COMET
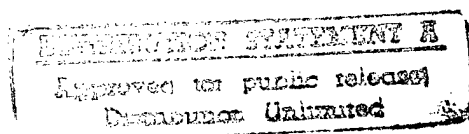
DTIC QUALITY INSPECTED 3

A Service of:

National Aeronautics and
Space Administration

**Scientific and Technical
Information Program Office**
Center for AeroSpace Information

19970814 069

CONTROL AUGMENTATION AND WORKLOAD REDUCTION BY

KINESTHETIC INFORMATION FROM THE MANIPULATOR

S.J. Merhav and O. Ben Ya'acov

Department of Aeronautical Engineering,
Technion - Israel Institute of Technology,
Haifa, Israel

SUMMARY

This paper is concerned with control augmentation and workload reduction by means of kinesthetic information provided by the manipulator. The control stick is loaded by a torque motor and the system is so interconnected that it presents complete kinesthetic input and output information from the controlled plant. Thus, the control task involves the same kinesthetic cues and the low workload as in nonintermediary handling of objects. It is demonstrated that within 20 rad/sec, which is the effective bandwidth in manual control, the method is realizable for a large variety of plants which may be unstable and time varying. Tracking and regulating tests demonstrate that very substantial improvements in accuracy and reduction in workload are obtained in comparison with ordinary isotonic, isomorphic or isometric manipulators. A test for the fixed set point regulation task involving a second order plant reveals that the control force law involved is strikingly similar to that of a linear regulator with an energy constraint obeying a quadratic performance criterion. The corresponding theoretical closed loop transfer function is in agreement with known linear models of the manual neuro-muscular system.

INTRODUCTION

With the advent of high performance aircraft, attention has focused on display augmentation and control augmentation systems (CAS). This paper is concerned with a special form of CAS, in which complete kinesthetic information is provided by the manipulator. Conventional manipulators are essentially passive linear transducers which translate manual commands into electrical input signals. In accordance with control theoretic man-vehicle models, e.g., McRuer et al [1], Kleinman et al [2], the generation of these manual commands require state estimation and optimum weighting which are executed by the functions of visual perception and cerebral data processing of the central nervous system. This explains the considerable workload generally experienced in the manual control of dynamical systems. Several studies in recent years attempted to reveal whether, and to what extent isotonic, isomorphic, isometric, inertia loaded, or other passive manipulators affect tracking and regulation performance [3, 4].

Since the muscle spindles and Golgi tendons in the manual neuromotor system provide position velocity and force measurements [5], different combinations of neuromotor loop closures should be involved in the operation of various types of passive manipulators. Recent laboratory open-loop tracking tests [6] have indeed revealed significantly different motor noise levels indicating such differences. They become, however, insignificant in closed loop tracking tasks as a result of the overriding supervisory visual loop closure. The dominant factors which determine performance and stress remain plant dynamics and system inputs, since the operations of state estimation and optimal weighting [2] are essentially the same with all types of passive manipulators. An interesting attempt to overcome this shortcoming of passive manipulators is due to Herzog [7] (1969), who studied the effect of a "matched manipulator". It ideally consists of a plant inverse operator at the input of the controlled plant. Thus, the human operator is always presented with a zero order system. Torque loading proportional to the plant input was applied to the manipulator so that an illusion of "natural feel" was provided. Significant improvement in tracking accuracies was reported [7] even when the manipulator match was not perfect. Two major shortcomings in this concept, have apparently prevented its emergence from the laboratory stage: 1) Inadequacy for systems with large parameter variations, as present in high performance aircraft. 2) Absence of response to external disturbances. Thus no advantage over passive manipulators exists in this important respect. Other investigations with similar techniques for the control of unstable systems were reported by Noggle [8] (1969) and more recently a tactile display of angle of attack was reported by Gilson et al [9] (1974), in particular when much attention was required in the visual channel.

The encouraging results obtained by these previous researchers were motivating factors in the work presented in this paper. Its specific objectives, however, are:

1) The method should improve control performance and reduce work-load for a large variety of dynamical systems and the design should not require adjustment of parameters for different systems.

2) The design should be realizable for time varying, high order stable or unstable plants.

3) The system should provide complete kinesthetic cues including the effect of external disturbances.

4) Comparative evaluations with conventional manipulators should consider both accuracy and workload.

These goals have been reached and the results have been experimentally demonstrated by means of a specially constructed single axis torque-motor-loaded manipulator suitably integrated into the control loop.

2. BASIC MANIPULATOR MODELS

Figs. 1a-1c schematically describe the interconnections of basic manipulators with the man-machine system, and their corresponding kinesthetic feedback paths. The diagrams suggest that the commanded scalar control u_c consists of a contribution u_c^v from the central nervous system which comprises visual perception and cerebral processing and a contribution u_c^y from the manual neuromuscular cent . associated with the cerebellum. In the sequel it is shown that the type of manipulator determines whether the visual-cerebral or the manual neuromotor center carries the main burden in the control task. A desired goal is clearly to achieve the latter. A control theoretic approach suggests that in either case, estimates $\hat{x}$ and $\hat{u}$ of the system state x and control force u are available so that an optimal weighting matrix $\underline{l}$ can be set in accordance with a suitable performance criterion. Fig. 1a represents the situation of the nonintermediary handling of an object (natural feel). In this case the system output y equals the manual deflection c. T_i, the torque exerted by the muscle output equals the reaction torque T_0 and is identical to the plant control input u. The muscle spindles G_{sp} measure position $x = x_1$ velocity $\dot{x} = x_2$ from y [1, 5]. The Golgi tendons [1] G_k measure T_i or u. These signals, corrupted by their corresponding measurement noises V_p and V_k yield the estimates $\hat{x}_N$ and $\hat{u}_N$. Thus, the optimal setting of $\underline{l}_N$ is possible
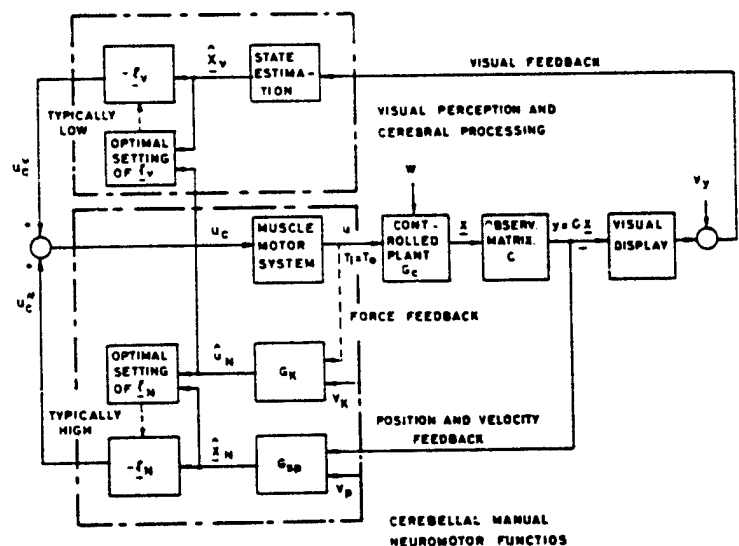

FIGURE 1a. Schematic description of the manual control system in ordinary nonintermediary handling tasks.

and $u_c^N = -\underline{l}_N \hat{x}_N$ is a substantial contribution to the control signal u_c. Consequently the contribution of the visual center $u_c^v = -\underline{l}_v \hat{x}_v$ will be comparatively small. This explains the small workload involved in nonintermediary handling of objects and the relative ease of manual operations in darkness or with closed eyes. Only in operations which require extreme precision (as the threading of a needle) the main burden is on the visual channel since a large $\underline{l}_v$ is required to suppress the effect of V_k and V_p. This is possible since V_y is very small by comparison.

Fig. 1b describes the man-machine system with a conventional isomorphic manipulator. The kinesthetic information path is now disconnected from the plant output y. c, the manipulator deflection is proportional to u. Since $T_o = T_i = ku$ (k - spring constant), G_k and G_p both provide measures of u only. Since $\hat{x}_N$ is not present, the setting of $\underline{l}_N$ must be zero so that $u_c^N = 0$. Consequently, the central nervous system must take the entire control task load and the optimal setting of $\underline{l}_v$ is consequently high. The lack of kinesthetic information from the system output thus explains the considerable workload which prevails with all types of passive manipulators, isotonic ($k = 0$), isomorphic ($k \neq 0$) and isometric ($k = \infty$). Only in the special case of a zero order plant, $y \propto c$, so that G_p provides information proportional to $\hat{x}$ and the setting of $\underline{l}_v$ is high. This explains the small work load experienced in the control of zero order systems.
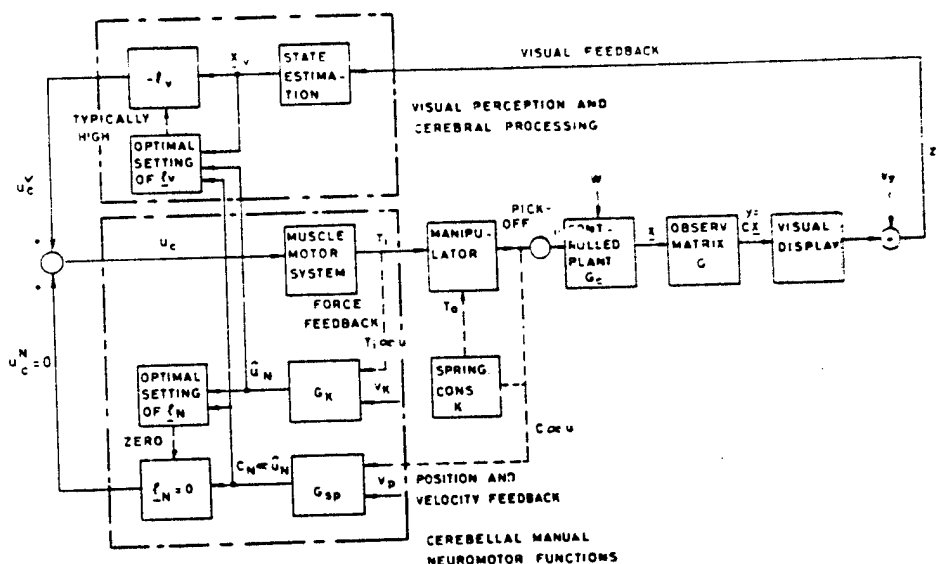

FIGURE 1b. Schematic description of the manual control system with a passive isomorphic manipulator.

FIGURE 1c. Schematic description of the manual control system with a "matched manipulator" according to Herzog [7].

Fig. 1c represents the idea of kinesthetic feedback by a "matched" manipulator according to Herzog [7]. The manipulator output signal is fed into an inverse plant operator. Thus, ideally y is proportional to c and effectively the system acts like the zero order system mentioned above. In addition, however, $T_0 = AHu$ (A - amplifier gain, H - torque motor constant) provides a measure of the actual control effort and the situation of "natural feel" as described in Fig. 1a, in principle, reestablished. However, since the kinesthetic information path is actually disconnected from y, the system cannot react to external disturbances w. Thus, in this important aspect - the method has no advantage over conventional passive manipulators. Another limitation is the impossibility of maintaining the match of the inverse operator if $G_c(s)$ undergoes substantial parameter variations. Moreover, the method is inadequate for unstable plants.

In the following section it is shown how complete kinesthetic input and output information can be provided and that the method involved can be implemented for a large variety of stable and unstable plants which may undergo large parameter variations.

3. REALIZATION OF MANIPULATOR SYSTEM WITH COMPLETE KINESTHETIC INFORMATION

Let $G_c(s)$ denote the plant dynamics. Instead of an inverse operator $G_c^{-1}(s)$ in tandem as indicated in Fig. 1c, the inverse operation can be approximated by placing $G_c(s)$ in the feedback path of a high gain amplifier K as shown in Fig. 2. N_1 and N_2 are compensation networks to ensure stability of the corresponding feedback loops. The plant input u is amplified by the power amplifier A driving the torque motor which is mechanically linked to the manipulator and the pick-off. Since $G_c(s) U(s) = Y(s)$ and $[Y_c(s)-Y(s)]KN_1(s) = U(s)$, it follows that:

$$\frac{Y(s)}{Y_c(s)} = \frac{K}{K + \dfrac{1}{N_1(s)G_c(s)}} \tag{1}$$

If it is possible to maintain the condition

$$K \gg 1/N_1(s)G_c(s) \tag{2}$$

up to the frequency of $\omega \approx 20$ rad/sec, which is the effective bandwidth in
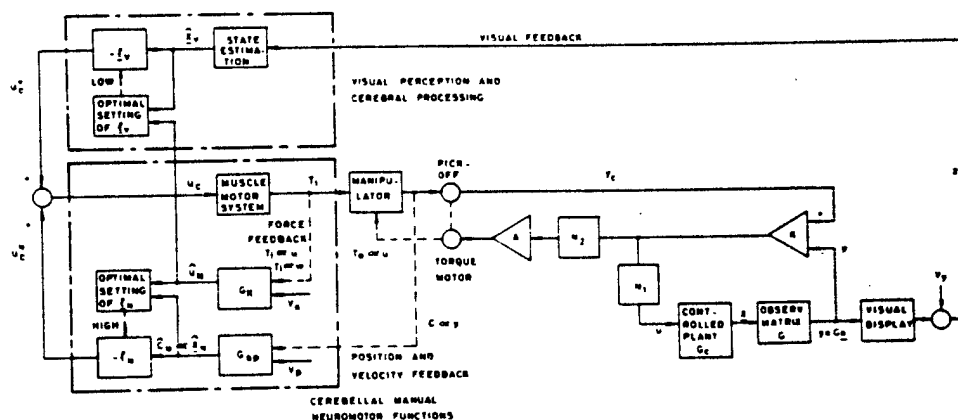
FIGURE 2. Realization of manual control system with complete kinesthetic information.

manual control, then from (1) one has:

$$Y(s) \simeq Y_c(s) \tag{3}$$

Since $y_c \propto c$ (Fig. 2), it follows that the kinesthetic feedback path from c is equivalent to that from y in Fig. 1c. Since $N_2(s)$ is in practice a wide band network, it follows that $T_0 \propto u$ in the relevant frequency band, and it is equivalent to the direct reaction torque T_0 in Fig. 1c. In view of (2), equality (3) is insensitive to wide parameter variations in $G_c(s)$ and if $N_1(s)$ is suitably designed, (3) holds for an unstable $G_c(s)$ as well.

It is easily verified that the reaction to the external disturbances $W(s)$ is satisfactorily provided by the system shown in Fig. 2:

$$Y(s) = G_c(s) \; [U(s) - W(s)] \tag{4}$$

$$U(s) = KN_1(s) \; [Y_c(s) - Y(s)] \tag{5}$$

Thus,

$$Y(s) = \frac{KN_1(s)G_c(s)}{1+KN_1(s)G_c(s)} \; Y_c(s) - \frac{G_c(s)}{1+KN_1(s)G_c(s)} \; W(s) \tag{6}$$

In view of (2) and since $N_1(s) \approx 1$ in the effective frequency band,

$$Y(s) \approx Y_c(s) - \frac{W(s)}{K} \tag{7}$$

Thus, due to the large gain K, if $y_c = 0$, the response to the disturbance is effectively eliminated. The torque required to maintain $Y_c(s) \equiv 0$ is determined by substituting (6) into (5), and deriving $U(s)$:

$$U(s) = KN_1(s) \; \frac{G_c(s)}{1+KN_1G_c(s)} \; W(s) \approx W(s) \tag{8}$$

Thus,

$$T_i(s) = AHU(s) \approx AHW(s) \tag{9}$$

The value of A must be so adjusted that for a typical disturbance level of $W(s)$, $T_i(s)$ should not cause muscular fatigue.

From the foregoing it follows that the system shown in Fig. 2 provides complete kinesthetic information in equivalence to Fig. 1a. It fulfills all the requirements regarding:

- Wide variations of plant parameters
- Unstable systems
- External disturbances

It now remains to show that the condition in (2) which underlies the validity

of the concept described, can indeed be guaranteed by practically realizable networks $N_1(s)$ and $N_2(s)$.

4. CONTROL LOOP DESIGN

The initial design of the control loop was carried out for $G_c(s) = 1/s^2$. This system is on the verge of instability. The networks $N_1(s)$ and $N_2(s)$ were then checked for other stable and unstable forms of $G_c(s)$. The detailed block diagram of the manipulator feedback loop is shown in Fig. 3. The brushless torque motor develops a maximum torque of 12 Kg-cm which is stepped up by a factor of 4 by means of an antibacklash gear. The transfer function of the torque motor is:

$$\frac{C(s)}{e_m(s)} = \frac{2145}{s(s+5.5)(s+167)} \tag{10}$$
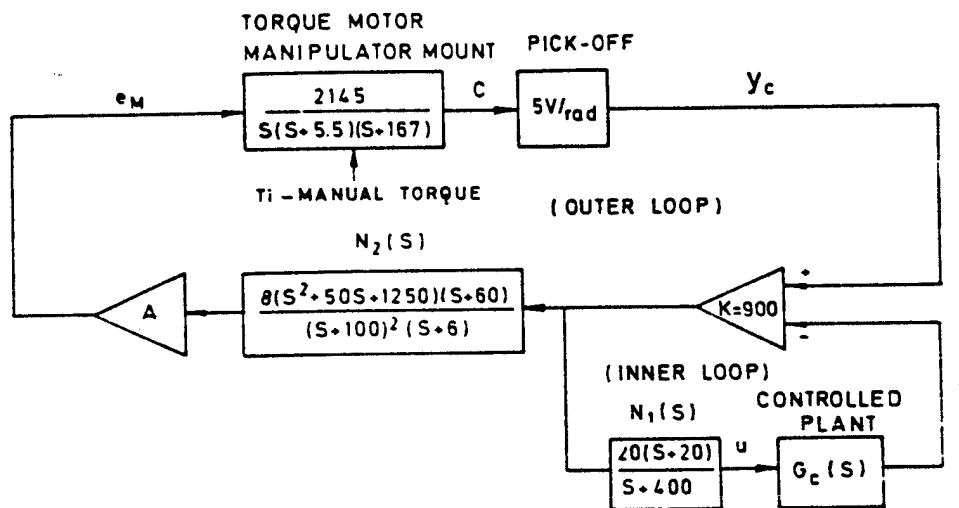
FIGURE 3. Block diagram of manipulator feedback loops.

The root locus of the inner loop involving $G_c(s)$, K and $N_1(s)$ is shown in Fig. 4. The complex zeros in $N_2(s)$ (Fig. 3) are intended to arrest the complex pole pair arising in the inner loop. The lag-lead network $(s+60)/(s+6)$ is introduced to increase the D.C. gain of the loop without impairing its dynamic performance within the 20 rad/sec band. The root locus of the complete
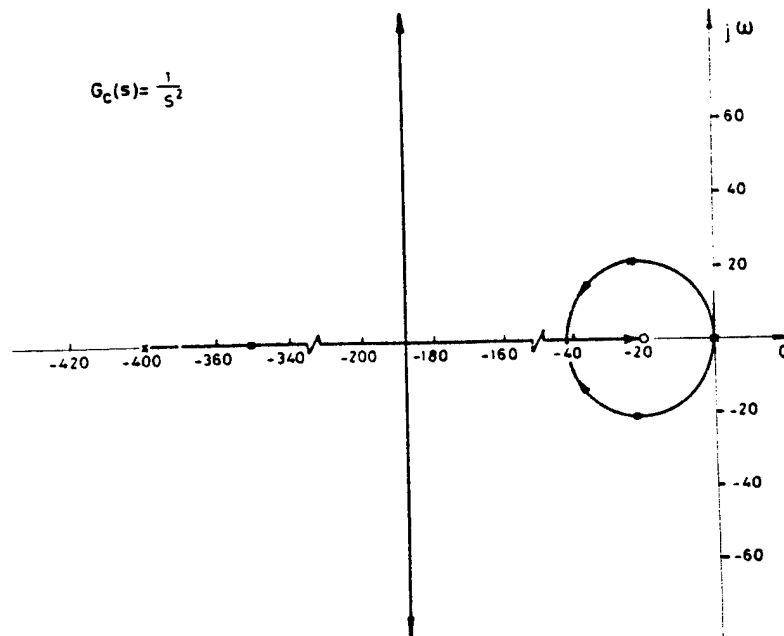
FIGURE 4. Root locus of inner loop, $G_c(s) = 1/s^2$.

manipulator system of Fig. 3 is shown in Fig. 5. Since all the closed loop poles are either compensated by neighboring zeros or are outside the 20 rad 20 rad/sec bandwidth, the required proportionality $c \propto y$ is effectively implemented. On replacing $G_c(s)$ by $1/s$, $1/s(s-1)$, $1/(s^2+0.66s+10)$ while retaining the same values for K, $N_1(s)$ and $N_2(s)$ as in Fig. 3, it was found that the closed loop pole locations vary only slightly so that $c \propto y$ is guaranteed. The gain yielded a control force of $\sim\pm2.5$ Kg for $c = \pm20°$. The complete manipulator is depicted in Fig. 6. It should be noted that though $c \propto y$ for different plants $G_c(s)$, large differences exist in the corresponding reaction torques T_0. For a given command output $Y_c(s)$, and since $Y(s) \approx Y_c(s)$, T_0 is given by

$$T_0(s) \simeq \frac{Y_c(s)}{G_c(s)} AH = uAH \qquad (11)$$

This display of u, characteristic of each $G_c(s)$ is essential in the ability of the human operator to execute optimal or near optimal control inputs. This is demonstrated in the next section.
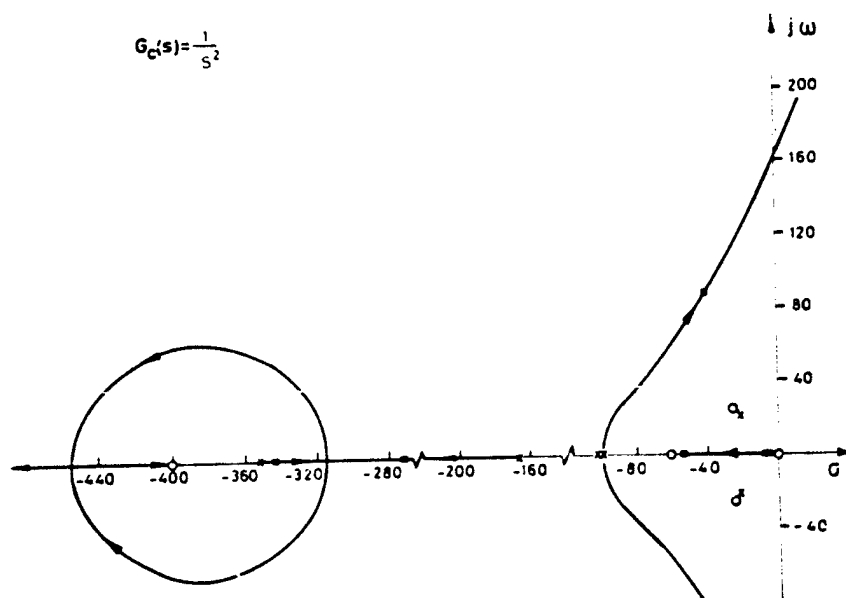
$G_c(s) = \dfrac{1}{s^2}$

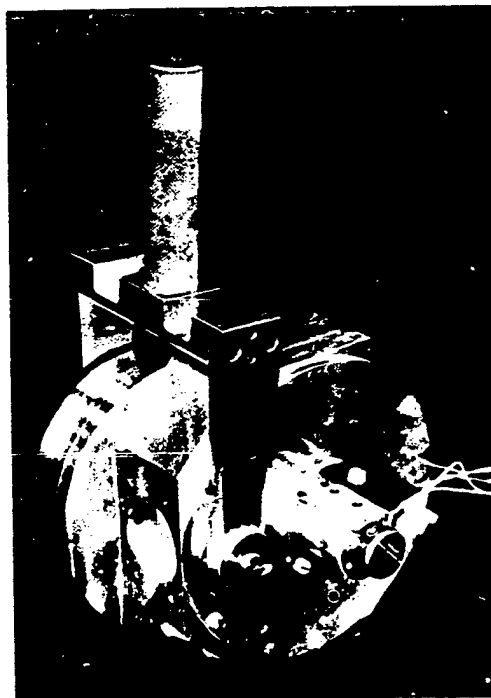FIGURE 5. Root locus of complete manipulator feedback system, $G_c(s) = 1/s^2$.

FIGURE 6. Torque motor loaded kinesthetic manipulator .

5. OPTIMAL CONTROL IN A SECOND ORDER PLANT

The control objective is to eliminate an initial deflection y_0 in minimum time, subject to constraints on the control effort u. The controlled plant was $G_c(s) = k/s^2$. A recorded sample of the time history of four such transient responses obtained in laboratory tests and the corresponding control inputs $u(t)$ are shown in Fig. 7. The results demonstrate the remarkable closeness between y and y_c and its excellent dynamic response. This, and the typical shape of the control time history $u(t)$, indicate that a linear control law is actually implemented by the human operator. This hypothesis was tested by the optimal solution of the corresponding analytical model as follows:

The state space representation of $G_c(s)$ is:

$$\dot{\underline{x}}(t) = A\underline{x}(t) + Bu(t) \tag{12}$$

The system matrix is 2×2, $x_1 = x$ and $x_2 = \dot{x}$. The controlled variable is

$$y(t) = C\underline{x}(t) \tag{13}$$

$$C(1,0) \quad ; \quad B = (0,k)^T \quad ; \quad A = \begin{pmatrix} 0 & 1 \\ 0 & 0 \end{pmatrix} \tag{14}$$
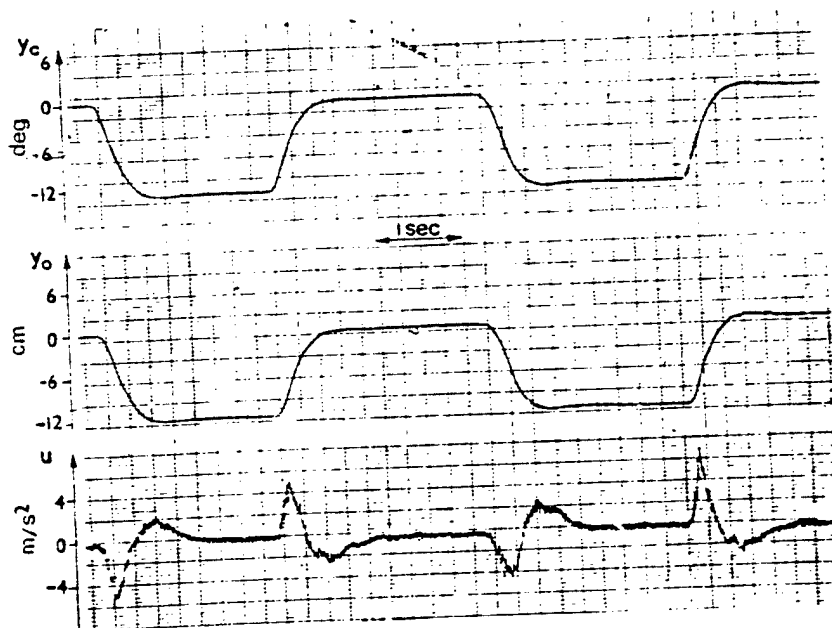
FIGURE 7. Time history of transient responses of a fixed set-point regulation task for $G_c(s) = 1/s^2$.

371

The performance criterion which is assumed to underly the control policy is the minimization of:

$$J = \int_0^\infty [y^2(t) + \rho u^2(t)] \, dt \tag{15}$$

$\rho \geq 0$ is the weight on the control effort.

In accordance with Fig. 1c, the observed variable is:

$$z(t) = C\underline{x}(t) + V_y(t) \tag{16}$$

where $V_y(t)$ represents white observation noise.

Let $\hat{\underline{x}} = (\hat{x}_1, \hat{x}_2)^T$ be the reconstructed state vector provided by a full state observer. The optimal control law is then given by:

$$u(t) = - \underline{l} \, \hat{\underline{x}}(t) \tag{17}$$

where $\underline{l} = (1/\rho) \, B^T P$ and P is the solution of the 2×2 Ricatti equation $C^T C - P B B^T P + A^T P + P A = 0$.

The result is:

$$\underline{l} = \left(\frac{1}{\sqrt{\rho}} \, , \, \sqrt{\frac{2}{\sqrt{\rho} k}} \right)^T \tag{18}$$

The full state observer is of the form:

$$\dot{\hat{\underline{x}}}(t) = A\underline{x}(t) + Bu(t) + K[y(t) - C\hat{\underline{x}}(t)] \tag{19}$$

where $y(t) = Cx(t)$, and $K = (k_1, k_2)^T$.

Defining $\underline{e}(t) \triangleq \underline{x}(t) - \hat{\underline{x}}(t)$, the resulting augmented differential equation interconnecting $\underline{x}(t)$ and $\hat{\underline{x}}(t)$ for the closed loop system [10] is given by

$$\begin{bmatrix} \dot{\underline{x}}(t) \\ \dot{\underline{e}}(t) \end{bmatrix} = \begin{bmatrix} A - B\underline{l} & -B\underline{l} \\ 0 & A - KC \end{bmatrix} \begin{bmatrix} \underline{x}(t) \\ \underline{e}(t) \end{bmatrix} \tag{20}$$

The characteristic values can be shown to be those of $A-B\underline{l}$ (regulator poles) and those of $A-KC$ (observer poles).

The characteristic equation of the observer is of the form $s^2 + k_1 s + k_2 = 0$. Given $k = 160$ and choosing $k_1 = \sqrt{2k_2}$, substituting (14) into (20), the numerical solution of $(\underline{x}, \underline{e})^T$ for the initial conditions $(x_0, e_0)^T = (x_1(0), 0, e_1(0), e_2(0))^T = (x_1(0), 0, x_1(0), 0)^T$ yields the best fit to Fig. 7 for the parameters $\rho = 64$, $k_1 = 25$ and $k_2 = 312$. The plot of the computed optimal $u(t)$ for these parameter values is shown in Fig. 8. It is
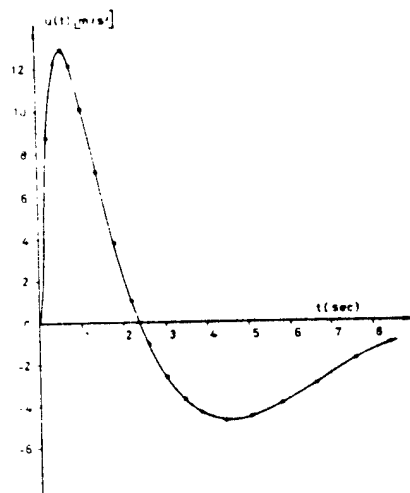
372

FIGURE 8. Computed optimal control force $u(t)$ for the fixed set point regulating task.

$$\rho = 64 \qquad k = 160, \qquad k_1 = 25, \qquad k_2 = 312.$$

easily verified that the closed loop transfer function H_c (s) relating $y(s)$ to $u(s)$ is given by:

$$H_c(s) = \frac{\dfrac{k}{\sqrt{\rho}}}{s^2 + \sqrt{\dfrac{2k}{\sqrt{\rho}}}\, s + \dfrac{k}{\sqrt{\rho}}} \tag{21}$$

It follows therefore that with torque feedback the human operator strongly resembles a linear optimal regulator with observation noise, subject to a quadratic performance criterion with an energy constraint (15).

It is also of interest to compare the closed loop transfer function of (20) with the neuromuscular limb-manipulator model according to McRuer et al [15]. From this model it follows that the closed loop transfer function for a purely inertially loaded manipulator, (equivalent to our example G_c (s) = k/s^2), the closed loop transfer function $C(s)/U_c$ (s) (Fig. 1c) is:

373

$$\frac{C(s)}{U_c(s)} \simeq \frac{\dfrac{K_{sp}\, C_f}{M}}{s^2 + \dfrac{B_m}{M} s + \dfrac{K_{sp}\, C_f}{M}} \tag{22}$$

where:

K_{sp}	–	Muscle spindle gain factor
$C_f = \partial P/\partial f$,	f –	neuromotor firing rate, P muscle tension
M	–	Combined limb-manipulator mass
B_m	–	$\partial p/\partial v$, muscle damping factor, V - velocity.

Since $T_0 = AHu$ and since $U(s) = Y(s)s^2/k$, it follows that $T_0(s) = AH/ks^2Y(s)$. Thus, AH/k is equivalent to a mass M. With the given torque motor gain settings, $M \simeq 0.3$ Kg. Since $c \propto y$, it is justified to compare (22) to $H_c(s)$ in (21). It is significant that they are of the same form.

The corresponding coefficients are:

$$\sqrt{\frac{2k}{\sqrt{\rho}}} = \frac{B_m}{M} \tag{23}$$

$$\frac{k}{\sqrt{\rho}} = \frac{K_{sp}\, C_f}{M} \tag{24}$$

The parameters B_m and C_f can vary widely [5]. Thus, for different values of M, the neuromuscular system has sufficient freedom to maintain the optimal parameter values dictated by the left hand sides of (23), (24). This is due to the independent control of B_m and C_f. By comparison, the measured and computed values of $u(t)$, it was found that $B_m = 1.9$ Kg sec/cm, which is in the region of values reported in the literature.

6. PERFORMANCE EVALUATION METHOD

From Sections 2 and 5 it follows that a major advantage of kinesthetic information must be workload reduction since the strenuous task of state estimation and optimal weighting by the visual perception and mental processing is nearly eliminated. In order to evaluate the method, two requirements had to be met:

1. The evaluation should be on a comparative basis.

2. It should involve workload measures.

Consequently all performance tests were carried out so that every type of $G_c(s)$ was tested both for the kinesthetic manipulator mode and the

374

conventional isomorphic manipulator mode. In practice, in order to keep all other factors unchanged, the same manipulator was switched into the system in either the isomorphic or the kinesthetic mode.

The specific requirements of the evaluation method were:

- It should provide an objective measure for the control task effort for any type of manipulator or controlled plant.

- The evaluation method should present a control task which is similar to that encountered in flight practice.

- The operator should not be able to influence the outcome by adopting "clever strategies."

In all tests the primary task was tracking and/or regulating $G_c(s)$ for a stationary random input or disturbance band limited to ~1 rad/sec. The control test was single axis and in the vertical plane.

In order to meet the foregoing requirements a secondary task method was developed and adopted in the evaluation. A general block diagram is given in Fig. 9. The method consists of reading out (to permit supervision) of two--digit random numbers displayed outside the foveal field of the primary task display. The random numbers change at a increasing rate $\lambda(t) = Bt$, where B is a constant. During the initial 20 seconds, the operator concentrates on the
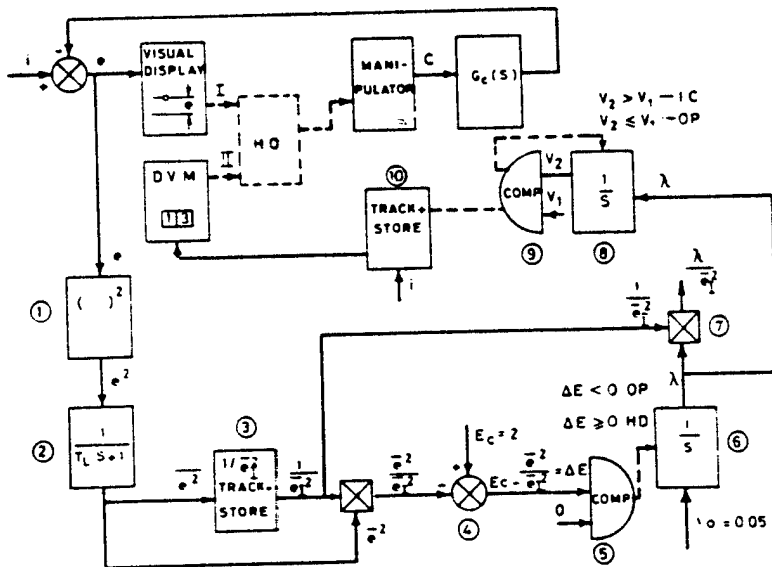

FIGURE 9. Block diagram of the secondary task evaluation system.

375

primary task only and the initial mean squared error $\overline{e_f^2}$ is determined. Thereafter the secondary task is activated. The operator has to control the primary task but simultaneously read out the random numbers the subsequent error variance $\overline{e2}$ is normalized to $\overline{e_f^2}$ as in Jex [11]. Due to the workload of the secondary task $\overline{e2}/\overline{e_f^2}$ gradually increases. When some predetermined level E_c is reached, the system automatically stops at $\lambda = \lambda_c$. The performance measure was chosen as $\lambda_c/\overline{e_f^2}$. A comparatively easy task will have a small $\overline{e_f^2}$ and a large λ_c and vice versa. Thus, a large value of $\lambda_c/\overline{e_f^2}$ indicates a system with good handling qualities. It easily verified that the method meets all three requirements listed above. In particular, the operator has no choice of "clever" strategies. For example, if he chooses initially to devote less attention to the primary task in order to reach a higher λ_c, his initial $\overline{e_f^2}$ will tend to be larger so that $\lambda_c/\overline{e_f^2}$ tends to remain constant. The noise generator output i provides both the primary task input and the random numbers to the secondary task display. Preliminary tests of the evaluation method with several subjects demonstrated that $\lambda_c/\overline{e_f^2}$ is significantly and consistently different for different types of $G_c(s)$ like $1/s$, $1/s^2$, $1/s(s-1)$. The method was therefore adopted for the comparative evaluation of the kinesthetic manipulator.

7. EXPERIMENTS AND RESULTS

The tracking and regulation experiments were carried out by a group of five students with no flying experience. They were selected from a larger group after undergoing preliminary screening tests of reaction time and tracking ability.

The experimental equipment used was:

- EAI-580 hybrid analog computer which was also used for the realization of the compensation networks $N_1(s)$ and $N_2(s)$ and gain Y

- HP H01-3722 noise generator for input, disturbance and secondary task signals.

- HP 1310A CRT display with a 30×40 cm screen.

- The single axis manipulator is loaded by medium power brushless torque motor and the pick off is linear low torque potentiometer.

- The power amplifier A has 200W output and a voltage gain amplification range of 10÷110.

The input i is obtained from a 1.5 Hz rectangular spectrum filtered by a single lag filter $1/(s+1)$. The disturbances w are obtained from the same source but after a delay τ to avoid correlation with i.

The first series of tests were tracking tasks with $i \neq 0$, $w \equiv 0$ for $G_c(s) = 1/(s^2+0.66s+10)$, $G_c(s) = 1/s^2$, $G_c(s) = 1/s(s-1)$. The duration of each test was approximately 2 min, depending on the instant $\overline{e2}/\overline{e_f^2} = E_c$.

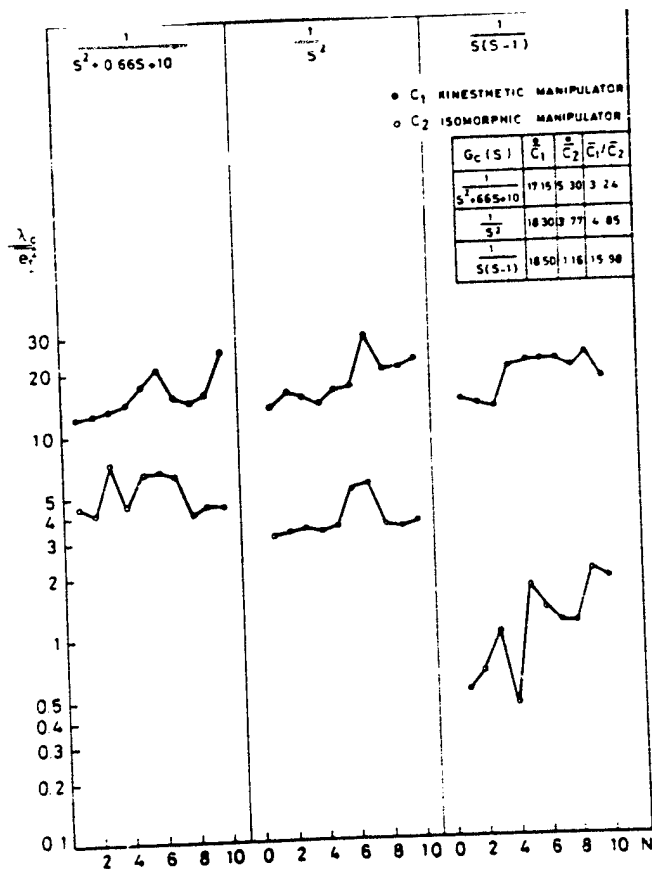A typical set of results of 10 tests for subject I is shown in Fig. 10.

FIGURE 10. Results of tracking experiments - Subject I.

The results of other subjects were quite similar. The following conclusions can be drawn:

1. For the isomorphic manipulator the performance measure $\lambda_c/\overline{e_I^2}$ is significantly lower, the harder the control task. This demonstrates the increasing work-load associated with difficult control tasks due to the load on the visual channel and mental processing. It also indicates the potential of the evaluation method in workload measurements, and task rating. A certain tendency of learning can be noticed for $1/s^2$ and $1/s(s-1)$. It was also present in the results of the other subjects.

2. For the kinesthetic manipulator, $\lambda_c/\overline{e_I^2}$ is practically the same for all types of $G_c(s)$, and it is considerably higher. This demonstrates the unloading of the visual channel by the provision of complete kinesthetic information paths. It is significant that even an unstable system yields the same performance measure.

The second series of tests were regulating tasks with $i \equiv 0$ and $w \not\equiv 0$. In this case the control task with the kinesthetic manipulator reduced to holding the manipulator in a "stick fixed" position against the jerks induced by $w(t)$. The visual feedback path was only required for occasional monitoring. Consequently $\lambda_c/\overline{e_I^2}$ was extremely high.
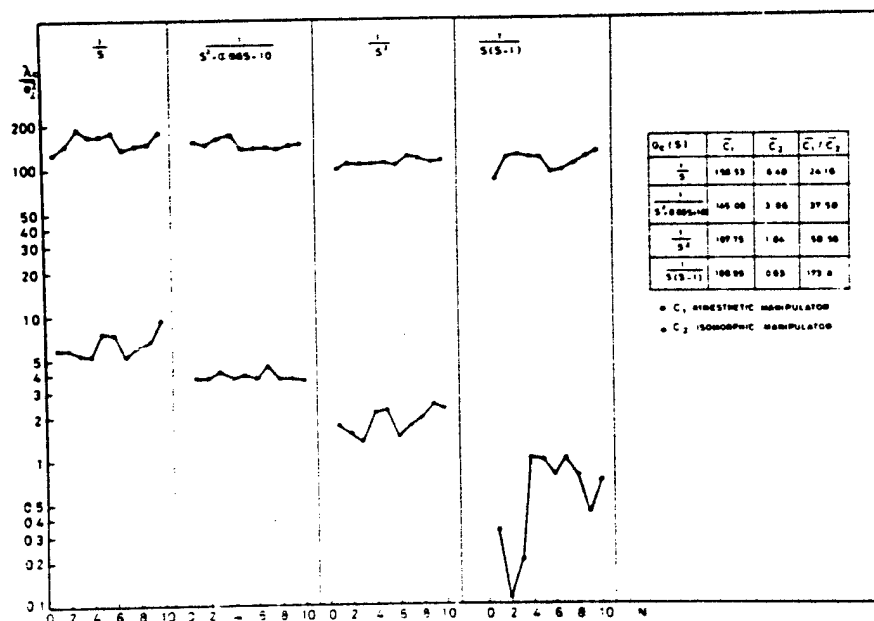
FIGURE 11. Results of combined tracking and regulating experiments - Subject I.

The third series of tests was a combined tracking and regulation, i.e., $i \neq 0$, $w \neq 0$. This is a typical situation in practical control tasks. The results are, as expected, intermediate between the first and second series of tests. The results for subject I are shown in Fig. 11 for $G_c(s) = 1/s$; $1/(s^2+0.66s+10)$; $1/s^2$; $1/s(s-1)$. The results for the other subjects again were very similar. In all tests $\overline{e_f^2}$ with the kinesthetic manipulator was between $3 \div 10$ times smaller than with the isomorphic manipulator, depending on the type of $G_c(s)$. The main observations are:

1. The performance measure $\lambda_c/\overline{e_f^2}$ deteriorates gradually by an order of magnitude from $1/s$ to $1/s(s-1)$ in a consistent manner. It is also considerably lower than for the pure tracking task shown in Fig. 10.

2. The performance measure $\lambda_c/\overline{e_f^2}$ for the kinesthetic manipulator deteriorates only by ~50% from $1/s$ to $1/s(s-1)$ and is higher by 170 as compared with the isomorphic manipulator.

3. The secondary task method and the criterion $\lambda_c/\overline{e_f^2}$ provide a consistent and sensitive yardstick for performance evaluation.

8. CONCLUSIONS

The kinesthetic information paths in manual control have been shown to play a vital role in workload reduction and that in the case of high order or unstable plants, this role may be decisive in stabilizing the system. It has also been shown that by the technique described in Sec. 3 it is possible to essentially close the same kinesthetic feedback paths that exist in the natural nonintermediary handling of objects. These loop closures provide the required state estimates for implementing near optimal control without loading the visual channel and mental processes. Comparative test demonstrates the superiority of the method both in precision and workload reduction.

9. REFERENCES

1. McRuer, D.T. et al, *New Approaches to Human-Pilot/Vehicle Dynamic Analysis*, AFFDL-TR-67-150, (1968).

2. Kleinman, D.L. et al, "An Optimal Control Model of Human Response, Part I: Theory and Validation," *Automatica*, Vol. 6, pp. 357-369, (1970).

3. McRuer, D.T., and Magdaleno, R.E., *Human Pilot Dynamics with Various Manipulators*, AFFDL-TR-66-138, (1966).

4. Kraiss, K.F., "Can Proprioceptive Cues Unload the Human Operator," *6th An. Conference on Manual Control*, (1970).

5. McRuer, D.T. et al, "A Neuromuscular Actuation System Model," *IEEE Transactions on Man Machine Systems*, Vol. MMS-9, No. 3, Sept. (1968), pp.61-71.

6. Ben Ja'acov, O., *Torque Feedback in Manual Control of Aircraft*, M.Sc. Thesis, Dept. of Aeronautical Engineering, Technion, May 1975.

7. Herzog, H.J., *Proprioceptive Cues and Their Influence on Operator Performance in Manual Control*, NASA CR-1248 (1969).

8. Noggle, P.L., *Manual Control of Unstable Vehicles Using Kinesthetic Cues*, MIT Report, MV-69-4 (1969).

9. Gilson, R.D., et al, "Kinesthetic Tactual Information Presentation-Inflight Studies," *IEEE Trans. on SMC*, Vol. 4, pp. 531-536 (1974).

10. Kwakernaak, H., and Sivan, R., *Linear Optimal Control Systems*, Wiley, Interscience (1972).

11. Jex, H.R., et al, "Development of the Dual Axis and Crosscoupled Critical Tasks, *8th Ann. Conference on Manual Control*, May 1972.

SESSION V

TRACKING AND OTHER PSYCHOMOTOR TASKS

Chairman: D. L. Baty

TIME OPTIMAL CONTROL OF AN UNDAMPED HARMONIC OSCILLATOR:

EVIDENCE FOR BIASES AND SCHEMATA[1]

By Richard J. Jagacinski, Michael W. Burke,
and Dwight P. Miller

The Ohio State University

SUMMARY

Choosing the appropriate environmental conditions for executing a given response is argued to be a task basic to many kinds of skilled performance. As an example of this skill, three experiments investigated how human subjects solve the problem of bringing an undamped harmonic oscillator to rest as quickly as possible by means of bang-bang control. Comparison with the optimal control theory solution to this problem suggests that subjects have difficulty in using acceleration information in both learning the form of the optimal switching pattern and also in executing their learned switching patterns when the harmonic oscillator is speeded up. Excellent transfer by several subjects in situations involving system positions and velocities not previously encountered constitutes evidence for stimulus recognition schemata underlying their performance.

INTRODUCTION

The optimal control patterns derived from optimal control theory can be used as a reference for examining the actual control patterns used by human subjects. Several control problems which have been investigated from this viewpoint have involved first order unstable systems (refs. 1, 2, 3, 4), pure inertia systems (refs. 5, 6, 7, 8, 9), and undamped harmonic oscillators (ref. 9). The present set of experiments investigates how human subjects solve the problem of bringing an undamped harmonic oscillator to rest as quickly as possible when they are limited to applying a rightward or leftward force of fixed magnitude.

A second aspect of these experiments is to investigate the level of generality of the subjects' control patterns by means of various transfer tasks. The term schema has been used in various ways in psychology to refer to a generalized response generating capability that is not limited to stimulus situations previously encountered. Adams (ref. 10) and Schmidt (ref. 11) have recently reviewed three uses of the term schema corresponding

to motor recall schema, motor recognition schema, and stimulus recognition schema. While there have been numerous studies supporting the notion of a stimulus recognition schema for various types of static visual forms (e.g., refs. 12, 13), the present authors are unaware of any previous experiments relating this concept to motor behavior or the control of dynamic systems. Motor theorists have tended to concentrate on the concepts of motor recall schema and motor recognition schema, which refer respectively to the capability of producing or recognizing movement patterns not previously experienced. However, a generalized ability for choosing the appropriate conditions in a dynamic environment for executing a given response would also appear to be an important aspect of many kinds of skilled performance. For example, a baseball player who has reached the limits of the outfield fence and who must leap to catch the baseball has to choose an appropriate point in the ball's trajectory to begin his response. Jumping either too early or too late may result in his missing the ball. Similarly, a rifleman attempting to hit a distant target on a windy day will introduce a certain amount of compensation into his aim for wind velocity, indicated by the state of specific visual cues such as the motion of tall grasses. He will wait for the instant when the wind velocity is appropriate for that precise amount of compensation before pulling the trigger. Both of these situations involve recognizing special conditions of a dynamic environment, and the notion of a stimulus recognition schema is appropriate for describing this kind of generalized skill.

An experimental strategy for demonstrating the existence of a schema using a within subject design is to show that over the course of an experiment a subject learns a new response pattern, and that he exhibits this learned pattern when he is transferred to a new situation in which he has no previous practice. The present experiments will involve a variety of transfer tasks to explore the applicability of the concept of a schema to controlling a dynamic system. The subject's responses in these tasks will be limited, however, to simple button pressings, thus making the selection of the appropriate environmental conditions more critical. Because evidence for motor recall schema and motor recognition schema must necessarily involve production or recognition respectively of new movements, any evidence for schemata in the present experiments will be interpreted as stimulus recognition schemata. These experiments will also attempt to determine the implications of the subject's transfer behavior for a process model of performance.

TIME OPTIMAL CONTROL OF AN UNDAMPED HARMONIC OSCILLATOR

The present set of experiments investigates one particular control problem -- bringing an undamped harmonic oscillator to rest as quickly as possible by the application of a leftward or rightward force of fixed magnitude. The problem is analogous to bringing an oscillating pendulum to rest by means of two magnets which can exert either a constant rightward or leftward force on the pendulum. The optimal switching locus for bringing the pendulum-like system to rest at the origin as quickly as possible is shown in figure 1. The locus consists of a string of dashed semicircular arcs
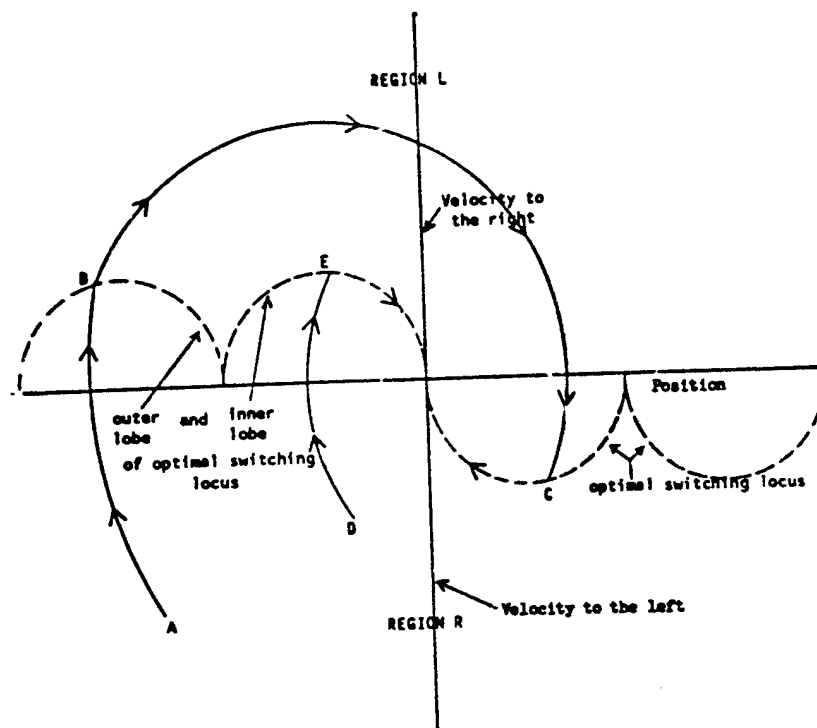
Figure 1. Optimal switching locus (— —) for bringing the system to rest at the origin as quickly as possible.

(ref. 14) that divides the phase plane into two regions, R and L. When the system has a position and velocity corresponding to Region R, the rightward force should be applied. In Region L, the leftward force should be applied. Two examples of the optimal switching strategy (A-B-C-Origin and D-E-Origin) are shown in figure 1.

Miller (ref. 9) instructed subjects as to the optimal switching strategy and measured their asymptotic performance using five different displays. Even when the optimal switching curve was available on a phase plane display, subjects experienced some difficulty in this control task. They tended to be least consistent in switches occurring near the cusp region between the inner and outer lobes and also tended to switch a little late along the outer lobe. These difficulties were considerably magnified with the least aided display, a single dimensional display of system position. Subjects' switches with this display tended to be both late and highly variable in the cusp region and out into the outer lobe. Miller was unable to account for this pattern of errors in terms of the subjects' psychophysical and reaction time limitations, and suggested that more research is necessary to clarify how subjects plan their responses in controlling such a system. The present experiments pursue this problem by investigating how subjects using a single

dimensional display learn to stop an undamped harmonic oscillator when they are given no prior instructions as to the optimal switching strategy.

EXPERIMENT 1

The first experiment examined subjects' performance with initial values of position and velocity that corresponded to optimal switching performance along the inner lobe in figure 1.

Method

Apparatus. The undamped harmonic oscillator system was simulated on an EAI Pace TR-48 analog computer, and system position was displayed as a 1/8-inch (.32-cm) diameter white dot moving horizontally across a 14-inch (35.56-cm) video monitor. The target region was represented by a 1/8-inch (.32-cm) wide mark in the middle of the television monitor. Above the monitor a pair of adjacent arrows pointing in opposite directions away from the center of the field alternately lighted, indicating whether a leftward or rightward force was being applied to the system. Subjects controlled the direction of the applied force with their right middle and index fingers by means of two pushbuttons. Momentarily depressing the left button caused the left arrow to light, produced a 500-Hz 110-msec tone over the earphones worn by the subject, and caused a leftward force to be applied to the pendulum-like system. The leftward force persisted until the right button was momentarily depressed. The right button functioned similarly.

Subjects. Four male, right-handed Ohio State University students participated in all four experiments.

Design. Each subject received 80 trials per session for 8 sessions. Each session lasted approximately 1 hour. The 80 trials consisted of four randomized blocks of the 20 initial conditions represented as black dots in figure 2. The undamped harmonic oscillator corresponded to the differential equation

$$(1/w^2)\, \ddot{x} + x = u \qquad (1)$$

where x is system position reltive to its natural resting position in inches, $\ddot{x}$ is system acceleration in inch/sec^2, $w = .4$ rad/sec, and $u = \pm 1.75$ inch (4.45 cm), depending on whether the right or left button was last depressed. At the beginning of each trial the system had one of the 20 initial conditions pictured in figure 2 and the rightward force was applied to the system. Optimal performance for bringing the system to rest at the origin as quickly as possible consisted of appyling a leftward force when the system intersected the inner switching lobe (figure 1). If a subject behaved in this manner, the time between the beginning of a trial to the optimal switch would range from 890 to 3,040 msec over the 20 initial conditions.

The system was considered to be at rest and on target when system velocity was less than 1/8 inch/sec (.32 cm/sec) and the system was within 1/16
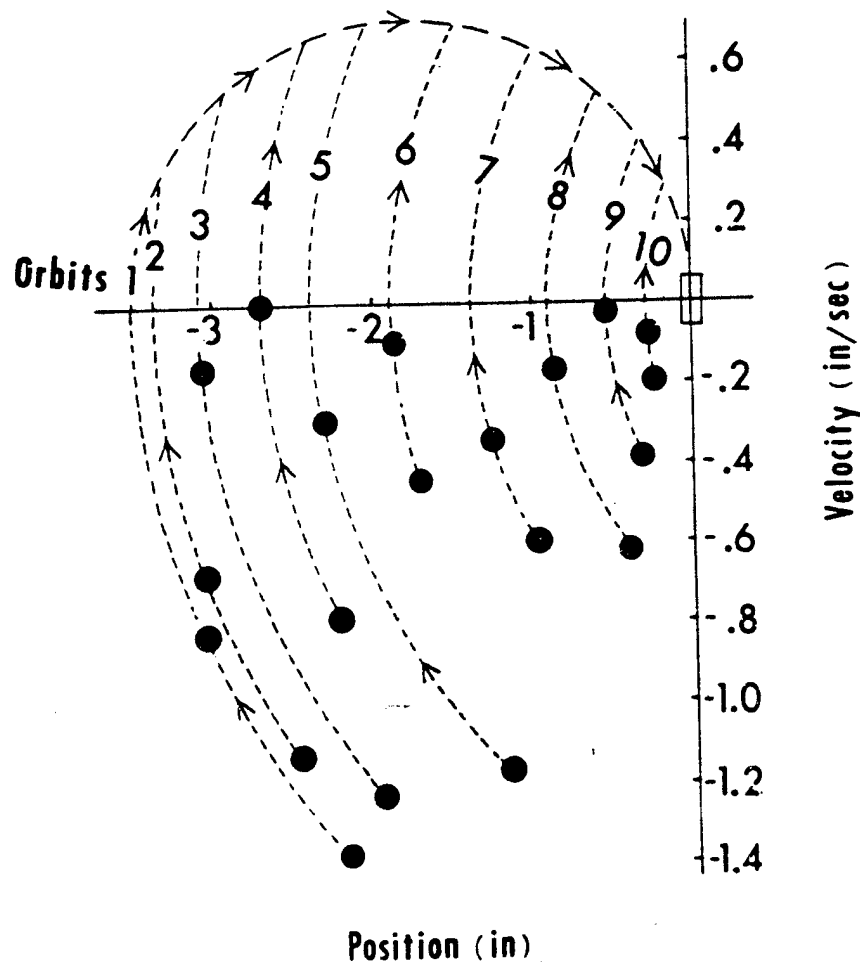
Figure 2. Initial positions and velocities for Experiments 1 and 3.

inch (.15 cm) of the center of the video monitor. Subjects were paid a base salary of $0.75 per session, and an additional amount per trial contingent on their performance. They received 4 cents per trial if they brought the system to rest on target as quickly as an ideal subject whose switching locus corresponded to the inner lobe in figure 1. For less than optimal perfor- mance, payoffs decreased linearly to zero as the time to bring the system to rest increased to 4 seconds longer than optimal performance.[2]

---

[2]Technically, the optimal switching locus is slightly different from the inner lobe shown in figure 1 because the effective target in the phase plane is a small rectangle about the origin rather than a single point at the origin. However, for the purposes of this experiment, the optimal switching locus for the point target was used to define optimal performance.

Procedure. Subjects were told that the dot represented a vehicle which would have a rightward force applied to it at the beginning of each trial. Their task was to stop the vehicle at the target region as quickly as possible by applying a leftward force at the appropriate instant. If the dot overshot or undershot the target, then the subjects were to apply right-ward and leftward forces until the dot finally slowed to criterion over the 1/8-inch (.32-cm) target region. The dot then disappeared from the screen, and the trial was over. Immediately after each trial, subjects were told how much they had earned for that trial to the nearest 1/10 cent. If at any time the dot exceeded the bounds of the 14-inch (35.56-cm) viewing window, the trial immediately ended and the subjects received zero payoff.

The data for each trial consisted of the position and velocity when the subject executed his first three switches for each trial, the elapsed time for the first two switches, and the total elapsed time for the trial.

Results

Median switching points were calculated for subjects' first switches with each of the 20 initial conditions. The medians were calculated in terms of elapsed time along a given orbit in the phase plane. In figure 3 the upper and the lower medians for each of the 10 orbits have been connected with straight lines to indicate the average switching patterns for two of the four subjects. The optimal switching pattern for a point target is indicated by the dashed semicircle.

One qualitative property of the optimal switching pattern is that it is a line through the phase plane. In other words, the two initial conditions lying along each orbit in figure 2 have the same optimal switching point. The width of the subjects' switching loci in figure 3 indicate how closely their performance approximated a line through the phase plane. All subjects markedly reduced their intra-orbit inconsistency over the first several days of practice (e.g., compare A-1 and B-1 with A-3 and B-3). However, Subjects B and E then exhibited increased inconsistency in the five orbits farthest from the target (e.g., see B-8). A 1% level multiple F_{max} ratio test (ref. 15) revealed that the increase in variance was statistically significant for Subject B (F_{max} (7, 5) = 67.92), but not for Subject E (F_{max} (5, 5) = 8.59).

If a subject's intra-orbit inconsistency is relatively small, one may then meaningfully compare the shape of his switching locus with the optimal locus. All four subjects achieved roughly monotonic switching loci with the root mean square difference between intra-orbit medians less than 200 msec (e.g., A-3, and B-3). However, the large intra-orbit variance exhibited by Subjects B and E late in practice was judged too large to warrant any more detailed analysis of the shapes of their switching loci. Further analyses were only conducted for Subjects A and C. Comparisons of the switching times on Days 2 and 3 with Days 7 and 8 revealed that by Days 7 and 8 both Subjects A and C switched significantly earlier on the outer orbits (1-5) and significantly later on the inner orbits (6-10). To test whether the shapes of the switching loci for Subjects A and C were non-monotonic in the phase
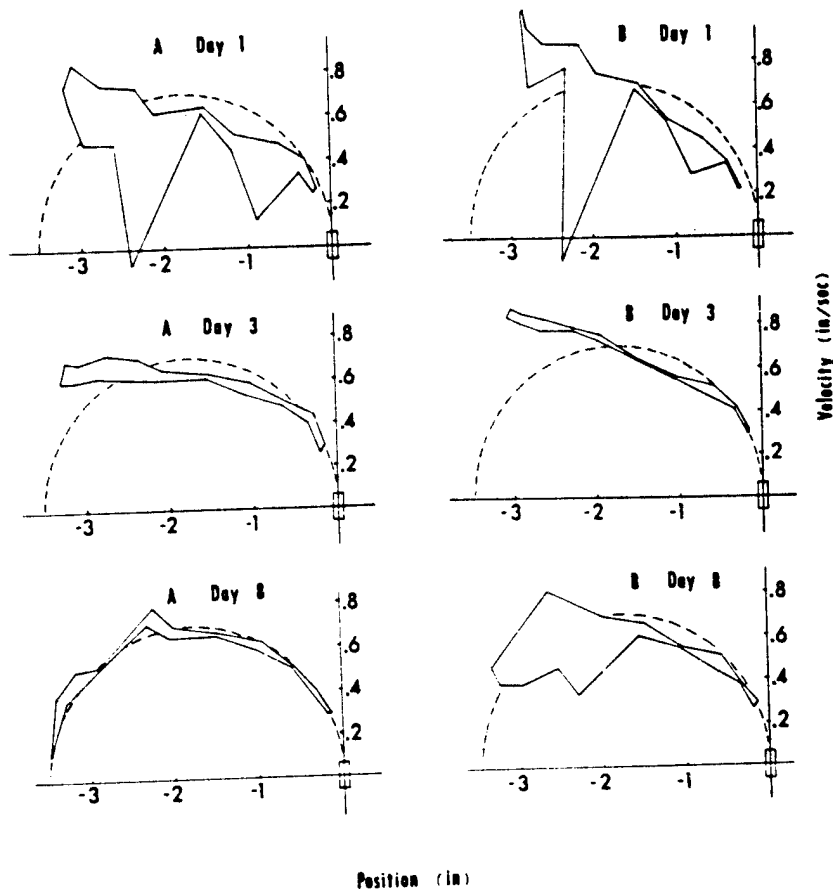
388

Figure 3. Median first switches in Experiment 1 for Subjects A and B.

plane, the switching velocity at the two middle orbits (5 and 6) was compared with the switching velocity at the outermost orbits (1 and 2) and at the innermost orbits (9 and 10). On Days 2 and 3, these two subjects had not achieved a non-monotonic switching pattern in that the switching velocity for the two outermost orbits was not significantly less than the switching velocity in the middle orbits. However, by Days 7 and 8 Subjects A and C did have a significantly lower switching velocity in the two outermost orbits.

One final measure of how closely these two subjects approximated optimal performance is the root mean square deviation from the dashed semi-circular locus shown in figure 2. This statistic equalled 114 msec for

Subject A and 160 msec for Subject C on Days 7 and 8, and both differences were significant at the .05 level.

Discussion

In order to interpret the manner in which the subjects' switching patterns changed over the 8 days of this experiment, it is useful to ask, "What must the subjects learn about the system in order to approximate the optimal control solution?" By trial and error subjects could arrive at a set of paired associations between the 20 initial conditions and the 20 corresponding switching points necessary to stop at the target without under-shooting or overshooting. Each of the initial conditions is uniquely speci-fied by a combination of position and velocity cues, and the switching points could be specified in terms of position, velocity, and/or elapsed time cues. As suggested by Preyss and Meiry (ref. 8), overshooting the target would cause the subjects to revise the switching point for a given initial condi-tion to occur sooner, and undershooting would result in a similar revision in the opposite direction, assuming that subjects are attempting to stop in the target region with a single switch. According to this model of learning behavior, one might expect an initially random-looking phase plane switching pattern to converge in a relatively uniform manner toward the optimal control solution. This simple model seems inadequate because of the extremely slow and non-uniform manner in which subjects did approach the optimal control solution after a more rapid initial convergence toward a monotonic switching pattern. The monotonic switching loci suggest that subjects are relying on control patterns that are appropriate for stopping a freely moving vehicle, but inappropriate for a pendulum-like system. More specifically, one typical property of braking systems for moving vehicles is that if one is traveling on a smooth level surface, stopping distance is an increasing function of the vehicle's velocity, but does not depend on its location. This property does not hold for the harmonic oscillator. As indicated in equation ' when the leftward force is applied to the system, the net braking force is an additive combination of the constant leftward force and the system's pendulum-like tendency to move rightward toward its natural equilibrium at the center of the target.

Assuming an initial bias toward characterizing the task as an ordinary vehicular braking task, one might expect the subjects' transition to a more veridical characterization of the system's dynamic properties to cover three stages of learning. In Stage 1 early in practice subjects assume that the braking force is not a function of position, and their switching velocity increases with distance from the target. Such behavior would be analogous to the manner in which car drivers traveling at higher velocities typically be-gin to apply the brakes farther from the intersection in order to stop in time. In Stage 2, subjects begin to realize that the braking force decreases with distance from the target and begin to apply the leftward force at correspondingly lower velocities. A switching pattern in which switching velocity continually increases with distance from the target is also con-sistent with this stage. If the subjects believe that the braking force actually decreases to zero for longer distances from the target. then they

390

should adjust their switching patterns so that the switching velocity becomes a constant for distances farthest from the target. Subjects cannot be in Stage 1 if they exhibit this switching pattern (e.g., figure 3, A-3), which represents the maximum downward adjustment possible in Stage 2. In Stage 3, subjects not only realize that the braking force decreases with distance from the target, but also realize that for longer distances from the target the system accelerates even though the leftward force is applied. This increasing acceleration with distance from the target requires the subjects to curve their phase plane switching patterns downward.

Within each of these three stages it is plausible that subjects might adjust their switching loci in accordance with the simple learning model previously mentioned. The stages place different limitations on how far such adjustment can proceed. Unless subjects reach Stage 3, they cannot produce a nonmonotonic switching locus. According to this interpretation, the slowness of subjects to approach the optimal control pattern can be attributed to their difficulty in making the two qualitative transitions to Stages 2 and 3. Subjects A and C showed clear evidence of reaching Stage 3 (e.g., figure 3, A-8). Whether Subjects B and E also reached Stage 3 is uncertain. Statistical tests of monotonicity were not performed for these latter two subjects due to the large intra-orbit variance they exhibited. The increase in intra-orbit variance shown by Subject B is still unexplained in this model.

The three stage theory just outlined deals with qualitative aspects of the phase plane switching patterns, namely their monotonicity. Further interpretation is possible if one assumes that subjects have non-veridical internal representations of the pendulum-like system, and that at any point in time subjects are attempting to behave optimally with respect to those non-veridical models. Assuming that subjects try to reach the origin without overshooting or undershooting, the pattern of switches must all lie on what the subjects believe to be a single trajectory to the target. One may therefore interpret the phase plane switching loci as trajectories of the subjects' internal models. An additional, but not very restrictive assumption is that the subjects' internal models do have unique trajectories that reach the origin when a constant force is applied. Under this interpretation the phase plane loci can be used to generate analytic representations of the subjects' internal models (R.A. Miller, personal communication). The detailed calculations and the problems of uniqueness of these analytic representations will not be pursued in the present paper.

EXPERIMENT 2

The second experiment extended the range of initial conditions so that on some trials it was necessary to use two switches in order to stop the system in the target area (see the outer lobe in figure 1). One aim of this experimental manipulation was to investigate how closely the subjects' first switch patterns would approximate the double lobe pattern of optimal performance for a point target. A second aim was to seek evidence for schemata by testing whether the observed switching patterns would transfer to new initial

positions and velocities. If subjects simply learn a set of paired associations between the initial conditions and corresponding switching points, then they should not be able to perform this transfer task.

Method

The same four subjects used in Experiment 1 received 8 days of practice with the 20 initial conditions represented as black dots in figure 4. The
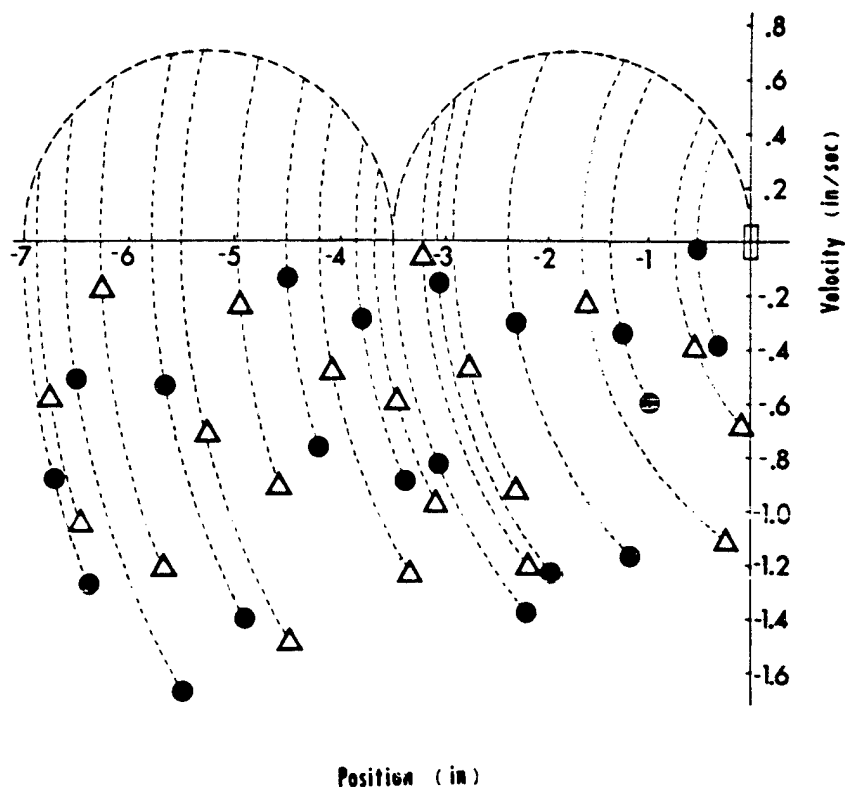

Figure 4. Well-practiced initial positions and velocities (●) and new initial positions and velocities (△) for the transfer test in Experiment 2.

10 initial conditions requiring only a single switch were identical to 10 of the initial conditions used in Experiment 1. Subjects were instructed that the range of starting positions would be extended, but that otherwise the system would be the same. Following Day 8 there were scheduling delays of 56, 54 and 11 days for Subjects A, B and C respectively. Each of these three subjects was therefore given 1 extra day of practice upon his return to the

experiment. All four subjects were then given 1 day of performance with the well-practiced initial conditions, 1 day of performance with 20 new initial conditions which are represented as triangles in figure 4, and a final day of performance with the well-practiced initial conditions. Subjects were not told that there had been any procedural change on the day with the new initial conditions.

Results

The median switch point was calculated for each initial condition as in the previous experiment. The means of each intra-orbit pair of medians have been connected with straight lines in figure 5 for the day with the new initial conditions (————————) and for the preceding (———————) and following (—··—···..) days using the well-practiced initial conditions.

To assure the subjects' performance on the new initial conditions cannot be attributed to previous practice on these very orbits, it was necessary to ascertain that second and third switches in Experiments 1 and 2 did not occur along these "new" orbits. Available records indicated that such switches were rare in the region of the outermost eight new orbits, and subsequent analysis was restricted to this region.

For each subject an F test was performed at the .05 level to determine whether there was a significant increase in intra-orbit variance with the new initial conditions. None of the F tests was significant. In order to test whether the switching pattern for the new initial conditions differed from the patterns on the preceding and following days, a polynomial was fit via multiple regression to the median switching points with the new initial conditions and a second polynomial was fit to the data for the preceding and following days. An F test was then performed to compare the sum of the residuals from these two polynomials with the residual when the data from all 3 days were fit by a single polynomial of the same degree. Only the reduction in residual for Subject B, F (2, 40) = 4.17, p < .05, was significant at the .05 level.

Two types of analyses were similarly conducted to test whether the performance of Subjects A, C and E with the new initial conditions differed from their performance on the outer seven orbits on the first 2 days of Experiment 2. First, an F test was performed for each subject at the .05 level to test whether the intra-orbit variance was larger at the beginning of Experiment 2. Subject C, F (14, 8) = 2.29, p < .001, did exhibit significantly larger intra-orbit variance at the beginning of Experiment 2; however, Subjects A and E did not. Polynomial regression analyses revealed that the shape of Subject A's switching pattern early in Experiment 2 was significantly different from the pattern for the new initial conditions; however, Subject E did not exhibit any significant difference.
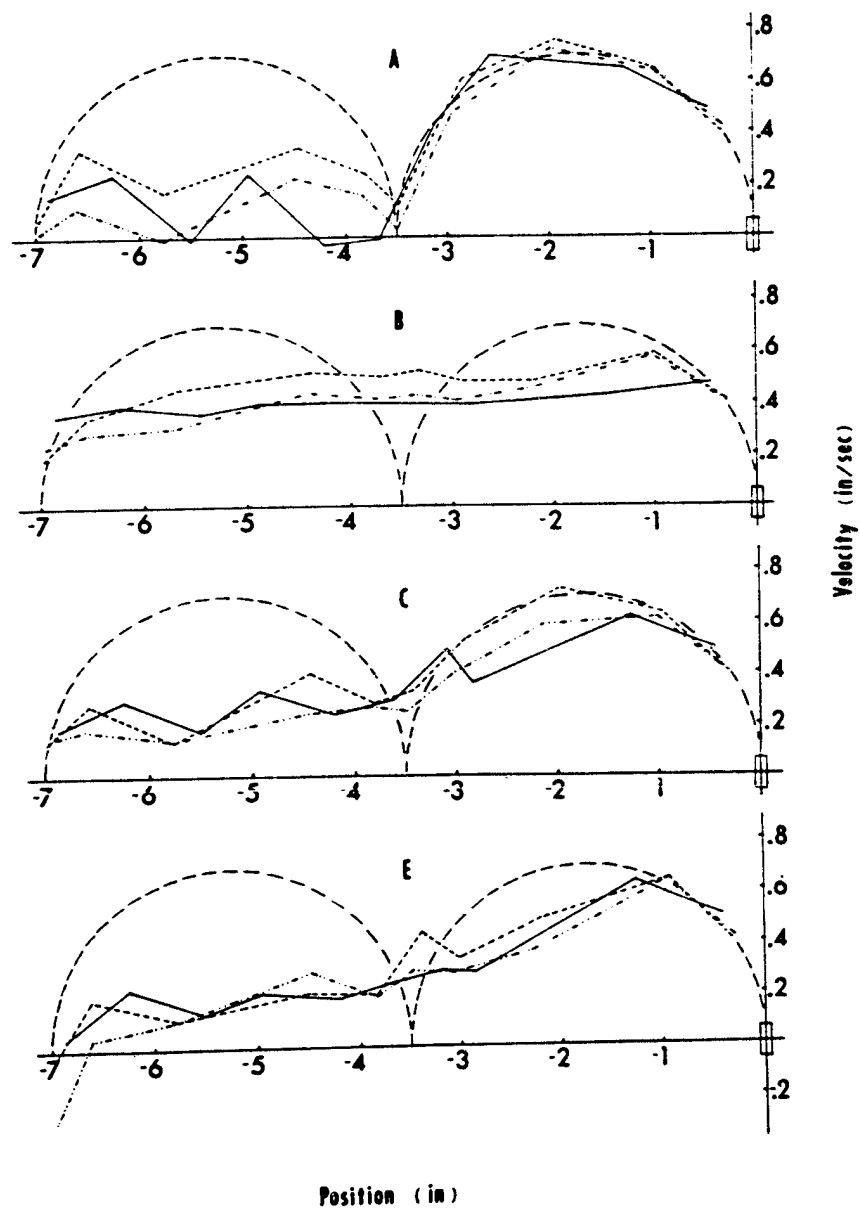
Figure 5. Means of median first switches for Subjects A, B, C, and E in Experiment 2 for well-practiced initial conditions (- - - and -·····) and new initial conditions (————).

Discussion

That none of the four subjects' switching loci resembled the double lobe optimal solution is perhaps not very surprising if one considers the difficulty involved in discovering such a solution by trial and error. The inner optimal lobe is part of a trajectory of the system through the phase plane, and subjects could have approached the optimal solution in this region by adjusting their switching points so as to eliminate undershoot or overshoot of the target. In contrast, the outer optimal lobe is not part of a trajectory, and subjects will overshoot the target for trials starting in this region of the phase plane no matter when their first switch occurs. The outer optimal lobe is not even the switching locus that minimizes overshoot of the target. A second reason for difficulty is that the total time to reach the target is not very sensitive to deviations from the outer optimal lobe. Engineers implementing automated switching devices typically take advantage of this fact by substituting a zero velocity switching locus in place of the outer optimal lobe. Such a locus is easier to construct and does not increase the total time to reach the target by more than 5% (ref. 16). In the present experiment it would probably be difficult for subjects to detect a 5% difference between optimal and sub-optimal loci because of variation in their second switch performance.

Within the accuracy of experimental measurement, Subjects A, C and E exhibited the same switching pattern for the new initial conditions as for the well-practiced initial conditions. Secondly, for Subjects A and C this pattern was significantly different from the switching pattern exhibited at the beginning of Experiment 2. Finally, records of previous performance indicate that these two subjects had negligible practice along the new orbits prior to the transfer task. Together these statements constitute evidence for the existence of schemata underlying the performance of Subjects A and C. While Subject E did show excellent transfer to the new initial conditions, this subject did not exhibit a significant change in switching pattern with practice. Therefore, this subject's performance does not constitute evidence for a schema. Subject B's performance also does not meet the strict criterion previously specified for the existence of a schema.

In order to further delineate the nature of the schemata implied by the performance of Subjects A and C, it is necessary to discuss alternative process models for behavior in this experiment. In the present task, the detailed time course of the button pressing responses was not measured; however, a simple, unvarying movement pattern would be sufficient to perform well. The concepts of motor recall schema and motor recognition schema, which respectively involve production and recognition of new movements, therefore need not be invoked for these experiments. What is necessary is that subjects know when to execute the button pressing response as the harmonic oscillator passes through states not previously observed. Stimulus recognition schema is an appropriate concept for describing this skill.

A more detailed question concerns what aspect of the subjects' performance is encoded in the recognition schema. Does the schema encode states of the oscillator system at which the subject should initiate the button pressing response, or does the schema encode states of the oscillator system at which

the actual depression of the switch should be completed? If the button pressing response could be executed instantaneously, this distinction would be meaningless. However, assuming at least a 200 msec reaction time in the subjects' execution of such a response, the distinction is important for this task. Unfortunately, the data in the present experiment do not distinguish between these two possibilities. These data do imply that subjects have learned a skill which is not specific either to the positions and velocities at the beginnings of trials or to particular orbits. However, subjects could perform the transfer task if they had learned a generalized locus of system states for either response initiation or for completing the switch depression. The basic difference between these two kinds of recognition schema is that the latter assumes subjects can predict when the system is one reaction time away from the switch completion locus. To distinguish between the two possible kinds of schemata, it is necessary to use a transfer task that necessitates the prediction capability postulated by the response completion schema. Such a test is provided by using a speeded simulation of the harmonic oscillator system.

EXPERIMENT 3

In order for subjects to achieve perfect transfer of a switching pattern with a speeded simulation of the oscillator system, three conditions must obtain. First, they must encode the switch completion locus rather than the switch initiation locus. Because the simulation is speeded, the oscillatory system will move through a larger fraction of its phase plane orbit during the subjects' reaction time. The locus of response initiation necessary to achieve the same switching locus will therefore be pushed farther back from the switch completion locus. Ability to make this necessary compensation is evidence for the use of a response completion locus. Secondly, subjects must be able to time scale their representation of the response completion locus if they use time or velocity cues to encode this locus. For example, assume subjects encode the locus at the accustomed speed as F_c ($\underline{t}$, $\underline{x}$, $\underline{v}$), where $\underline{t}$ is elapsed time, $\underline{x}$ is system position, and $\underline{v}$ is system velocity. If the speeded simulation is twice as fast as the accustomed speed, the subjects' new locus should be F_c ($\frac{1}{2}\underline{t}$, $\underline{x}$, $2\underline{v}$). Elapsed time cues must be halved, position cues need not be changed, and velocity cues must be doubled, because the speeded simulation covers the same distances as before with twice the velocity and in half the elapsed time. Thirdly, subjects' ability to predict when the system is one reaction time away from F_c must be of such quality as not to deteriorate significantly in its predictive accuracy when applied over a relatively longer fraction of the phase plane orbit. For example, a simple constant velocity extrapolation of the system's motion might provide adequate predictive accuracy when the simulation is slow, because the fraction of the phase plane orbit covered in one reaction time is small, and the system undergoes relatively little acceleration over the prediction interval. This approximation may break down, however, with a speeded simulation. In summary, perfect transfer with a speeded simulation will be evidence that all three of these necessary conditions obtain. Less than perfect transfer will be evidence that at least one of these conditions does not obtain.

At a more general level of description, this experiment also provides a further test of the subjects' ability to transfer to a new situation.

Perfect transfer would provide additional support for stimulus recognition schemata.

Method

The same four subjects used in the first two experiments were given 1 day of practice with the initial conditions used in Experiment 1. Subjects were then given another day at the accustomed speed, 2 days with the simulation running twice as fast as usual, and a final day at the accustomed speed. On the first day with the fast simulation, subjects were told that the system had been speeded up, but that nothing else was changed.

Results

The first switch data for the day immediately preceding and the day immediately following the speeded simulation were analyzed to determine how closely subjects approached the optimal switching locus. To test for a non-monotonic switching pattern, the average switching velocity in the middle two orbits (5 and 6) was compared with the average switching velocity in the innermost and outermost pairs of orbits. Subjects A, C and E all exhibited a non-monotonic pattern. However, for Subject B the switching velocities for the middle and outermost orbits were not significantly different (figure 6).
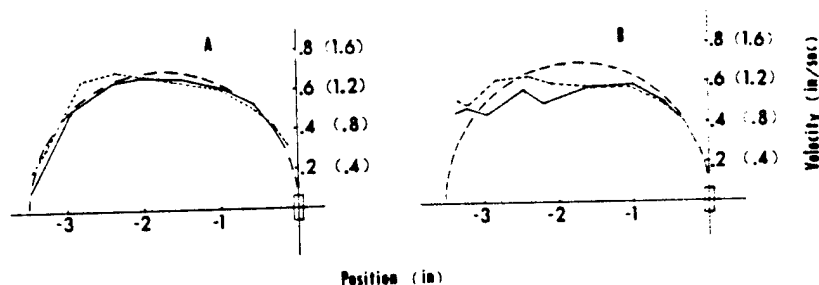

Figure 6. Means of median first switches for Subjects A and B in Experiment 3 with the speeded simulation (----) and the simulation at the accustomed speed (————). The ordinate values in parentheses refer to performance with the speeded simulation.

A second analysis compared the first switch data on the two speeded simulation days with the immediately preceding and the immediately following day at regular speed. In order to facilitate comparison, switching times on the two speeded days were all multiplied by a factor of 2 for the following analyses. F tests were conducted for each subject to determine whether

intra-orbit variance on the five outer orbits (1-5) and the five inner orbits (6-10) increased with the speeded system. For the outer orbits, Subject E exhibited a large increase in intra-orbit variance, F (10,10) = 9.10, p <.001, and Subject C exhibited a smaller increase, F (10,10) = 2.97, that approached significance at the .05 level. No other statistically significant increases were detected.

In order to test whether a change in the shape of the switching locus had occurred with the speeded system, separate analyses of variance were performed on the outer five and inner five orbits for Subjects A, B and C, but only for the inner orbits for Subject E, because of the large increase in variance he exhibited on the outer orbits on the speeded days. As shown in

Table 1

Mean Differences Between Non-speeded and 2 x Speeded

Switching Times in Experiment 3

Subjects	Outer orbits (1-5) (msec)		Inner orbits (6-10) (msec)	
	Obtained difference	Difference necessary for significance, p <.05	Obtained difference	Diff. necessary for significance p < .05
A	106*	±86	-6	±60
B	119*	±107	-15	±25
C	77*	±55	4.	±57
E	--	--	21	±115

*p < .05

Table 1, Subjects A, B and C all switched significantly later in the outer orbits with the speeded simulation. None of the four subjects exhibited a significant difference in the inner orbits. In order to indicate the sensitivity of these contrasts, the mean differences between speeded and non-speeded switching times necessary to achieve statistical significance at the .05 level have been listed in Table 1. The power of the contrasts for detecting differences as large as these is about .56; the power for detecting differences twice as large is about .97.

Given that subjects did show excellent transfer for the inner orbits, it becomes important to test whether this switching pattern was learned over the course of the experiment. Accordingly, F tests were conducted to test

whether the intra-orbit variance on the 2 days with the speeded system was significantly less than intra-orbit variance on the first 2 days of Experiment 1 for these five orbits. Subjects A, F (10,10) = 26.35, p < .001, Subject C, F (10,10) = 6.65, p < .01, and Subject E, F (10,10) = 12.15, p < .001, all exhibited significantly higher intra-orbit variance on Days 1 and 2 of Experiment 1. Only Subject B, did not exhibit a significantly higher variance and this subject also exhibited no significant change in his mean switching times with practice.

Discussion

Subjects A, C and E all exhibited non-monotonic phase plane loci; however Subject B did not. In terms of the three stage model described in Experiment 1, Subjects A, C and E reached Stage 3, but Subject B only reached Stage 2. In other words, in adjusting his switching locus Subject B still did not take into account the system's increasing acceleration for orbits farthest from the target. This subject's failure to converge on the optimal solution after such prolonged practice lends further credence to the three stage model as a necessary elaboration of the simple learning model.

The perfect transfer exhibited by Subjects A, C and E in the inner orbits constitutes evidence for the existence of schemata. The transfer was to a new situation not previously practiced; within the limits of experimental measurement the pattern was identical to the pattern exhibited on the immediately preceding and following days at the usual speed; and the pattern of behavior was different from the behavior exhibited by the subjects at the very beginning of practice in Experiment 1. These results imply that over the course of the experiments Subjects A, C and E learned a general response generating strategy, which may be called a schema. Although one cannot conclude that Subject B learned his switching pattern in the inner orbits over the course of these experiments, his transfer behavior did exhibit the same general pattern as Subjects A and C. In the following discussion of possible underlying process models the construct r_c should therefore be called a response completion locus rather than schema for Subject B. However, for ease in exposition, this point will not be constantly reiterated.

The perfect transfer exhibited in the inner five orbits is consistent with the assumptions that subjects used a stimulus recognition schema for switch completion, that they were able to time scale this locus if it involved time and velocity cues, and that their ability to extrapolate the system's motion pattern was relatively accurate. If subjects used a response initiation schema and appropriately time scaled any time and velocity cues, the measured switching locus with the speeded simulation would be shifted upward by one-half the duration of the subjects' reaction time. Assuming a reaction time of at least 200 msec, the shift would amount to at least 100 msec in real time, and at least 200 msec on the doubled time scale used for comparing the two simulations. In fact, no statistically significant shift was observed in the inner orbits, and the power for detecting a 200 msec shift was approximately .94 for Subject E and considerably greater than .99 for Subjects A, B and C.

The hypothesis that subjects used a response initiation schema must therefore be rejected unless one additionally assumes that subjects used velocity cues and failed to time scale them sufficiently. Failure to time scale would lead to initiating the response at a lower velocity and would move the measured switching locus downward in the phase plane, reducing the prediction of a full 200 msec shift. A similar explanation would also need to be invoked to account for the considerably less than 200 msec shift observed in the outer five orbits for Subjects A, B and C. The large increase in intra-orbit variance in the outer orbits for Subject E does not fit this description, and suggests that the decision of when to switch is based on different information for the two initial conditions within each orbit. In this regard Subject E's behavior appears to differ in a more fundamental manner from normative switching behavior than the performance of the other three subjects and will not be included in the discussion that follows.

While it is not possible to rigorously rule out the above response initiation schema hypothesis on the basis of the present data, the assertion of nearly equal, but opposite effects to account for the excellent transfer in the inner orbits is not very plausible. A second explanation of the data for Subjects A, B and C is that they did use a response completion schema, but failed to sufficiently time scale the locus in the region of the outer five orbits. Failure to time scale elapsed time cues by a factor of one-half would result in subjects' switching at too long an elapsed time, and hence the observed switching locus for the speeded system would be shifted upward. The excellent transfer in the inner orbits would then be attributed to the subjects' using position and/or velocity cues to specify the switching locus in that region of the phase plane.

In evaluating the plausibility of this explanation it is important to note that subjects must estimate elapsed time relative to some easily identified starting point. The only two likely starting points in the present task are the beginning of the trial and the point at which the system reverses direction from left to right. The beginning of the trial cannot be the starting point, or subjects would not have been able to exhibit the excellent transfer observed in Experiment 2. The point at which the system reverses direction is also implausible. Subjects having to wait for this event before starting their prediction process could not exhibit switching times less than one reaction time after the system reversed direction. However, for the orbits farthest from the target Subjects A and C exhibited switching times less than 200 msec. Without a likely starting point for estimating elapsed time, this second explanation also appears implausible.

A third explanation of the upward shift for Subjects A, B and C is that in using a response completion schema their ability to predict the motion of the system over the duration of one reaction time was relatively accurate for the inner orbits, but not for the outer orbits. In the outer orbits, the motion of the system more nearly approximated a constant acceleration in the period immediately prior to the observed switching loci. Rosenbaum (ref. 17) has reported correlational data indicating subjects can extrapolate constantly accelerated motion to a fixed reference point with considerable accuracy. There are, however, a number of other studies in which subjects have had

400

considerable difficulty in extrapolating accelerated motion in manual tracking tasks (refs. 18, 19, 20) and in predicting collision with a second object moving at constant velocity (ref. 21). In these latter experiments, subjects tended to underestimate or ignore the increase in velocity of an accelerated motion. In the present experiment, this kind of bias would lead to subjects initiating their switching response too late and overshooting the desired switching locus in agreement with the observed data. This bias would have much less effect in the inner orbits because of the lower level of acceleration in these orbits.

While it is not possible to rigorously exclude any of the above three explanations on the basis of the present data, the third explanation does lend itself as the most plausible alternative both because of its agreement with previous studies showing difficulty in extrapolating accelerated motion and because this explanation does not have to postulate any different kind of information processing for the inner and outer orbits. One special case of a process model fitting this third explanation is a model used by Miller (ref. 9). He assumed that subjects specify the switch completion locus in terms of position cues and use a constant velocity extrapolation of the system's motion over a 200 msec reaction time. For each of the four subjects in the present experiment, this model predicts an upward shift of the speeded switching locus on the inner five orbits of approximately 50 msec on the doubled time scale used to compare performance on the two simulations. The probability of failing to reject the null hypothesis for at least one of the four subjects given a true shift of this magnitude is approximately .005, which suggests that this model should be rejected. The probability value is so low primarily due to the data of Subject B.

A model assuming constant acceleration extrapolation predicts shifts of less than 6 msec on the doubled time scale for both the inner and outer orbits, even with an assumed reaction time as long as 350 msec. This model can also be rejected by the present data. One cannot, however, reject the possibility that subjects made some, though insufficient, use of acceleration information. This latter kind of model can approximate the present data more accurately than Miller's model by assuming some usage of acceleration extrapolation and a reaction time longer than 200 msec.

CONCLUDING REMARKS

One aspect of these experiments was to compare subjects' switching patterns with optimal switching behavior. The optimal control theory solution to stopping the harmonic oscillator was not used in a direct way to generate a process model for the human controller as has been done by Kleinman, Baron, and Levison (ref. 22) for tasks involving continuous correction of random disturbances. Rather, the optimal control solution was used as a reference for examining qualitative aspects of the subjects' performance such as intra-orbit switching variance and the monotonicity of the switching locus. The Kleinman, Baron, and Levison model assumes that the human controller has a veridical representation of the system he is attempting to control, and when necessary the criterion function that the subject is assumed to be optimizing

is adjusted away from nominal values in order to match the model to subjects' behavior. In the present experiments it has been assumed that subjects are always attempting to minimize time, and that deviations from optimal performance can be attributed to a non-veridical characterization of the pendulum-like system. The plausibility of this interpretation would be enhanced if incorporating evidence for non-veridical internal models into the more detailed process models of continuous tracking behavior led to superior prediction of subjects' performance in those tasks.

According to the three stage learning model described in Experiment 1, the subjects' difficulty in approaching the optimal control solution is attributable to their not taking into account the system's tendency to accelerate toward its natural equilibrium position at the center of the target. However, even after Subjects A and C overcame this difficulty, their lack of perfect transfer on the outer orbits with the speeded simulation has been attributed to insufficient use of acceleration cues in predicting the system's motion over the duration of their reaction times. These results are not surprising in that only ordinal knowledge of the increasing acceleration of the system with distance from the target is necessary to permit subjects to curve their switching loci downward. In contrast, more than ordinal knowledge of acceleration is necessary for appropriate short-term prediction of the system's motion to permit perfect transfer with the speeded simulation. The data for Subject B are surprising, however, because this subject showed the most evidence of using acceleration information for short-term prediction in the inner orbits, but did not take the system's acceleration into account in the shape of his switching locus.

Another aspect of these experiments was their support for the existence of schemata. Subjects' ability to exhibit the same switching locus with new initial conditions not previously encountered and with the speeded simulation are evidence that a generalized skill was learned. The three different types of transfer tasks used in these experiments occurred at different points in practice and tested different segments of the overall first switch pattern. By combining some of these transfer tests, future research may begin to ask more specific questions about developmental aspects of the skill involved in controlling a dynamic system.

In their schema theories of motor skills, both Pew (ref. 23) and Schmidt (ref. 11) have treated the conditions of the external environment and the performer's musculature as inputs which determine the choice of an appropriate motor response. However, the converse relationship is also quite plausible for many skills -- namely, that the range of possible reponses determines the performer's choice of internal and external environmental conditions for beginning a response. In the present experiments it has been assumed that subjects had only a single possible motor response, a stereotyped button press, and the choice of external environmental conditions for response initiation was therefore the only choice available to them. In more complex skills involving a variety of possible responses, both kinds of choices are probably involved. For example, the skilled tennis player described by Bartlett (ref. 24) may possess the versatility to begin his stroke over an entire range of possible conditions of the ball, the racket, and his muscula-

ture and be capable of altering the form of his stroke accordingly. However, to at least some extent, he has the ability to choose the internal and external environmental conditions for his stroke by appropriately positioning himself and waiting for a particular point in the ball's trajectory. The form of the stroke he wishes to execute will determine his choice of environmental conditions, as well as vice versa. The conception of a motor recall schema as emphasized by motor theorists is appropriate for describing a generalized ability to choose the form of the response given the environmental conditions. The conception of stimulus recognition schema as emphasized in the present experiments is appropriate for describing a generalized ability to choose the environmental conditions given the desired form of the response. An issue that any general theory of skilled performance must ultimately address is how these two aspects of choice are related in situations where neither the form of the response nor the environmental conditions are fixed.

REFERENCES

1. Ray, H. W.: The application of dynamic programming to the study of multistage decision processes in the individual. Unpublished Doctoral Dissertation, The Ohio State University, 1963.

2. Rapoport, A.: A study of human control in a stochastic multistage decision task. Behavioral Science, 1966, 11, 18-32.

3. Rapoport, A.: A study of a multistage decision making task with an unknown duration. Human Factors, 1966, 8, 54-61.

4. Rapoport, A.: Dynamic programming models for multistage decision-making tasks. Journal of Mathematical Psychology, 1967, 4, 48-71.

5. Pew, R. W.: A model of human controller performance in a relay control system. Proceedings of the Fifth National Symposium on Human Factors in Electronics, San Diego, California, May, 1964, 241-251.

6. Pew, R. W.: Performance of human operators in a three-state relay control system with velocity-augmented displays. IEEE Transactions on Human Factors in Electronics, 1966, HFE-7, 77-83.

7. Pew, R. W.: Acquisition of hierarchical control over the temporal organization of a skill. Journal of Experimental Psychology, 1966, 71, 764-771.

8. Preyss, A. E., and Meiry, J. L.: Stochastic modeling of human learning behavior. IEEE Transactions on Man-Machine Systems, 1968, MMS-9, 36-46.

9. Miller, D. C.: Behavioral sources of suboptimal human performance in discrete control tasks. Massachusetts Institute of Technology, Engineering Projects Laboratory Technical Report, No. DSR 70283-9, January, 1969.

10. Adams, J. A.: Issues for a closed-loop theory of motor learning. In G. E. Stelmach (Ed.), Motor control: Issues and trends. New York: Academic Press, 1976.

11. Schmidt, R. A.: A schema theory of discrete motor skill learning. Psychological Review, 1975, 82, 225-260.

12. Attneave, F.: Transfer of experience with a class-schema to identification-learning of patterns and shapes. Journal of Experimental Psychology, 1957, 54, 81-88.

13. Posner, M. I., and Keele, S. W.: On the genesis of abstract ideas. Journal of Experimental Psychology, 1968, 77, 353-363.

14. Athans, M., and Falb, P. L.: Optimal control. New York: McGraw-Hill, 1966.

15. David, H. A.: The ranking of variances in normal populations. Journal of the American Statistical Association, 1956, 51, 621-626.

16. Knudsen, H.: Maximum effort control for an oscillatory element. Unpublished M.S. Thesis, University of California, Berkeley, 1960. As cited in M. Athans & P. L. Falb, Optimal control. New York: McGraw-Hill, 1966, 587.

17. Rosenbaum, D. A.: Perception and extrapolation of velocity and acceleration. Journal of Experimental Psychology: Human Perception and Performance, 1975, 1, 395-403.

18. Gottsdanker, R. M.: The accuracy of prediction motion. Journal of Experimental Psychology, 1952, 43, 26-36.

19. Gottsdanker, R. M.: Prediction-motion with and without vision. American Journal of Psychology, 1952, 65, 533-543.

20. Gottsdanker, R. M.: A further study of prediction-motion. American Journal of Psychology, 1955, 68, 432-437.

21. Runeson, S.: Visual prediction of collision with natural and nonnatural motion functions. Perception and Psychophysics, 1975, 18, 261-266.

22. Kleinman, D. L., Baron, S., and Levison, W. H.: A control theoretic approach to manned-vehicle systems analysis. IEEE Transactions on Automatic Control, 1971, AC-16, 824-832.

23. Pew, R. W.: Human perceptual motor performance. In B. Kantowitz (Ed.), *Human information processing: Tutorials in performance and cognition*. New Jersey: Lawrence Erlbaum, 1974, 1-39.

24. Bartlett, F. C.: *Remembering*. Cambridge, England: University Press, 1932.

405

CONTINUOUS COMPENSATORY AUDIO MANUAL TRACKING

Richard Gray Costello

The Cooper Union For The Advancement Of Science And Art
Electrical Engineering Department
Cooper Square
New York, N.Y. 10003

SUMMARY

For the purpose of this investigation, continuous compensatory audio manual tracking is defined as the set of circumstances under which a human operator manipulates a manual control in response to a continuous audio input or command signal; and attempts to null out any changes in the audio command by generating appropriate manual responses.

The investigation was prompted by several recreational glider pilots, who commonly employ a device called an audio variometer to adjust their flight path. The audio variometer is a sensitive differentiating altimeter, which produces an audio output proportional to the glider's rate of climb (or rate of sink, as the case may be). If the glider is climbing, the pitch of the audio tone output climbs, if the glider is falling, the audio pitch falls. The glider pilot is thus able to adjust his control tactics in response to the audio tone output, and use his eyes for enjoying the scenery.

An analog computer, a voltage controlled oscillator, and a side arm controller were employed to simulate a single axis continuous compensatory audio manual trucking task. A student built digital interface sampled four channels of real time simulation data, for later analysis by a dedicated NOVA 1200 mini computer.

The rather limited results indicated a corner frequency for this task in the region of 1/10 hz., well below the corner frequency for visual manual tracking tasks. It was observed that those subjects who had had some musical training produced consistently better audio-manual tracking results, when compared to subjects who had had no musical training.

INTRODUCTION

Intermittent control of a human operator system, utilizing an audio feedback link, has been with mankind for a surprising long period of time. An eighteenth century helmsman piloting a sailing vessel through fog used his ears to select a course in response to bells, foghorns, and perhaps the sound of breaking waves. A mule skinner, backing his rig, with its team of twenty mules into a borax loading station, responded to yelled audio commands. Under such circumstances, where both decision and system time constants easily exceeded one second, audio control worked and still works admirably.

406

In more recent times, intermittent audio control is used in an expanding variety of applications. Audio warning systems, which call for one or more human operator actions in response to a bell, whistle, woop, or siren, are seen everywhere - from the controversial atomic reactor scramming controls to the surly sounding automobile ignition on buzzer. Recently, electronically generated voice commands have been investigated and then applied as a possibly improved audio feedback control link. Simpson and Williams (6) investigated such an audio control link in the context of aircraft collision avoidance; specifically they discussed the ground proximity warning system which is now being installed in commercial airlines, and which electronically yells "Whoop, Whoop - Pull up! Pull up!" Here again, a discrete action or set of actions is required in response to the audio signal, and the audio systems appear to work admirably.

Vinje, who wrote his Ph.D. thesis on audio compensatory tracking, has written several papers dealing with aural compensatory tracking. His 1972 paper, co-authored with Pitkin (9), enumerates several early investigations of a pilot's ability to control an aircraft in response to audio control signals; including DeFlorez's (1) 1936 paper dealing with "True blind flight", Forbes et al.'s (2) 1957 description of the "Flybar" experiments, (Flybar = Flying by auditory reference), and Katz, et al.'s (3) 1966 paper concerning "***Acoustic displays***" in a simulated aerospace vehicle".

Conversely, when continuous manual responses are required of an operator in response to an audio control input, the quality of system performance reported in the literature is somewhat vague. A small to fair amount of experimental work can be found in the literature, primarily dealing with flying an airplane blind under instrument flight rules (IFR), with a primary flight display instrument, such as a pitch, roll, or yaw display replaced by some sort of audio whistle, chirp, buzz or other continuously variable aural display.

1972 was a good year for audio manual tracking papers. Mirchandani (4) discussed, "An Auditory Display in a Dual-Axis Tracking Task", based upon his MIT Master's thesis of 1971. Mirchandani suggested that "supplementary auditory displays in existing systems, such as, in airplanes (especially helicoptors and VTOL) *** could improve the performance of the operators and make the systems more efficient". Vinje wrote his second paper of 1972 (8) on audio displays for IFR Hover Control, and presented the results at almost the exact same time that Mirchandani suggested the application.

Vinje concluded that, "*** pilots could control an aurally displayed function and another visually displayed function better that if the two functions were both presented visually and separately displayed".

That is, Vinje concluded that audio tracking could be superior to visual tracking, when more than one display had to be simultaneously tracked.

This is directly opposed to the conclusion reached three years later,

407

in 1975, by Uhlemann and Geiser (7), when they reported on "Multivariable Manual Control with Simultaneous Visual and Auditory Presentation of Information". Uhlemann and Geiser specifically state that "*** visual displays are indispensable". Furthermore, if visual displays are widely separated, by, say 70 degrees of arc, so that the pilot must turn his head to watch various displays, then, in this case, auditory support of the visual display can help - but - "the auditory support should be attached to the least important control system". This is exactly opposite to Vinje's 1972 conclusion, that "An audio display was most effective when it presented a signal which was important to the pilot, e.g., a nonredundant signal which changed rapidly and which was directly related to a controlled variable".

Clearly, uniform agreement on the value of auditory control does not presently exist.

Furthermore, agreement on the most suitable type of audio display does not exist either. Vinje found the best display to be continuously varying tones from 330 to 4300 hz., interrupted near the zero error point, and presented to either the left or the right ear as the operator's input function switched sign. Vinje's audio display is illustrated in Figure 1. Uhlemann and Geiser found the best display to be a constant frequency 800 hz. tone, of varying amplitude or volume, presented to either the left or the right ear as the operator's input functions switched sign. Uhlemann and Geiser's audio display is illustrated in Figure 2.

To the best of my knowledge, none of these experimentally investigated audio-control systems has seen the light of day to day use. Intermittent or discrete audio-manual control systems do not exist in quantity. Continuous audio-manual control systems do not exist in quantity.

However, at least one continuous audio-manual control system does commercially exist and is used with same degree of regularity.

This investigation was prompted by several recreational glider pilots, who commonly employ a device called an audio variometer to adjust their flight path. The audio variometer is a sensitive differentiating altimeter, which produces an audio output proportional to the glider's rate of climb (or rate of sink, as the case may be). If the glider is climbing, the pitch of the audio tone output climbs, if the glider is falling, the audio pitch falls. The glider pilot is thus able to adjust his control tactics in response to the audio tone output, and use his eyes for enjoying the scenery. Figure 3 displays the response of such an audio variometer.

AUDIO VARIOMETERS

Several types of Audio Variometers are marketed by the firm of GRAHAM THOMSON LTS.,* who kindly supplied the information concerning variometers that is presented here. A most significant point concerns the establishment of a set point or zero point, when continuous audio tones are employed to convey information which varies both in magnitude and in polarity, or

algebraic sign.

Consider the tone assignments, shown in Figure 4, which were used for one experiment concerning a model for a "Zero-Reader" Speed Director and Variometer (A Compensatory Tracking System).

A relatively high audio frequency of 3000 hz. as shown in Figure 4 represented the maximum positive error in the flight vector allowed, and a relatively low audio frequency of 333 hz. represented the maximum negative error allowed. The geometric midpoint frequency of 1000 hz. represented the set point of zero error. For compensatory tracking, the human operator or pilot wishes to keep the error at zero. For the audio case illustrated in Figure 4, this means keeping the audio tone at the zero set point of 1000 hz. Zero error does not correspond to zero sound or zero frequency, but rather to some intermediate frequency. Without a sense of perfect audio pitch, keeping a frequency reference in mind is extraordinarily difficult, if not impossible. Hence, another audio tactic is almost invariably employed to distinguish positive errors from negative errors, and to indicate zero or tolerably small errors.

The commercial "Cambridge Triple-Range Variometer with Speed Director and Mark II Audio" uses an interrupted tone for positive rate of climb errors and a continuous whistle tone for negative rate of climb errors. This is illustrated in Figure 5.

Note that the audio information is identically displayed to both ears. Glider pilots do not usually wear earphones, which essentially precludes switching the tracking signal from the right ear to the left ear as the signal changes sign. Thus, the audio display modes favored by Vinje or Uhlemann and Geiser are not used in this particular application of audio manual tracking to the control of a glider.

Several glider pilots with thousands of hours of experience were interviewed, and two of them claimed that the audio variometer was a big improvement over the visual variometer. A third stated that he liked it at first, but later stopped using it entirely, because the whistle got on his nerves. The two pilots who held favorable opinions concerning the effectiveness and usefulness of the audio variometer also mentioned that they often disconnected or turned down the audio output in order to hear the rush of the wind, or just plain silence.

This application of audio manual tracking by glider pilots was the first and only such application the author has knowledge of. Commercial airline pilots, NASA researchers, and every control expert that was questioned agreed that actual applications of audio-manual tracking were as rare as a quiet politician in an election year - that is, there were not any applications at all, aside from the glider system.

*Graham Thomson Ltd., 3200 Airport Avenue
 Santa Monica, California 90405 (213) 398-4714

EXPERIMENTAL APPARATUS

The investigation consisted of a simulation, flown by students who, with only one exception, had no musical training. The basically simple experimental set-up is depicted by the block diagram of Figure 6. The TR-20 analog computer generated the single sine wave input signal, and formed the system error in response to the input signal and the system dynamics modeled by the analog computer. The results presented later on deal only with the case of unity controlled dynamics, although other higher order dynamics were investigated. A NOVA model 1200 digital computer sampled the system input signal (sine and cosine components), the operator's input signal (which was the system error), and the operator's output signal (which was the system output for unity dynamics). Sampling was performed ten times a second, and the analog information was digitized, and stored on a magnetic disk file for later data analysis. Figure 7 displays the major digital components utilized.

The simulation was run as part of a special projects electrical engineering course taught at the Cooper Union in N.Y.C. One group of students designed and built the multiplexer, another group built the analog to digital converter and the requisite computer interface, another group built the digital to analog converter and computer interface, and the last group built the voltage controlled oscillator and amplifier, which produced the actual audio output signal. After much trial and an astounding amount of error, the entire instrument package was pronounced up and running all in its own bright blue relay rack. Funding was obtained from the field, stream and sponge department, with the exception of a $200 hard cash IEEE research prize won by the supervising student group that performed the actual experiment.

RESULTS

The results of the audio-manual glider pilot tracking simulation are bothersome. The results appear to indicate that audio-manual tracking is decidedly inferior to visual manual tracking - even though some glider pilots claim otherwise.

To allow for a ready comparison of results, the three minute tracking runs were performed by the same subject three different ways. The subject performed via audio tracking alone, via visual tracking alone, and via audio plus visual tracking.

The order of runs was reversed, to see if this made any difference. It did not. Several different audio diaplays were used. Some were clearly inferior, some were clearly superior. Head phones were superior to a loudspeaker, even with no ear switching - apparently the phones cut our extraneous audio noise. A pure variable tone signal with no absolute zero reference was cleary inferior. See Figure 8. The best audio tracking signal found in these experiments is shown in Figure 9. The signal consists of a continuously variable tone of constant amplitude, to which is

added a constant center frequency tone, corresponding to a zero error. When the tracking tone equals or is nearly equal to the center frequency reference tone, beats are heard. The beats grow lower in frequency as the error is nulled out, from either error polarity. Zero error yields zero beat, an extremely easy to perceive condition. Large errors produce tones of either high or low frequency, which clearly give polarity information.

Without such polarity information, sign reversals are common - the operator does not know which way to move his stick. An example of polarity reversal is shown in the recordings of Figure 10, for the case of audio-manual tracking with no zero tone reference. Figure 11 shows the operator's response for the case of compensatory visual manual tracking, using an oscilloscope display. It is effectively identical to Figure 12, which shows the operator's response for the case of compensatory audio-visual-manual tracking, with a zero beat reference tone. In both these cases, the data indicate an approximate magnitude corner frequency of approximately 0.4 hz. When the very best data for the compensatory audio-manual tracking task with a zero beat reference tone is examined, the approximate magnitude corner frequency is found to be slightly less than 0.2 h3, or almost an octave lower than the visual case. Note that these frequencies are all significantly lower than the figures generally reported for trained operators performing tracking experiments.

CONCLUSIONS

This data indicates that visual tracking performance enjoys a bandwidth advantage nearly double that for audio-manual tracking, for the idealistically simple case of unity dynamics and a single axis tracking task, with sinusoidal inputs. It is interesting to note that the single students who had had musical training learned far faster than the other students, and consistently outscored them in minimizing total mean square error.

In conclusion, it may be worthwhile to speculate upon how a glider pilot actually utilizes his audio variometer. It is the author's opinion that the glider pilot does not continuously track the audio signal, but rather uses it in an intermittant fashion, to provide directional goals for his flight path, which he controls via visual tracking of the horizon and other visual cues. That is, it is conjectured that the glider pilot actually uses visual information for the second by second fine control of his glider, and uses the audio variometer to provide relatively long term information concerning his overall performance (is he going up? or down?) which he then uses to alter his flight strategy, in a long term fashion.

REFERENCES

1. DeFlorez, L., "True Blind Flight", _Journal of The Aeronautical Sciences_, Vol. 3, March 1936, pp. 168-170.

2. Forbes, T.W., Garner, W.R., and Howard, J.G., "Flying by Auditory Reference ("FLYBAR")" _Applied Experimental Psychology - Human Factors in Engineering Design_, Chapanis, A., Ed., New York, N.Y., John Wiley & Sons, 1957, Ch. 9.

3. Katz, D., et al., "Experimental Study of Acoustic Displays of Flight Parameters in a Simulated Aerospace Vehicle", _NASA Technical Report, CR-509_, July 1966.

4. Mirchandani, Pitu, B., "An Auditory Display in a Dual-Axis Tracking-Task", _IEEE Transactions on Systems, Man, and Cybernetics_, Vol. SMC-2, No. 3, July 1972, pp. 375-380.

5. Pitkin, Edward T., and Vinje, Edward W., "Comparison of Human Operator Critical Tracking Task Performance with Aural and Visual Displays". _IEEE Transactions on Systems, Man, and Cybernetics_, March 1973, pp. 184-187.

6. Simpson, C.A., and Williams, D.H., "Human Factors Research Problems in Electronic Voice Warning System Design", _Eleventh Annual Conference on Manual Control_, Ames Research Center, Moffett Field, California, NASA TM X-62, 464, May 1975, pp. 94-106.

7. Uhlemann, Hartmut, and Geiser, George, "Multivariable Manual Control with Simulataneous Visual and Auditory Presentation of Information", _Eleventh Annual Conference on Manual Control_, Ames Research Center, Moffett Field, California, NASA TM X-62, 464, May 1975, pp. 3-18.

8. Vinje, E. Wayne, "Flight Simulator Evaluation of Audio Displays For IFR Hover Control", _Proceedings of the Eigth Annual Conference on Manual Control_, held at the University of Michigan, AFFDL-TR-72-92, May 1972, pp. 625-649.

9. Vinje, Edward W. and Pitkin, Edward T., "Human Operator Dynamics for Aural Compensatory Tracking", _IEEE Transactions on Systems, Man, and Cybernetics_, Vol. SCM-2, No. 4, Sept. 1972, pp. 504-512.

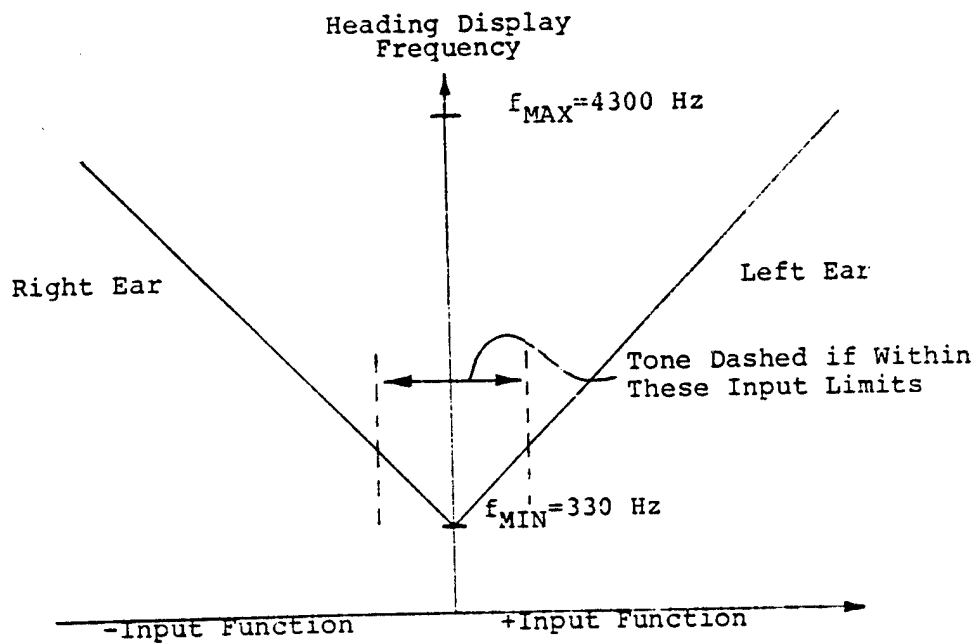Figure 1 - Pilot's Input Signal, Varying Tone, From Vinje (8)

Heading Display
Frequency

$f_{MAX}=4300$ Hz

Right Ear

Left Ear

Tone Dashed if Within
These Input Limits

$f_{MIN}=330$ Hz

-Input Function   +Input Function

Figure 2 - Pilot's Input Signal, Varying Volume,
From Uhlemann and Geiser (7)

Volume of 800 Hz Constant Frequency Tone

Right Ear

Left Ear

-Input
Function

Zero Volume
At Zero Input

+Input
Function
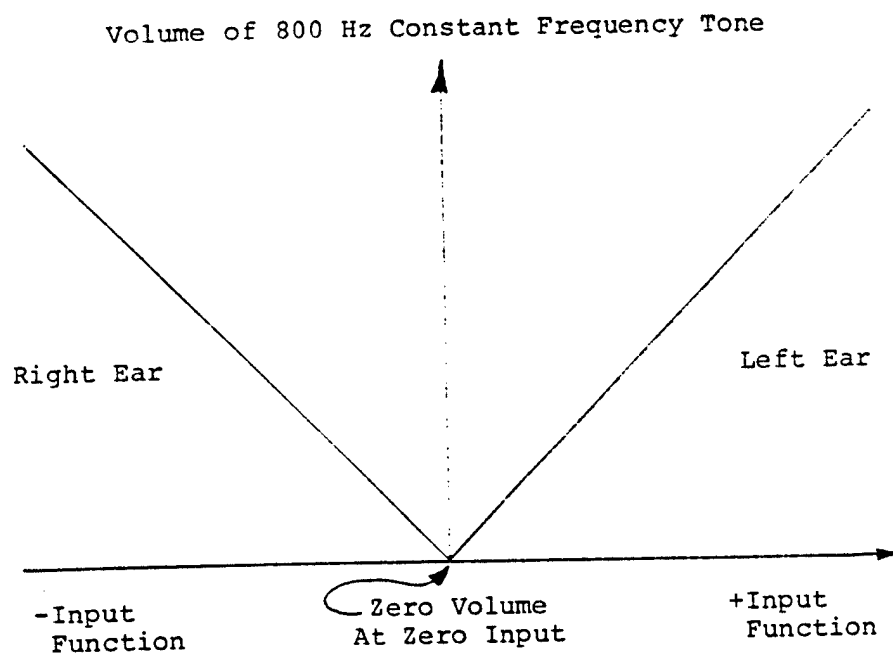
Figure 3 - Response Of The PIEP Audio
Unit For Variometers

Frequency Of Audio Tone

The zero frequency cut
in point is adjunstable
to positive, zero, or
negative rate of climb.
(It is usually set near
zero).

Very low frequency tone,
sounds like the "peeps"
of a baby chick

- Rate of Climb   0   + Rate of Climb
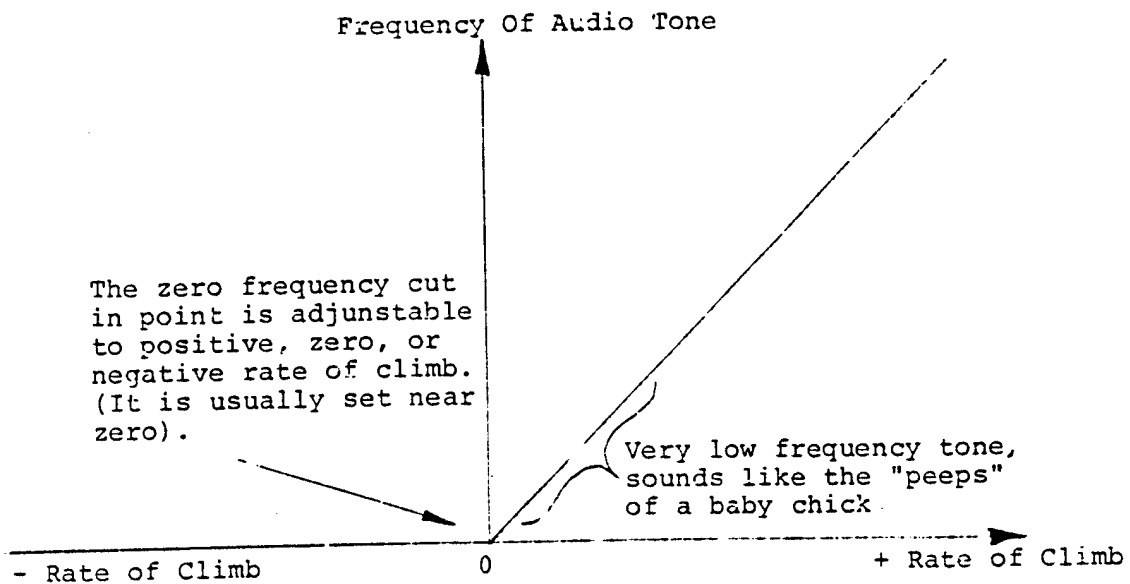
Figure 4 - Continuous Audio Pitch Versus
Flight Vector Error For A Model Of A
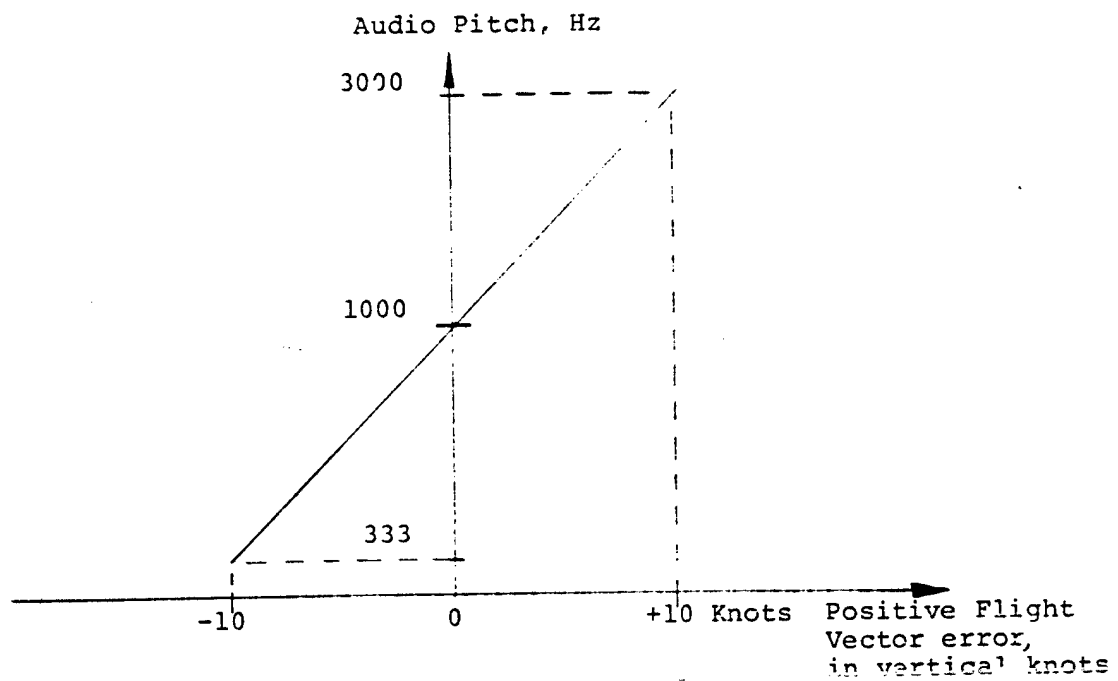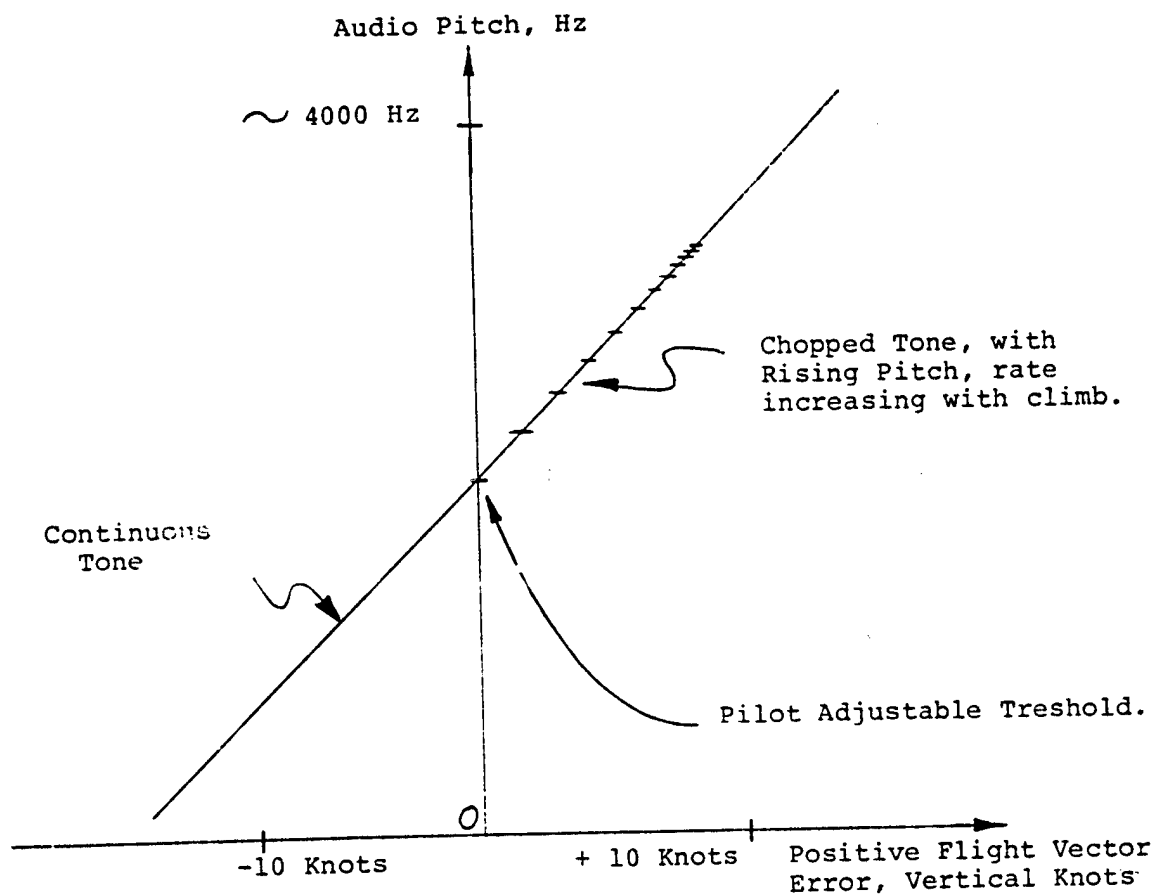"Zero-Reader" Speed Director And Variometer
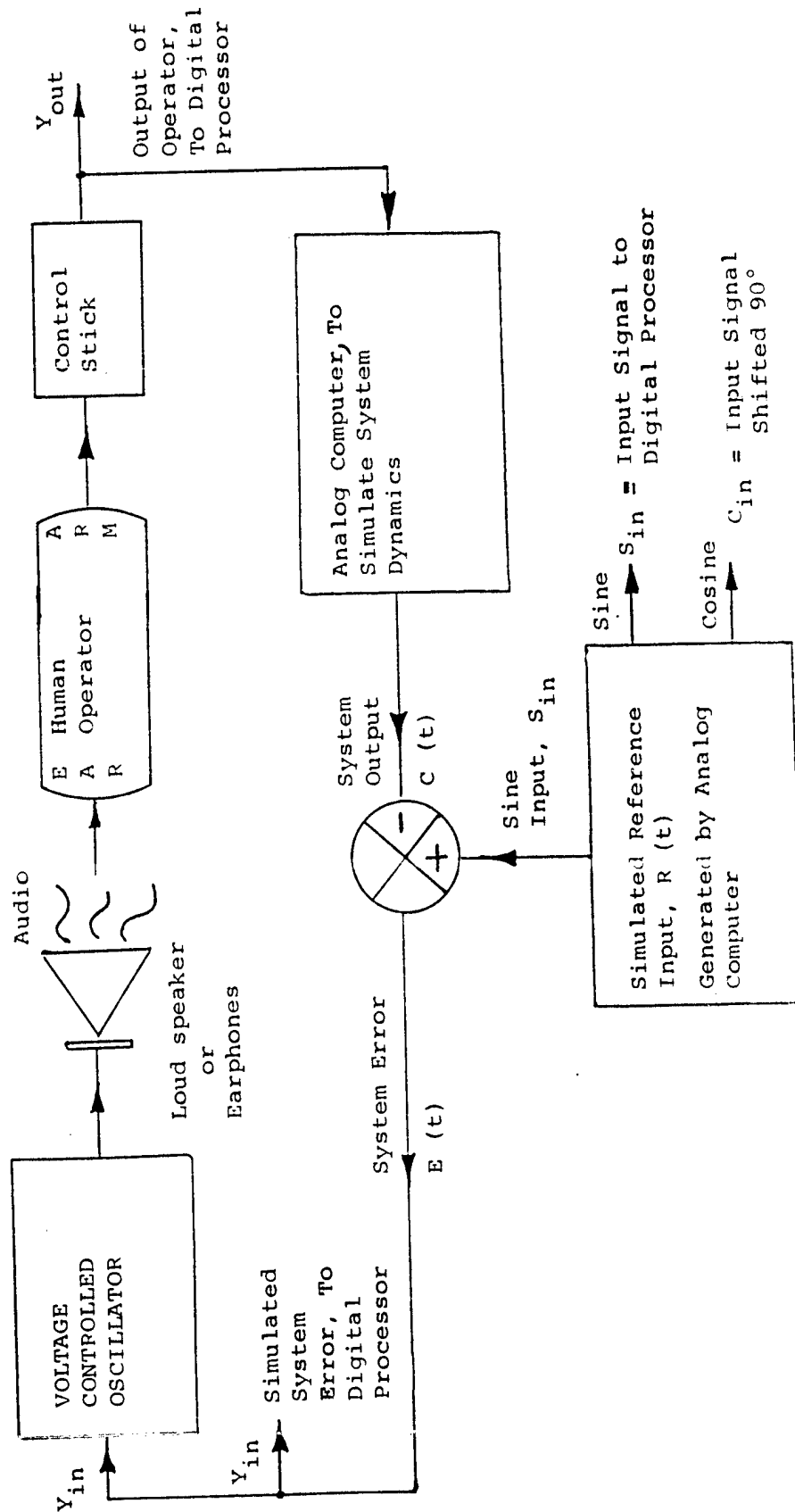(Compensatory Tracking System)

Audio Pitch, Hz

3000

1000

333

-10   0   +10 Knots   Positive Flight
Vector error,
in vertical knots

414

Figure 5 - Audio Output Of The Cambridge
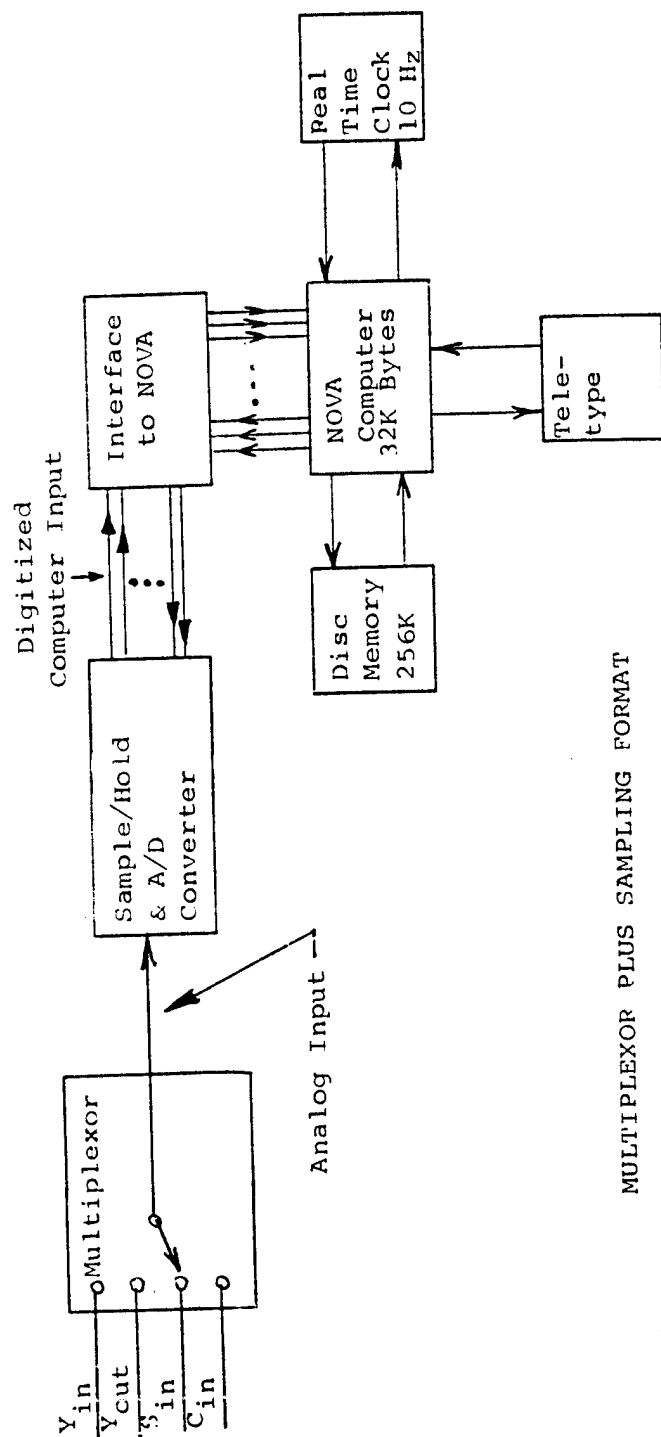Triple-Range Variometer With Speed Director
And Mark II Audio Unit

Figure 6

ANALOG SIMULATION SEGMENT OF THE
COMPENSATORY AUDIO-MANUAL TRACKING EXPERIMENT

Y_{out}

Output of Operator, To Digital Processor

Control Stick

E A R Human Operator E A R M

Audio

Loud speaker or Earphones

Analog Computer, To Simulate System Dynamics

VOLTAGE CONTROLLED OSCILLATOR

System Output

C (t)

Y_{in}

Simulated System Error, To Digital Processor

Y_{in}

System Error

E (t)

Sine Input, S_{in}

Simulated Reference Input, R (t) Generated by Analog Computer

Sine

S_{in} = Input Signal to Digital Processor

Cosine

C_{in} = Input Signal Shifted 90°

416

DIGITAL DATA PROCESSING SEGMENT OF THE AUDIO-MANUAL TRACKING EXPERIMENT

Figure 7

Multiplexor

Y_{in}
Y_{out}
S_{in}
C_{in}

Analog Input

Sample/Hold & A/D Converter

Digitized Computer Input

Interface to NOVA

Real Time Clock 10 Hz

NOVA Computer 32K Bytes

Disc Memory 256K

Tele-type

MULTIPLEXOR PLUS SAMPLING FORMAT

Samples

Y_o Y_i S_i C_i

0 4 8 12

Real Time Clock, T=100 msec.

Y_o Y_i S_i C_i

100 104 108 112

msec.

Time

417
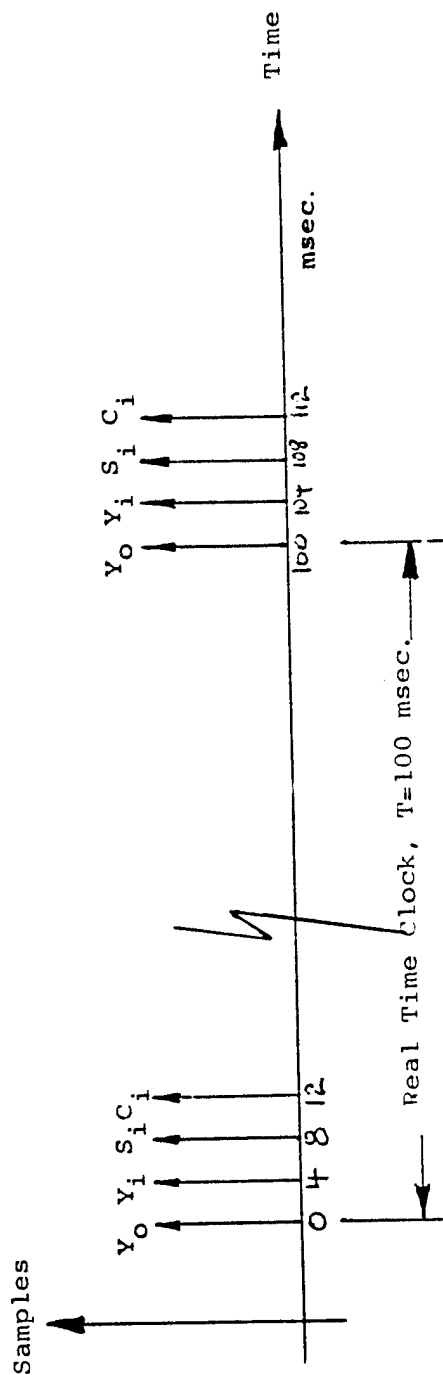
Figure 8ₐ - Compensatory Audio Manual Tracking Performance
With No Zero Reference Tone

Sinusoidal Audio Frequency Tracking Tone

1000Hz

650Hz

300Hz

-1
Maximum
Negative
Error

0

+1
Maximum
Positive
Error

Error
Magnitude,
Normalized
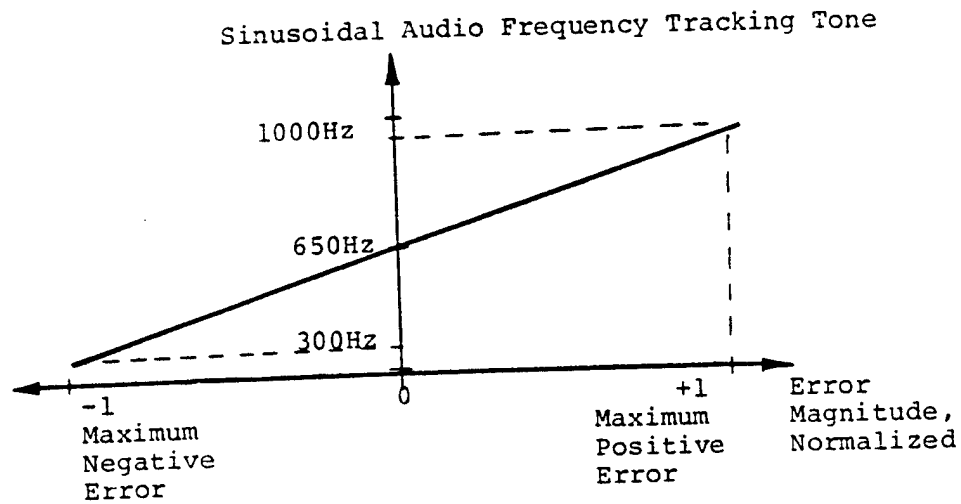
Figure 8ᵦ - Normalized Operator's Response to Single Sinusoidal
Inputs (average of 10 runs)

Approximate Magnitude
Corner Frequency = 0.05Hz

Phase

Magnitude

0 db.

Magnitude

0 degrees

Phase

-90 degrees

-20 db

0.01   0.1   1.0   Frequency, Hz
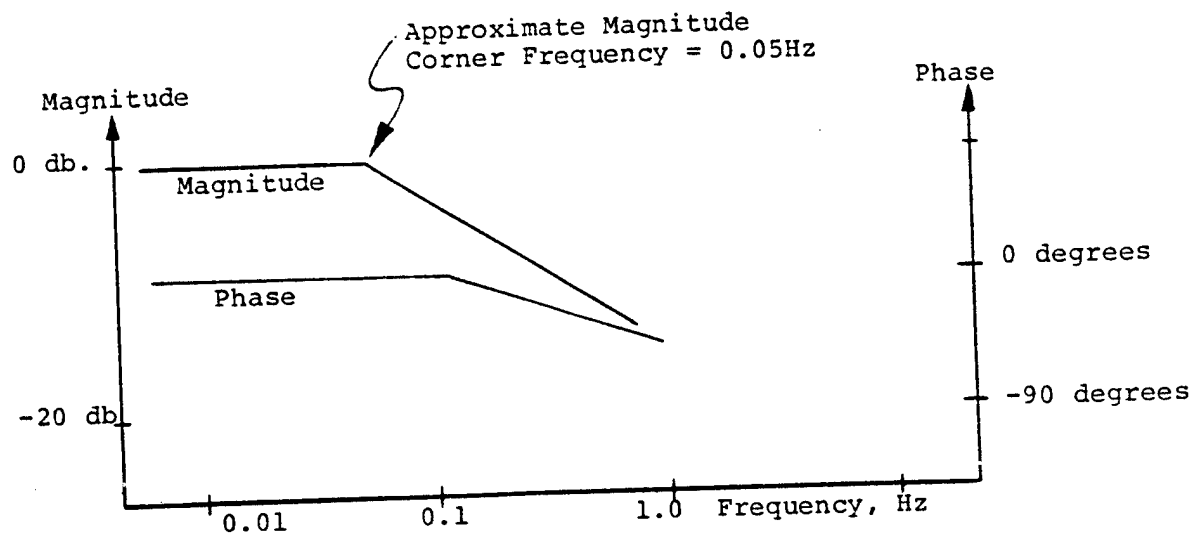
Figure 9ₐ - Compensatory Audio-Manual Tracking With
         A Zero Beat Reference Tone

Audio Frequency Tracking Tone

1000Hz

Beat Frequency
Superimposed On
Tracking Tone

650Hz

Zero Beat
At Zero
Error

300Hz

-1   0   +1

Normalized
Error
Magnitude
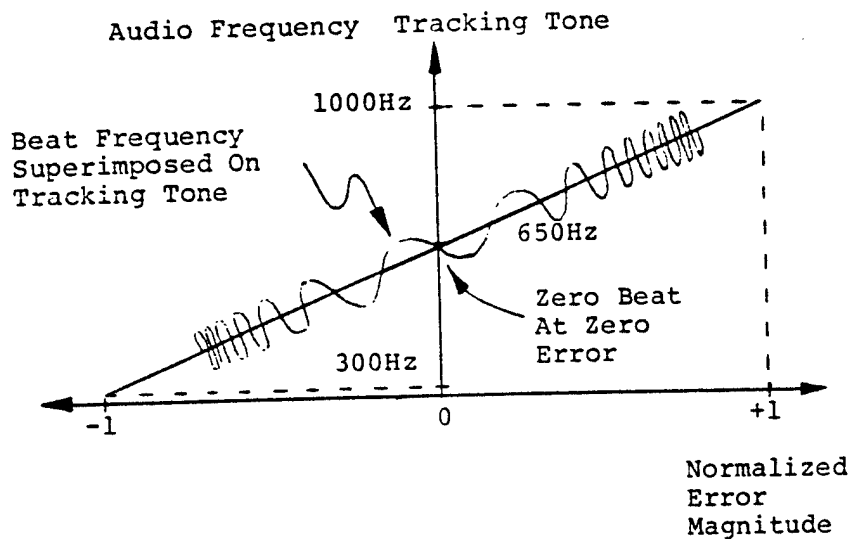
Figure 9ᵦ - Operator's Performance For Compensatory Audio-
         Manual Tracking With A Zero Beat Reference Tone

Approximate
Corner
Frequency = 0.2Hz

Phase

Magnitude

0 db

Magnitude

0 degrees

Phase

-90 degrees

-20 db

0.01   0.1   1.0   Frequency, Hz

419

Operator's Output

$c(t)$

ω

Note Operator's
Polarity
Reversed

System Output

$m(t)$

System Input
0.05Hz

$x(t)$

System Error = Operator's Input

$e(t)$
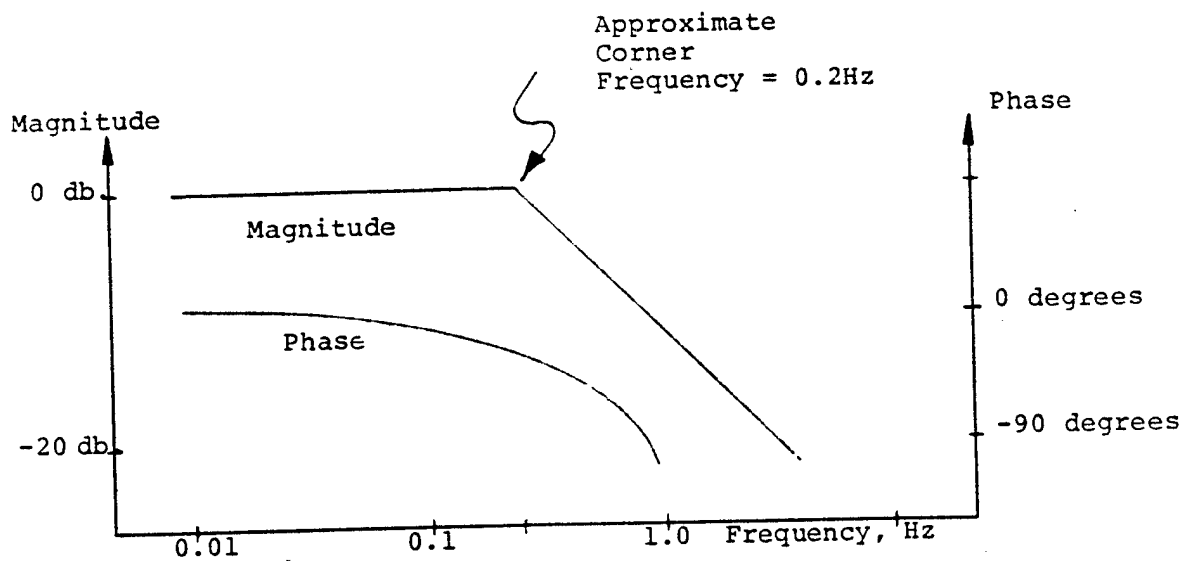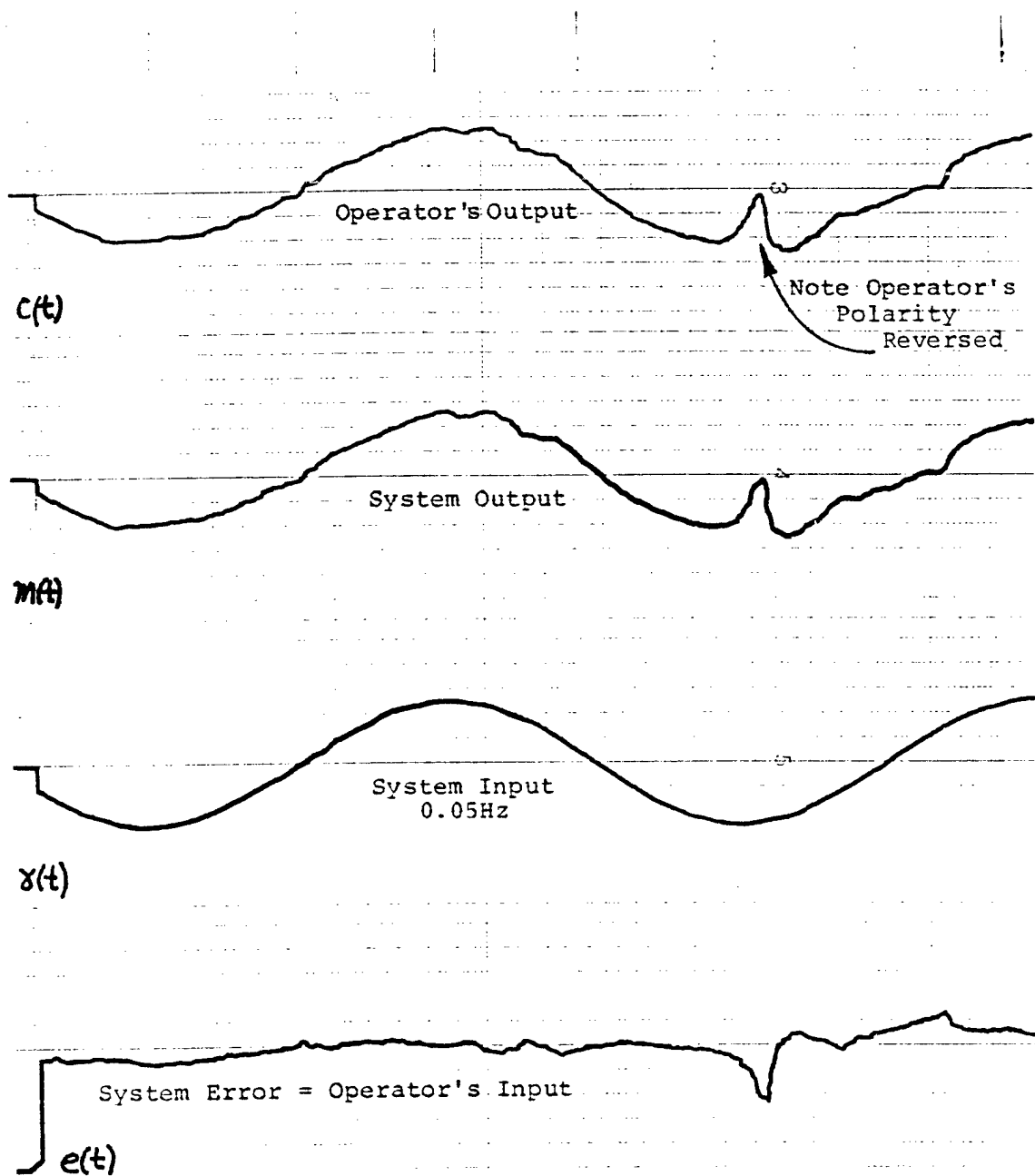
Figure 10 - Analog Outputs Recorded From An Audio-Manual
Tracking Simulation Utilizing A Pure Tone Signal
With No Zero Reference Tone. (As shown in Figure 4)

420

Figure 11 - Compensatory Visual Manual Tracking Performance,
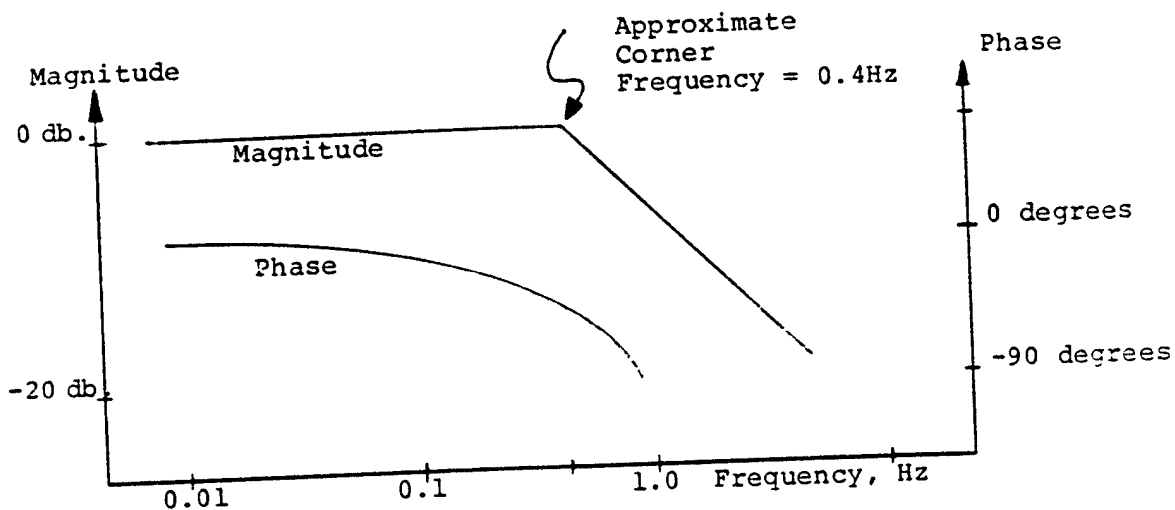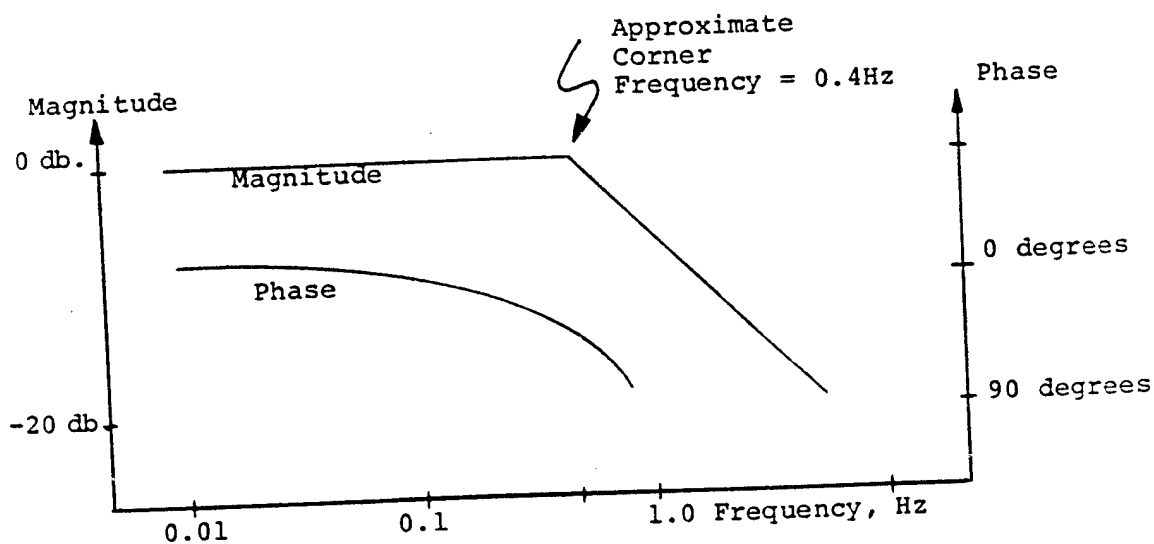Oscilloscope Display, 10 runs of 3 minutes

Figure 12 - Compensatory Audio-Visual Manual Tracking Performance,
With A Zero Beat Frequency Reference Tone, And
Oscilloscope Display.

421

EYE TRACKING: HORIZONTAL VS. VERTICAL

By John Hornseth, Gary Stanley, James Porterfiel
Crew Station Integration Branch
Human Engineering Division
6570 Aerospace Medical Research Laboratory
Wright-Patterson AFB, Ohio 45433

Paul Carson
University of Dayton Research Institute
300 College Park Avenue
Dayton, Ohio 45409

SUMMARY

The Honeywell Remote Oculometer was used to obtain eye pursuit tracking data on eight subjects. A three-minute recording of Gaussian noise, bandwidth limited to 1.5 Hz served as the forcing function. A galvo-laser system rear projected the forcing function onto a vertical viewing screen as a spot of light randomly moving in one dimension (horizontally or vertically) with a maximum excursion of $\pm 5°$ visual angle as viewed by the subject. Each subject tracked the forcing function twice vertically and twice horizontally in a balanced design. Frequency analysis of the data showed: (1) coherence values were essentially the same for both horizontal and vertical eye tracking, (2) average vertical gain (.70) was significantly higher than average horizontal gain (.62) with both showing no drop with frequency, and (3) phase was essentially the same for both vertical and horizontal eye tracking, was linearly correlated (-.99) with frequency, and could be represented as a transport delay of .125 seconds.

INTRODUCTION

Stated similarities, or differences, between horizontal and vertical eye tracking capabilities, in smooth pursuit tracking, are based upon meager experimental evidence. This study was designed to obtain substantial eye tracking data on eight subjects. Of specific interest were possible differences in coherence, gain, and phase.

APPARATUS

A three-minute recording of a Hewlett-Packard 3722A Noise Generator, set at infinite sequence length and at 0.0 to 1.5 Hz Gaussian Noise Bandwidth, served as the forcing function. An optical projection system consisting of a low power laser and a pair of galvo-mirrors rear projected the forcing function onto a cloth screen in the form of a 1/2" diameter spot of red light

randomly moving in one dimension, either horizontally or vertically, about a center spot marked on the screen. The maximum excursion of the forcing function was $\pm 5°$ visual angle, as viewed by the subject. The $\pm 5°$ visual angle positions were also marked on the screen and, along with the center spot, served as calibration points for both the forcing function and the subject's eye movement response. The subject tracked the forcing function from a position on the opposite side of the screen from the optical projection system and equidistant from the screen.

The subject's eye line-of-sight was computed using the AMRL Honeywell Remote Oculometer. For a complete description of the Oculometer see reference 1. Calibration of the Oculometer prior to each tracking run was accomplished by using a second optical projection system positioned adjacent to the forcing function optical projection system. The Oculometer-driven laser spot was turned off during the tracking run.

Five channels of a seven channel 1/2-inch Ampex 300 instrumentation tape recorder were used to record: (1) time code, (2) forcing function on horizontal runs, (3) forcing function on vertical runs, (4) horizontal eye movements, and (5) vertical eye movements.

PROCEDURE

Eight male students from the University of Dayton were tested using an ABBA order of presenting the horizontal and vertical tracking runs. Four subjects were given the horizontal run first and four subjects were given the vertical run first in a balanced design. After seating the subject, the operation of Oculometer was checked and calibrated. The subject was instructed to sit in a natural, comfortable position. The only constraint placed upon the subject was the instruction to refrain from making large head movements. The subject was not given any practice trials. The subject was instructed to follow (pursue) the moving spot of light with his eyes as the spot moved horizontally (or vertically) on the screen. The subjects were screened for uncorrected 20/20 vision. Between runs subjects were given a short rest while the forcing function tape was rewound to its starting position and the equipment calibration was checked.

RESULTS

Frequency analyses of the tracking sessions for the eight subjects were accomplished by the Dynamics Technology Applications Branch (AFDL/FBG) at Wright-Patterson Air Force Base. For each run the power spectral density of the forcing function, the power spectral density of the eye response output, the cross power spectral density, the cross correlation, the coherence, and the transfer functions in gain and phase were computed. Only the statistical analyses of these data are presented in this report. Development of a de-

423

scriptive model representing subjects' performances will be accomplished at a later date.

The data for the two horizontal runs and for the two vertical runs for each subject were averaged for each of fifteen frequency points between 0 and 1.5 Hz. Analyses of variance were performed on these averaged data to obtain the horizontal and vertical comparisons presented in this report.

An 8 x 2 x 15 analysis of variance was performed on the coherence, gain, and phase data. The results of these analyses are presented in Tables I, II, and III for coherence, gain, and phase respectively. Plots of coherence by frequency, gain by frequency, and phase by frequency were obtained by averaging the data across subjects for each axis (Figures 1, 2, and 3).

The analysis of variance of the coherence data (Table I) shows no significant difference between horizontal and vertical coherence. In addition, there was no significant interaction between axes and frequency. However, the effect of frequency on coherence was significant and can be observed in Figure 1.

Vertical gain was significantly higher than horizontal gain (Table II and Figure 2). Vertical gain, averaged across subjects and frequency, was .70 and average horizontal gain was .62. No interaction between axis and frequency was present as can be observed in Figure 2.

No significant difference between horizontal phase and vertical phase was observed (Table III and Figure 3) although a small, but significant, interaction between axis and frequency was found. The increase of phase lag with frequency was highly significant. The regression of phase and frequency for both axes is plotted in Figure 4. Both horizontal and vertical phase showed a high linear correlation (-.99) with frequency. The slopes of the regression lines, -71.13 for the horizontal data and -66.85 for the vertical data, represent transport delays of .131 seconds and .119 seconds for horizontal and vertical eye tracking respectively. (The transport delay of 1/15 sec introduced by the Oculometer was subtracted before computing these values.)

DISCUSSION

The major finding of this study was the significantly higher vertical gain as compared with the horizontal gain. This result confirms the observation made last year by Shirachi and Black (Reference 2). However, two of the eight subjects tested showed slightly higher horizontal than vertical gains. Further study is planned to examine the range of these individual differences (emphasized by Huddleston in Reference 3) and the persistence of this observed horizontal-vertical gain difference with training.

Figure 3 does not appear to reflect the significant, but small, interaction between axes and frequency observed in the analysis of variance of the phase data (Table III). However, the difference in slopes of the regression lines shown in Figure 4 does reflect this interaction.

CONCLUDING REMARKS

In this study comparing horizontal and vertical eye tracking performance, vertical gain was found to be significantly higher than horizontal gain. No differences were found in coherence or in phase.

REFERENCES

1. Merchant, John; Morrissette, Richard; and Porterfied, James L: Remote Measurement of Eye Direction Allowing Subject Motion over one Cubic Foot of Space. IEEE Transactions in Biomedical Engineering, Vol. BME-21, No. 4, July 1974.

2. Shirachi, D.K.; and Black, J.H., Jr.: Head-Eye Tracking in Two-Dimensional Pursuit Tasks. Eleventh Annual Conference on Manual Control, NASA TM X-62, 464, 1975.

3. Huddleston, H.F.: Oculometer Pursuit of Vertical Sinusoidal Targets. Nature, Vol. 222, May 10, 1969.

TABLE I

ANOVA for Coherence

Source	Error Term	df	Mean Square	F
Axis (A)	AxS	1	0.0814	0.5458
Frequency (F)	FxS	14	0.0923	13.0216*
Subject (S)		7	0.4214	
AxS		7	0.1492	
FxS		98	0.0071	
AxF	AxFxS	14	0.0044	0.9451

* p < .001

TABLE II

ANOVA for Gain

Source	Error Term	df	Mean Square	F
Axis (A)	AxS	1	0.3810	6.6652*
Frequency (F)	FxS	14	0.0325	3.8734**
Subject (S)		7	0.2967	
AxS		7	0.0572	
FxS		98	0.0084	
AxF	AxFxS	14	0.0064	1.7109
AxFxS		98	0.0038	

 * p < .05
** p < .001

TABLE III

ANOVA for Phase

Source	Error Term	df	Mean Square	F
Axis (A)	AxS	1	22.26	0.0980
Frequency (F)	FxS	14	13010.20	145.7360**
Subject (S)		7	1409.12	
AxS		7	227.21	
FxS		98	89.27	
AxF	AxFxS	14	60.57	1.8996*
AxFxS		98	31.88	

* p < .05
** p < .001
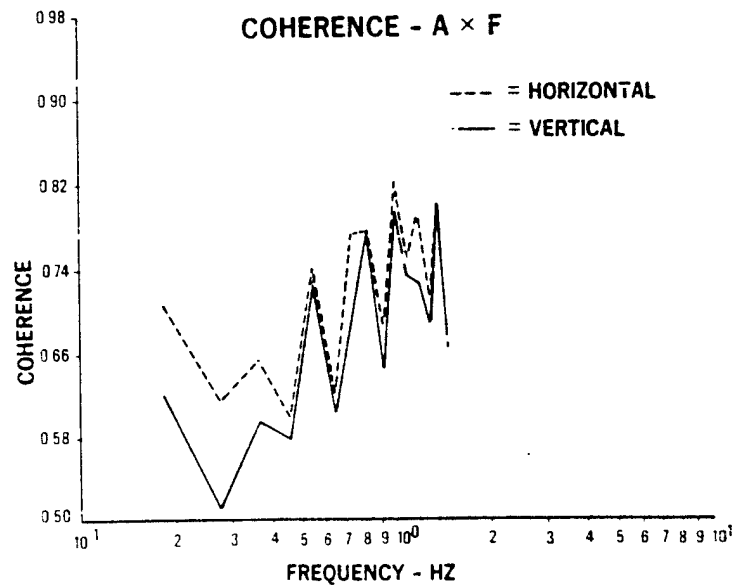
Figure 1. Horizontal and Vertical Coherence as a Function of Frequency.
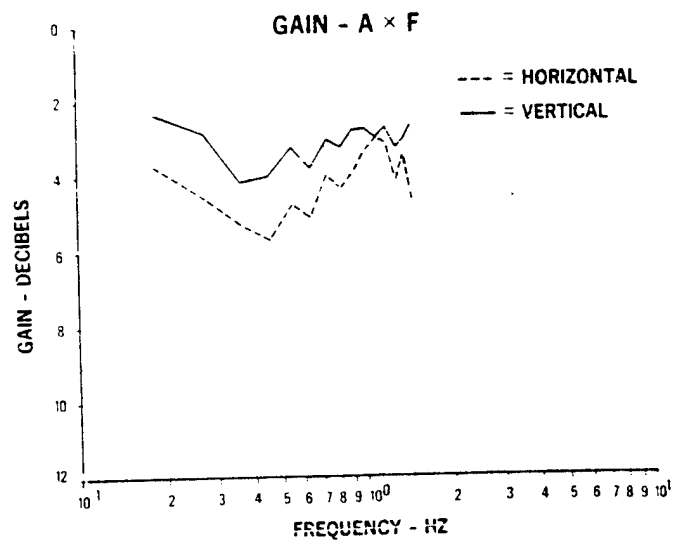
Figure 2. Horizontal and Vertical Gain as a Function of Frequency.

428

PHASE - A × F

---- = HORIZONTAL
—— = VERTICAL
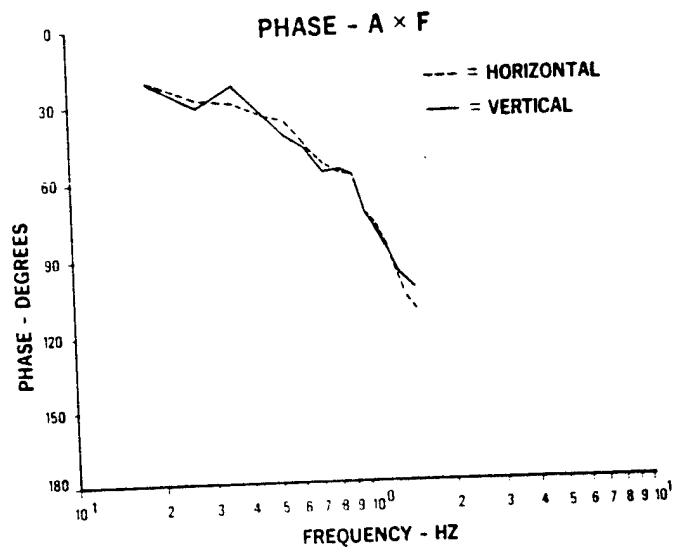
Figure 3. Horizontal and Vertical Phase as a Function
of Frequency.

REGRESSION - A × F

= HORIZONTAL
= VERTICAL
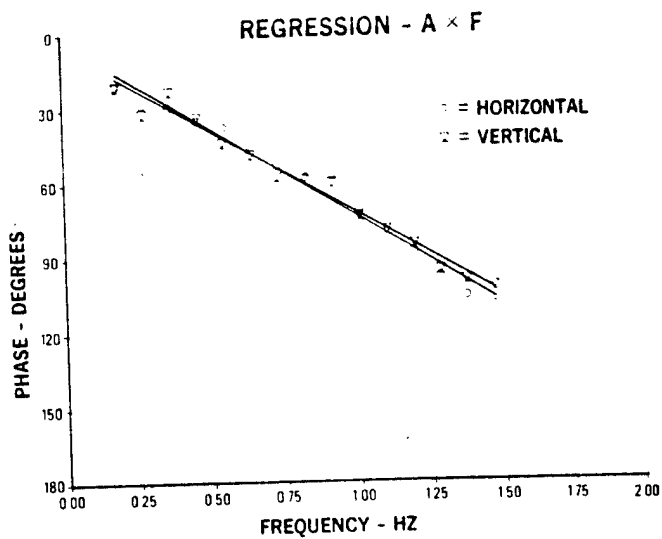
Figure 4. The Regression Between Frequency and Phase for
Horizontal and Vertical Data.

429

HEAD TRACKING: A FATIGUE STUDY

By John Hornseth and Gary Stanley
Crew Station Integration Branch
Human Engineering Division
6570 Aerospace Medical Research Laboratory
Wright-Patterson AFB, Ohio 45433

Paul Carson
University of Dayton Research Institute
300 College Park Avenue
Dayton, Ohio 45409

SUMMARY

A Helmet-Mounted Sight was used .to obtain two dimensional head pursuit tracking data on eight subjects. For each dimension, Gaussian noise, bandwidth limited to 0.5 Hz or 1.5 Hz, was alternately recorded (for four minutes and 2.5 minutes respectively) five times to obtain a 32.5 minute continuous forcing function. A galvo-laser system projected the forcing function as a (target) spot randomly moving in two-dimensions with a maximum excursion of $\pm10°$ visual angle. The follower spot (computed head position) was projected by a second galvo-laser system. Frequency analysis of the beginning and final tracking periods for the 0.5 Hz tracking data revealed: (1) no change in horizontal or vertical coherence with trials; (2) a significant reduction in gain from trial 1 to trial 5; (3) a significant increase in phase lag from trial 1 to trial 5; (4) significant differences between horizontal and vertical tracking dimensions in coherence and phase lag; and (5) several significant higher order interactions involving trials, axes, and frequency. Coherence analysis of the 1.5 Hz tracking data revealed a breakdown in linear tracking performance.

INTRODUCTION

This study was conducted to determine whether extended continuous pursuit tracking in two-dimensions with a helmet-mounted sight would produce significant changes in tracking performance. Of specific interest were possible changes which might occur in coherence, gain, and phase.

APPARATUS

Gaussian noise was recorded for 32-1/2 minutes independently on two channels of an instrumentation tape recorder. The bandwidth of the noise generator was alternately set at .5 Hz, for four minutes, and then at 1.5 Hz, for 2-1/2 minutes, five times to make up a 32-1/2 minute, two-dimension-

al, forcing function consisting of a sequence of slow and fast tracking sessions.

An optical projection system consisting of a low-power laser and a pair of mirror galvanometers rear projected the forcing function onto a cloth screen in the form of a target spot of red light randomly moving in two dimensions about a center point on the screen. The maximum excursion of the forcing function in both X and Y dimensions was $\pm 10°$ visual angle, as viewed by the subject. Lower left and upper right 10° visual angle positions marked on the screen served as calibration points for both the forcing function and subject's line-of-sight, as computed by the helmet-mounted sight. The Honeywell Helmet-Mounted Sight (HMS) used in this study is described in Reference 1. The output of the HMS was used to drive a second optical projection system which produced the follower spot of light controlled by the subject. The subject tracked the target laser beam from a position on the opposite side of the screen from the optical projection system and equidistant from the screen.

Five channels of a second instrumentation tape recorder were used to record: (1) time code generator signal, (2) horizontal forcing function, (3) vertical forcing function, (4) horizontal (azimuth) head tracking response, and (5) vertical (elevation) head tracking response.

PROCEDURE

Eight male students from the University of Dayton served as subjects for this study. After seating the subject and adjusting the helmet as snugly and comfortably as possible to his head, the HMS was boresighted and calibrated for proper alignment and gain settings. The subject then tracked the forcing function (target spot) with his follower spot continuously for 32-1/2 minutes. Subjects received no practice trials prior to the experimental session. The helmet visor and reticle were up and out of sight during the tracking run.

RESULTS

Frequency analyses of the first and fifth slow-fast tracking sessions for the eight subjects of this study were performed by the Dynamics Technology Applications Branch (AFDL/FBG) at W-PAFB. Only a statistical treatment of the data is presented in this report. Development of a descriptive model representing subjects' performance will be accomplished at a later date.

Slow (.5 Hz) Tracking Data

The analysis of variance (Table I) of the coherence data for the first and fifth slow (.5 Hz) tracking runs showed no significant overall change in

coherence with extended tracking. However, the presence of significant higher order interactions indicates that changes did occur at specific frequencies (observable in Figure 1) and for specific axis by frequency combinations. The analysis also shows that while horizontal coherence was significantly greater than vertical coherence, this difference was also specific to certain frequencies (observable in Figure 2) and for certain frequency by trial combinations.

A significant reduction in gain from Trial 1 to Trial 5 was noted (Table II, Figure 3). However, a significant interaction between trials and frequency was present (observable in Figure 3). No overall difference between horizontal and vertical gain was found, but a significant interaction between axes and frequency was observed, as can be seen in Figure 4.

A significant increase in phase lag from Trial 1 to Trial 5 was observed with no interaction effect between trial and frequency (Table III and Figure 5). Vertical phase lag was found to be significantly greater than horizontal phase lag but a significant interaction between axes and frequency was present as can be seen in Figure 6. Linear regression plots of phase lag with frequency are shown in Figure 7, comparing Trial 1 and Trial 5, and in Figure 8, comparing horizontal and vertical axes. The coefficient of correlation for these regression lines are between -.98 and -.99. The slopes of the regression lines shown in Figure 7 for Trial 1 and Trial 5 are essentially the same and represent a transport delay of .176 seconds. The slopes of the regression lines shown in Figure 8 represent transport delays of .123 seconds for the horizontal axis and .232 seconds for the vertical axis. (A transport delay of 1/30 second introduced by the helmet-mounted sight was subtracted before computing these values.)

Fast (1.5 Hz) Tracking Data

Coherence values for the 1.5 Hz tracking runs averaged well below .5. Consequently the analysis of the gain and phase data was not considered appropriate. An analysis of variance of the coherence data was carried out (Table IV). The analysis reveals no significant trial effect, but a significant interaction between trial and frequency (Figure 9). Horizontal coherence was significantly higher than vertical coherence. However, a significant interaction between axes and frequency was also present (Figure 10).

DISCUSSION

The coherences observed for the fast tracking runs were surprisingly low. It is believed that the chief reason for these low coherence values was the subject's lack of experience in head tracking. A study to examine the effect of practice in head tracking upon subject's coherence scores, as a function of forcing function bandwidth, is planned. Further study is also needed to determine whether the significant interactions between trials and frequency and between axes and frequency, as observed in the coherence

432

analyses of both the slow and fast tracking sessions, are meaningful. For the slow tracking coherence data, the interaction effects do not appear to be large enough to be practically significant. For the fast tracking coherence data, the reduced vertical coherence, as compared with the horizontal coherence, at the higher frequencies (Figure 10) may be meaningful in terms of helmet mass. However, it is more difficult to account for the reduction in coherence at low frequencies on Trial 5 as compared to Trial 1 as seen in Figure 9.

The significant trial by frequency and axis by frequency interactions present in the analysis of variance of slow tracking gain (observable in Figures 3 and 4) do not appear to be of sufficient magnitude to be meaningful. Although it was anticipated that trials (fatigue) would have more of an effect upon the vertical axis gain than upon the horizontal axis gain, it is interesting to note that the trial (fatigue) effect is similar for both the horizontal and vertical axes.

As anticipated, the significant axis by frequency interaction found in analyzing phase angle data showed (Figure 6) that vertical phase was larger than horizontal phase at the higher frequencies. However, this effect was not enhanced by trials (fatigue) as was expected (i.e., the trial by axis by frequency interaction was not significant). Of final interest is the observation that trials (fatigue) did not affect subject's transport delay (as represented by the slopes of the regression lines) but instead affected the Y intercepts (see Figure 7) which presumably represents an increase in the operation of some sort of non-linear dead zone by the subject. Further study is needed to establish the significance of this observation.

CONCLUDING REMARKS

Extended continuous pursuit tracking, in two dimensions, with a helmet-mounted sight does produce significant changes in tracking performance. The results of this study showed that 32-1/2 minutes of continuous tracking produced a significant reduction in gain and a significant increase in phase.

REFERENCES

1. Ferrin, F.J.: "F4 Visual Target Acquisition System," Proceedings of A Symposium on Visually Coupled Systems: Development and Application, sponsored by Aerospace Medical Division, Brooks Air Force Base, Texas and 6570th Aerospace Medical Research Laboratory, Wright-Patterson AFB, Ohio. AMD-TR-73-1, September 1973, pp. 15-32. AD 916572.

TABLE I

ANOVA for Slow Coherence

Source	Error Term	df	Mean Square	F
Axis (A)	AxS	1	0.0684	10.6386*
Trial (T)	TxS	1	0.3766	5.2078
Frequency (F)	FxS	8	0.0226	11.4054***
Subject (S)		7	0.2008	
AxS		7	0.0064	
TxS		7	0.0723	
AxT	AxTxS	1	0.0066	1.6285
FxS		56	0.0020	
AxF	AxFxS	8	0.0054	2.9605**
TxF	TxFxS	8	0.0079	2.5036*
AxTxS		7	0.0041	
AxFxS		56	0.0018	
TxFxS		56	0.0032	
AxTxF	AxTxFxS	8	0.0094	4.6307***
AxTxFxS		56	0.0020	

   * p < .05
  ** p < .01
 *** p < .001

TABLE II

ANOVA for Slow Gain

Source	Error Term	df	Mean Square	F
Axis (A)	AxS	1	0.1753	0.5626
Trial (T)	TxS	1	1.6763	9.1965*
Frequency (F)	FxS	8	0.3962	26.7230***
Subject (S)		7	0.1868	
AxS		7	0.3116	
TxS		7	0.1823	
AxT	AxTxS	1	0.0446	1.5769
FxS		56	0.0148	
AxF	AxFxS	8	0.0225	3.3025**
TxF	TxFxS	8	0.0301	2.4085*
AxTxS		7	0.0282	
AxFxS		56	0.0068	
TxFxS		56	0.0125	
AxTxF	AxTxFxS	8	0.0049	0.9502
AxTxFxS		56	0.0052	

  * p < .05
 ** p < .005
*** p < .001

TABLE III

ANOVA for Slow Phase

Source	Error Term	df	Mean Square	F
Axis (A)	AxS	1	5597.5	35.6682**
Trial (T)	TxS	1	2056.6	5.8132*
Frequency (F)	FxS	8	5670.7	64.3181**
Subject (S)		7	1277.9	
AxS		7	156.9	
TxS		7	353.8	
AxT	AxTxS	1	21.5	1.0928
FxS		56	88.2	
AxF	AxFxS	8	397.8	9.2252**
TxF	TxFxS	8	18.5	0.6683
AxTxS		7	19.6	
AxFxS		56	43.1	
TxFxS		56	27.6	
AxTxF	AxTxFxS	8	33.6	1.1698
AxTxFxS		56	28.8	

  * p < .05
** p < .001

TABLE IV

ANOVA for Fast Coherence

Source	Error Term	df	Mean Square	F
Axis (A)	AxS	1	0.5696	7.8571*
Trial (T)	TxS	1	1.1553	3.6152
Frequency (F)	FxS	15	0.0429	2.7184**
Subject (S)		7	1.3447	
AxS		7	0.0725	
TxS		7	0.3196	
AxT	AxTxS	1	0.0181	1.2516
FxS		105	0.0158	
AxF	AxFxS	15	0.0613	5.4819***
TxF	TxFxS	15	0.0352	2.5506**
AxTxS		7	0.0145	
AxFxS		105	0.0112	
TxFxS		105	0.0138	
AxTxF	AxTxFxS	15	0.0351	2.8318**
AxTxFxS		105	0.0124	

```
  * p < .05
 ** p < .005
*** p < .001
```

SLOW COHERENCE - T × F
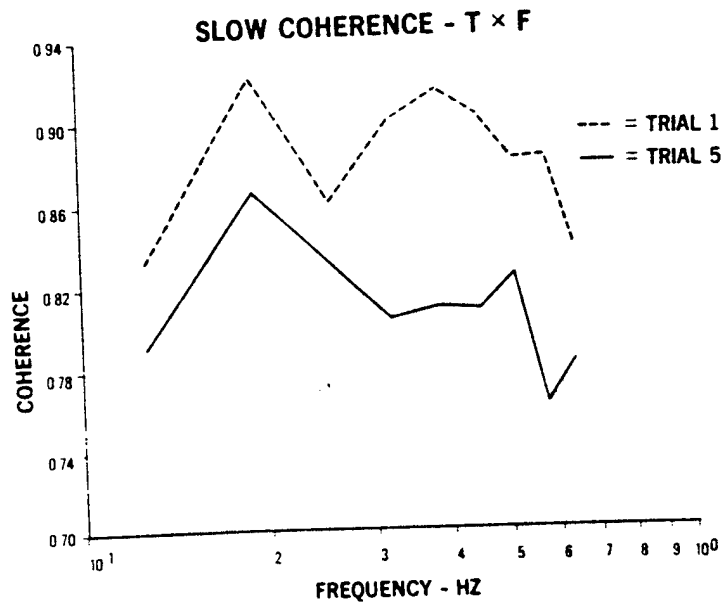
Figure 1. Coherence as a Function of Frequency for Trial 1
and Trial 5: Slow (.5 Hz) Tracking Data.
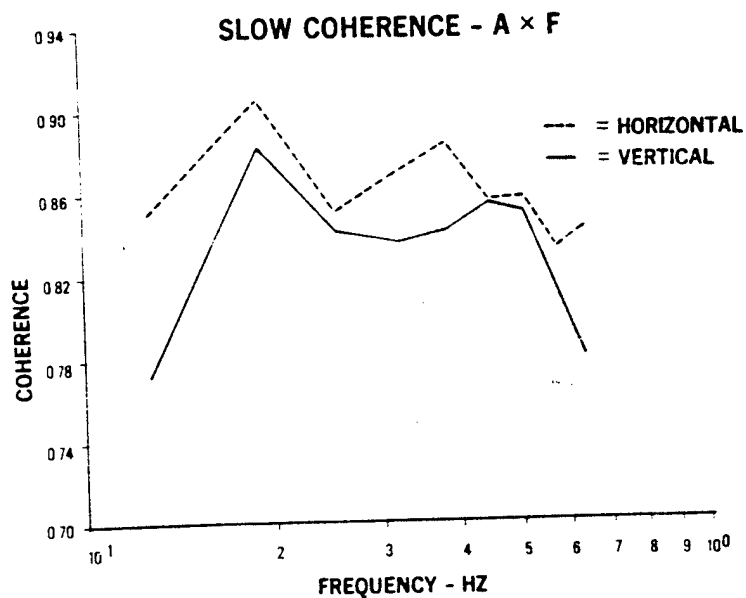
SLOW COHERENCE - A × F

Figure 2. Coherence as a Function of Frequency for Horizontal
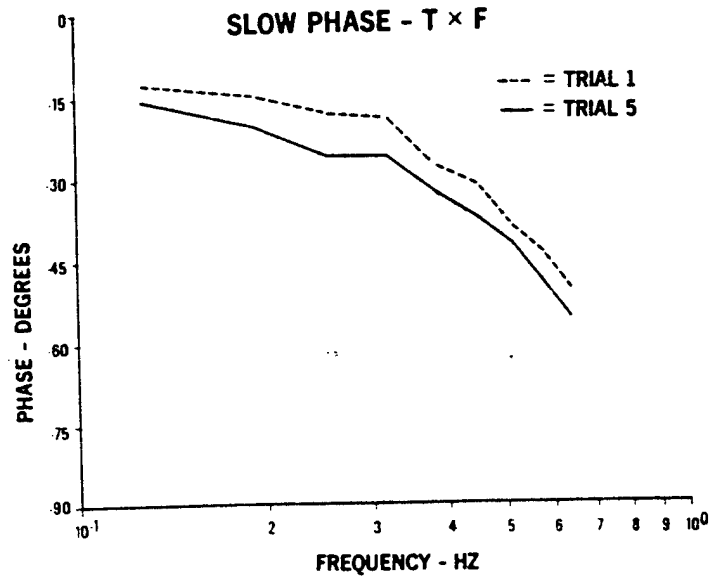and Vertical Tracking Dimensions: Slow (.5 Hz) Tracking
Data.

438
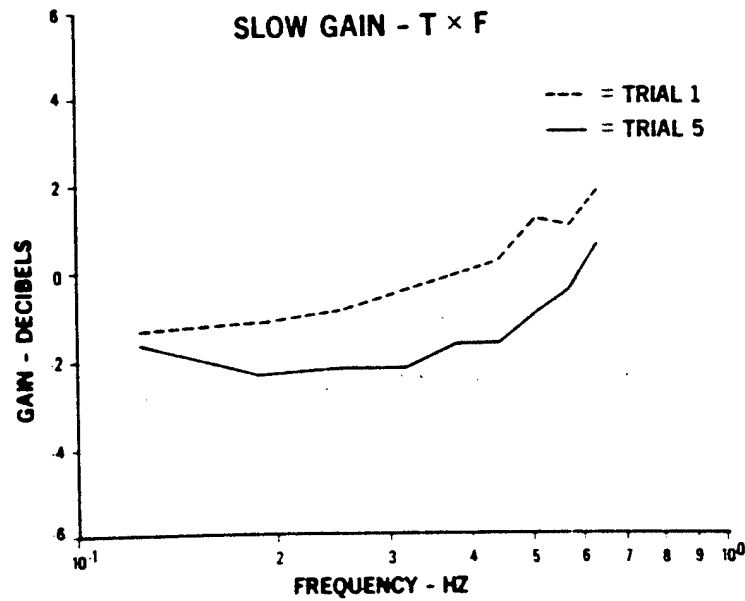
Figure 3. Gain as a Function of Frequency for Trial 1 and Trial 5: Slow (.5 Hz) Tracking Data.
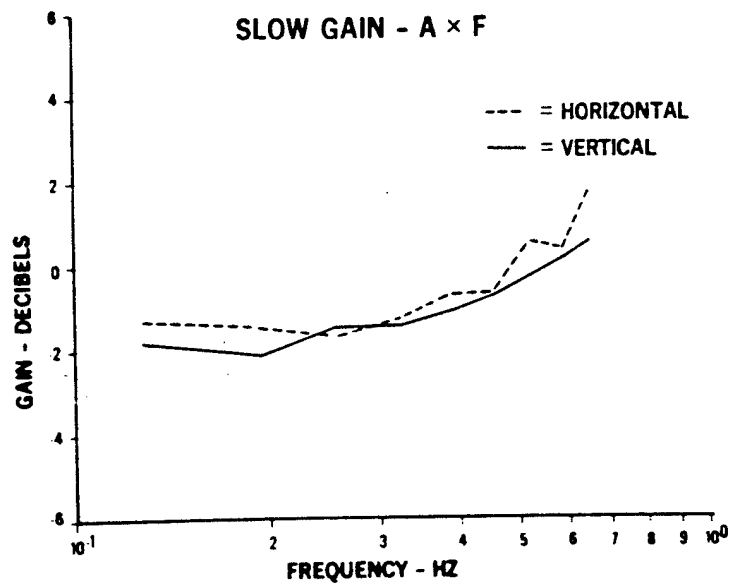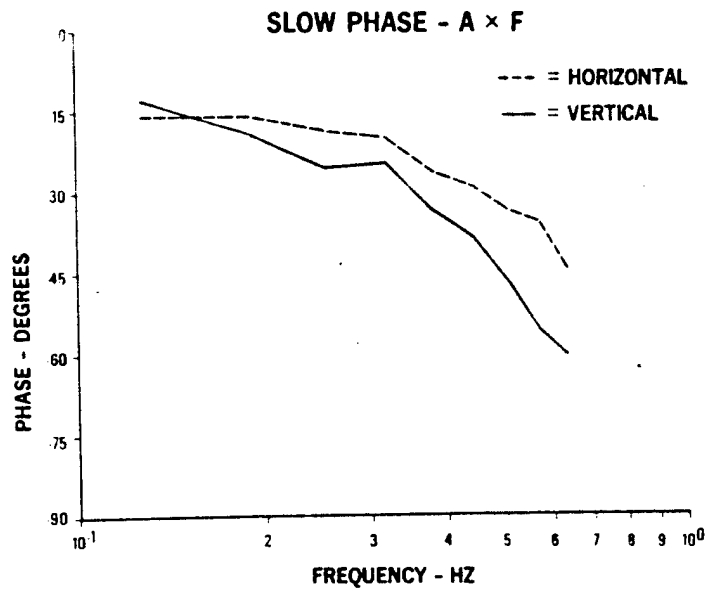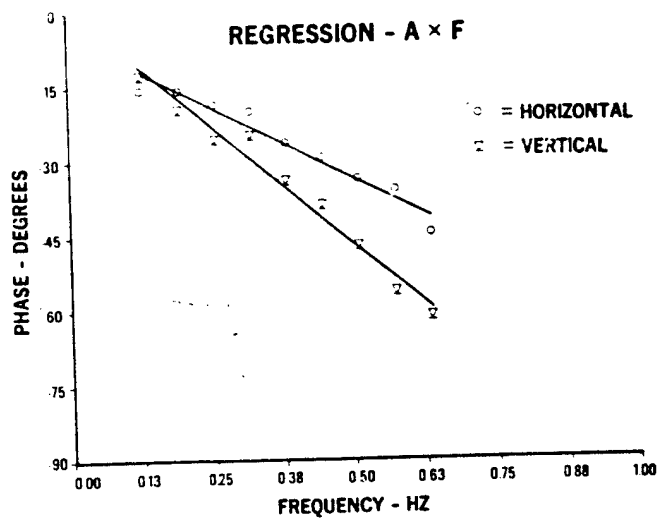

Figure 4. Gain as a Function of Frequency for Horizontal and Vertical Tracking Dimensions: Slow (.5 Hz) Tracking Data.

SLOW PHASE - T × F

--- = TRIAL 1
— = TRIAL 5

Figure 5. Phase as a Function of Frequency for Trial 1 and
Trial 5: Slow (.5 Hz) Tracking Data.

SLOW PHASE - A × F

--- = HORIZONTAL
— = VERTICAL

Figure 6. Phase as a Function of Frequency for Horizontal and
Vertical Tracking Dimensions: Slow (.5 Hz) Tracking
Data.

440
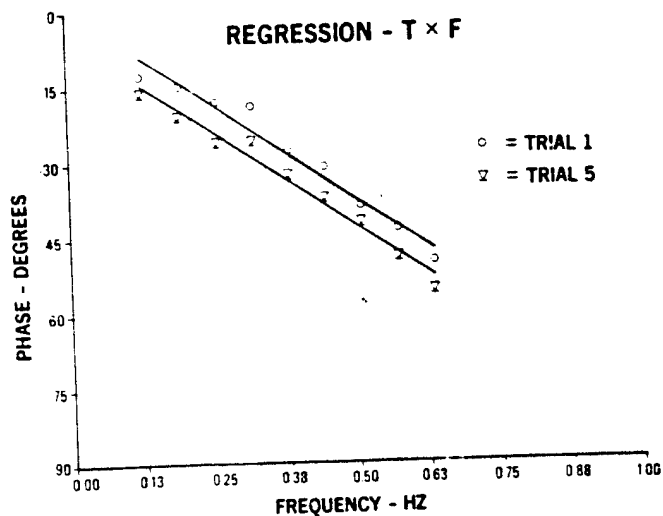
Figure 7. Regression Between Phase and Frequency for Trial 1 and Trial 5: Slow (.5 Hz) Tracking Data.

Figure 8. Regression Between Phase and Frequency for Horizontal and Vertical Tracking Dimensions: Slow (.5 Hz) Tracking Data.

441
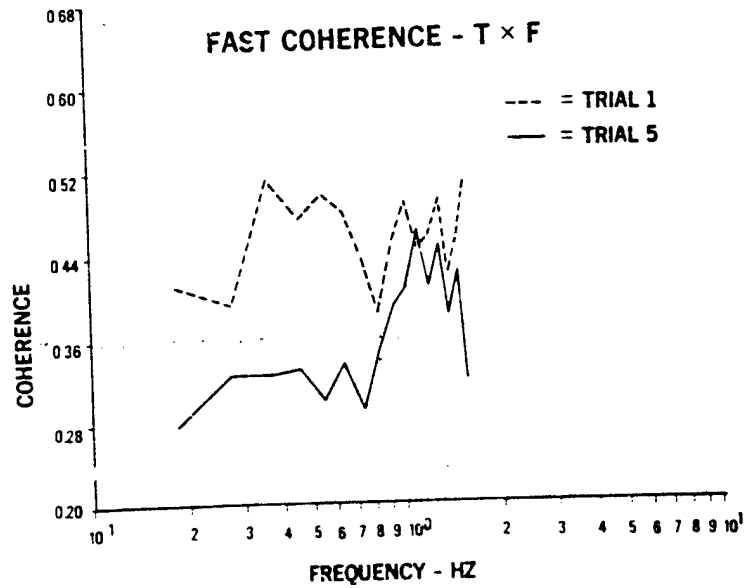
Figure 9. Coherence as a Function of Frequency for Trial 1 and Trial 5: Fast (1.5 Hz) Tracking Data.
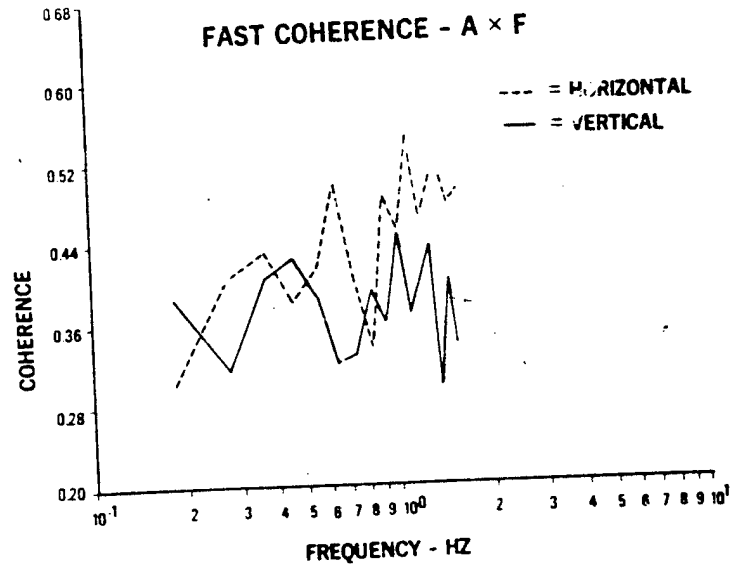

Figure 10. Coherence as a Function of Frequency for Horizontal and Vertical Tracking Dimensions: Fast (1.5 Hz) Tracking Data.

442

A COMPARISON OF IN-FLIGHT AND GROUND-BASED PITCH ATTITUDE

TRACKING EXPERIMENTS

by M.F.C. van Gool and H.A. Mooij

National Aerospace Laboratory NLR

SUMMARY

Servo-analysis, applying mathematical models of human pilot behaviour, is an efficient approach to broaden the understanding of the "match" between the characteristics of the flight control system-aircraft combination, the human pilot and the displays. Quasi-linear models can be used in this type of analysis.

The influence of motion on the human pilot characteristics in command-type pitch attitude tracking experiments is investigated in flight and in a moving-base flight simulator (also used fixed-base).

The results are compared with results of similar investigations published in the literature.

INTRODUCTION

Research directed at the development of criteria for good handling qualities of aircraft under manual control has been in the past and will be in the future an important on-going activity. The emergence of new techniques in aircraft design and the associated changes in operational use forms the most important reason for these activities. Recent emphasis on CCV/FBW (Control Configured Vehicle/Fly-By-Wire) technology to be applied in production type aircraft emphasizes the need for development of adequate handling quality criteria.

Handling quality criteria formulated in the form of "specifications" or "regulations" are in many cases not directly applicable to aircraft with the electrical, closed-loop, primary flight control systems as they are proposed in contemporary design studies.

Servo-analysis, applying mathematical models of human pilot control behaviour, is an efficient approach to broaden the understanding of the "match" between the characteristics of the flight control system/aircraft combination, the human pilot and the displays and can therefore be used in the formulation of handling quality criteria.

Quasi-linear models can be used in this type of analysis. Available quasi-linear models have been developed for certain simple piloting control tasks such as single-loop compensatory tracking, using data which

have been mainly obtained under laboratory-type experimental conditions. It is considered valuable to be able to validate the applicability of these models for particular circumstances such as handling qualities investigations using flight simulators. Following such a validation, servo-analysis studies can be carried out to predict stability and performance of the pilot-aircraft system for a wide range of dynamical configurations in the flight simulator. In addition, if knowledge on the relation between the pilot's control behaviour in flight simulators and in-flight is available, the prediction can be extended to the in-flight situation.

A discussion of the correlation of in-flight and ground-based measured pilot transfer characteristics based on results obtained during three experiments will be presented.

HUMAN OPERATOR DYNAMICS IN CLOSED-LOOP CONTROL SYSTEMS

Because many piloting problems involve principally one axis and because experimental analysis of the multiloop control situation is very complex, most of the research effort reported in the literature up to now has been related to the investigation of single-loop compensatory control systems. In such control situations, the pilot, characterized by the describing function Y_p, driving the controlled element, characterized by its transfer function Y_c, pays his attention to one control task having a visual stimulus which shows the "error" between command input and system output.

A helpful concept for describing the relation between the human pilot and the controlled element transfer characteristics in single-loop compensatory control systems is the "crossover model" as formulated by McRuer and others (Refs. 1 and 2).

Based on the observations of compensatory control systems covering a wide range of dynamic properties of the controlled element, the open-loop transfer function $Y_p Y_c$ can be represented by a single two-parameter model in the frequency range where $|Y_p Y_c| = 1$.

The model has the following form:

$$Y_p(j\omega) Y_c(j\omega) = \frac{\omega_c e^{-j\omega\tau_e}}{j\omega}$$

where ω_c = crossover frequency
τ_e = effective time delay

Up to now the majority of accurate describing functions have been determined only on the ground (and mostly from fixed-base experiments). The set of experiments, described in this paper covers in-flight as well as moving-base flight simulator and fixed-base flight simulator environments.

The dynamic characteristics of the controlled element (flight control system/aircraft combination) and the operational environment were the principal experimental variables during the investigations, listed below:
- Experiment I The controlled element was a pitch attitude controller with

pitch-rate-command/attitude-hold properties and selectable dynamic characteristics.

The experiments were carried out in flight with a Beechcraft Queen Air aircraft fitted with a model-following flight control system. The general expression for the transfer function of the controlled element is:

$$\frac{\theta}{\delta_s} = \frac{K_\theta(s+1/\tau_\theta)}{s(s^2+2\zeta_\theta\omega_\theta s+\omega_\theta^2)}$$

$1/\tau_\theta$, ω_θ and K_θ were selectable over a wide range while ζ_θ was maintained close to 0.7 in all cases.

The variable dynamics were mechanized according to the so-called Prefilter Model Following principle as described in reference 3.

- Experiment II The dynamics of the flight control system/aircraft combination were identical to those used in Experiment I, but the experiments were carried out in the moving-base flight simulator of the Department of Aeronautics and Space Engineering of the Delft University of Technology which was also used fixed-base.

- Experiment III The controlled element again was of the pitch-rate-command/attitude-hold type, although this characteristic was not obtained through model-following but was inherent to a pitch attitude controller designed around a simulated jet transport aircraft having neutral static stability as described in reference 4.

In one configuration Direct Lift Control (DLC) "augmentation" was provided for improving manoeuvring. Lift modulation was commanded directly by stick displacement through a wash-out filter. These experiments were carried out in the same flight simulator used in Experiment II.

This paper presents only a small part of the result of these experiments. More controlled elements than presented here have been evaluated. Furthermore remnant data, measured for all controlled elements, are not presented in this paper. However these results are presented in the complete report on these experiments, reference 5.

For Experiment I and II a comparison of the tracking results for one of the controlled elements (C-3) in different environments (in-flight, moving-base and fixed-base simulator) will be presented to demonstrate the effect of motion on human tracking behaviour. For Experiment III a comparison of the tracking results for two controlled elements having identical pitch attitude characteristics, but differing due to direct lift control augmentation (B-4 with, and A-1 without DLC), will be presented to demonstrate the effect of DLC-heave motion. The transfer functions of these controlled elements are presented in figure 1.

PILOT DESCRIBING FUNCTIONS AND MATHEMATICAL MODELS

Experiment I and II
The forcing function, injected into the display was a sum of 10 sinusoids with a cut-off frequency of 1.5 rad/sec. (4 sinusoids were used as low

amplitude high-frequency shelf). The average pilot describing functions for three environmental conditions are presented in figure 2.

In accordance with the crossover model a large amount of pilot lead has been generated. This can be demonstrated by the parameters of a 4-parameter pilot model that has been fitted to the describing functions:

$$Y_p = K_p \frac{\tau_L j\omega + 1}{\tau_I j\omega + 1} e^{-j\omega\tau_e}$$

K_p = gain
τ_L = lead time constant
τ_I = lag time constant
τ_e = effective time delay

With a fitting procedure that emphasizes a good fit in the neighbourhood of crossover frequency, the following average results are obtained:

	$K_p(\frac{deg\ stick}{cm\ display})$	$\tau_I(sec)$	$\tau_L(sec)$	$\tau_e(sec)$
In-Flight (2 pilots, 5 runs each)	0.5	0.1	8.0	0.26
Moving-Base (4 pilots, 5 runs each)	0.5	0.1	7.0	0.31
Fixed-Base (2 pilots, 5 runs each)	1.6	0.1	2.2	0.30

Fixed-base results are different from results with motion. With motion higher lead time constants and lower steady state gains are obtained.

Experiment III

The forcing function consisted of a sum of sinusoids forming a spectrum with a first-order roll-off shape with a cut-off frequency of 1 rad/sec (again augmented with a low-amplitude high-frequency shelf). The average pilot describing functions for the configurations with and without direct lift control are presented in figure 3.

The parameters of the 4-parameter pilot model, obtained in the same way as for Experiment I and II, are as follows.

	$K_p(\frac{deg\ stick}{cm\ display})$	$\tau_I(sec)$	$\tau_L(sec)$	$\tau_e(sec)$
With DLC (4 pilots, 5 runs each)	13.4	0.6	1.2	0.32
Without DLC (2 pilots, 5 runs each)	17.8	0.3	0.8	0.35

It is observed that with additional translational motion due to DLC, the gain decreases and the lead time constant increases.

Pilot-aircraft performance

Loop bandwidth and stability as expressed in crossover frequency and phase margin and the performance measures Score ($= 1 - \dfrac{\sigma_e^2}{\sigma_i^2}$), and relative remnant, ($\rho_{a_e}^2 = \dfrac{\sigma_{e_i}^2}{\sigma_e^2}$), related to the pilot's input, are as follows.

	ω_c	φ_m	Score	$\rho_{a_e}^2$
Exp. I In-Flight	1.7	35	0.34	0.66
Exp. II Moving-Base	2.0	31	0.55	0.74
Exp. II Fixed-Base	2.0	16	0.48	0.66
Exp. III Moving-Base with DLC	1.4	54	0.81	0.86
Exp. III Moving-Base without DLC	1.9	44	0.84	0.82

With respect to Experiments I and II it can be observed that in-flight the crossover frequency is lower, the phase margin is higher and the Score is lower than moving-base.

With respect to Experiment II, it is observed that moving-base the phase margin, Score and the relative remnant are higher than fixed-base.

With respect to Experiment III it can be observed that for the controlled element with DLC the crossover frequency is lower and the phase margin is higher than for the controlled element without DLC.

INFLUENCE OF MOTION

In the evaluation of the influence of motion on the outcome of the experiments it has to be kept in mind that command-type tracking has been carried out in which the displayed error signal is not congruent with the actual pitching motion and in which a frequency dependent relation exists between pitch and heave motion.

In general, sensing of angular motion, usually associated with the "semicircular canals" can be characterized as a second-order response to angular acceleration (Ref. 6). It is believed that a threshold is incorporated in this mechanism which has a value of 0.5 deg/sec^2. The dynamics of the second-order system are such that from 0.2 to 10 rad/sec, angular motion perception is proportional to angular rate. For prolonged turning the "subjective" signal

washes out. The treshold value for angular rate based on this number is 2.6 deg/sec for the pitch axis (Ref. 2)

Sensing of linear motion is ordinarily associated with the "utricles" which are sensitive to the total applied force (Because the utricles do not respond only to inertial accelerations but to the total applied force, they have to be considered specific force indicators).

For the discussion here, the inputs to the utricles will be referred to as accelerations. The model for linear motion sensing presented by the author of reference 6 can be characterized as that of a second-order system responding to linear acceleration. Because it is estimated that the two first-order break-points are located at frequencies of 0.1 and 1.5 rad/sec, the subjective perception of acceleration over the frequency range of interest is accompanied by large phase lags. It is believed that also in this case a threshold is present which has a value of 0.1 m/sec^2 (Ref. 6) for the vertical axis.

Possibly the mentioned threshold values are even higher in tracking experiments, because the pilot experiences both visual and motion inputs, as opposed to the experiments described in reference 6 were the subject concentrated solely on the task of detection motion.

To be able to estimate the amount of motion during the experiments, the level of motion in each of the three experiments has been computed. Root mean square (r.m.s.) values of pitch rate and vertical acceleration are as follows

	r.m.s. pitch rate (deg/sec)	r.m.s. vertical acceleration (m/sec^2)
Exp. I In-Flight	1.0	1.24
Exp. II Moving-base	1.1	0.08
Exp. III with DLC	1.9	0.08
Exp. III without DLC	2.1	0.05
Threshold of perception suggested	2.6	0.1

For Experiments I and II the r.m.s. values of pitch rate have been below the threshold of perception. The difference between Experiment I and II with respect to motion was the r.m.s. value of vertical acceleration which has been well above the perception threshold for Experiment I and of the same magnitude as the perception threshold for Experiment II.

For Experiment III the r.m.s. of pitch rate was somewhat below the perception threshold. With respect to the r.m.s. value of vertical acceleration an increase of 50 % is observed for the experiment with DLC as compared to the experiment without DLC. Assuming that during an appreciable part of the time a level of motion equal to twice the r.m.s. value existed, the vertical acceleration with DLC has been above the perception threshold.

Turning to the literature it is observed that most tracking investigations including rotational motion have been performed with disturbance-type

448

forcing functions, thus having rotational motion congruent to the displayed error signal; this type of investigations are described in references 7 to 11.

Although not directly applicable to the test described in this study it is remarked in reference 11 that previous work by R.S. Shirley (Sc.D. Thesis, M.I.T., 1968) has shown that addition of congruent motion (disturbance tracking) in a single-axis tracking task is beneficial if the lead information that the motion supplies is not redundant and can be used to maintain better control of the system. Another way of saying this is that the merits of motion are dependent on task difficulty in single-axis control tasks. However, it should be observed that the improved performance for Exp. II moving-base as compared to fixed base shows the same trend.

Stapleford, Peters and Alex (Ref.12, 1969) state that their studies indicated that motion cues will be used except when tracking a random-appearing command input with a compensatory display. Due to the fact that with a command input the visual system will only sense the difference between the input and the vehicle motion, while the vestibular system senses the actual vehicle motion there is a "conflict" between the two modalities involved. The authors of reference 12 conclude that when this conflict exists, the pilots apparently ignores the motion inputs.

A study on the effect of rotational motion using a large amplitude command-type forcing function is reported by Junker and Replogle (Ref. 13, 1975). The authors conclude from their investigations that, "the human operator will make use of large amplitude motion information when controlling a moving platform with dynamics of the general form K/s^2". A controlled element with K/s^2 characteristics discussed in the present paper is Controlled Element C-3, although the level of rotational motion was small.

No literature with respect to translational motion in command tracking could be located. Although not directly applicable to the tests described in this study it is considered interesting to mention that Ringland and Stapleford (Ref. 14, 1973) state that among others the following conclusions can be drawn from the work they performed with respect to disturbance tracking:

- Low level linear acceleration cues can be effectively used by pilots to improve performance in tracking tasks
- Performance improvements with linear motion cues are highly subject dependent.

CONCLUSIONS

Command-type tracking experiments have been carried out with a pitch-rate-command/attitude-hold flight control system controlled by side stick with and without motion.

The results of the experiments give reason to believe that the effect of rotational motion during the experiments resulted in an increase in system stability as well as in improved performance for a controlled element requiring low-frequency lead generation. This is observed for an experiment during which the simulator motion level was lower than the commonly

449

accepted threshold of human motion perception. This result is in accordance with an observation made by Junker and Replogle (1975) for large amplitude motion.

Translational motion existing during the tracking tasks (aircraft dynamics) lowered the values of crossover frequency and Score and thus degraded the pilot-aircraft performance in the pitch tracking tasks as compared to the performance obtained fixed-base.

REFERENCES

1. McRuer, D.T.; Graham, D.; Krendel, E.S. and Reisener, Jr. W.: Human Pilot Dynamics in Compensatory Systems: Theory, Models and Forcing Functions Variations. AFFDL TR-65-15 1965.

2. McRuer, D.T. and Krendel E.S.: Mathematical Models of Human Pilot Behaviour. AGARDograph No. 188 1974.

3. Mooij, H.A.: Flight Experience with an Experimental Electrical Pitch-Rate-Command/Attitude-Hold Flight Control System. AGARD-CP-137 1974.

4. Mooij, H.A.: Handling Quality Criteria Development for Transport Aircraft with Fly-by-Wire Flight Control Systems. NLR TR 74141 U 1975.

5. Gool, M.F.C. van and Mooij, H.A.: Human Pilot Describing Function, Remnant and Associated Information for Pitch Attitude Control: Results from In-Flight and Ground-Based Tracking Experiments. NLR TR 75062 U 1975.

6. Peters, R.A.: Dynamics of the Vestibular System and their Relation to Motion Perception, Spatial Disorientation and Illusions. NASA CR-1309 1969.

7. Guercio, J.C. and Wall, R.L.: Congruent and Spurious Motion in the Learning and Performance of a Compensatory Tracking Task. Human Factors, 14(3) 1972.

8. Bergeron, H.P. and Adams, J.J.: Measured Transfer Functions of Pilots during Two-Axis Tasks with Motion. NASA TN D-2177 1964.

9. Ringland, R.F.; Stapleford, R.L. and Magdaleno, R.E.: Motion Effects on an IFR Hovering Task-Analytical Predictions and Experimental Results. NASA CR-1933 1971.

10. Ringland, R.F. and Stapleford, R.L.: Experimental Measurements of Motion Cue Effects on STOL Approach Tasks. NASA CR-114458 1972.

11. Bergeron, H.P.; Adams, J.J. and Hurt, G.J.: The Effects of Motion Cues and Motion Scaling on One- and Two-Axis Compensatory Control Tasks. NASA TN D-6110 1971.

12. Stapleford, R.L.; Peters, R.A. and Alex, F.R.: Experiments and a Model for Pilot Dynamics with Visual and Motion Inputs. NASA CR-1325 1969.

13. Junker, A.M. and Replogle, C.R.: Motion Effects on the Human Operator in a Roll Axis Tracking Task. Aviation, Space and Environmental Medicine. June, 1975.

14. Ringland, R.F. and Stapleford, R.L.: Pilot Describing Function Measurements for Combined Visual and Linear Acceleration Cues. Proceedings of the Eight Annual Conference on Manual Control, AFFDL-TR-72-92. (1973).
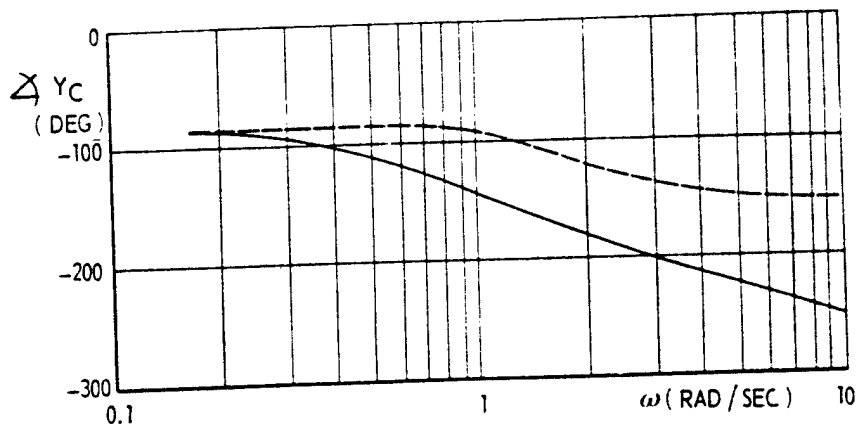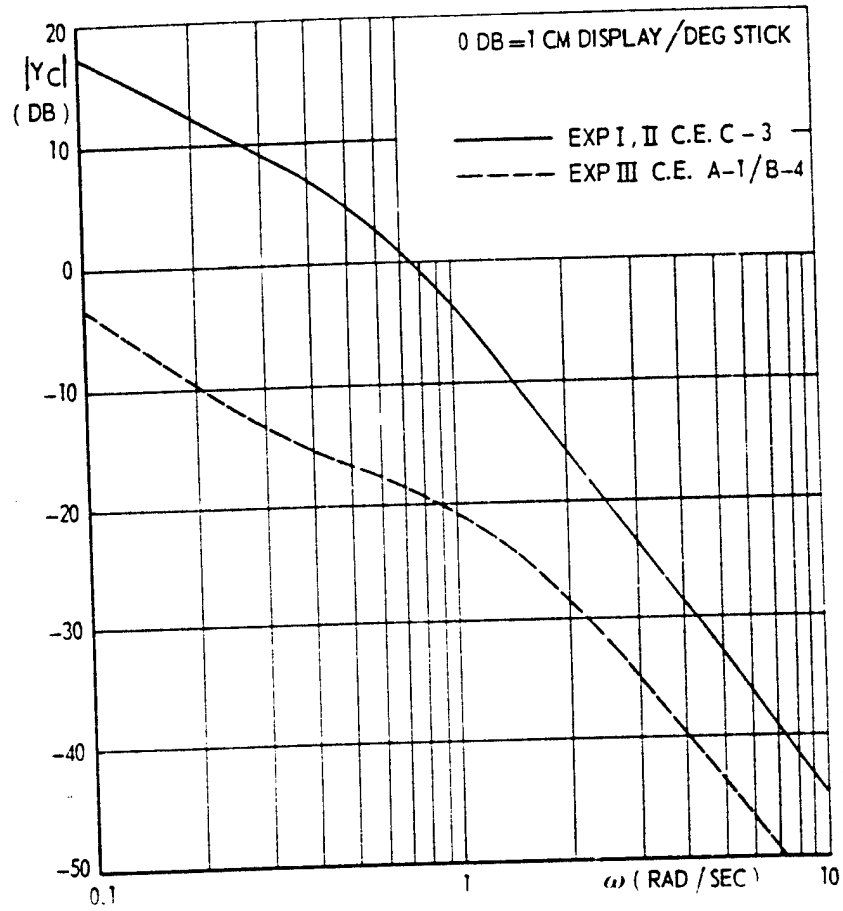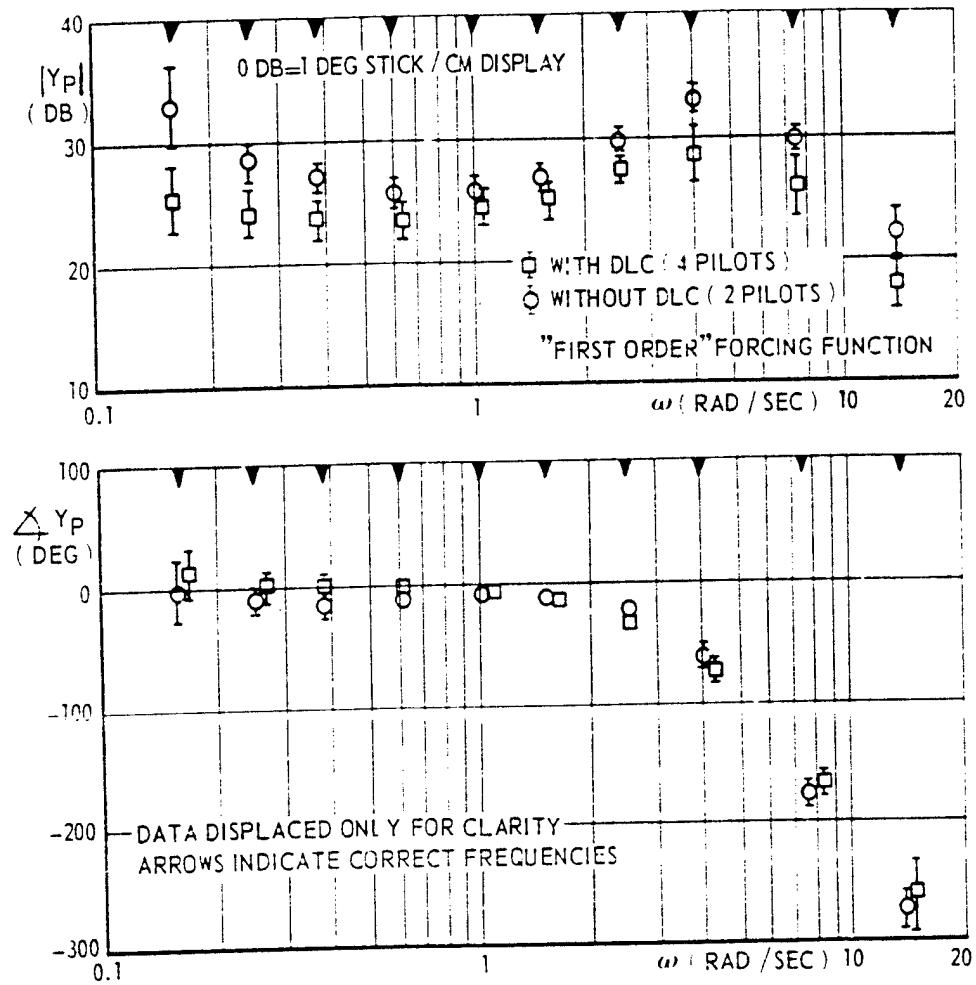
CONTROLLED ELEMENT DYNAMICS

Fig. 1
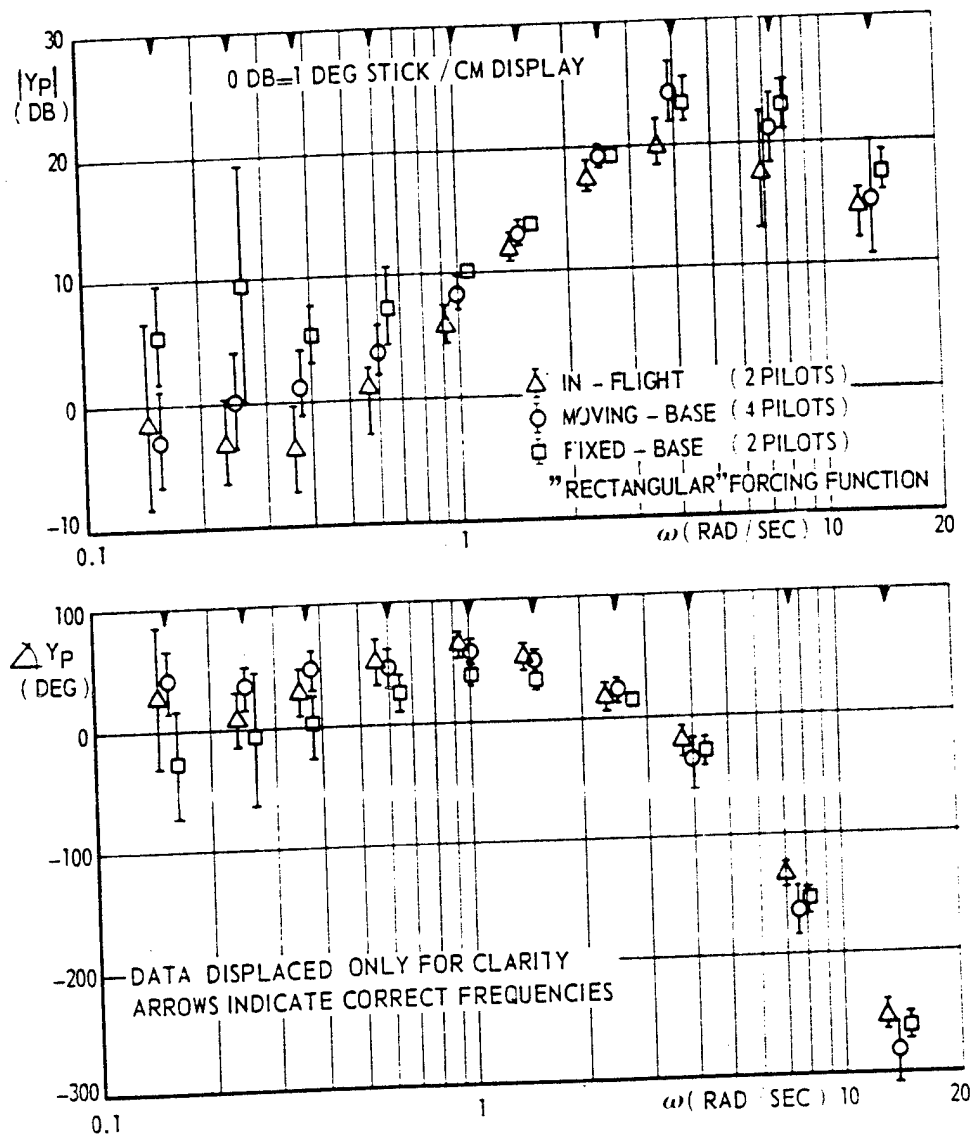
PILOT DESCRIBING FUNCTION FOR EXPERIMENT I AND II

Fig. 2

PILOT DESCRIBING FUNCTION FOR EXPERIMENT III

Fig. 3

EFFECTS OF HEADGEAR AND VISUAL ANGLE
ON HEAD ROTATION SPECTRAL CHARACTERISTICS

By D. K. Shirachi[1]

National Research Council
Resident Research Associate

D. L. Monk and J. H. Black, Jr.

Crew Station Integration Branch
Human Engineering Division
6570 Aerospace Medical Research Laboratory
Wright-Patterson AFB, Ohio 45433

SUMMARY

Dynamic characteristics of the unrestrained human head movement control system are measured as a function of headgear weight and size of the stimulus trajectory envelope. The coherence, gain and phase spectral characteristics are unaffected by variations in the weight of the helmet and associated head line-of-sight measurement hardware; however, a gain amplitude nonlinearity related to stimulus visual field size is shown to exist.

INTRODUCTION

Significant hardware developments during recent years now permit practical, remote measurement of an operator's head line-of-sight with good accuracy and reliability. The advent of this practical capability has stimulated numerous proposed applications of Visually Coupled Systems, control systems which are directed by natural head movements with feedback information displayed in the operator's visual

[1]Present address: Computer Sciences Corporation
1101 San Antonio Road
Mountain View, California 94043

field. The purpose of this investigation of head pursuit tracking was to provide dynamic performance data to aid in the evaluation of the head movement system as an active contro'' ' to identify important design considerations in the future development o   _d line-of-sight measurement systems.

Several DoD agencies and NASA are seriously consideri g potential applications of head-aimed control systems for aircraft flight control, head slaved simulator displays, navigation and reconnaissance sensor control, and target designation. Chouet and Young [1] have shown that a head position measurement device can be used as an efficient means of controlling vehicular attitude, especially for three-axis manual control, and other investigations of Visually Coupled Systems [2] have demonstrated the feasibility of head-controlled sensors and weapon systems. Head line-of-sight measurements are also being considered for selection and control of aircraft cockpit information displays and as a means of providing accurate bearing to way points for precision updating of onboard navigation systems.

All these applications of head control take advantage of the operator's proprioceptive feedback and utilize the rapid, precise head movement coordination which is a natural physiological activity in man and is coupled to his perception of and reaction to his environment. The research reported herein describes the characteristics of unrestrained head movement as a function of headgear weight and angular size of the visual field in which the pursuit task occurs.

METHODS

Experimental Apparatus

A Honeywell Helmet-Mounted Sight (HMS) which measures the operator's helmet angular line-of-sight in real-time was used to observe dynamic head movements. The Honeywell HMS [3] computed head line-of-sight coordinates from information generated by scanning infrared light beams transmitted from fixed-coordinate "light fans" mounted beside the experimental subject and received by infrared detectors mounted on a helmet worn by the subject. An electronic computation unit provided analog voltages corresponding to the horizontal and vertical coordinates of the head line-of-sight. The following three helmet configurations weighing 4-1/4, 3 and 2 pounds respectively were used in the experiments: a Navy Model LG1065; a Phase I, lightweight prototype, Model LG1087; and a modified Air Force Model LG1063 with visor, oxygen mask recepticles and associated hardware removed to reduce weight.

The moving target stimuli for the head pursuit tracking were generated by projecting a laser beam directed by an X-Y mirror galvanometer system onto a vertical viewing screen which subtended a visual angle of $\pm 20^\circ$ in both vertical and horizontal axes. The vertical and horizontal inputs to the galvanometer system were

uncorrelated and consisted of band-limited, Gaussian noise with a half-power bandwidth of 3 Hz. The helmet weight experiments used a $\pm 10^{\circ}$ visual field as the stimulus projection envelope, and the angular field experiments used amplitudes of $\pm 5^{\circ}$, $\pm 10^{\circ}$ and $\pm 15^{\circ}$ for the stimulus field.

The helmet weight experiments were conducted on two experimental subjects; the angular field experiments were performed on three experimental subjects. For all of the experiments, one subject was trained and the other subjects were untrained. The angular field experiments were performed with both the 2 and 4-1/4 pound helmets; however, since the results were identical, only data for the 2 pound helmet is presented here.

DATA ANALYSIS

The data analysis method chosen for investigation of the head movement system dynamics was power spectral analysis [4, 5], and the frequency information of the spectral analysis permitted a comparison of the authors' data with those in the literature. Using power spectral analysis techniques, one may directly compute the system's linear, input-output transfer function and coherence function which is a quantitative measure of the credibility associated with the computed linear transfer function.

It is assumed that the measured output response, $x(t)$, is the sum of an input stimulus, $u(t)$, multiplied by the system transfer function, $h(t)$, plus an additive noise source, $n(t)$, which is uncorrelated with the input.

$$x(t) = h(t) \ u(t) + n(t)$$

$$E[n(t) \ u(t)] = 0; \quad 0 \le t \le T$$

Performing a Fourier transformation of the input and output variables and converting to power spectra

$$G_{ux} = H \ G_{uu} + G_{nx}$$

where G_{uu} = auto-power spectrum of $u(t)$

G_{ux} = cross-power spectrum of $u(t)$ and $x(t)$

G_{nx} = cross-power spectrum of $n(t)$ and $x(t)$

E[ ] = expected value operator

457

Assuming that n(t) is uncorrelated with x(t), and n(t) is zero mean, Gaussian noise, then the use of ensemble averaging for the auto- and cross-power spectra for many segments of frequency computations causes G_{nx} to approach zero. Therefore,

$$\overline{G}_{ux} = H \, \overline{G}_{uu}$$

and

$$H = \frac{\overline{G}_{ux}}{\overline{G}_{uu}}$$

where $\overline{G}$ denotes the ensemble average.

The coherence function, γ^2, is defined as

$$\gamma^2 = \frac{\overline{G}_{ux}{}^2}{\overline{G}_{uu} \, \overline{G}_{xx}} \; ; \qquad 0 \le \gamma^2 \le 1.0$$

where G_{xx} = auto-power spectrum of x(t).

The coherence function is the proportion of input power contained by the output power spectrum and is a quantitative measure of the linear causal relationship between the input and output of a system.

Input-output cross-correlations were computed to determine the time delay of the output response relative to a given input stimulus. The lag time corresponding to the maximum value of the cross-correlation function is considered as the time delay of the measured input-output relationship.

The following time responses were recorded: horizontal stimulus, vertical stimulus, horizontal head movement response and vertical head movement response. For each of the stimulus-response pairs, cross-correlation functions, coherence functions and transfer function gain and phase angle spectra were computed so that direct and cross-coupled characteristics of each coordinate axis could be determined.

RESULTS

Helmet Weight

Data recorded from the helmet weight experiments showed no appreciable

differences in the coherence, phase angle or gain characteristics when HMS helmet weight was increased. The spectral characteristics for two subjects are shown on Figures 1 through 6, and these curves show no appreciable differences between helmets of different weight.

Based upon the definition of half-power bandwidth which is the frequency region in which the input-output signal power transfer function remains above 0.5 of maximum signal transmissibility (Bendat and Piersol [4]) and forming an analogous definition for the coherence function where a coherence value of 0.5 is analogous to the half-power point, the bandwidth of the head movement system was found to be approximately 2.0 Hz.

The transfer function gain varied between 0.3 and 0.4 for horizontal movements and 1.0 and 1.5 for vertical movements (figures 3 and 4). One can easily observe that the vertical gain was much greater than the horizontal gain, and these results agree with those of Shirachi and Black [6].

The phase angle curves showed no differences as a function of increasing helmet weight (figures 5 and 6), and the phase angle was a linear function of frequency as determined by a linear least squares fit of the data points with a correlation coefficient greater than 0.98.

Visual Field Size

In contrast with the results for the helmet weight experiments, there was a significant effect of visual field size on the transfer function gain (figures 7, 8 and 9). An increase of visual field size produced sizeable increases of gain throughout the response bandwidth of the head movement system. It should also be noted that the vertical gains were always greater than the horizontal gains, just as in the helmet weight experiments. The $\pm 5^{o}$ stimulus envelope produced quite small gains in the region of 0.07 to 0.15 (horizontal) and 0.2 to 0.7 (vertical) and the $\pm 15^{o}$ envelope produced gains of 0.6 to 1.5 (horizontal) and 1.1 to 3.0 (vertical). These results indicate that an interaction exists between the transfer function gain and size of the stimulus visual field.

The coherence functions for the visual field experiments were similar to those for the helmet weight experiments. Stimulus amplitude appeared to have negligible effect on coherence (figure 10a).

The phase angle curves also showed no amplitude effects (figure 10b), and they were linear with frequency just as in the helmet weight experiments. However, the phase angles in the high frequency region near 1.5 Hz showed less phase lag than the phase curves for the helmet weight experiments.

459

CONCLUSIONS

The head movement system had previously been thought to exhibit linear behavior which can be modeled by a constant gain term in series with a time delay element (Shirachi and Black [6]). However, new experimental evidence which shows an amplitude-dependent transfer function gain relationship has been presented in this paper which appears to challenge the linear model of Shirachi and Black. The invariance of the coherence and phase angle characteristics with stimulus field size combined with an amplitude-dependent gain characteristic do not conform to the linear system model. It is not readily apparent what mechanism or mechanisms are operating to produce the amplitude-dependent behavior presented here. Transfer function gain may be influenced by head and eye interaction at small stimulus amplitudes. Another probable factor is target angular velocity which varies as a function of stimulus amplitude when the forcing function bandwidth is constant. However, future experimentation is necessary in order to provide sufficient data to explain the transfer function gain behavior.

REFERENCES

1. Chouet, B. A. and L. R. Young. Tracking with head position using an electro-optical monitor. IEEE Trans. Syst., Man and Cybernetics. SMC-4: 192-204, 1974.

2. Birt, J. A. and H. L. Task, ed. Proc. Symp. Visually Coupled Systems: Development and Application. AMD TR-73-1. (AD 916572) 1973.

3. Ferrin, F. J. F4 visual target acquisition system. Proc. Symp. Visually Coupled Systems: Development and Application. AMD TR-73-1. (AD 916572) 1973.

4. Bendat, J. S. and A. G. Piersol. Random Data: Analysis and Measurement Procedures. Wiley-Interscience, New York. 1971.

5. Roth, P. R. Effective measurement using digital signal analysis. IEEE Spectrum. 8: 62-70, 1971.

6. Shirachi, D. K. and J. H. Black, Jr. Head-eye tracking in two-dimensional pursuit tasks. Proc. Eleventh Annual Conf. Manual Control. NASA TM X-62,464, 1975.

LIST OF FIGURES

COHERENCE FUNCTION

FIGURE 1

FIGURE 2

462
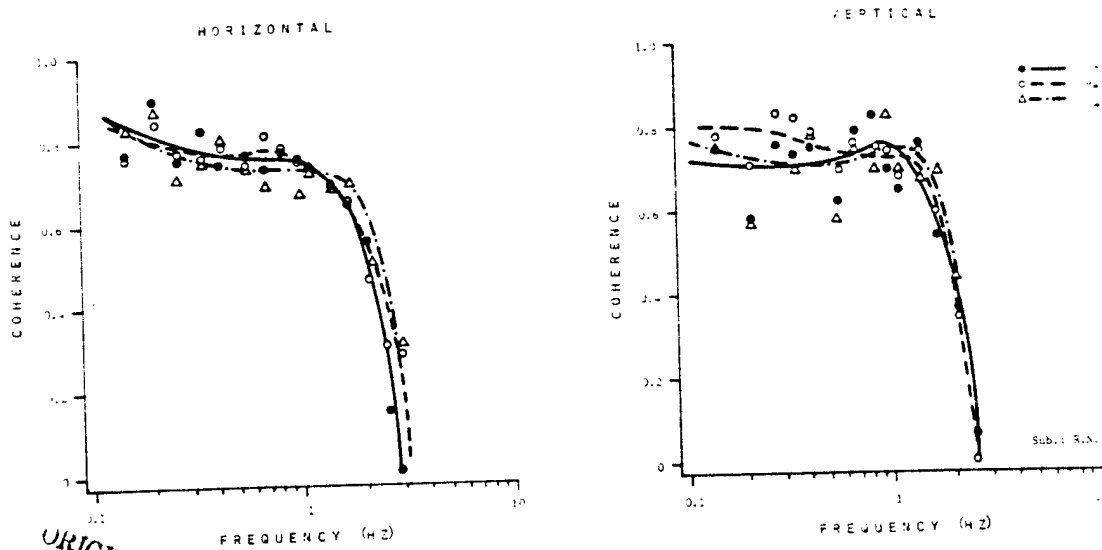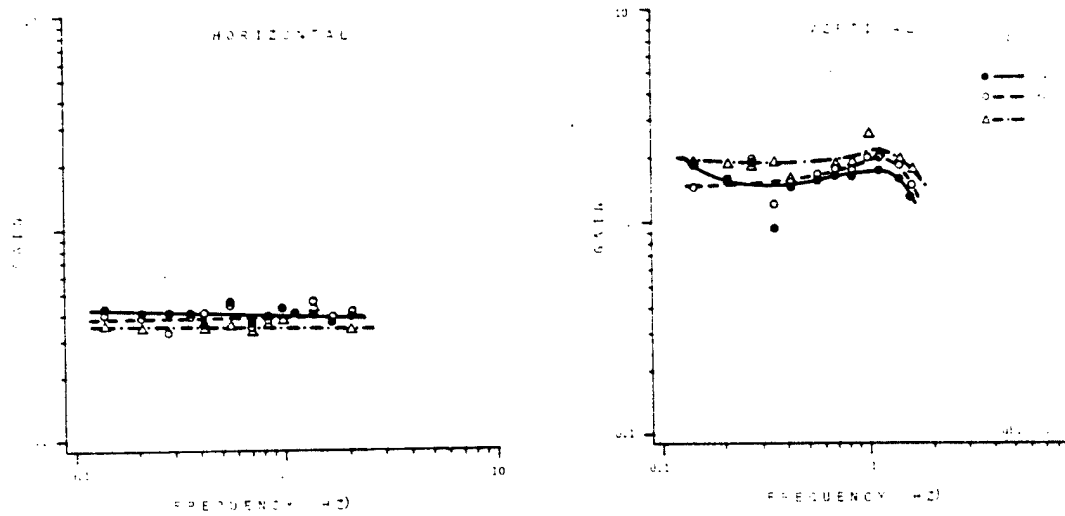
FIGURE 3

FIGURE 4

TRANSFER FUNCTION PHASE

HORIZONTAL   VERTICAL

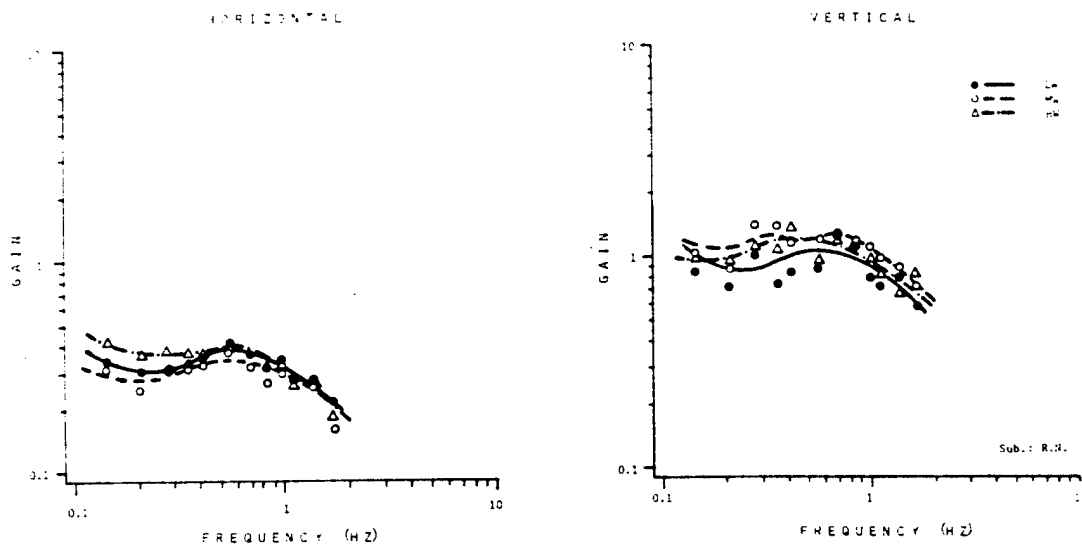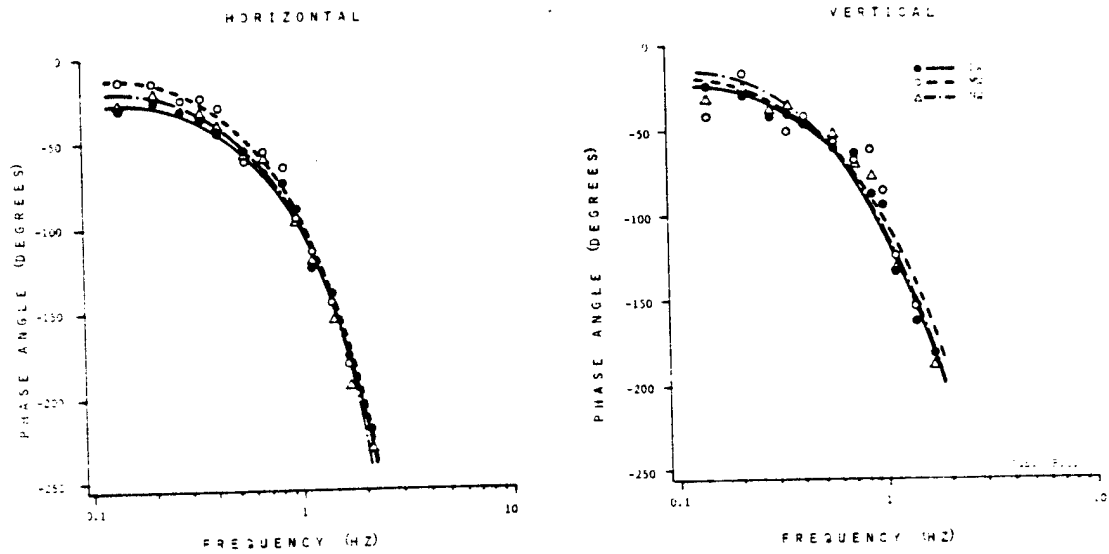FIGURE 5

FIGURE 6
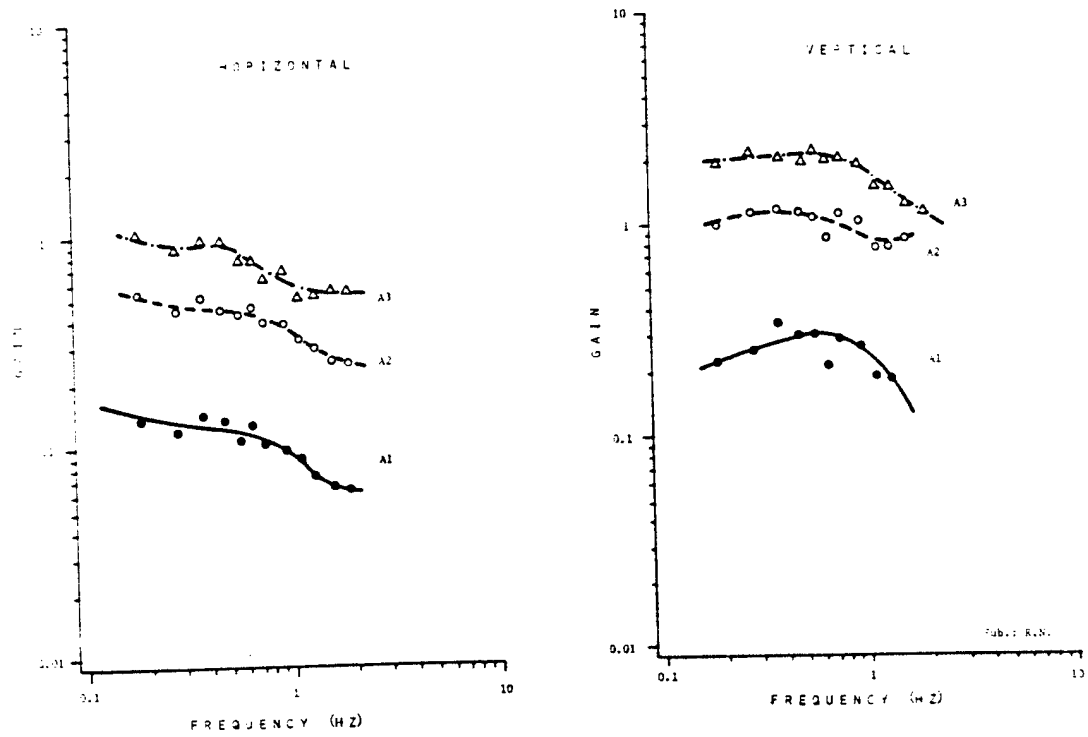
TRANSFER FUNCTION GAIN
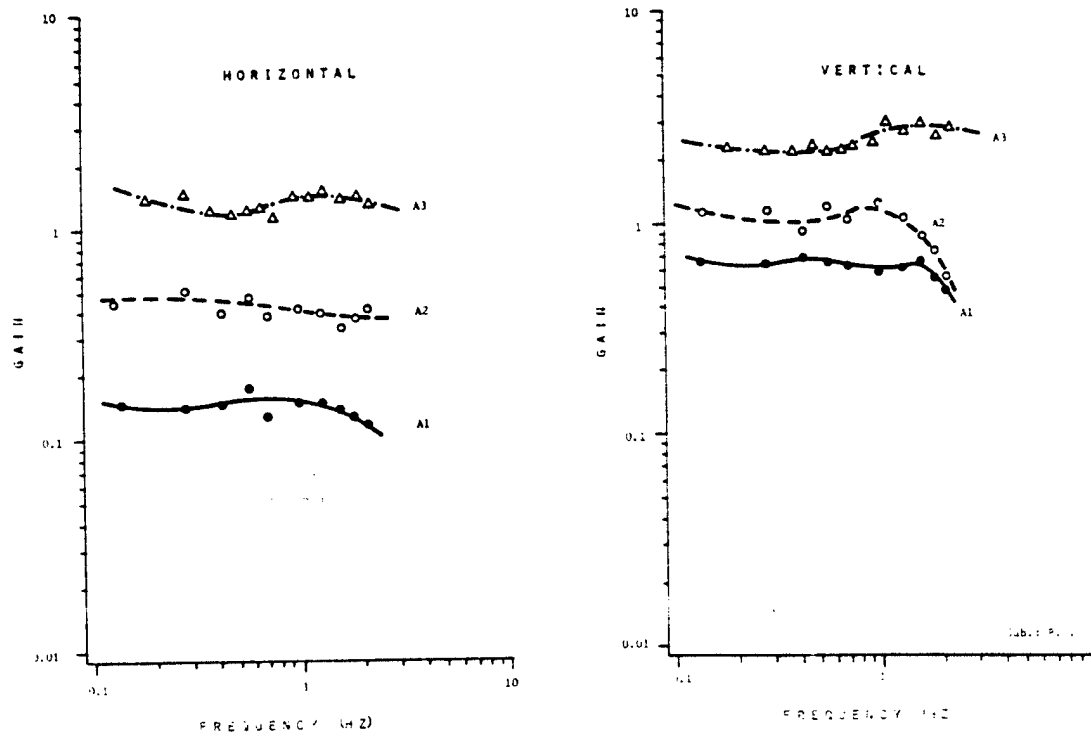
FIGURE 7

TRANSFER FUNCTION GAIN

FIGURE 8

466

TRANSFER FUNCTION GAIN
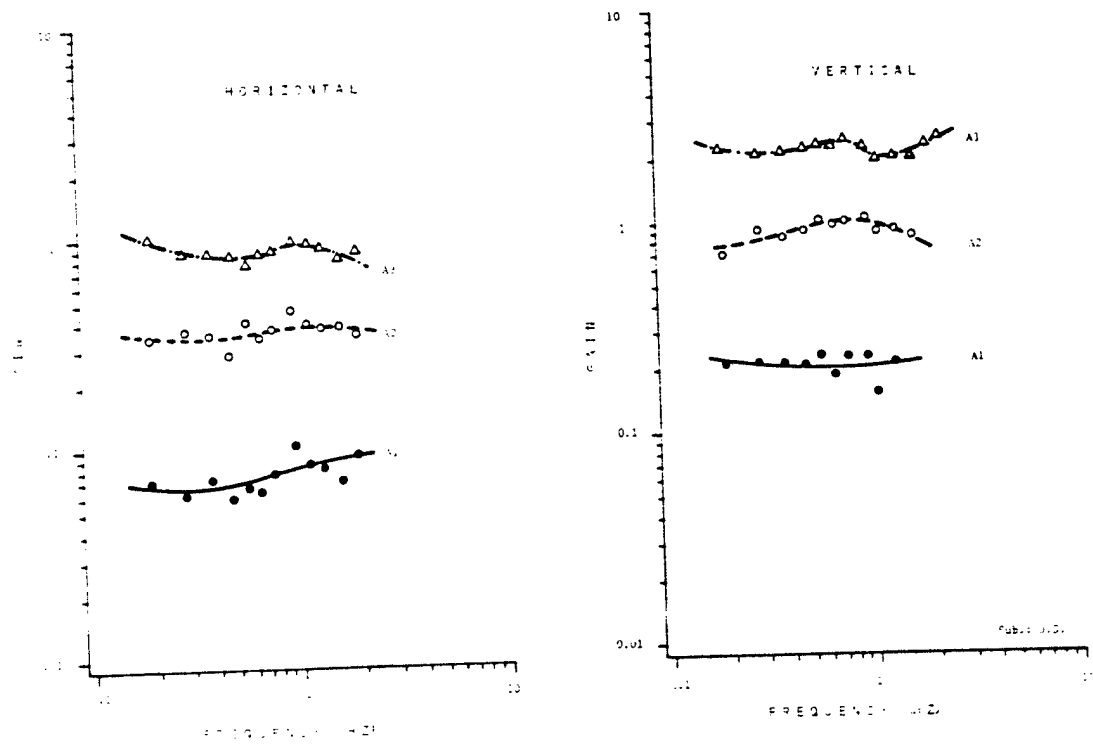

FIGURE 9

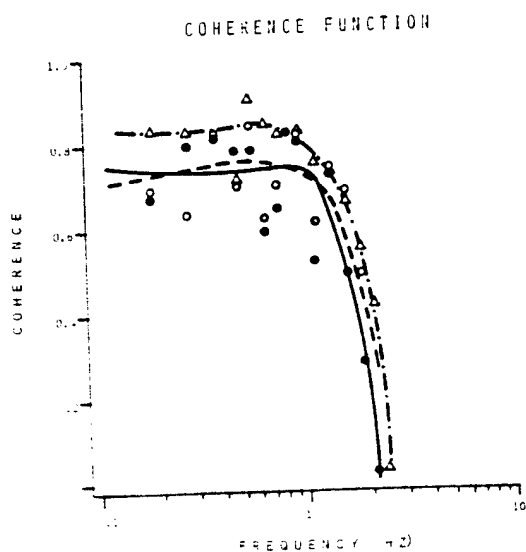COHERENCE FUNCTION

TRANSFER FUNCTION PHASE
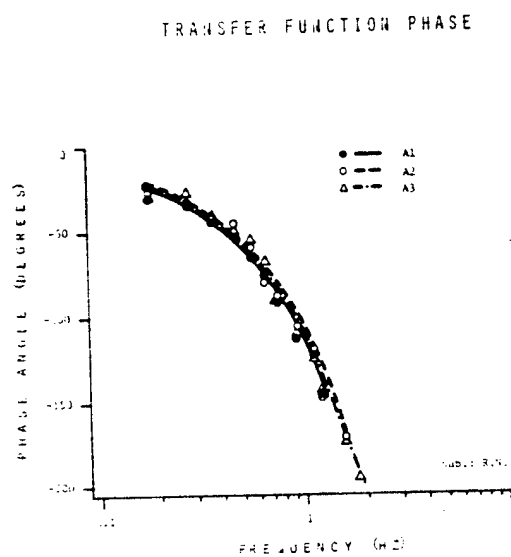

FIGURE 10a

FIGURE 10b

HUMAN ENGINEERING LABORATORY HELICOPTER OBSERVER PERFORMANCE STUDIES

By John A. Barnes

U. S. Army Human Engineering Laboratory
Aberdeen Proving Ground, Maryland

The Systems Performance and Concepts Directorate of the U. S. Army Human Engineering Laboratory has, since 1972, been conducting a series of flight studies relating to some of the typical tasks performed by the U. S. Army helicopter observer. The first series of observer performance studies were called the Human Engineering Laboratory Helicopter Acquisition Tests (HELHAT).

HELHAT I

The initial study, reference 1, was conducted in October 1972 at the Naval Weapons Center, China Lake, California. This study was performed in conjunction with a tri-service target detection/acquisition test. The test was designed to help determine which was the most advantageous location for the observer position in operational helicopters, figure 1. The 68 simulated tactical low level route reconnaissance missions were flown by pilot observers from the 1st Cavalry Division using AH-1 and OH-58 helicopters. The targets were twenty items of 1950-60 era ordnance and three bridges set along a three leg, seven mile flight course over rough terrain with a cover of scrub growth.

The results indicated that although the observers detected a slightly larger number of targets from the left seat of the OH-58, there were no significant differences in the number of detections that could be attributed to the location of the observer in the helicopter.

HELHAT II

The second flight study, reference 2, was conducted in July and August of 1973 at Aberdeen Proving Ground, Maryland. This study was designed to allow us to determine whether a single observer or the pilot and observer team could perform a better job of target detection/acquisition during low level route reconnaissance using the OH-58. The 36 pilots and pilot observers who flew the 24 flights that made up this study were again from the 1st Cavalry Division, and many of them had flown in the previous study at China Lake.

The flight course was set up along a three leg, 15 mile route over the flat wooded area of Aberdeen Proving Ground and nine items of 1950-60 era ordnance and six "Fire Orange" boxes were the targets. The boxes, which measured 4 feet by 8 feet by 1 foot were used as control targets.

| OH-58 | AH-1 | AH-1 |
| O P | 0 / P | P / 0 |
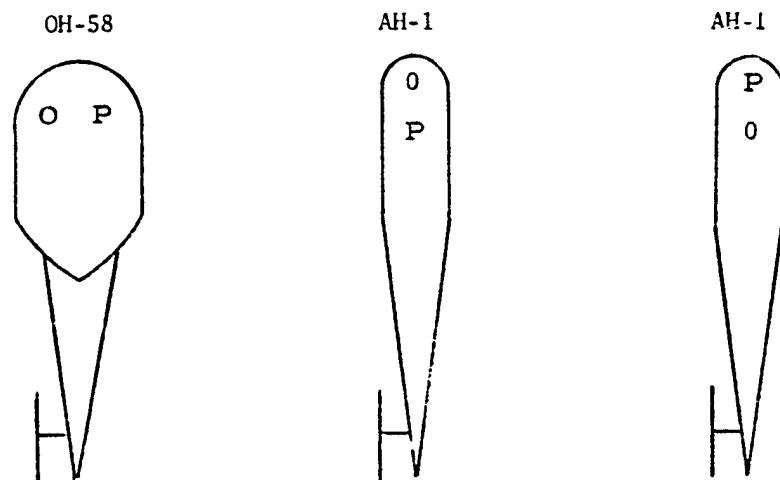
CONFIGURATION

| Pilot Right | Observer Front | Pilot Front |
| Observer Left | Pilot Rear | Observer Rear |

Fig. 1.   Experimental Configurations

An ancillary six flight Nap-of-the-Earth (NOE) test was flown after the main study had been completed. This test was flown at the lowest possible altitude depending upon the height of the ground cover; the altitudes varied from three to thirty feet as the crews flew an "S" pattern reconnaissance along the last leg of the low level course in the reverse direction. The NOE crews had great difficulty in maintaining their geographical orientation: crews 4 and 6 became lost and had to be told by the over-flying control aircraft to climb out and return to the base. Crew 5 also became disorientated, but they momentarily went to a higher altitude to reorient themselves and then proceeded to finish the mission NOE. All of these crewmen had combat experience and had had some NOE training.

The results of HELHAT II are shown in Tables 1 and 2.

470

TABLE 1. TARGETS DETECTED

TARGET TYPE	CREWS	OBSERVERS	NOE
ORDNANCE	40%	42%	44%
ORANGE BOX	76%	42%	67%
OVERALL	55%	42%	55%

TABLE 2. NOE DETECTION RANGE (METERS)

TARGET

CREW	15	14	13	12	11	10
1	520	120		470		640
2	160	370	350	770	220	1110
3				780	400	
4	460	200		1470		1280
5	340	100	90	600		
6						

HELHAT

The final portion of this series, reference 3, was published in 1974 and contained the major portions of HELHAT I and II as well as the target detection ranges achieved by the subjects during these two flight studies. The maximum detection ranges and the helicopter altitudes that accompanied them are shown in Table 3. These data, along with other pertinent facts about each detection, were processed using a multiple regression technique to try to determine the significant factors that contribute to successful target detection.

TABLE 3

Low Altitude Target Detection Efforts
(APG and NWC)

Target	Description	Volume (Cubic Feet)	Minimum Detection AGL Minimum AGL (Feet)	Range (Meters)	Maximum Detection Range Maximum Range (Meters)	AGL (Feet)
NWC 3	M-211 Trucks (3)	1674 ea	80	1060	1800	280
NWC 6	M-4 Tractor	1273	100	930	1020	210
NWC 10	V-62 Van	1715	80	580	740	320
APG 5	V-62 Van w Antenna[a]	3405	84[b]	570	640	249[c]
NWC 23	Bridge, 2 lane	148,200	100	460	785	150
NWC 22	Supply Dump	69,445	100	420	660	250
NWC 24	Bridge, 1 lane	102,400	90	380	1470	260
NWC 19	M-37 Truck (3)	578 ea	90	280	1130	190
NWC 26	Pickup Truck	665	90	280	890	230
NWC 11	75mm Sky Sweep Gun (3)	1944 ea	90	230	550	270
NWC 16	V-62 Van w Antenna	2910	90	220	1060	340
APG 4	Day-Glo Orange Box	32	80[b]	140	840	214[b]
NWC 15	M-47 Tank	2620	110	250	510	200
NWC 17	Truck, Amphibious	2259	110	580	1290	310
NWC 4	M-535 Van	1678	120	1160	2200	330
APG 1	M-258 Van	2397	120[c]	620	1800	362[b]
NWC 12	Searchlight (3)	307 ea	120	310	441	150
NWC 13	M-38 Jeep (2)	177 ea	120	190	470	300
NWC 14	75mm Sky Sweep Gun	1944	120	190	280	160
NWC 7	Bridge, 1 lane	21,760	140	370	760	280
NWC 27	Tractor and Tanker	3115	160	880	1030	220
APG 2	Day-Glo Orange Box	32	186[b]	230	600	351[c]
NWC 9	V-62 Van	1715	190	670	830	250
APG 3	M-259 Van w Antenna	3394	189[c]	570	1880	251[b]
NWC 2	105mm Howitzer (3)	720 ea	210	1060	1060	210
NWC 1	M-48 Tank	2881	220	610	2320	340
APG 12	Day-Glo Orange Box	64	239[b]	220	400	328[b]
NWC 5	90mm Gun Mount	1637	250	637	1000	330
APG 10	Day-Glo Orange Box	32	268[b]	210	640	361[b]
APG 13	M-21 Rocket Launcher (3)	422 ea	296[b]	950	950	296[b]
APG 15	Day-Glo Orange Box	32	316[b]	400	600	419[b]
APG 14	M-21 Rocket Launcher	422	310[b]	200	500	362[b]
APG 6	M-38 Hard-Top Jeep	434	307[c]	100	500	434[b]
APG 7	Day-Glo Orange Box	64	329[c]	1600	1600	329[c]
APG 9	XM387E1 Missile Truck	1316	370[c]	1240	1290	392[c]
NWC 8	Truck, Amphibious	2259	370	700	700	370

[a]This van had been extended by 3 feet.

[b]Crew score

[c]Observer score

The results of the stepwise multiple regression analysis of the 268 detections in which the desired 29 measures for each detection were available indicated that the significant aspects of target detection were;

        Sighting Angle
        Terrain Slope/Roughness
        Target Background Conspicuity
        Target Foreground Conspicuity
        Target Distance from Flight Path
        Aircraft Heading
        Aircraft Altitude Above Ground Level
        Aircraft to Target Range
        Apparent Target Size
        Bearing Estimate Error

When the HELHAT data were analyzed, not considering Conspicuity and Range and Bearing Estimate Errors, there were some changes in the significant variables. These 831 detections added;

        Target Difficulty
        Relative Bearing to Target
        Cloud Cover
        Target Length
        Target Volume

and caused the deletion of Terrain Slope/Roughness and Apparent Target Size.

POP-UP STUDY

A third flight study, reference 4, investigated the effectiveness of a helicopter using the pop-up tactic and a simulated wire-guided missile against a heavy tank's main gun. This test was flown in August of 1975 at Aberdeen Proving Ground. This was a dynamic encounter rather than a passive one such as HELHAT; the study was primarily to test the ability of the tank crews of two different types of heavy tanks to defend themselves against a helicopter gunship, therefore it was the tank crew that changed rather than the air crew. The test scenario called for the Forward Observer to direct the helicopter to move to one of the eight preselected positions to perform the pop-up tactic. The tank crews had been briefed that they would be liable to encounter helicopter missile fire on certain portions of the extensive tank road course.

The mean Air-to-Ground and Ground-to-Air detection ranges are shown in Table 4. The "LOS Range" entry is the maximum possible range at which either vehicle could have seen the other from that position. The "ND" entry indicates that the tank crew did not detect the helicopter during the attack from that position. A typical engagement plan is shown in figure 2. The Forward Observer located in the area of CP 22G alerts the helicopter to proceed to pop-up position II for the attack as the tank will be in his line-of-sight
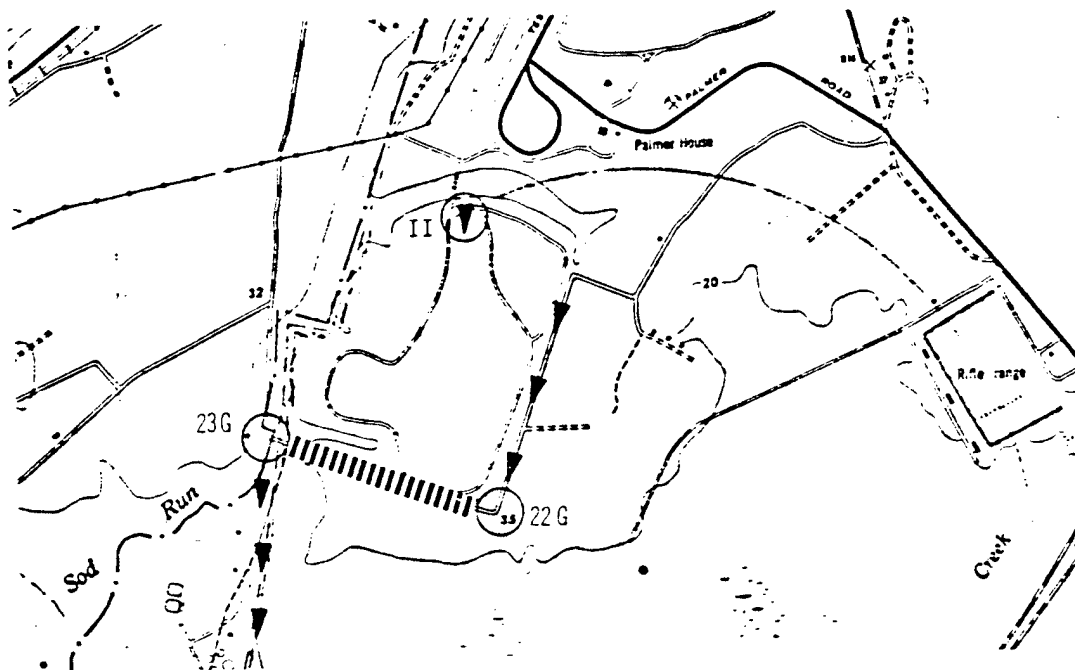
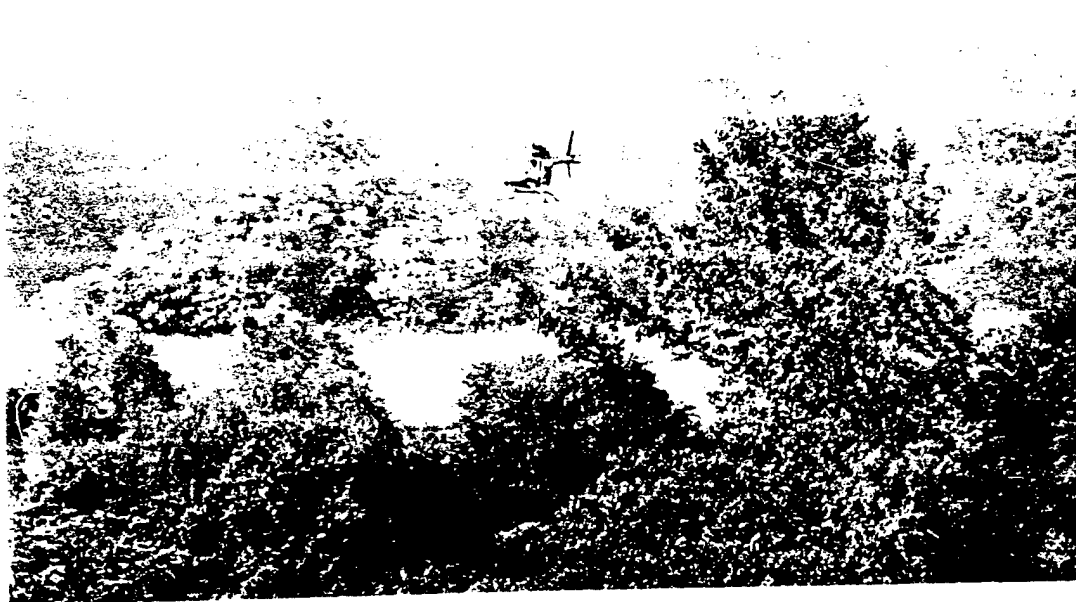Fig. 2. CP 22G to CP 23G Course Segment, Pop-Up Position II

Fig. 3. Helicopter At Pop-Up Position II, Ready For Missile Launch

474

after it passes CP 22G enroute to CP 23G. Figure 3 shows the helicopter in firing position at position II; an OH-58 was used as a substitute for the AH-1 because of scheduling problems. Figure 4 shows the helicopter on a simulated gunnery run against the tank; this procedure was used to alert the tank crew that they had been under missile attack and that if they had not seen the helicopter before, it was too late!

TABLE 4. POP-UP RESULTS (METERS)

POP-UP POSITION	LOS RANGE	MEAN A-TANK RANGE		MEAN F-TANK RANGE	
		AIR/GND	GND/AIR	AIR/GND	GND/AIR
1	2250	1640	1511	1631	1070
2	1000	1000	1000	1000	1000
3	3000	1480	1125	1700	1125
4	1400			1100	1120
5	1800	1200	720		
6	1750	1420	485	1303	840
7	2100			2030	ND
8	2950			2100	ND

HELCAT

The current effort, Human Engineering Laboratory Camouflage Application Test (HELCAT), is the air-to-ground portion of a larger, interagency camouflage application test in which the detectability of pattern painted tanks is being compared to that of camouflaged tanks. The day and night airborne phases will be flown in mid-June. During the day phase we will, for the first time, record the observer's actual eye point of regard during an air-to-ground target search. We will measure the single glance dwell time, the total dwell time and the observer field of view for each of the day target detections. The night phase will use the AN/PVS5 Night Vision Device as an observer aid.

The results of the study will compare observer's daytime target detection performance, against pattern painted and camouflaged tanks, with and without the eye movement measurement device. The night portion will compare the observer target detection performance, against the same tanks, with and without the AN/PVS5 Night Vision Device, and the unencumbered day performance with the night AN/PVS5 performance. These results should tell what part of.

Fig. 4. Helicopter On Firing Pass From Pop-Up Position II.

the camouflage on the tanks needs to be improved to prevent detection, the amount of detection degradation from day conditions to be expected when the AN/PVS5 devices are used, and the gain in night detection capability to be expected when the AN/PVS5 devices are used.

REFERENCES

1. Barnes, John A.: HELHAT I, The Effect of Observer Position On Target Detection. HEL TM 7-73, 1973.

2. Aviation Team, Systems Performance and Concepts Directorate: HELHAT II, Scout Crew/Observer Target Detection Flight Tests. HEL TN 1-74, 1974.

3. Barnes, John A.: Human Engineering Laboratory Helicopter Acquisition Test (HELHAT). HEL TM 20-74, 1974.

4. Barnes, John A.: Use of the Tank Main Gun for Defense Against Helicopter Attack. HEL TM 14-76, 1976.

INTERACTION BETWEEN WARNING SIGNAL AND FORE-PERIOD

IN SIMPLE FOOT REACTION TIME

Nataraj S. Nataraj
Engineering Technologies
Sinclair Community College
Dayton, Ohio 45402

John M. Howard
Dept. of I.E. and O.R.
Wayne State University
Detroit, Michigan 48202

ABSTRACT

This paper reports in part the results of an experiment set up to study the effects of interaction between the fore-period and warning signal on a simple foot reaction time task. The task required the subject to respond with a lateral movement of the right foot from right to left after observing the onset of a temporal visual event. Reaction times were recorded for various combinations of fore-periods and warning signals. Interpretation of results are made with respect to design and operation of foot controls.

INTRODUCTION

In the operation of machine-foot controls the human operator is sometimes required to respond after a varying interval of time which is preceded by a warning signal of variable length. Man/machine interface of this type is most common in an industrial environment. In this setting it is common to find an operator monitoring a set of machine-readiness lights, manipulating material with his hands and operating the machine functions with one or both of his feet. Successful operation of this type of machine is dependent upon many variables, such as working environment, operator experience and motivation, and machine design. In certain situations operator speed of response is crucial to successful and safe machine operation. One factor that may have an observable effect upon the operator's speed of

477

response is temporal expectancy. Temporal expectancy is defined as an increasing readiness to respond to events (signals) that occur over time. The measurement of simple reaction time can be used as an observation of an increasing readiness to respond. In general, as readiness increases, reaction time decreases.

Naatanen (1970) in a review of the literature points out two diverging tendencies with respect to the relationship between fore-period and simple reaction time: (1) when the fore-period is not varied, a general observation is that the longer the fore-periods, and (2) when fore-periods of different duration are randomly presented, the reaction time—in addition to its being generally longer than in the aforementioned case, is longest after the shortest fore-period in a series. It has also been observed that the longest fore-period in a series yields the shortest reaction time. Naatanen in conclusion proposed that four factors exert an influence on the relationship between fore-period and the reaction time when varying fore-periods with a given range are delivered in a random order. Two of these factors act via the variables called "expectancy": (1) the expectancy-reducing effect of the flow of time after the warning signal, because longer periods are more difficult to estimate than shorter ones; and (2) the expectancy-increasing effects of the flow of time after the warning signal, because the objective probability of the occurence of the stimulus increases.

Several earlier studies used the term expectancy to describe the subject's change in reaction time over a range of time intervals. Deese (1955: 363) hypothesized that "expectancy should be low immediately after a signal, should increase as the mean intersignal interval approaches, and

finally should become quite high as the intersignal interval goes beyond the mean." Baker (1959) offered another hypothesis suggesting that expectancy increases as intersignal interval increases until the mean intersignal interval and then expectancy decreases as fore-period increases further. Both hypotheses have been supported by research. The major difference between the studies supporting one or the other of the hypotheses was in the size of the range of fore-periods.

In experiments that supported the theory of increasing expectancy, ranges of less than 5 sec. were used, while in experiments that supported a U-shaped function the ranges were 18 sec. or greater. In those experiments the varying fore-periods were always preceded by a warning signal of fixed length.

Since the intervals appropriate to the operation of foot-operated industrial machines (such as described previously) are relatively short, and usually include a warning signal (machine ready signal) of varying length, the range of fore-periods and warning signals used in this experiment were short.

Following from those earlier studies it was expected that temporal expectancy and therefore speed of reaction time would vary as a function of the interaction between the duration of both a fore-period (FP) interval within a range of FP and a warning signal (WS) within the range of WS. To test this hypothesis a range of eight common values of WS and FP were paired with itself and with each of the other seven values, producing 64 paired presentations of WS and FP. The eight common values were 250 msec., 500 msec., 1, 2, 3, 4, 5, and 7 sec.

METHOD

Subjects. Forty-eight (30 males, 18 females) volunteer college students served as subjects. All subjects were screened for the absence of visual color defects, corrected 20/20 visual acuity and physical disability with regard to the right leg and foot movement. Twenty-nine male and 15 female subjects were right leg dominant. Table 1 gives the subject characteristic for age, weight and stature.

Apparatus. The foot reaction time measurement apparatus is shown in Figure 1. It consisted of a vertical-horizontal adjustable seat that provided for control of subject knee angle, 30° off vertical. The start and experimental targets were each 6 cm. in diameter and placed 15 cm. apart. The display consisted of a yellow warning signal (WS) and red stimulus light which were mounted vertically (WS below) on a gray panel 15 cm. apart. The gray panel was positioned 266 cm. in front of the subject at seated eye height from the floor. Each light was 6 cm. in diameter. The recording equipment included a sandal sole approximating a 9 1/2 shoe with a brass spike (protruding 2 cm. downward) affixed to the center of the sole. The sandal was attached to the subjects' right foot with straps. The targets were brass plates. An electronic timing measuring device (Beckman Universal Timer) was used to measure response time in 1/1000 sec. Response time was measured from onset of the red stimulus light until the experimental target was contacted.

Experimental Design. Using a table of random numbers, the experimenters assigned a random sequence for the presentation of 64 combinations of WS and FP. The presentation order was counterbalanced to minimize the effects

TABLE I

BIO DATA OF SUBJECTS

	MALE (30)		FEMALE (18)		TOTAL (48)	
	MEAN	STD. DEV.	MEAN	STD. DEV.	MEAN	STD. DEV.
Age (years)	23.45	3.77	23.37	5.08	23.21	4.31
Stature (meters)	1.79	0.07	1.64	0.05	1.73	0.10
Weight (kg.)	75.33	13.91	56.20	10.00	68.70	14.74
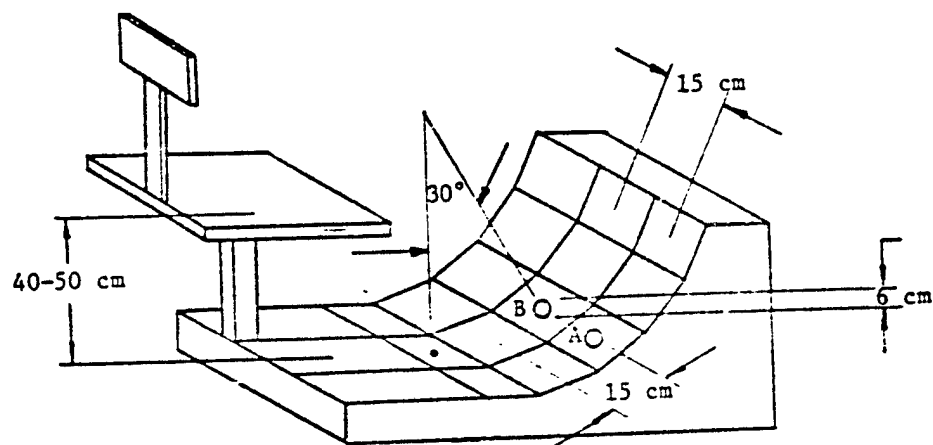
A - Starting Position

B - Experimental Target (6 cm. in diameter)

FIGURE 1 - DIMENSIONS OF THE FOOT REACTION-TIME MEASUREMENT APPARATUS

of subject learning and fatigue. The complete test session took approximately 50 min. All subjects were tested between the hours of 10:00 A.M. and 4:00 P.M. Subjects were not provided with knowledge of results during testing. Subjects were given 5 unscored practice trials (3 sec. WS, 3 sec. FP), during which they became familiar with the foot reaction time measurement apparatus. All subjects were debriefed following testing.

Instruction Given to the Subject. The subject was instructed to sit comfortably but straight, his thighs horizontal, with his right foot over the target. The knee angle was measured 30° off vertical. If necessary, the chair was adjusted to achieve this body posture. The subject was instructed to fixate on the black dot located on the gray panel before them. A yellow light would appear in the circle toward the bottom of the panel and a red light would appear in the circle to the top. The yellow light appeared first, went off and then was followed by the red light. When the red light appeared, the subject was asked to move as rapidly as possible from the start position (right plate) to the experimental target on the left. The speed of this movement was the main objective, and therefore the subject was told not to worry about the accuracy of the foot movement, although hitting the target plate was essential to achieving timed scores. After each trial the subjects were free to rest their right leg in any desired position. When the next trial was to begin the subjects were asked to reset their leg to the start position and again fixate on the black dot. Subjects were not permitted to hold onto the apparatus seat during testing.

TABLE II

REACTION TIMES FOR WS OR FP KEPT CONSTANT AT 250 M.SECS.

WARNING SIGNAL OR FORE PERIOD	WARNING SIGNAL KEPT CONSTANT AT 250 M.SEC.			FORE PERIOD KEPT CONSTANT AT 250 M.SEC.		
	N*	MEAN (m.sec.)	STD. DEV. (m.sec.)	N*	MEAN (m.sec.)	STD. DEV. (m.sec.)
250 m.sec.	48	170.93	38.00	48	170.98	46.03
500 m.sec.	47	178.96	40.76	48	173.17	43.58
1 sec.	48	182.27	49.87	48	184.19	45.30
2 sec.	48	190.27	47.88	48	179.58	40.65
3 sec.	48	196.65	61.15	48	181.13	37.38
4 sec.	48	189.08	50.71	47	186.94	36.62
5 sec.	48	189.75	44.68	48	180.58	38.56
7 sec.	48	187.69	48.19	48	184.56	45.13

TABLE III

REACTION TIMES FOR WS OR FP KEPT CONSTANT AT 500 M.SECS.

WARNING SIGNAL OR FORE PERIOD	WARNING SIGNAL KEPT CONSTANT AT 500 M.SEC.			FORE PERIOD KEPT CONSTANT AT 500 M.SEC.		
	N*	MEAN (m.sec.)	STD. DEV. (m.sec.)	N*	MEAN (m.sec.)	STD. DEV. (m.sec.)
250 m.sec.	47	172.04	42.33	47	178.96	40.76
500 m.sec.	43	180.31	39.74	48	179.90	39.62
1 sec.	47	190.32	49.15	48	199.77	60.19
2 sec.	47	187.36	47.45	47	197.13	57.35
3 sec.	47	191.02	38.48	48	179.58	44.94
4 sec.	47	188.36	44.74	48	182.81	43.18
5 sec.	47	193.19	46.99	48	194.35	50.18
7 sec.	48	210.96	49.68	48	189.73	43.70

* NUMBER OF SUBJECTS

TABLE IV

REACTION TIMES FOR WS OR FP KEPT CONSTANT AT 1 SEC.

WARNING SIGNAL OR FORE PERIOD	WARNING SIGNAL KEPT CONSTANT AT 1 SEC.			FORE PERIOD KEPT CONSTANT AT 1 SEC.		
	N*	MEAN (m.sec.)	STD. DEV. (m.sec.)	N*	MEAN (m.sec.)	STD. DEV. (m.sec.)
250 m.sec.	48	184.19	45.31	48	182.06	49.93
500 m.sec.	48	198.21	58.95	47	190.32	50.43
1 sec.	48	204.10	53.08	48	204.15	55.57
2.sec.	48	195.15	50.77	48	189.15	42.42
3 sec.	48	194.13	50.78	48	187.31	51.20
4 sec.	48	194.88	44.22	48	188.73	46.14
5 sec.	48	200.25	45.52	48	193.52	49.51
7 sec.	44	191.41	49.17	48	192.90	53.01

* NUMBER OF SUBJECTS

TABLE V

REACTION TIMES FOR WS OR FP KEPT CONSTANT AT 2 SECS.

WARNING SIGNAL OR FORE PERIOD	WARNING SIGNAL KEPT CONSTANT AT 2 SEC.			FORE PERIOD KEPT CONSTANT AT 2 SEC.		
	N*	MEAN (m.sec.)	STD. DEV. (m.sec.)	N*	MEAN (m.sec.)	STD. DEV. (m.sec.)
250 m.sec.	48	179.63	41.03	48	190.46	48.57
500 m.sec.	48	196.35	57.40	47	187.23	47.51
1 sec.	48	189.15	42.42	48	195.15	50.77
2 sec.	47	194.28	46.79	47	194.06	49.20
3 sec.	48	203.31	58.75	48	187.96	49.18
4 sec.	48	188.75	41.59	48	189.77	48.90
5 sec.	48	191.25	52.27	48	188.70	45.81
7 sec.	47	190.38	43.09	48	186.83	56.21

*NUMBER OF SUBJECTS

TABLE VI

REACTION TIMES FOR WS OR FP KEPT CONSTANT AT 3 SECS.

WARNING SIGNAL OR FORE PERIOD	WARNING SIGNAL KEPT CONSTANT AT 3 SEC.			FORE PERIOD KEPT CONSTANT AT 3 SEC.		
	N*	MEAN (m.sec.)	STD. DEV. (m.sec.)	N*	MEAN (m.sec.)	STD. DEV. (m.sec.)
250 m.sec.	48	181.27	37.35	48	196.02	61.63
500 m.sec.	48	179.60	44.95	48	192.71	38.76
1 sec.	48	188.88	53.16	48	196.48	52.25
2 sec.	48	188.02	46.86	48	203.31	61.12
3 sec.	47	189.81.	44.63	48	187.71	43.50
4 sec.	48	192.04	46.52	48	183.10	39.08
5 sec.	48	205.04	49.33	48	204.71	50.47
7 sec.	48	192.81	48.53	48	192.92	46.66

* NUMBER OF SUBJECTS

TABLE VII

REACTION TIMES FOR WS OR FP KEPT CONSTANT AT 4 SECS.

WARNING SIGNAL OR FORE PERIOD	WARNING SIGNAL KEPT CONSTANT AT 4 SEC.			FORE PERIOD KEPT CONSTANT AT 4 SEC.		
	N*	MEAN (m.sec.)	STD. DEV. (m.sec.)	N*	MEAN (m.sec.)	STD. DEV. (m.sec.)
250 m.sec.	47	189.06	39.04	48	188.60	50.63
500 m.sec.	48	182.81	42.81	47	188.40	44.71
1 sec.	48	188.31	48.86	48	190.52	50.01
2 sec.	48	189.81	48.55	48	187.50	43.30
3 sec.	48	183.21	39.03	48	181.94	46.59
4 sec.	48	185.58	39.94	48	185.69	40.04
5 sec.	48	192.23	41.58	48	192.25	50.23
7 sec.	48	192.60	44.76	47	187.66	45.88

* NUMBER OF SUBJECTS

TABLE VIII

REACTION TIMES FOR WS OR FP KEPT CONSTANT AT 5 SECS.

WARNING SIGNAL OR FORE PERIOD	WARNING SIGNAL KEPT CONSTANT AT 5 SEC.			FORE PERIOD KEPT CONSTANT AT 5 SEC.		
	N*	MEAN (m.sec.)	STD. DEV. (m.sec.)	N*	MEAN (m.sec.)	STD. DEV. (m.sec.)
250 m.sec.	48	176.63	44.59	48	189.75	44.68
500 m.sec.	48	193.83	48.33	48	192.63	51.18
1 sec.	48	194.56	50.46	48	200.25	45.27
2 sec.	48	188.79	46.43	48	190.96	51.74
3 sec.	48	204.71	46.11	48	205.04	49.33
4 sec.	48	192.38	48.11	48	192.23	43.93
5 sec.	48	192.46	49.92	48	192.88	53.13
7 sec.	42	196.15	56.17	48	190.92	50.30

* NUMBER OF SUBJECTS

TABLE IX

REACTION TIMES FOR WS OR FP KEPT CONSTANT AT 7 SECS.

WARNING SIGNAL OR FORE PERIOD	WARNING SIGNAL KEPT CONSTANT AT 7 SEC.			FORE PERIOD KEPT CONSTANT AT 7 SEC.		
	N*	MEAN (m.sec.)	STD. DEV. (m.sec.)	N*	MEAN (m.sec.)	STD. DEV. (m.sec.)
250 m.sec.	48	182.48	41.80	48	184.77	51.93
500 m.sec.	47	190.47	51.15	48	210.96	49.68
1 sec.	46	193.72	52.02	44	191.34	48.37
2 sec.	46	187.83	46.27	48	190.19	42.66
3 sec.	46	192.78	47.31	48	192.81	48.53
4 sec.	47	183.59	51.64	48	193.02	44.72
5 sec.	45	191.19	42.10	47	196.38	56.07
7 sec.	47	186.26	39.58	47	186.26	44.85

* NUMBER OF SUBJECTS

TABLE X

REGRESSION VALUES OF REACTION TIMES FOR WS-FP KEPT CONSTANT

WARNING SIGNAL OR FORE PERIOD	WARNING SIGNAL KEPT CONSTANT		FORE-PERIOD KEPT CONSTANT	
	Y-INTERCEPT (m.sec.)	SLOPE	Y-INTERCEPT (m.sec.)	SLOPE
250 m.sec.	180.030	1.996	175.800	1.526
500 m.sec.	177.484	4.118	185.870	0.672
1 sec.	-195.307	-0.007	190.140	0.308
2 sec.	190.570	0.376	191.750	-0.601
3 sec.	182.707	2.454	195.467	-0.337
4 sec.	185.660	0.808	189.150	-0.026
5 sec.	188.546	1.368	195.070	-0.260
7 sec.	189.012	-0.166	195.804	-0.910

RESULTS

Results are presented first for the eight common values of FP and WS; these are followed by the regression analysis for each FP and WS kept constant. Data were eliminated from the analysis for trials which subjects failed to respond to stimulus or evidenced unusually long reaction time.

The mean, standard deviation and the number of subjects for each WS-FP combination are shown in Tables II through IX. For 128 combinations of WS-FP, the mean reaction time values ranged from 170.98 m.secs. to 210.96 m.secs. The variability of reaction time varied from 36.62 m.secs. to 61.63 m.secs. The linear regression values for WS-FP kept constant are presented in Table X. The negative regression slope was found when WS was 1 sec. and 7 sec. and for FP values of 2, 3, 4, 5 and 7 secs. In all cases
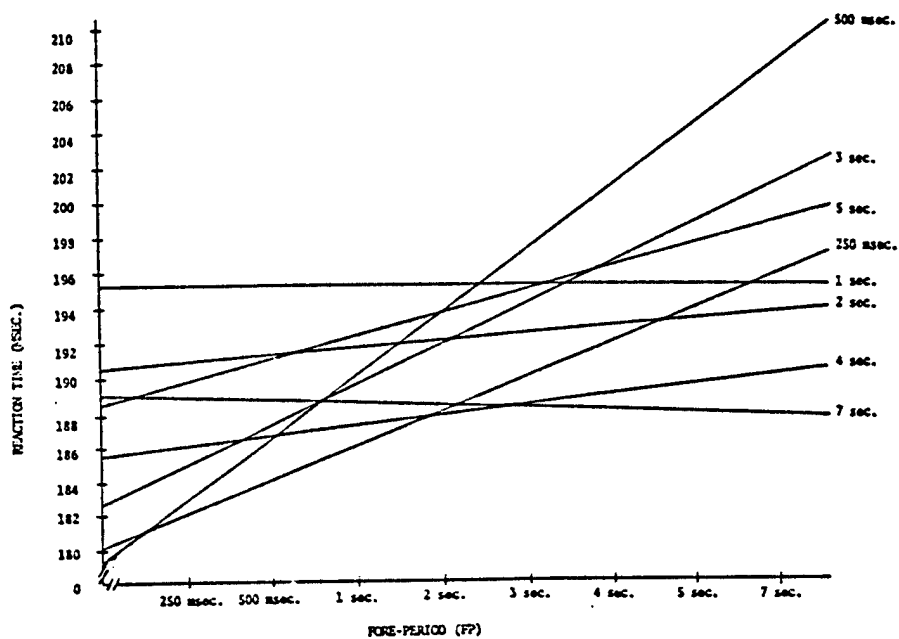
FIGURE 2: REGRESSION PLOT OF REACTION TIME VS. FP
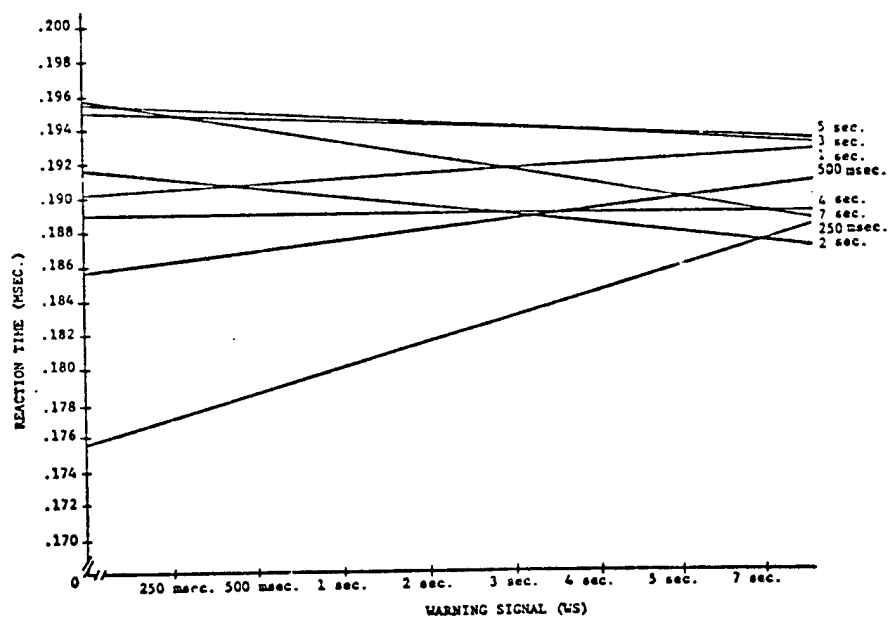(WS KEPT CONSTANT)

FIGURE 3: REGRESSION PLOT OF REACTION TIME VS. WS
(FP KEPT CONSTANT)

488

except for the 1 sec. WS, the WS regression intercept value was less than the corresponding FP value.

SUMMARY

To study the interactive effects of variable FP and WS on temporal expectancy of foot simple reaction time, forty-eight college students responded to a red visual stimulus by moving the right foot laterally left to a disc target. The WS and FP were paired for 64 combinations with the following common values: 250 m.secs., 500 m.secs., 1, 2, 3, 4, 5 and 7 secs.

Results of the present study suggest that when the FP value is larger than the WS value, the reaction time (temporal expectancy) is usually less than when the WS-FP values are reversed. This finding is indicated mainly for the WS-FP values of 250 m.secs., 500 m.secs., 1 and 2 secs., with the reverse found for the values of 3 through 7 secs. In addition, when a FP value was kept constant at 2 secs. or greater, the reaction time decreased as WS increased. The combination of WS-FP that produced the least variable effect on RT was shown to be a WS kept constant at 1 sec. or FP kept constant at 4 secs.

While the results of this study are not conclusive with regard to the interactive effects of variable warning signals and fore-periods, they do indicate that the speed of human operator response (foot reaction time) can be enchanced by controlling the duration of WS-FP intervals. Further analysis of this data and additional studies are in process.

REFERENCES

1. Baker, C. H. Towards a Theory of Vigilance. Canadian Journal of Psychology, 1959, 13, 35-49.

2. Deese, J. Some Problems in the Theory of Vigilance. Psychological Review, 1955, 62, 359-368.

3. Naatanen, R. The Diminishing Time-Uncertainty with the Lapse of Time After the Warning Signal in Reaction-Time Experiments with Varying Fore-Periods. Acta Psychologica, 1970, 34, 399-419.

SESSION VI

AUTOMOBILE DRIVING

Chairman: G. A. Bekey

A SIMULATOR FOR DRIVING RESEARCH[1]

By Rudolph G. Mortimer and Russell L. Adkins

Department of Health and Safety Education
University of Illinois

SUMMARY

A fixed-base simulator is described which is to be used in research on driving skills and the effects of alcohol, as well as other studies of driver-vehicle performance.

INTRODUCTION

In a previous research study by Mortimer and Sturgis (reference 1), a fixed-base simulator was used to evaluate the effects of alcohol on the lateral control cues and motor skills used by drivers. In addition, a preliminary study was carried out of the effect of alcohol on car-following performance. Subsequently, some additional studies were carried out in a vehicle operated on public highways for a comparison with results using the driving simulator. In order to conduct further studies of this type, and having similar objectives, but in addition to assess the effects of stress, incentives and information loading, as well as alcohol on these basic driving skills, a driving simulator is under development at the University of Illinois.

The objective of this report is to provide an overview of the general operating characteristics of the device.

THE DRIVING SIMULATOR

The driving simulator consists of a number of major components, including the following: an automobile in which the driver is seated, a roadway display generation and projection system, a vehicle dynamics simulation, a control console and a data recording and acquisition capability.

The Automobile

A 1969 Simca automobile, cut-off about 0.5 m rear of the front seats is mounted on a supporting structure. The rack has been removed from the rack and pinion steering box and a spring has been attached to the steering column by a nylon cord which winds around the column if the steering wheel is rotated, thereby creating a return force. Steering feel thus achieved was modeled after an American automobile having power steering. A multi-turn rotary potentiometer is attached to the end of the steering column to measure steering wheel displacement. The conventional accelerator and brake pedals are left intact. Depressing the accelerator actuates a linear potentiometer whose output is fed to the analog computer. Similarly, depressing the brake pedal actuates the vehicle's master cylinder which is connected to a hydraulic brake transducer, the electric signal from which is also sent to the analog computer. A position servo which is actuated by a signal proportional to simulated vehicle speed drives the speedometer cable which is directly coupled to the speedometer pointer.

The driver's seat is adjustable in fore and aft position as well as in the rake of the seat back, as is conventional with this vehicle.

Roadway Display Generation and Projection System

At present, a Raytheon 704 digital computer is used to generate a roadway display on a CRT. A television camera views the CRT display and sends the image to an Advent video projector which is mounted above the automobile, in the same longitudinal plane as the driver's position. A curved projection screen 1.8 m wide and 1.3 m high is positioned 2.5 m in front of the driver.

The display consists of a horizon line, the dashed center line and the edge lines of a two-lane road which responds appropriately in lateral translation and yaw to steering inputs and to speed commands originating from the accelerator and brake controls. In addition, the display can show the rear of another vehicle in the right hand lane (presently configured as a straight truck) which will provide the stimulus in car-following studies.

Longitudinal Dynamics Simulation

The automobile dynamics were implemented with the use of an EAI TR-20 analog computer and some additional integrators and multipliers. The extra components were required due to the size of the simulation. The longitudinal dynamics were assumed to be independent of the lateral steering dynamics. Because the car model is to be used in car-following experiments a relatively elaborate model was used for the longitudinal dynamics of the car.

The forces resisting the motion of the car are composed of three parts: a factor proportional to the speed of the car, a factor proportional to the square of the speed, and a constant term. The constant term is

negative and is used to simulate the effects of an automatic transmission. It will accelerate the car from rest without any driver input. The other two factors are positive and may be adjusted to match the coastdown curve of the car to any other desired curve. By eliminating the speed-squared term a linear resistance force may be obtained and the stability derivatives of various cars utilized (see references 2 and 3). Figure 1 shows the coastdown curve for a typical configuration. Note the acceleration of the car from rest due to the negative resistance factor.

The available acceleration force is equal to the rolling radius of the rear tires times the torque applied to them from the driveshaft with the engine at full throttle. For a given car this acceleration force is assumed to be a function of car speed only. This functional relationship is simplified to consist of two linear segments with one breakpoint. By eliminating the breakpoint a linear available acceleration force is obtained and the published stability derivatives may again be used.

The accelerator pedal attenuates the available acceleration force in a linear fashion and thus gives the driver control over the speed of the car. Figure 2 shows the acceleration of the car for various throttle positions.

The driver controls the deceleration of the car by applying a force to the brake pedal. A pressure transducer on the brake line provides an output to the analog computer proportional to the force applied to the brake. To provide the effect of the tires skidding on the road the output of the pressure transducer is diode-limited at a level which provides a deceleration corresponding to the maximum deceleration of a real car. Up to the cutoff level the car will decelerate at a rate proportional to brake pedal force.

Lateral Steering Dynamics Simulation

The lateral steering dynamics are speed dependent and consist of a two-degree-of-freedom model, the roll axis being neglected. For a development of these equations and a comparison to a three-degree-of-freedom model see reference 2. The tire characteristic curves are generated by two diode function generators (one for the front tires and one for the rear tires) which have three positive and three negative breakpoints. The function generators permit a fairly accurate representation of the tire characteristics and also provide a limit on the lateral force provided by the tires. Figure 3 shows the steering response of the car at 30 mph for various step inputs, the input angle being measured at the front tires. Note that the curves are all exponentials. Figure 4 shows the steering response at an increased speed of 50 mph. In this case the response curves are damped oscillations, illustrating the speed dependence of the lateral steering dynamics.
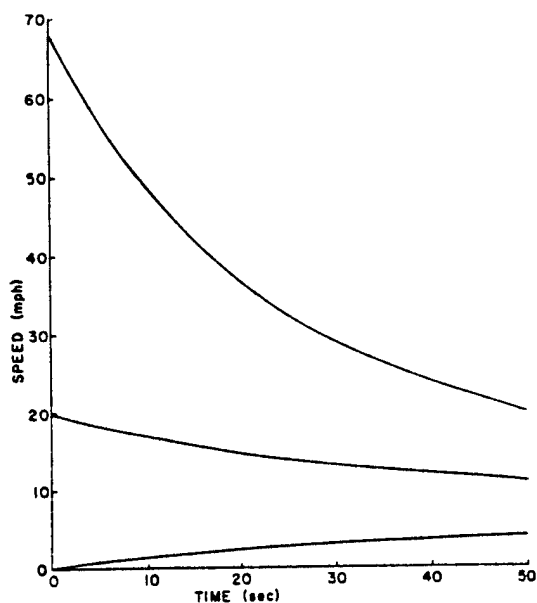
Fig. 1. Coastdown curve for a typical vehicle configuration.
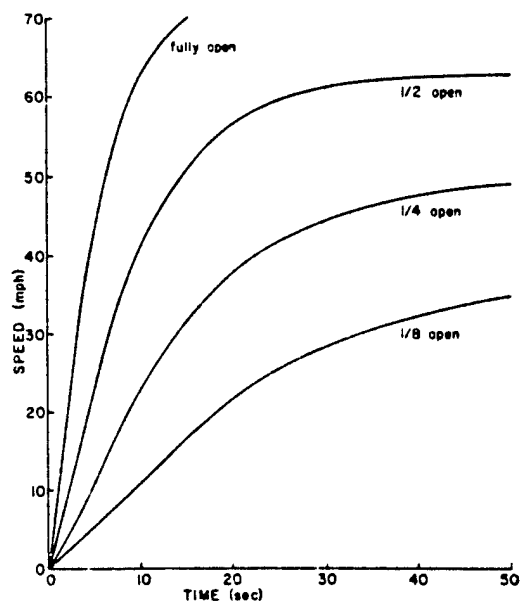

Fig. 2. Acceleration of the car for various throttle positions.
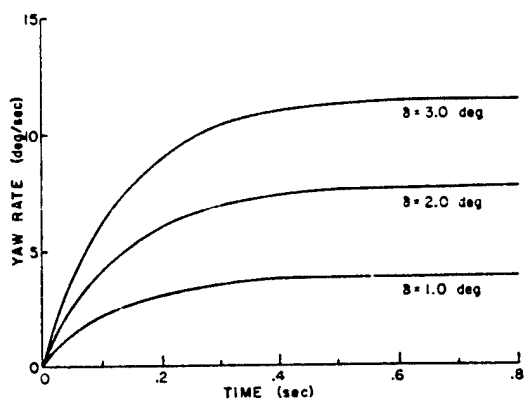

Fig. 3. Steering response of the car at 30 mph for various step inputs to the front wheels.
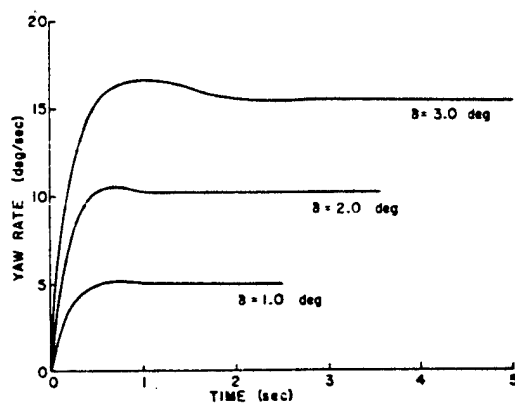

Fig. 4. Steering response of the car at 50 mph for various step inputs to the front wheels.

496

Control Console

A control console provides the experimenter with status displays, such as the speed and lateral position of the subject's vehicle, as well as a number of control functions, such as to label, initiate and terminate the test trials. Two types of forcing functions will be provided in the lateral control studies, besides road curvature. At all times a low amplitude pseudo-random signal will be added to the subject's steering wheel position output signal to act as a low-level background tracking task, simulating minor inputs from the road, wind or other sources to require continuous vigilance on the part of the driver. Similar signals of higher amplitude will also be used as forcing functions to create a more complex continuous steering task as one type of test input. The second type will consist of a discrete step input signal added to the subject's steering wheel position to simulate a persistent, sudden wind gust.

Additional controls are concerned with setting up initial conditions in car-following studies and for providing both manual or automatic control of the lead-vehicle's speed-time history.

Data Recording and Acquisition

In order to provide continuous monitoring of system operation, including acquisition of data signals, an eight-channel strip chart recorder will be used at all times. This recorder will also be used to monitor physiological recording of heart rate or EMG which will be taken on all subjects. A number of the analog data signals which can be used to describe driver-vehicle performance, such as speed, lateral position, heading angle, yaw rate, etc. in steering and headway, relative velocity, etc. in car-following will be recorded on magnetic tape after digitization at 20 Hz by the same computer used to generate the roadway display. Time series and other analyses will then be carried out on these data.

REFERENCES

1. Mortimer, R.G.; and Sturgis, S.P.: The Effects of Low and Moderate Levels of Alcohol on Steering Performance. Proceedings, 6th International Conference on Alcohol, Drugs and Traffic Safety, The Addiction Research Foundation, Toronto. 329-346. 1975.

2. Weir, D.H.; Shortwell, C.P.; and Johnson, W.A.: Dynamics of the Automobile RElated to Driver Control. Tech. Report, 157-1, Systems Technology, Inc. July, 1966.

3. Wojcik, C.K.; and Allen, R.W.: Studies of the Driver as a Control Element, Phase 3. UCLA Eng. Rept. No. 7148, Inst. of Transportation and Traffic Eng. July, 1971.

SESSION VII

HANDLING QUALITIES AND PILOT RATINGS

Chairman: S. J. Merhav

A STATISTICAL APPROACH TO THE ANALYSIS OF

PILOT BEHAVIOR IN MULTILOOP SYSTEMS

By Norihiro Goto[*]

NASA Ames Research Center

SUMMARY

This work aims at examining the feasibility of a statistical approach to studying the correlation of the pilot rating with pilot behavior in multiloop control situations. Moving-base simulator experiments were conducted at the Ames Research Center with emphasis placed upon the lateral-directional control of an aircraft under gusty air conditions in the landing approach phase. Analyses have been made of the pilot behavior variation with respect to three experimental variables, using the recently developed identification method that utilizes the so-called autoregressive scheme. The effects of one experimental variable, SAS ON or OFF, are particularly discussed in this report to show that the method is quite practical and feasible to obtain unknown pilot dynamics and spectral quantities associated with multiloop control systems and that the correlation can be well understood by this analytical approach.

INTRODUCTION

It would be superfluous to say that the pilot in control of an aircraft is a multivariable processor and controller. He receives more than one feedback cue through visual displays or through his own visual and/or vestibular organs. Then he exerts controls over more than one quantity to offset the gap, if any, between the current states and the desired states of the aircraft, thereby constructing a multiloop feedback system. The evaluation of the aircraft handling qualities made by the pilot in flight tests or simulator tests is considered to be based, except for some particular flight phases, upon the results of the multiloop control. Understanding pilot behavior in multiloop control situations is therefore fundamental to properly interpreting the pilot rating and comments, and also fundamental to setting up the pilot model that might be used as an analytical design tool in making assessments of the handling qualities of aircraft. As pointed out in reference 1, however, there have been instrumental, measurement, and analytical difficulties inherent in identifying the pilot behavior, especially in finding unique pilot describing functions in multiloop systems. This situation may be reflected in the fact that less than half a dozen experimental series pertinent to aircraft multiloop control have been carried out so far to identify pilot behavior (e.g., refs. 2-4). As far as the analytical difficulties are concerned, recent development of identification methods seems to be encouraging us to go

---

[*]National Research Council Research Associate.

a step ahead into the area of determining human pilot dynamics for some multi-loop situations.

In this work, one of the identification methods, which makes use of the so-called autoregressive scheme, is applied to the analysis of the pilot's lateral-directional control of an airplane in the landing approach phase under gusty air conditions. The simulator experiments, conducted at the NASA Ames Research Center with the use of the FSAA (Flight Simulator for Advanced Aircraft) moving simulator, employed three experimental variables to investigate the variation of the pilot rating and behavior with respect to the variables. This report discusses particularly the correlation of one of the three variables, Roll/Yaw SAS ON or OFF, with the pilot behavior, emphasizing the influence of the aircraft dynamics change. The general objective is directed toward examining the feasibility of the statistical identification approach to understanding and interpreting the pilot rating and behavior. Results may help to define pilot models in realistic multiloop control situations.

SYSTEM MODEL AND THE ANALYTICAL METHOD (AR-MODEL METHOD)

Let us assume the system model to be a typical compensatory control system as shown in figure 1. Although we do not have a definite ground on which the system model like the one shown in the figure is set up by the pilot for aircraft control, we shall proceed with this model for the understanding of the analytical procedure. For the lateral-directional control in the landing approach phase on IFR, however, it will be shown that the model in figure 1 is appropriate.

In figure 1, the vectors $\Pi(n)$ and $\Theta(n)$ $(n = 1, 2, \ldots, N)$ may be set for the lateral-directional control of the aircraft as

$$\Pi(n) = [\delta_a(n)\delta_r(n)]' \tag{1}$$

and

$$\Theta(n) = [\phi(n)\psi(n)\beta(n)]' \tag{2}$$

where

$\delta_a(n)$ = pilot's wheel movements (rad),

$\delta_r(n)$ = pilot's pedal movements (cm (in.)),

$\phi(n)$ = roll angle output of the aircraft (rad),

$\psi(n)$ = yaw angle output of the aircraft (rad),

$\beta(n)$ = sideslip angle output of the aircraft (rad) , $\left.\begin{matrix} \\ \\ \\ \\ \\ \end{matrix}\right\}$ (3)
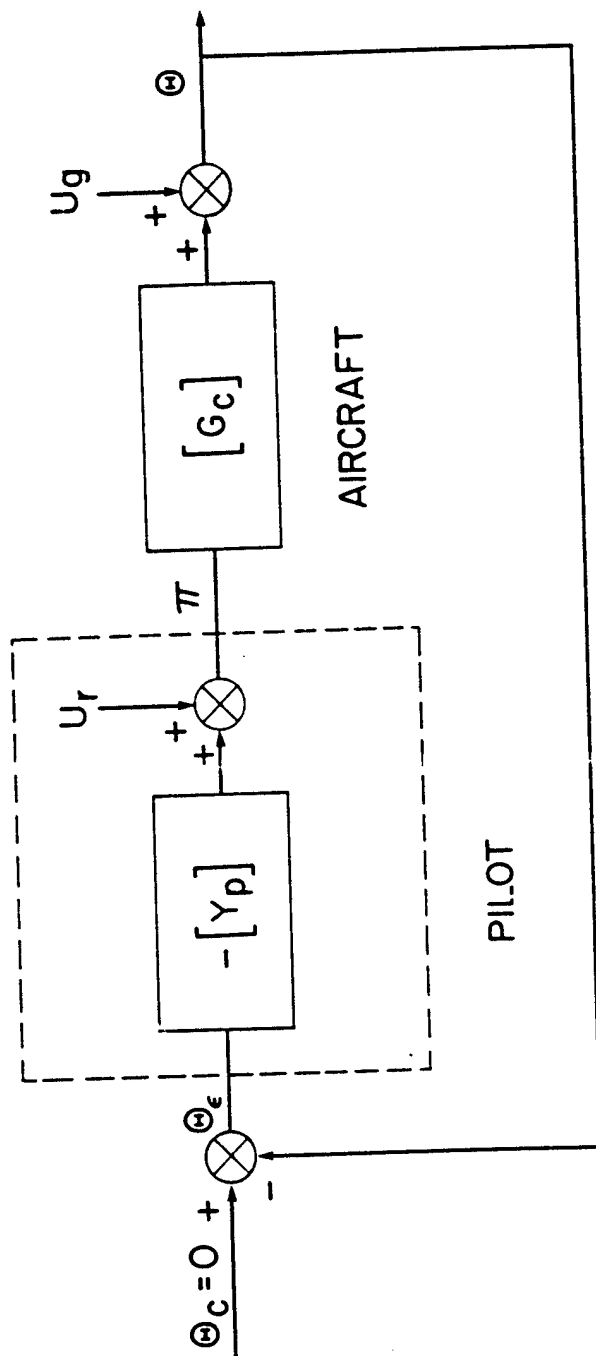
502

Figure 1.- Block diagram of a compensatory closed system.

and ' denotes the transpose. The matrices $[Y_p(z)]$ and $[G_c(z)]$ represent the pilot dynamics and the aircraft dynamics, respectively. They are defined, if we employ the definitions of equation (3), as

$$[Y_p(z)] = \begin{bmatrix} \dfrac{\delta_a}{\phi}(z) & \dfrac{\delta_a}{\psi}(z) & \dfrac{\delta_a}{\beta}(z) \\[3mm] \dfrac{\delta_r}{\phi}(z) & \dfrac{\delta_r}{\psi}(z) & \dfrac{\delta_r}{\beta}(z) \end{bmatrix} \tag{4}$$

and

$$[G_c(z)] = \begin{bmatrix} \dfrac{\phi}{\delta_a}(z) & \dfrac{\phi}{\delta_r}(z) \\[3mm] \dfrac{\psi}{\delta_a}(z) & \dfrac{\psi}{\delta_r}(z) \\[3mm] \dfrac{\beta}{\delta_a}(z) & \dfrac{\beta}{\delta_r}(z) \end{bmatrix} \tag{5}$$

where z is the backward shift operator, i.e., $z^k y(n) = y(n - k)$. Expand the transfer function matrices $[Y_p(z)]$ and $[G_c(z)]$ into the series in z as

$$[Y_p(z)] = \sum_{m=1}^{\infty} [y_p(m)]z^m \tag{6}[1]$$

$$[G_c(z)] = \sum_{m=1}^{\infty} [g_c(m)]z^m \tag{7}[1]$$

where $[y_p(m)]$ and $[g_c(m)]$ show the impulse response matrices. Then, using the impulse response matrices, we may describe the system of figure 1 by the following equations:

$$\Pi(n) = \sum_{m=1}^{\infty} [y_p(m)]\Theta(n - m) + U_r(n) \tag{8}$$

$$\Theta(n) = \sum_{m=1}^{\infty} [g_c(m)]\Pi(n - m) + U_g(n) \tag{9}$$

_____

[1] It is assumed here that $[y_p(0)] = 0$ and $[g_c(0)] = 0$. See reference 5 for the discussion on the inclusion of $[y_p(0)]$ and $[g_c(0)]$.

where $U_r(n)$ is the 2×1 noise vector injected by the pilot, $[u_{\delta_a}(n) u_{\delta_r}(n)]$, and $U_g(n)$ is the 3×1 external noise vector, such as the gust-induced quantities, $[u_\phi(n) u_\psi(n) u_\beta(n)]$. The feedback system model of equations (8) and (9) was first studied by Akaike (refs. 5 and 6).

We set assumptions as follow:

1. $\Pi(n)$, $\Theta(n)$, $U_r(n)$, and $U_g(n)$ are all stationary and zero mean.

2. The feedback system is stable, i.e., all the roots of the determinant of $\{I - [Y_p(z)][G_c(z)]\}$ must lie outside the unit circle.

3. The noise vectors $U_r(n)$ and $U_g(n)$ are uncorrelated with each other, i.e., every element of $U_r(n)$ is uncorrelated with every element of $U_g(n)$.

4. The noise vectors $U_r(n)$ and $U_g(n)$ satisfy the following autoregressive (AR) relationships for a properly selected L:

$$U_r(n) = \sum_{\ell=1}^{L} C_r(\ell) U_r(n - \ell) + W_r(n) \qquad (10)$$

$$U_g(n) = \sum_{\ell=1}^{L} C_g(\ell) U_g(n - \ell) + W_g(n) \qquad (11)$$

where $W_r(n)$ and $W_g(n)$ are white noise processes, and $C_r(\ell)$ (2×2) and $C_g(\ell)$ (3×3) are coefficient matrices.

Operating the AR filters of equations (10) and (11) conceptually on equations (8) and (9), respectively, we get

$$\Pi(n) = \sum_{\ell=1}^{L} C_r(\ell) \Pi(n - \ell) + \sum_{\ell=1}^{\infty} A_p(\ell) \Theta(n - \ell) + W_r(n) \qquad (12)$$

$$\Theta(n) = \sum_{\ell=1}^{L} C_g(\ell) \Theta(n - \ell) + \sum_{\ell=1}^{\infty} A_c(\ell) \Pi(n - \ell) + W_g(n) \qquad (13)$$

where

$$A_p(\ell) = [y_p(\ell)] - \sum_{k=1}^{\ell-1} C_r(k)[y_p(\ell - k)] \qquad (14)$$

$$A_c(\ell) = [g_c(\ell)] - \sum_{k=1}^{\ell-1} C_g(k)[g_c(\ell - k)] \qquad (15)$$

505

By putting together equations (12) and (13) we arrive at the matrix form

$$X(n) = \sum_{\ell=1}^{\infty} A(\ell)X(n - \ell) + W(n) \tag{16}$$

if we set

$$X(n) = [\Pi(n) \quad \Theta(n)]' \tag{17}$$

$$W(n) = [W_r(n) \quad W_g(n)]' \tag{18}$$

$$A(\ell) = \begin{bmatrix} C_r(\ell) & A_p(\ell) \\ \hline A_c(\ell) & C_g(\ell) \end{bmatrix} \tag{19}$$

and $C_r(\ell) = C_g(\ell) = 0$ for $\ell > L$. Equation (16) is the AR model of the vector $X(n)$ of infinite order, which cannot be fitted to the given data.

Instead of having the AR model of infinite order, consider an AR model of finite order M,

$$X(n) = \sum_{\ell=1}^{M} A(\ell)X(n - \ell) + W(n) \tag{20}$$

satisfying the relationships

$$\left. \begin{array}{l} E[W(n)] = 0 \text{ (zero vector)} \\[6pt] E[W(n) \cdot X'(n - \ell)] = 0 \text{ (zero matrix) for } \ell \geq 1 \\[6pt] E[W(n) \cdot W'(\ell)] = \delta_{n,\ell} \sum_w \end{array} \right\} \tag{21}$$

where $\delta_{n,\ell} = 1$ $(n = \ell)$, $= 0$ $(n \neq \ell)$, $\sum_w$ is the covariance matrix of $W(n)$, and E denotes the expectation. In equation (20) it is assumed that

$$A(\ell) = 0 \text{ (zero matrix), for } \ell > M. \tag{22}$$

Suppose we have completed the fitting of the AR model in the form of equation (20). We first partition the estimated AR coefficient matrix $A(\ell)$ as shown by equation (19). Then, the impulse response matrices $[y_p(\ell)]$ and $[g_c(\ell)]$ are calculated from equations (14) and (15) up to any desired ℓ under the assumption of equation (22). The frequency response function matrix of the pilot is obtained by replacing z by $\exp(-j\omega\Delta T)$ in the following equation:

$$[Y_p(z)] = [I - C_r(z)]^{-1}A_p(z) \tag{23}$$

506

where I is the unit matrix, ΔT the sampling interval, ω the frequency in rad/sec,

$$C_r(z) = \sum_{\ell=1}^{M} C_r(\ell) z^\ell$$

and

$$A_p(z) = \sum_{\ell=1}^{M} A_p(\ell) z^\ell$$

The estimation of the AR coefficient matrix $A(\ell)$ is made along the least squares method. From equation (20) we have

$$R_{xx}(n) = \sum_{\ell=1}^{M} A(\ell) R_{xx}(n - \ell), \quad n = 1, 2, \ldots, M \tag{24a}$$

$$= \sum_{\ell=1}^{M} A(\ell) R'_{xx}(\ell) + \Sigma_w, \quad n = 0 \tag{24b}$$

where $R_{xx}(\ell)$ is the covariance matrix of the vector $X(n)$. Equation (24a) is solved for $A(\ell)$ ($\ell = 1, 2, \ldots, M$). Practically, we may use the efficient recursive computational algorithm of the least squares based upon the formulas developed by Whittle (refs. 7 and 8). Note that the estimate of the covariance matrix Σ_w, which is obtained by using the relationship of equation (24b), is important in that it may be used to check assumption 3 stating the uncorrelatedness of U_r and U_g, and thus can be used to check the propriety of the system model.

The determination of the optimal order M in equation (20) is made by the use of an objective judgment criterion MFPE (Multiple Final Prediction Error) proposed by Akaike (ref. 8). This criterion is defined by

$$\text{MFPE} = \left(1 + \frac{Mk + 1}{N}\right)^k \left(1 - \frac{Mk + 1}{N}\right)^{-k} \|d_M\| \tag{25}$$ [2]

where k = number of the components in the vector X, N = number of the data points, M = order of the AR model, d_M = the estimate of the covariance matrix Σ_w, when the AR model of order M is fitted, and $\|d_M\|$ = determinant of d_M. The criterion MFPE gives the optimal order M that best approximates the possibly infinite-order system such as equation (16) in the sense of the minimization of the mean square error of the one-step-ahead prediction obtained by using the least squares estimates of the AR coefficients.

---

[2]Akaike later generalized the judgment criterion to propose the information criterion called AIC (ref. 9). The use of MFPE and AIC in this work has shown that both give the same order.

The power spectral density matrix $P_x(j\omega)$ of the time series vector $X(n)$ is given by

$$P_x(j\omega) = \Delta T [A(j\omega)]^{-1} \sum_w \overline{[A'(j\omega)]}^{-1} \qquad (26)$$

where

$$A(j\omega) = \sum_{\ell=0}^{M} A(\ell)\exp(-j\omega\ell)$$

and $A(0) = -I$ (I: unit matrix), and $\overline{A(j\omega)}$ is the complex conjugate of $A(j\omega)$.

In order to see the effectiveness of our results, given by equation (23) for example, we have to look into the linear coherency, which can be estimated by the use of the spectral density matrix $P_x(j\omega)$. When Σ_w is diagonal, meaning that the components of the vector $W(n)$ are mutually independent, we reach a simple expression which gives the indication of the linear coherency characteristics as

$$r_{ij}(j\omega) = q_{ij}(j\omega)/p_{ii}(j\omega) \qquad (27)$$

In equation (27), $p_{ii}(j\omega)$ is the power spectrum of the i-th component of the vector $X(n)$ (e.g., the power spectrum of δ_a if $i = 1$), and $q_{ij}(j\omega) = |[A(j\omega)]_{ij}^{-1}|^2 \sigma_{jj}$, where $[A(j\omega)]_{ij}^{-1}$ indicates the (i, j)-th component of $[A(j\omega)]^{-1}$, and σ_{jj} is the (j, j)-th component of Σ_w; r_{ij} shows the contribution in power of the j-th noise source to the power of the i-th component of $X(n)$, and

$$\sum_{j=1}^{k} r_{ij}(j) = 1 \qquad (28)$$

This quantity is called the relative power contribution, and it is worth checking even when the off-diagonal elements of Σ_w are not zero but practically small.

EXPERIMENT

Simulator experiments were conducted at the NASA Ames Research Center, using the FSAA 6-degrees-of-freedom moving-base simulator. The simulated flight phase was the final landing approach under gusty air conditions. Thus, the pilot's task was to track the glideslope and the localizer while also keeping the airspeed and the attitude of the aircraft at some desired values. The flight configuration is visualized in figure 2. The flight loading conditions of the STOL transport used are shown in table I, together with the lateral-directional stability dynamics data which were measured prior to the
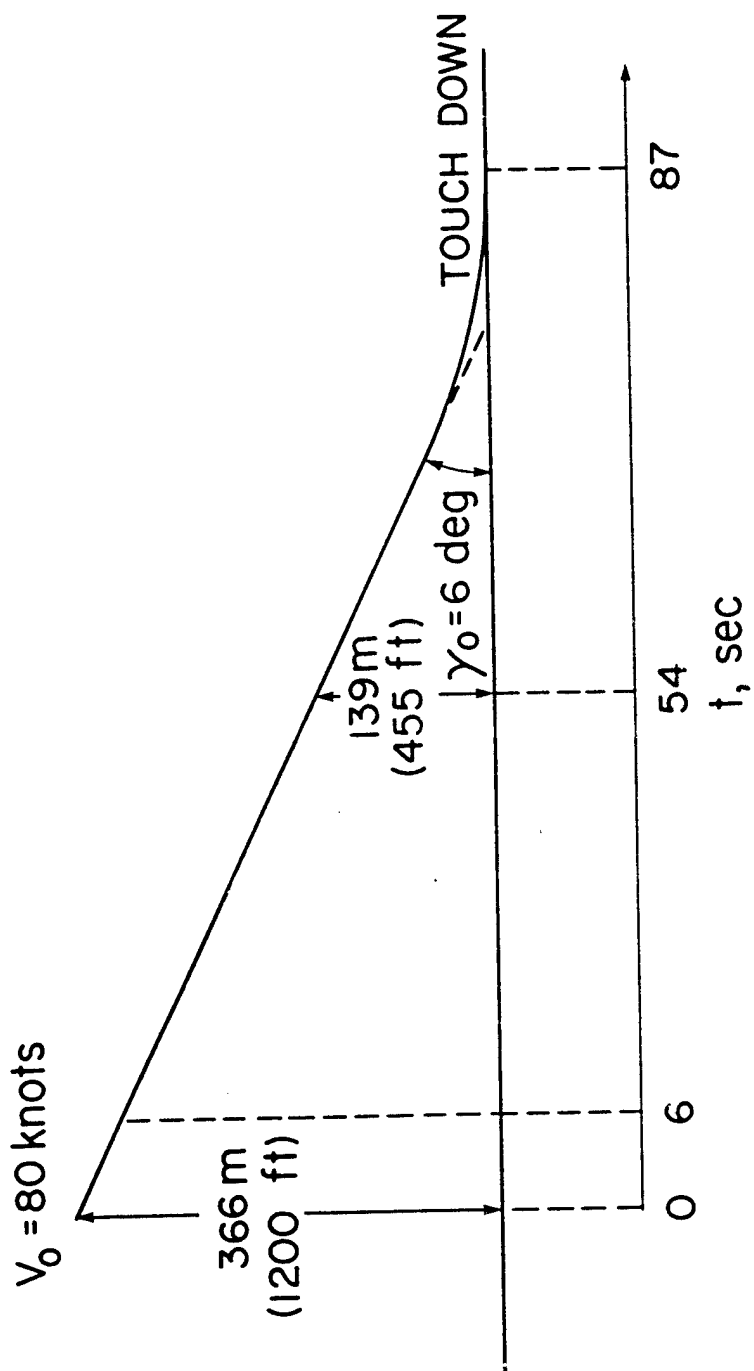
508

Figure 2.- Landing approach flight configuration.

TABLE I.- FLIGHT LOADING CONDITIONS AND STABILITY DERIVATIVES DATA

Initial conditions	Aircraft dimensions
V_o = 80 knots	W = 68,040 kg (150,000 lb)
H_o = 366.8 m (1203.5 ft)	S = 154.9 m^2 (1667 ft^2)
γ_o = -6.0°	b = 34.0 m (111.6 ft)
α_o = -0.33° deg	I_x = 255,776 kg-m-sec^2 (1,850,000 slug-ft^2)
	I_z = 483,900 kg-m-sec^2 (3,500,000 slug-ft^2)
	I_{xz} = 37,385 kg-m-sec^2 (270,400 slug-ft^2)
Stability derivatives (body axis)[a]	Response characteristics
Y_v = -0.1431 1/sec	Roll time constant
L_β = -0.4894 1/sec^2	$1/T_r$ = 0.7778 1/sec
N_β = 0.4397 1/sec^2	Spiral time constant
Y_p = 0.007266 m/sec (0.02384 ft/sec)	$1/T_s$ = -0.09317 1/sec
L_p = -0.5518 1/sec	Dutch-roll mode damping
N_p = -0.08578 1/sec	ζ_D = 0.08798
Y_r = 0.7919 m/sec (2.598 ft/sec)	Dutch-roll mode undamped
L_r = 0.6812 1/sec	natural frequency
N_r = -0.1618 1/sec	ω_D = 0.7938 rad/sec
Y_{δ_a} = 0.0	
$L\delta_a$ = 0.4428 1/rad-sec^2	
$N\delta_a$ = -0.01632 1/rad-sec^2	
$Y\delta_r$ = 0.1276 m/sec^2/cm (1.063 ft/sec^2/in.)	
$L\delta_r$ = 0.01486 1/sec^2/cm (0.03775 1/sec^2/in.)	
$N\delta_r$ = -0.02341 1/sec^2/cm (-0.05945 1/sec^2/in.)	

[a]To obtain primed stability derivatives, refer to reference 10, p. 257.

experiment. See reference 11, for example, for the details of the FSAA simulator system.

Three experimental variables were selected for this work:

1. Flight rules (VFR or IFR)

2. SAS (Roll/Yaw SAS ON or OFF)

3. Gust intensity $\sigma = 1.2$ or 1.8 m/sec (4 or 6 ft/sec)

where σ is the rms value of the vertical gust component. Experimental runs analyzed in this work consisted of six runs with four different configurations as listed in table II. An experienced NASA pilot participated in this experiment, and his rating on each configuration by the Cooper-Harper scale (ref. 12) is also given in table II. It should be mentioned here that seven preliminary runs preceded the six runs for data taking, and the pilot ratings and the greater part of the pilot comments were collected in the preliminary runs. The emphasis of the experiment and of the analysis was placed on the lateral-directional control of the aircraft. Therefore, Pitch-SAS was kept in the ON position so that the influence of the longitudinal control on the lateral-directional control could be made as small as possible. Roll/Yaw SAS utilizes

TABLE II.- SIMULATOR EXPERIMENT FLIGHT CONFIGURATIONS AND PILOT
RATING FOR EACH CONFIGURATION

Configuration	Base	Flight rule	Roll/yaw SAS	Gust condition	Pilot rating
A-1	Moving	VFR	OFF	Turbulent[a] $\sigma = 1.2$ m/sec (4.0 ft/sec)	5.5 ~ 6.0
A-2	Moving	VFR	OFF	Turbulent $\sigma = 1.2$ m/sec (4.0 ft/sec)	5.5 ~ 6.0
B-1	Moving	IFR	OFF	Turbulent $\sigma = 1.2$ m/sec (4.0 ft/sec)	6.5
B-2	Moving	IFR	OFF	Turbulent $\sigma = 1.2$ m/sec (4.0 ft/sec)	6.5
C-1	Moving	IFR	OFF	Turbulent $\sigma = 1.8$ m/sec (6.0 ft/sec)	7.0
D-1	Moving	IFR	ON	Turbulent $\sigma = 1.2$ m/sec (4.0 ft/sec)	2.0

[a]Every turbulent condition includes 20 knots headwind. Pitch-SAS is ON for every configuration.

roll angle and roll rate feedback to aileron and roll angle and roll rate in addition to washed-out yaw rate feedback to rudder. The Yaw SAS was also supplemented with an aileron-to-rudder crossfeed, in which the aileron movement signal filtered by a first-order lag was cross-fed to the rudder, principally to remove the effect of aileron yaw. A typical example of the aircraft response to a relay-type wheel input is shown in figure 3 for both SAS-OFF and SAS-ON configurations.

The gust simulated in this experiment was based on the one-dimensional spectral density functions of the Dryden form. References 11 and 13 contain the details of the model and the method to generate it. One point to note is that the gust characteristics are a function of the altitude as the result of employing the assumption of the two-dimensional isotropy near the ground. Setting $t = 0$ at the I.C. ($h = 366$ m (1200 ft)), the time sector used for the analysis was from $t = 6.0$ sec to $t = 54.0$ sec as shown in figure 2. However, the change in altitude may not be so large as to make it necessary to take into account the nonstationary characteristics of the gust (see ref. 14, for example).

Six quantities, δ_a, δ_r, ϕ, ψ, β, y_ε (where y_ε is the deviation angle from the localizer beam and the others are defined by eq. (3)), in addition to some other quantities useful for the analysis, were recorded for each run on RUNDUM tape (ref. 11) and were processed by a TSS/360 computer system at the Ames Research Center. Note that δ_a and δ_r are wheel angle and pedal travel, respectively, instead of forces applied by the pilot to wheel and pedal. So, the pilot dynamics results shown later may contain the wheel and pedal dynamics. The sampling time was 0.06 sec.

Results of the analysis by the AR-model method are shown in figures 4-10 and in table III. The power spectral densities of the pilot control outputs and the aircraft outputs for configuration B-1 (SAS-OFF) and configuration D-1 (SAS-ON), respectively, together with their rms values are shown in figures 4 and 5. Figure 6 is an example of the relative power contribution for configuration B-1. Note that in figures 4, 5, and 6, the abscissa is in the linear scale of the frequency. Figures 7, 8, and 9 are the pilot describing function data (i.e., fig. 7 shows the wheel-related describing functions for configuration B-1; fig. 8 shows the pedal-related describing functions for configuration B-1; and fig. 9 shows the wheel-related describing functions for configuration D-1). The pedal-related describing functions for configuration D-1 are not shown here since the pedal movement of the pilot in this configuration is so small (as indicated by the rms value in fig. 5) that it is not considered to be of any significance. Figure 10 is an example of the comparison of a particular describing function, $\delta_a/\phi(j\omega)$, between configurations B-1 and D-1. Table III gives the normalized d_M's, i.e., the element is given by $d_{ij}/\sqrt{d_{ii}d_{jj}}$, if $d_M = [d_{ij}]$. These data provide a basis for examining the propriety of the system model. Also, the order of the AR model determined by MFPE is shown in table III.
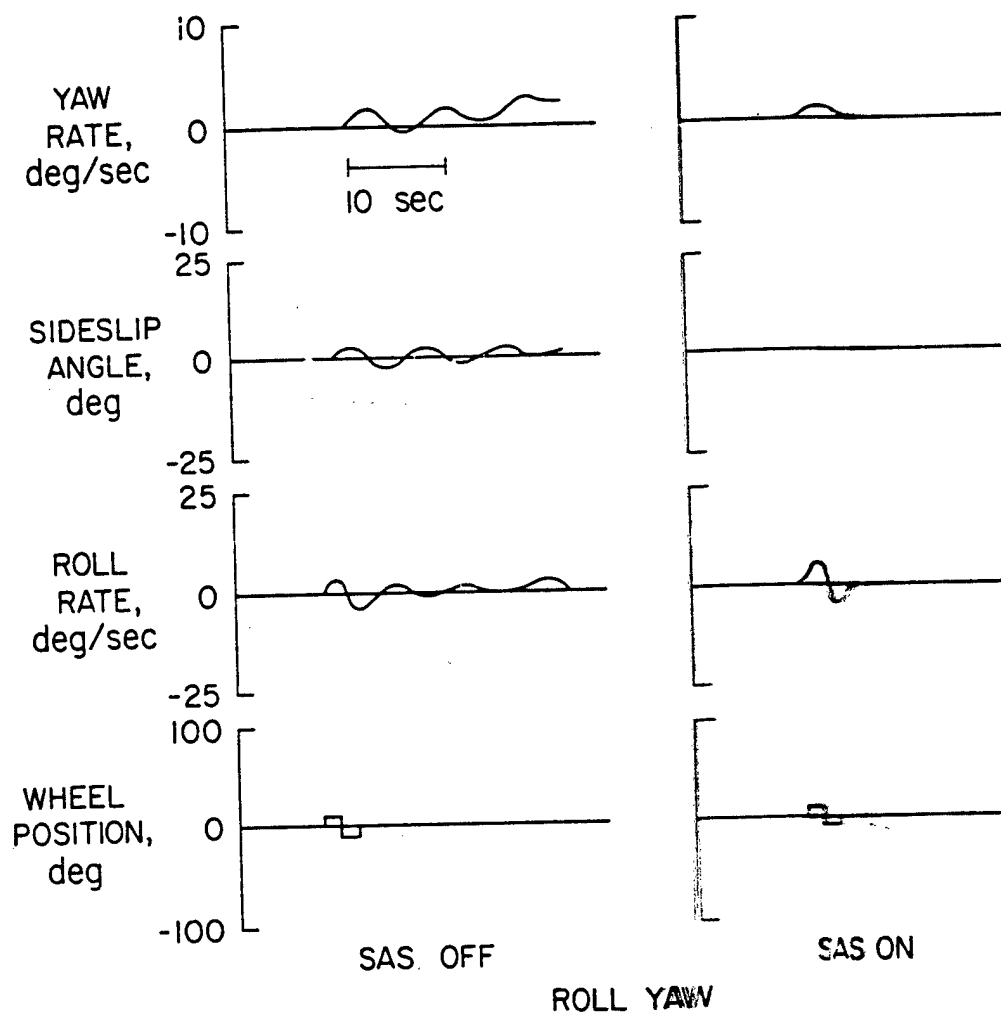
YAW
RATE,
deg/sec

SIDESLIP
ANGLE,
deg

ROLL
RATE,
deg/sec

WHEEL
POSITION,
deg

10

0

-10

25

0

-25

25

0

-25

100

0

-100

10 sec

SAS OFF

SAS ON

ROLL YAW

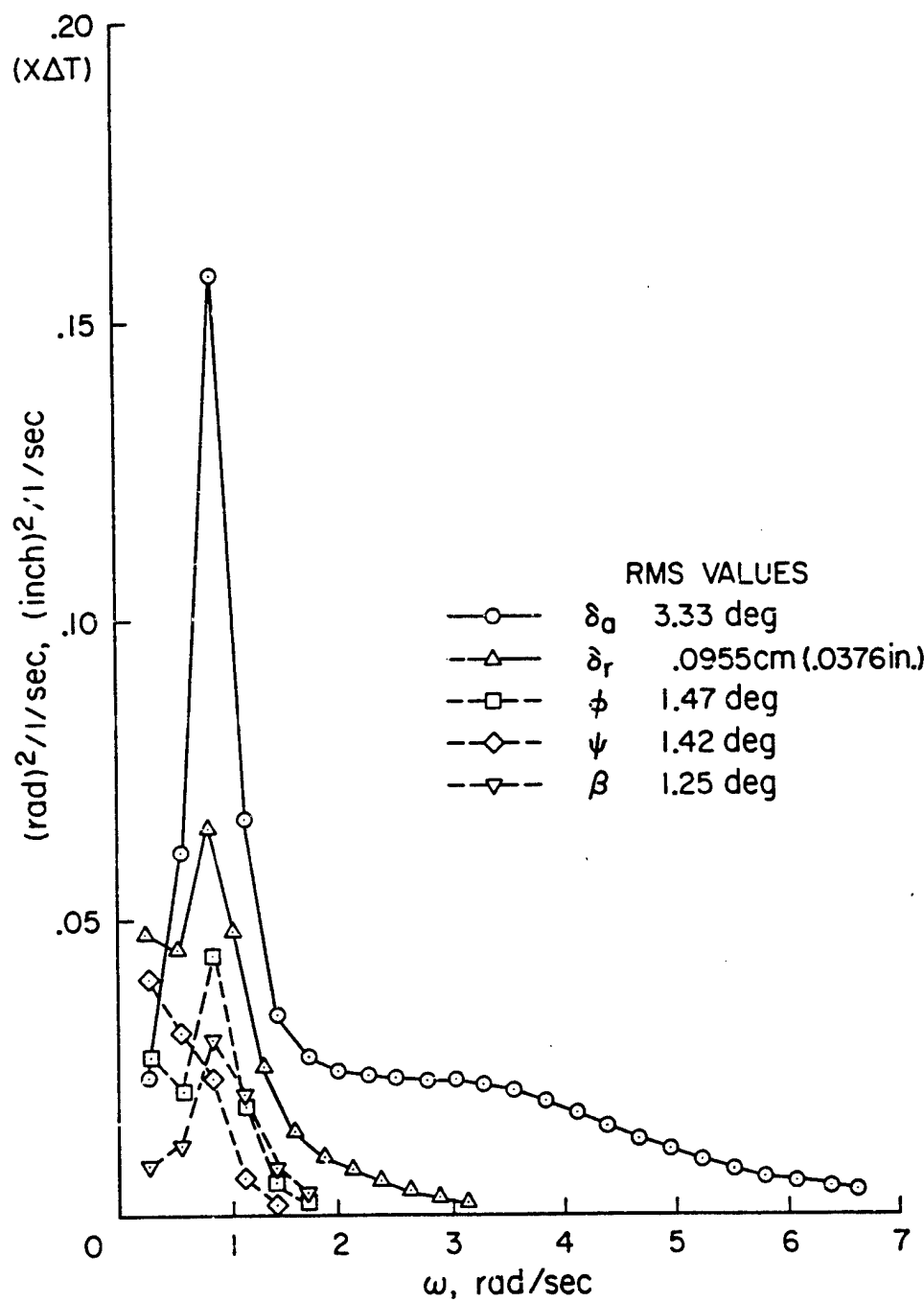Figure 3.- Effects of Roll/Yaw SAS.

513
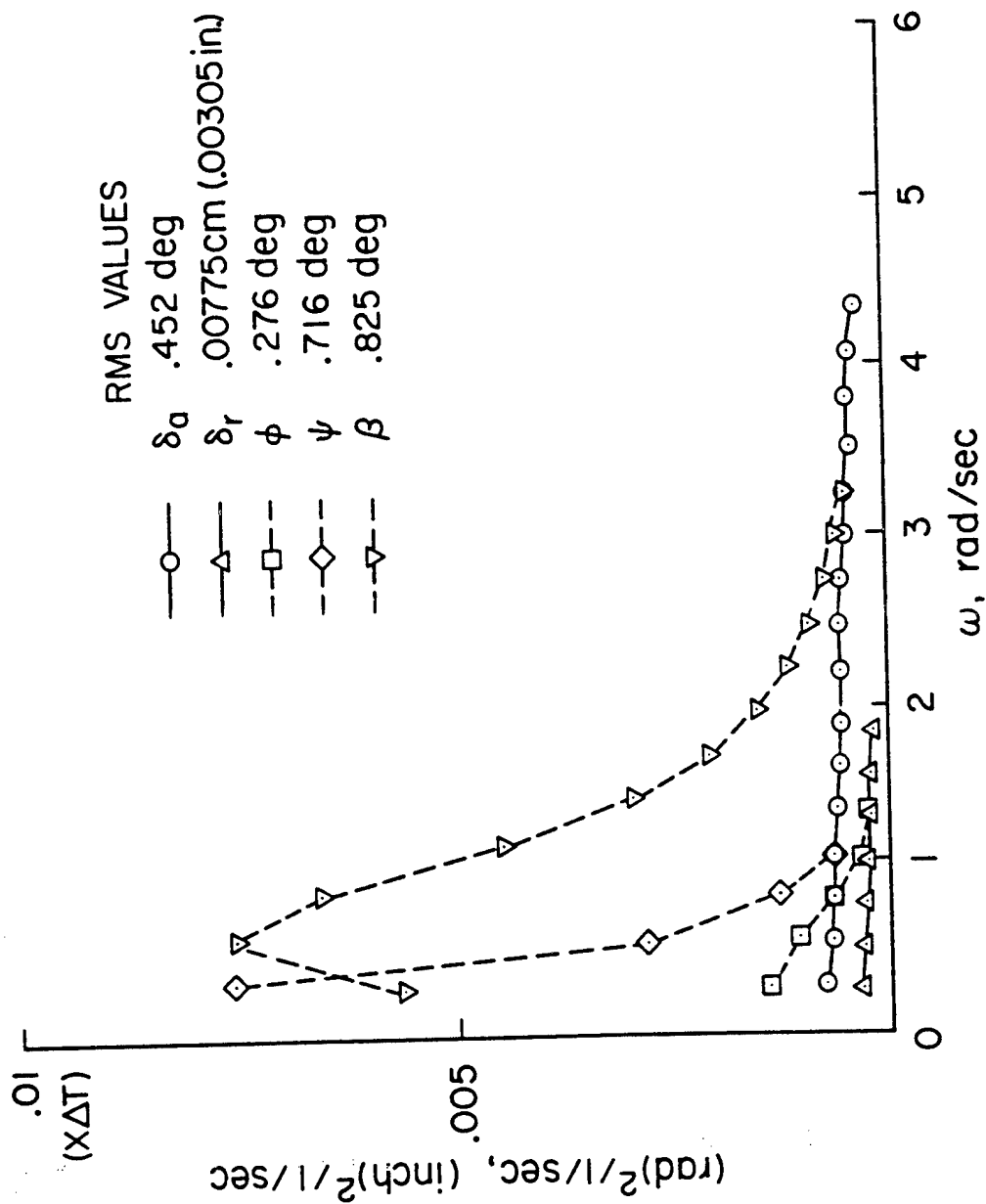
Figure 4.- Power spectra: configuration B-1.
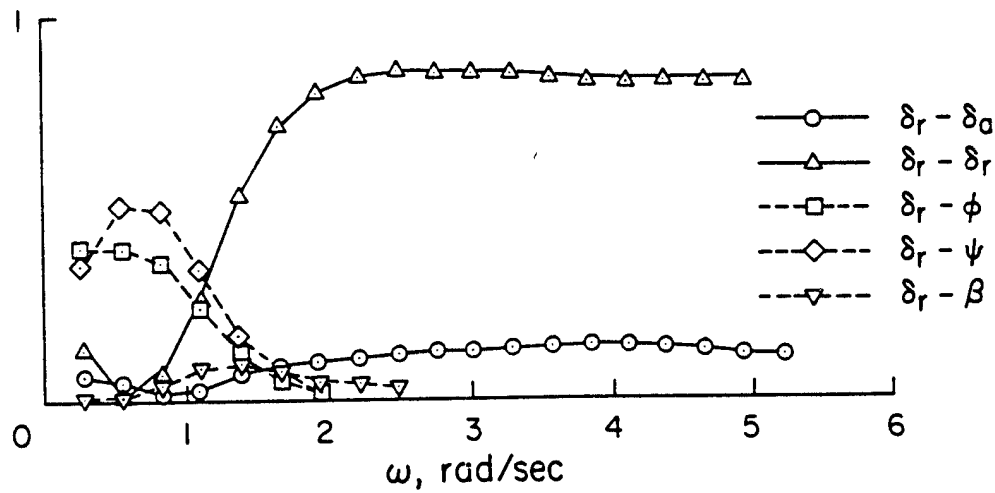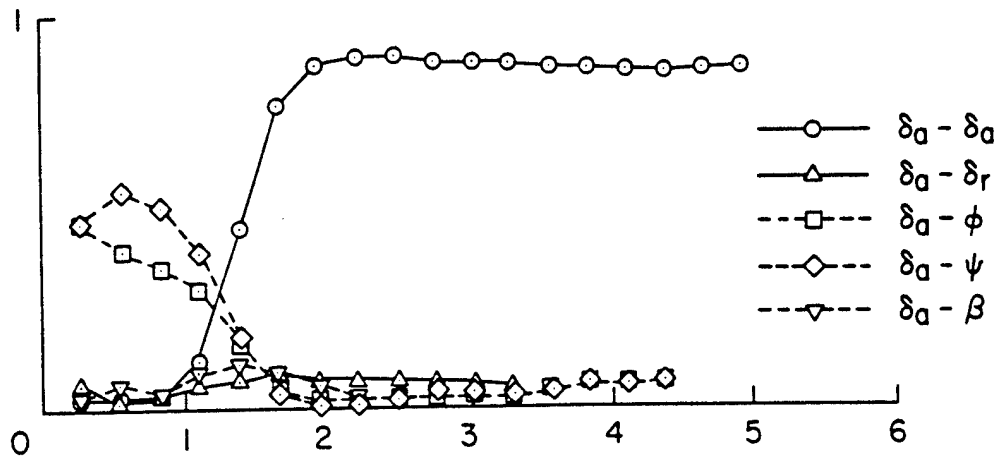
514

Figure 5.- Power spectra: configuration D-1.

Figure 6.- An example of the relative power contribution: configuration B-1.
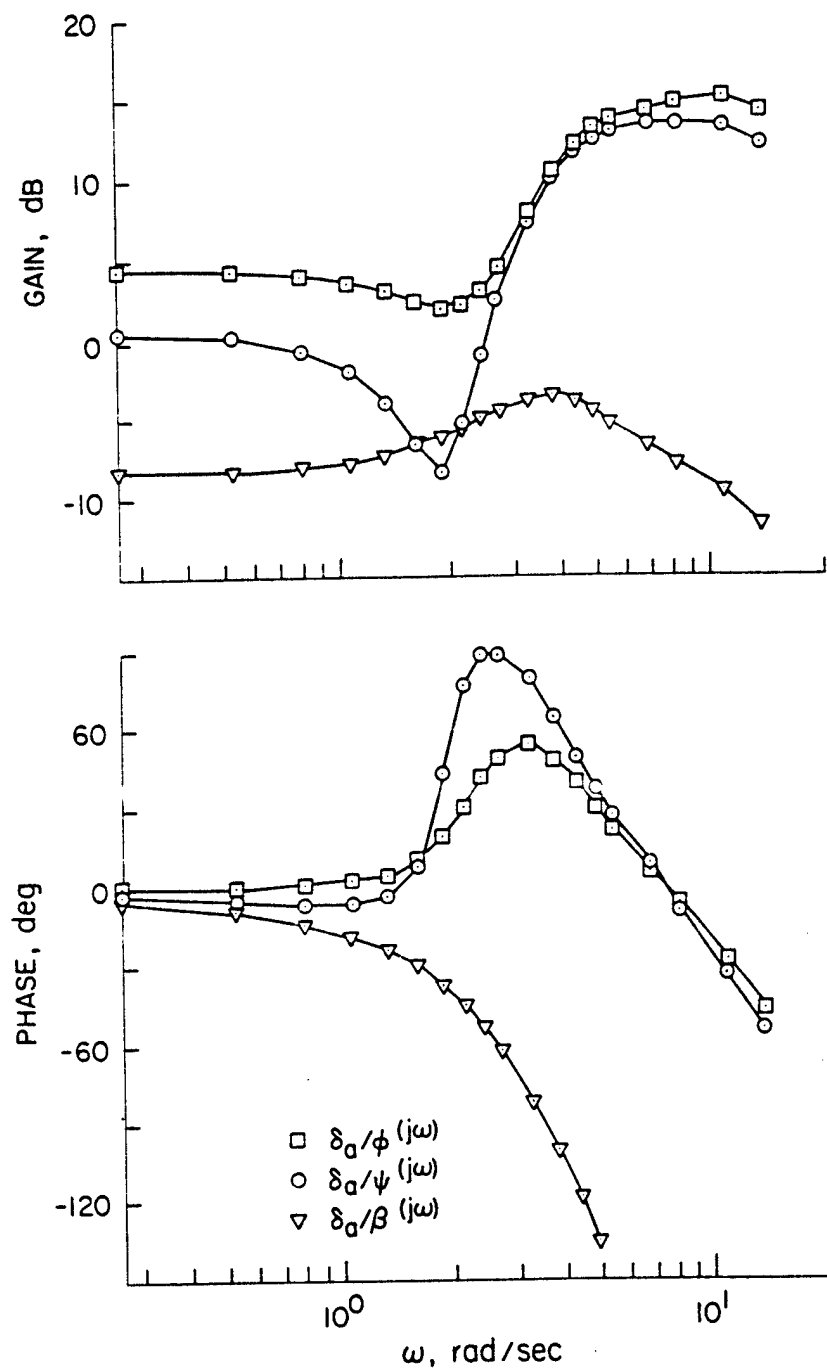
Figure 7.- Wheel-related describing functions of the pilot: configuration B-1.
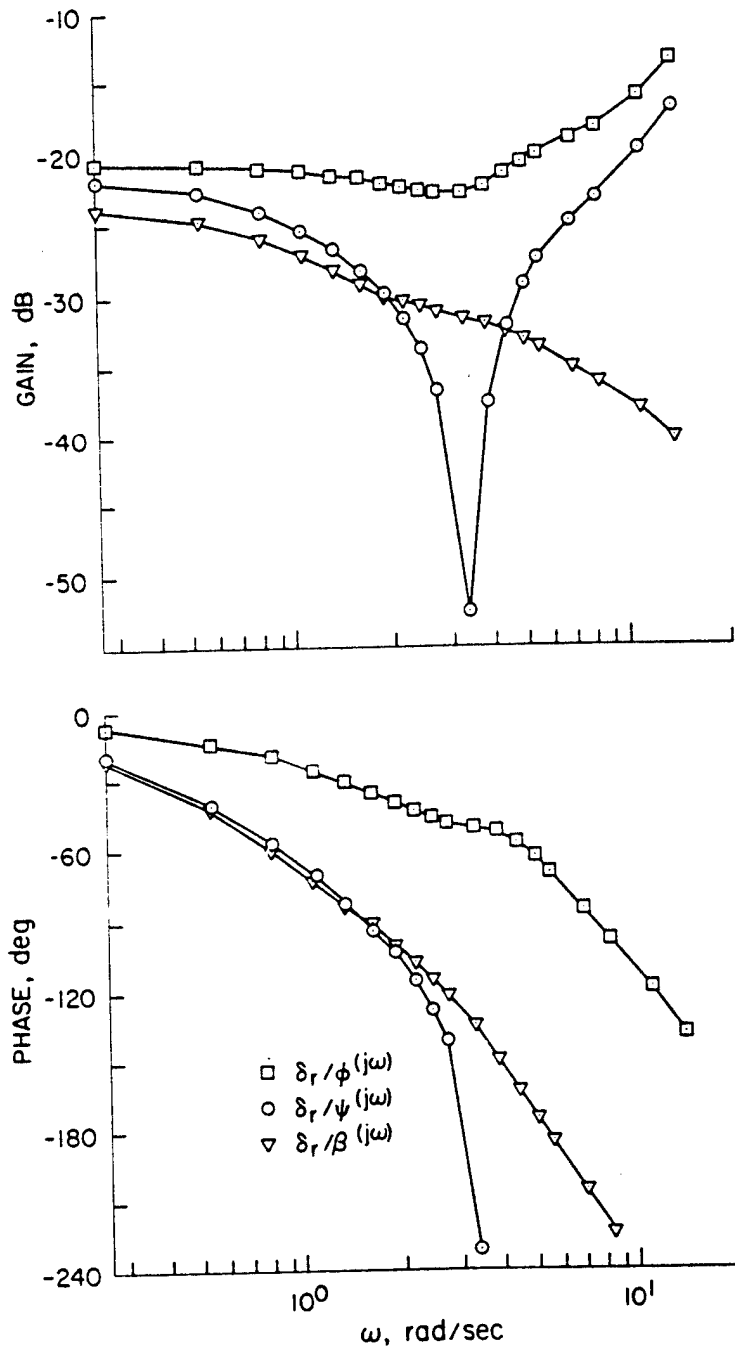
517

Figure 8.- Pedal-related describing functions of the pilot: configuration B-1.
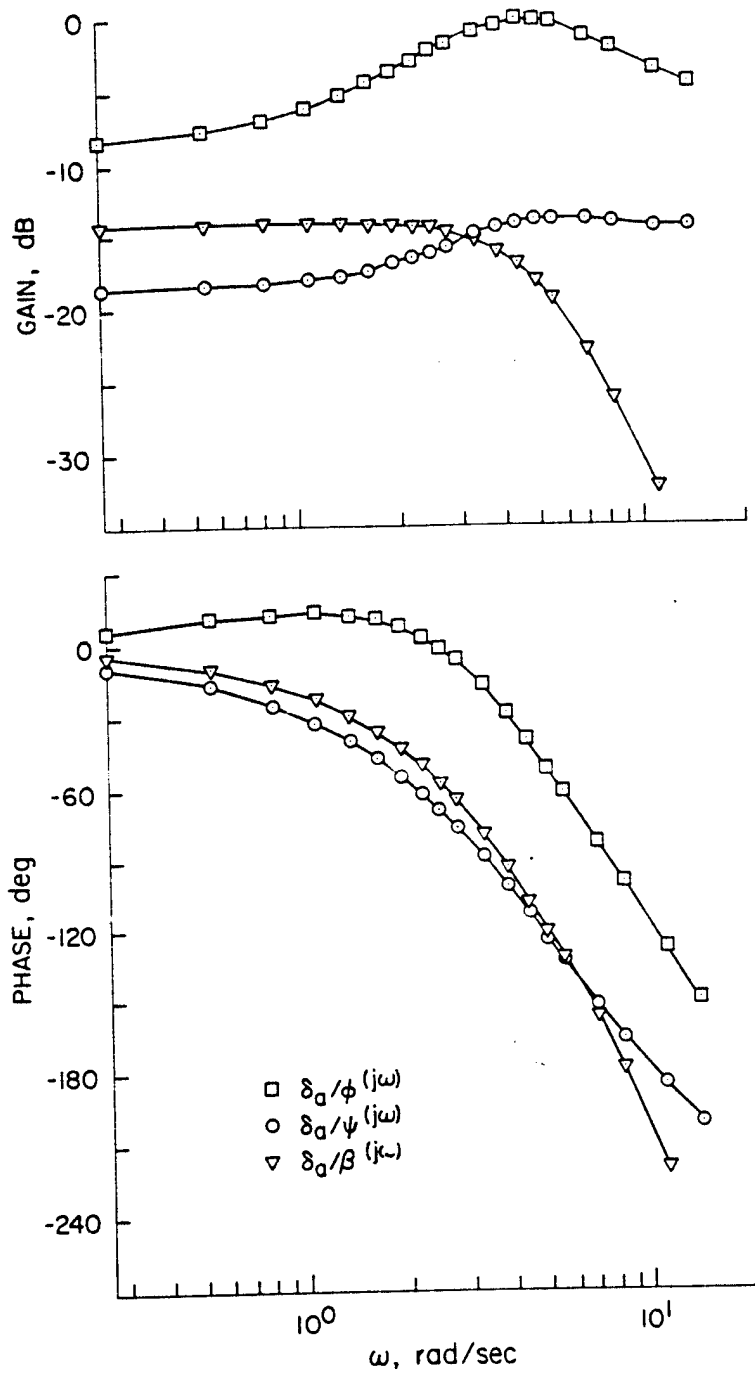
518

Figure 9.- Wheel-related describing functions of the pilot: configuration D-1.

519

EXPERIMENTAL FITTING   FITTED FUNCTIONS

SAS OFF   □ $\delta_a/\phi(S) = K_p e^{-0.4S}(1+0.35S+0.21S^2)$

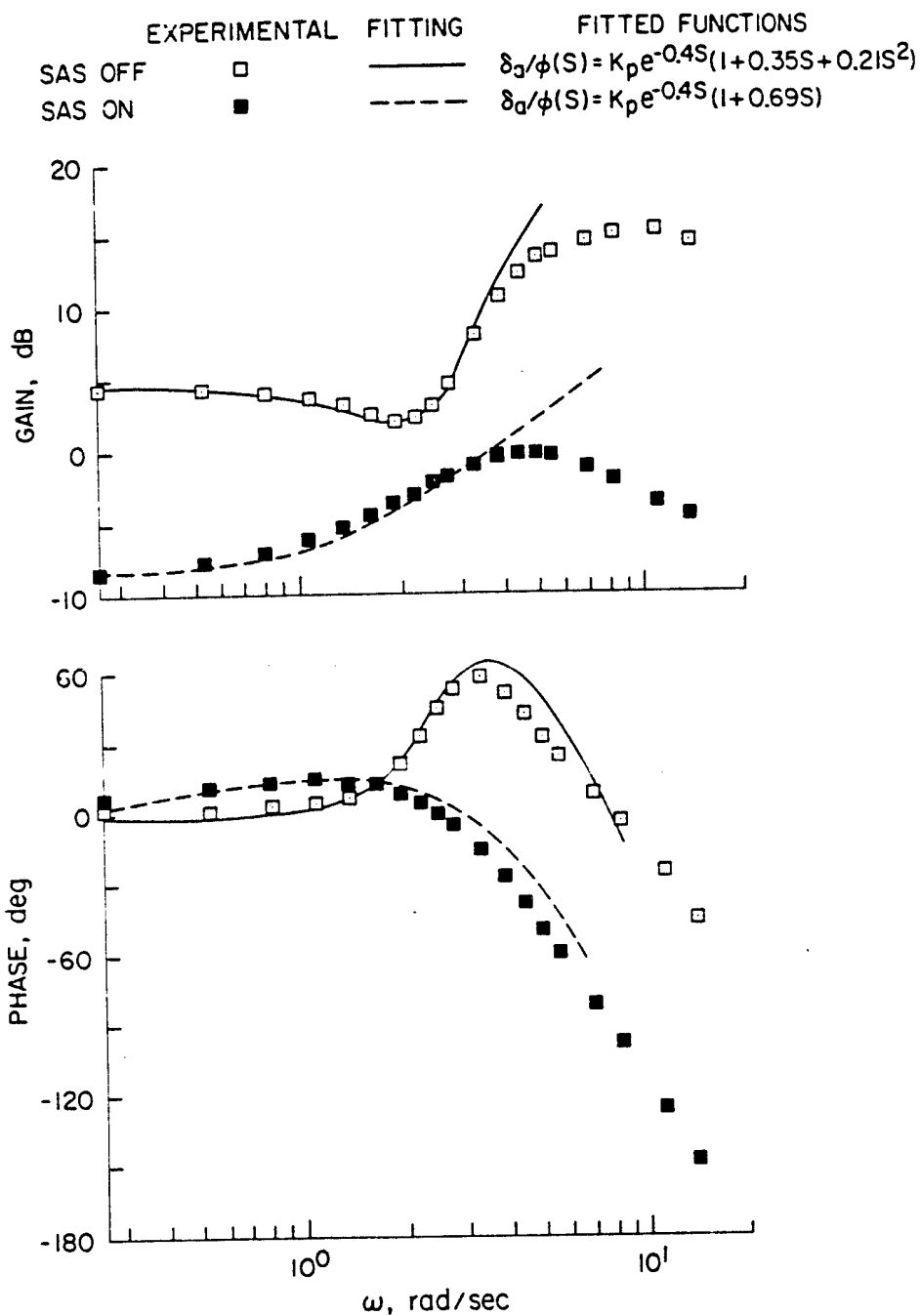SAS ON   ■ $\delta_a/\phi(S) = K_p e^{-0.4S}(1+0.69S)$

Figure 10.- Comparison of a describing functions, δ_a/ϕ, between configurations B-1 and D-1.

TABLE III.- NORMALIZED COVARIANCE MATRIX d_M AND THE ORDER OF THE AR MODEL

	δ_a	δ_r	ϕ	ψ	β
Configuration B-1 (M = 7)					
δ_a	0.1000000D 01	0.1005529D 00	0.4019349D-02	0.1793190D-01	0.1280636D-01
δ_r	0.1005529D 00	0.1000000D 01	-0.1968628D 00	0.6887329D-02	-0.1113333D 00
ϕ	0.4019349D-02	-0.1968628D 00	0.1000000D 01	-0.9248254D 00	0.3880180D-01
ψ	0.1793190D-01	0.6887329D-02	-0.9248254D 00	0.1000000D 01	0.2108075D-01
β	0.1280636D-01	-0.1113333D 00	0.3880180D-01	0.2108075D-01	0.1000000D 01
Configuration D-1 (M = 4)					
δ_a	0.1000000D 01	0.5945739D-01	0.6133936D-01	-0.1641999D 00	-0.4559047D-01
δ_r	0.5945739D-01	0.1000000D 01	0.1626071D 00	-0.1138606D 00	0.1799904D-01
ϕ	0.6133936D-01	0.1626071D 00	0.1000000D 01	-0.6793050D 00	-0.3196776D-01
ψ	-0.1641999D 00	-0.1138606D 00	-0.6793050D 00	0.1000000D 01	0.2076136D 00
β	-0.4559047D-01	0.1799904D-01	-0.3196776D-01	0.2076136D 00	0.1000000D 01
Digital simulation study (M = 6)					
δ_a	0.1000000D 01	0.6229741D-01	0.1938894D 00	-0.1840873D 00	0.1226025D 00
δ_r	0.6229741D-01	0.1000000D 01	0.1642078D 00	-0.1619289D 00	0.9192547D-01
ϕ	0.1938894D 00	0.1642078D 00	0.1000000D 01	-0.9793968D 00	0.6785351D 00
ψ	-0.1840873D 00	-0.1619289D 00	-0.9793968D 00	0.1000000D 01	-0.7119448D 00
β	0.1226025D 00	0.9192547D-01	0.6785351D 00	-0.7119448D 00	0.1000000D 01

DIGITAL SIMULATION STUDY

Before going into the discussion of the results of the simul or experiment, we now briefly refer to the results of the digital simulation that was made as a credibility study of the AR-model method. The digital simulation made use of the system model of figure 1 with the known pilot dynamics matrix [Y_p] and the aircraft lateral-directional dynamics of table I. For the pilot noise $U_r(n)$, two mutually independent white noises were used. The rms values of these noises were 0.4° for the wheel control and 0.005 cm (0.002 in.) for the pedal control. The gust simulation system was different from that used for the simulator experiment and was based upon the method described in reference 15. The gust intensity was $\sigma = 1.2$ m/sec (4 ft/sec). All equations described by the Laplace operator S were reduced to the corresponding difference equations (ref. 16). From the records of the vectors $\Xi(n)$ and $\Theta(n)$, the matrix [$Y_p(j\omega)$] was identified as unknown.

Results of this simulation study are shown in figures 11 and 12. The normalized estimate of the covariance matrix d_M is seen in table III, by which we may say that the noise correlation is even worse than those in the simulator experiment, possibly because of the different gust generation system; however, the model of figure 1 is appropriate (see the off-diagonal elements in the bracket of the matrix). The estimated [$Y_p(j\omega)$] appears to be in reasonably good agreement with the theoretical one, at least qualitatively, up

521

ESTIMATED   SIMULATED DYNAMICS

δ_a/ϕ ☐ $\delta_a/\phi(S) = 2.0e^{-0.06S}(1+0.3S)$

δ_a/ψ ○ $\delta_a/\psi(S) = 0.1e^{-0.06S}S$

δ_a/β ▷ $\delta_a/\beta(S) = 0.5e^{-0.06S}/(1+0.3S)$

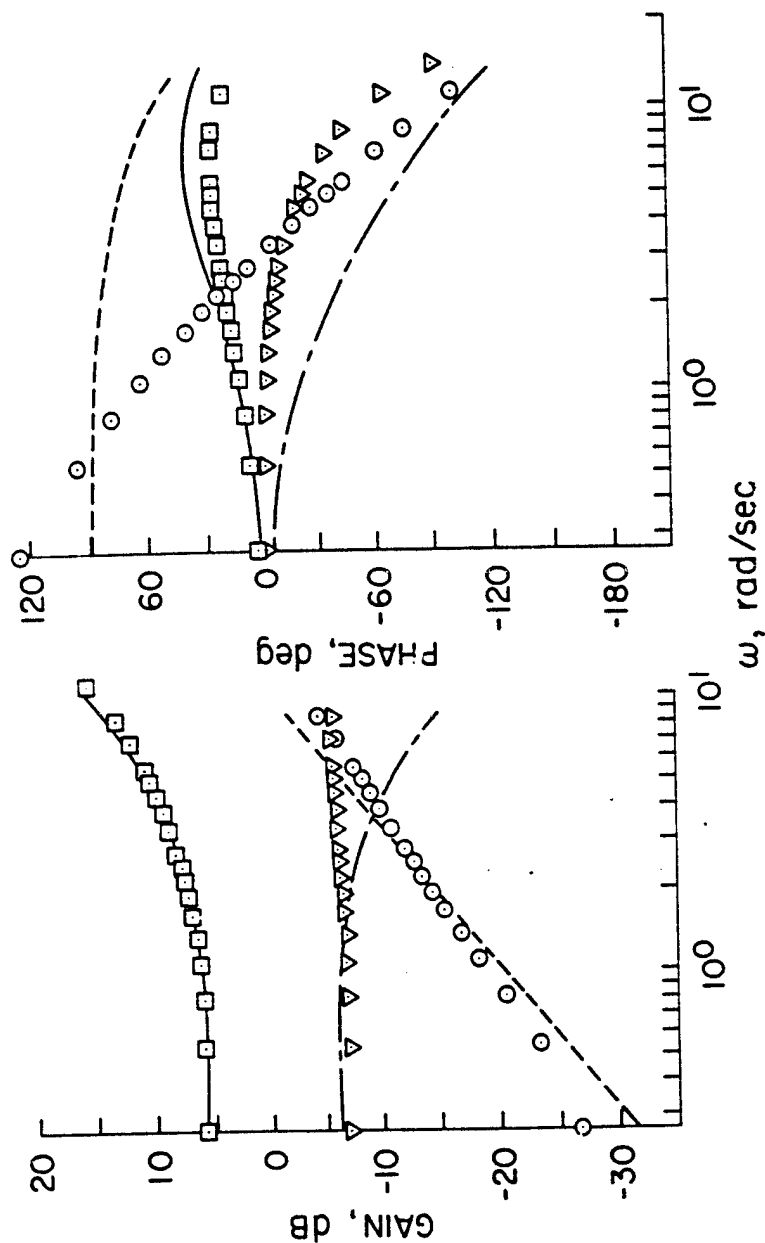Figure 11.- Results of the digital simulation study: wheel-related frequency response functions.

Figure 12.– Results of the digital simulation study: pedal-related frequency response functions.

ESTIMATED   SIMULATED DYNAMICS

δ_r/ϕ □ $\delta_r/\phi(S) = 0.15e^{-0.06S}S$

δ_r/ψ ○ $\delta_r/\psi(S) = 0.15e^{-0.06S}(1+0.3S)$

δ_r/β ▷ $\delta_r/\beta(S) = 0.1e^{-0.06S}/(1+0.3S)$

to a certain frequency. Sepcifically, the roll-angle-related frequency response functions δ_a/ϕ and δ_r/ϕ are quite good due to the large magnitude of their static gains compared with the others. The discrepancy in δ_a/ψ, especially in its phase, between the simulated dynamics and the estimated dynamics may be due to its relatively small static gain and the computational difficulty to realize a pure differentiator. Since many off-diagonal elements outside the brackets in the normalized d_M shown in table III take on large values compared with 1, it makes little sense to check the relative power contribution. It should be noted that the signal-to-noise ratio deteriorated rapidly from the frequency of 4.0 rad/sec because of the use of white noises as the pilot remnants. Also it should be mentioned that the data are influenced by the computational method of the digital simulation and that the influence of the magnitude and the frequency characteristics of the pilot noises on the estimated results should be studied further in conjunction with the external noise characteristics.

DISCUSSION

With the digital simulation study in mind, we now proceed to the discussion of the results of the simulator experiment, using configurations B-1 and D-1 to see the effects of the Roll/Yaw SAS on pilot behavior. It can be seen that the effects of SAS-ON are very conspicuous. For configuration D-1, pedal movements are zero in actuality, wheel movements are small, and the variation of the aircraft outputs is also small. As seen in table III, most off-diagonal elements in the normalized d_M are small compared with 1 for both configurations, and the correlation between W_r and W_g of equation (18) is small, thereby assuring the propriety of the system model of figure 1. In addition, it is worthwhile to examine the relative power contribution in these configurations for the purpose of looking into the linear coherency characteristics and the effectiveness of the pilot's control in the frequency domain. Figure 6 shows the wheel- and pedal-related relative power contributions only for configuration B-1, but these values are sufficient to find that the pilot's wheel and pedal movements are responding to the variation mainly in roll and yaw angle in the low-frequency region up to about twice the Dutch-roll frequency, beyond which the pilot appears to be just a noise generator. Accordingly, the pilot describing functions are considered to be reliable only in the low-frequency region.

Looking at figure 9 which shows the wheel-related pilot describing functions for configuration D-1, and comparing with figure 7, it can be noticed that the SAS-ON does not require much compensation effort from the pilot; static gains are much lower for configuration D-1 than for B-1, and the first-order lead control is noticeable only for the wheel-to-roll-angle describing function. On the other hand, for configuration B-1, the pilot seems to be employing the second-order lead control for δ_a/ϕ, δ_a/ψ, and δ_r/ψ. This may be suggesting that the pilot is utilizing motion cues for this particular run, or that he is employing a special control technique to cancel out the aircraft's oscillatory Dutch-roll motion (ref. 17).

A comparison of the wheel-to-roll-angle describing function is made in figure 10 between configurations B-1 and D-1. Solid and dotted curves in the figure show an attempt at the function fitting, although there is a great uncertainty in the high-frequency region because of the bad linear coherency. Physically realizable pilot models may have to include the first- or second-order lag terms.

Putting together all the results and the consideration described thus far, details of pilot behavior that may contribute to determining the pilot rating can be understood fairly well. More systematic measurements are necessary in order to develop the multiloop pilot model that can be used as an analytical design tool in making assessments of the aircraft handling qualities.

CONCLUDING REMARKS

The AR-model method has been applied for the first time to the identification of pilot behavior in multiloop tasks. Results show that this is a practical and promising technique for obtaining a general idea of the unknown pilot dynamics in multiloop systems. However, more work is needed to identify pilot describing functions that are reliable over a wide frequency range.

In the experiment described here, three experimental variables were used, and their effects, particularly the effects of the Roll/Yaw SAS, have been made clear to some extent. Pilot behavior and its correlation with the handling quality variable may be further defined by this line of approach.

ACKNOWLEDGMENT

REFERENCES

1. McRuer, D. T.: Development of Pilot-in-the-Loop Analysis. J. Aircraft, vol. 10, no. 9, 1973, pp. 515-524.

2. Stapleford, R. L.; McRuer, D. T.; and Magdaleno, R.: Pilot Describing Function Measurements in a Multiloop Task. NASA CR-542, 1966.

3. Weir, D. H.; and McRuer, D. T.: Pilot Dynamics for Instrument Approach Tasks: Full Panel Multiloop and Flight Director Operations. NASA CR-2019, 1972.

4. Beppu, G.: A Study of Pilot Behavior During Controlling the Lateral-Directional Motion of Airplanes in Turbulent Air. NASA TM X-62,464, 1975, pp. 625-644.

5. Akaike, H.: On the Use of a Linear Model for the Identification of Feed-back Systems. Ann. Inst. Statist. Math., vol. 20, 1968, pp. 425-439.

6. Akaike, H.: On a Decision Procedure for System Identification. IFAC Kyoto Symposium on System Engineering Approach to Computer Control, 1970, Preprint, pp. 485-590.

7. Whittle, P.: On the Fitting of Multivariate Autoregressions and the Approximate Canonical Factorization of a Spectral Density Matrix. Biometrica, vol. 50, 1963, pp. 129-134.

8. Akaike, H.: Autoregressive Model Fitting for Control. Ann. Inst. Statist. Math., vol. 23, 1971, pp. 163-180.

9. Akaike, H.: A New Look at the Statistical Model Identification. IFEE Trans., vol. 19, no. 6, 1974, pp. 716-723.

10. McRuer, D.; Ashkenas, I.; and Graham, D.: Aircraft Dynamics and Auto-matic Control. Princeton University Press, Princeton, N.J., 1973.

11. McFarland, R. E.: A Standard Kinematic Model for Flight Simulation at NASA-Ames. NASA CR-2497, 1975.

12. Cooper, G. E.; and Harper, R. P., Jr.: The Use of Pilot Rating in the Evaluation of Aircraft Handling Qualities. NASA TN D-5153, 1969.

13. Parris, B. L.: Modeling Turbulence for Flight Simulations at NASA Ames. CSCR No. 4, prepared by Computer Sciences Corporation for NASA, 1975.

14. Chalk, C. R.; Neal, T. P.; Harris, T. M.; Pritchard, F. E.; and Woodcock, R. J.: Background Information and User Guide for MIL-F-8785B(ASG); Military Specification - Flying Qualities of Piloted Airplanes. AFFDL-TR-68-72, Air Force Flight Dynamics Laboratory, 1969, p. 427.

15. Franklin, J. A.: Turbulence and Lateral-Directional Flying Qualities. NASA CR-1718, 1971, p. 89.

16. Neuman, F.; and Foster, J. D.: Investigation of a Digital Automatic Aircraft Landing System in Turbulence. NASA TN D-6066, 1970.

17. Goto, N.; and Washizu, K.: On the Dynamics of Human Pilots in Marginally Controllable Systems. AIAA J., vol. 12, no. 3, 1974, pp. 310-315.

RIDE QUALITY SENSITIVITY TO

SAS CONTROL LAW AND TO HANDLING QUALITY VARIATIONS

Philip A. Roberts, David K. Schmidt, and Robert L. Swaim
School of Aeronautics and Astronautics, Purdue University

SUMMARY

State variable techniques are used to generate the vertical and lateral fuselage loadfactor distributions for the B-52H and B-1 bombers. A comparison of loadfactors resulting from cruise turbulence excitation, reveals that ride quality is not significantly improved by increasing the control law complexity. Control law complexity is meant to imply rate feedback in comparison to full state feedback. Handling quality parameterizations show pronounced effects on the loadfactors. Finally variations under relaxed static stability implementation show that the ride quality is degraded by restoration of handling characteristics to original short period values.

INTRODUCTION

Control Configured Vehicle (CCV) technology is just beginning to affect the design and manufacture of aerospace vehicles. Current technology aircraft like the F-16 fighter and B-1 bomber are utilizing concepts such as ride control, Relaxed Static Stability (RSS), and fatigue reduction. Future vehicles will certainly incorporate active controls, maneuver load control, direct lift, flutter mode control, and gust load alleviation concepts. These future vehicles will be optimized under many manifolds to include Ride Quality (RQ).

The objective of this paper is to discuss the RQ trends which large flexible aircraft exhibit under various parameterizations of control laws and handling qualities. The information was generated as a data base for research supported by NASA Dryden Flight Research Center under grant NSG 4003. The ultimate aim of the project is delineation of handling qualities specifications for highly flexible CCV vehicles. This paper contains a summary of the assumptions and solution technique, a control law parameterization review, a discussion of ride sensitivity to handling qualities, and finally the RQ effects generated by implementing relaxed static stability configurations.

SYMBOLS

A'   Transpose of the A matrix

$\bar{c}$ — Mean aerodynamic chord length

cg — Center of gravity

E{ } — Expected value

HQ — Handling Qualities

ℓ_x — Distance from cg along fuselage centerline, positive forward

$\bar{\ell}_t$ — Distance between the tail and wing-body aerodynamic centers

$N_{z,y}$ — Loadfactor at a particular body station;
    z denotes vertical
    y denotes lateral

rms — Root mean square

RQ — Ride Qualities

RSS — Relaxed static stability

S — Wing planform area

S_t — Tail planform area

U_0 — Averaged Steady State Flight Velocity

u — Control(s) vector; elevator, aileron, and/or rudder

$\bar{V}$ — Tail volume coefficient

x — State vector; usually associated with physical outputs in this paper

α — Perturbation angle of attack

β — Perturbation side slip angle

ζ — Damping value

η — Scalar unit white noise

θ — Perturbation pitch angle

ξ_i — ith elastic mode generalized displacement

$\phi_i(\ell_x)$ — ith orthogonal elastic mode shape value at body station ℓ_x

ϕ — Perturbation roll angle

ψ Perturbation yaw angle

ω Natural frequency

PROBLEM FORMULATION

Equations of Motion for Flexible Vehicles

Time domain representations for the flexible vehicles were decoupled into longitudinal and lateral state variable formats. The Gaussian white noise representation of turbulence was modeled as a state vector system as suggested in reference 1. The gust state vector was appended to the vehicle state equations resulting in the familiar control form (1).

$$\dot{x}(t) = Ax(t) + Bu(t) + Gn(t) \tag{1}$$

where: x $(n+p) \times 1$
        u $m \times 1$
        n number of physical vehicle states
        m number of **controls**
        p number of gust states
        G $(n+p) \times 1$
        A $(n+p) \times (n+p)$
        B $(n+p) \times m$

Loadfactor Expression

The major contributions to vertical and lateral loadfactors at cruise conditions can be represented by equations (2a) and (2b).

$$N_z(\ell_x,t) = \frac{1}{g}[U_0(\dot{\theta}-\dot{\alpha}) + \ell_x\ddot{\theta} - \sum_{i=1}^{K} \phi_i(\ell_x)\ddot{\xi}_i] \tag{2a}$$

$$N_y(\ell_x,t) = \frac{1}{g}[g\phi - U_0(\dot{\beta}+\dot{\psi}) - \ell_x\ddot{\psi} - \sum_{i=1}^{K} \phi_i(\ell_x)\ddot{\xi}_i] \tag{2b}$$

where: K is the number of elastic modes included in the model.

Throughout this paper the standard right hand stability axis system is utilized with the x axis positive forward from the cg as shown in figure 1.

The sign conventions for the vertical and side bending elements are shown in figures 2 and 3.

The loadfactor expressions can be reformulated as functions of the physical state variables by simple substitution.
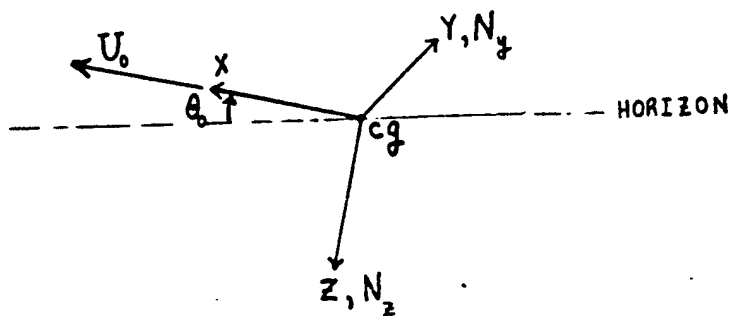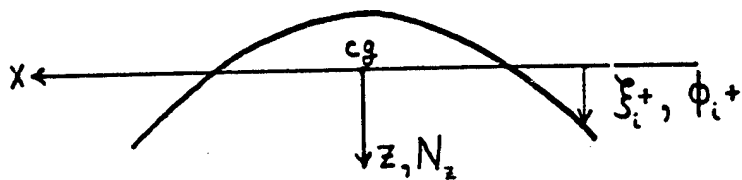
Figure 1: Stability Axis Sign Convention

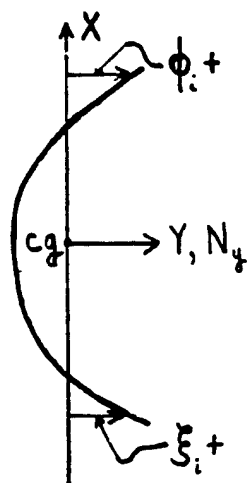Figure 2: Fuselage Vertical Bending Sign Convention

Figure 3: Fuselage Side Bending Sign Convention

531

$$N_z(\ell_x, t) = P_z\, x_z(t) \qquad\qquad (3a)$$

$$N_y(\ell_x, t) = P_y\, x_y(t) \qquad\qquad (3b)$$

The 1x(n+p) row vectors, $P_{z,y}$ are deterministic for a given vehicle equation of motion set, specific control, and specified gain value. Equations (3) can be manipulated into a mean square value expression for the loadfactor.

$$E\{N_{z,y}^2\} = P_{z,y}\, E\{xx'\}_{z,y}\, P'_{z,y} \qquad\qquad (4)$$

Assuming a stationary, zero mean process for the state differential system (1) leads to an algebraic matrix Riccati equation. This equation can be solved for the symmetric covariance matrix, $E\{xx'\}$. Utilizing one algorithm suggested by Gelb in reference 2, convergence can be obtained within 35 seconds on a CDC 6500 for a 16x16 Riccati system. A simple matrix multiplication routine completes the solution utilizing equation (4).

Study Vehicle Descriptions and Flight Conditions

The B-52H and B-1 were chosen for this study because they exemplify the trend toward more elastic structures for future large vehicles. The B-52, and commercial derivatives thereof, was a member of the first generation of elastic vehicles. Since that era, improved structural design techniques and composite materials have made possible vehicles like the highly elastic B-1.

The flight conditions were chosen because they represent cruise conditions which are mission essential and because turbulence encounters at low altitudes must be included in future design considerations.

The B-52H is used by the US Air Force as a long range bomber. It is 47.55 meters long and has a wing span of 56.4 meters. Originally designed as a high altitude bomber, it must now cope with penetration problems by combined high/low altitude profiles. Table 1 describes the flight condition for the B-52H.

```
Mass = 158,757 kilograms  (350,000 lbs.)
Mach = .55
Velocity = 185.56 meters/sec  (608.8 fps)
cg at 25% mean aerodynamic chord
Altitude = 609.6 meters  (2000 ft)
```

TABLE 1: B-52H Flight Condition

The B-1 is currently being test flown in a major pre-production effort by Rockwell International and the USAF. It is designed as the replacement vehicle for the aging B-52 fleet. The advanced structures and integrated technology make this vehicle an outstanding example for loadfactor

contributions due to elasticity. The overall length of the B-1 is 46 meters. The reference wing span utilized at the flight condition in Table 2 is 41.8 meters.

Mass = 103,315 kilograms (227,770 lbs)
Mach = .85
Velocity = 289.4 meters/sec (949.45 fps)
cg is at fuselage station 40.67 (meters)
Altitude = 30.48 meters (100 feet)

TABLE 2: B-1 Flight Condition

CONTROL LAW VARIATIONS

Both vehicles were modeled as stable, unaugmented systems in the vertical and lateral cases with the exception of the B-52H which required a small roll subsidence mode stabilization before proceeding. Each vehicle model was theoretically modified utilizing pitch rate, yaw rate, pitch rate/pitch attitude, blended pitch rate with acceleration, and full state feedback control laws. No significant differences in RQ were generated by these variations for identical (or nearly equivalent) handling quality values.

It should be mentioned here that the B-1 Structural Mode Control System was purposely not included or utilized because this study is involved with general control design parameterizations and not the specific RQ optimization of the B-1. For both aircraft studies, only the primary control surfaces (elevator, rudder, and aileron) were used for RQ determinations.

To establish a basis for comparison, the unaugmented vehicle loadfactors were computed for .3048 meter/sec (1 fps) rms (root mean square) gust velocities.

Figure 4 depicts the loadfactor curves for the unaugmented B-52H. The nearly linear loadfactors labeled "rigid body only" include all terms except the summations in equations (2a) and (2b). Hence any interactive rigid body and elastic dynamics from the Riccati solution are included in this output. The second line which has a more pronounced curvature includes all the modes that were utilized in the model. For the B-52H at this flight condition, the maximum elastic contribution to vertical loadfactors is about 15% of the total. (The lateral fuselage modes used in this data were primarily aftbody modes. Hence the rise in elastic effects near the tail.)

Figure 5 shows an impressive increase in the elastic contribution to vertical loadfactors on the unaugmented B-1. The discerning reader will immediately note the changes in vertical scale in figures 4 and 5. The different flight conditions and elastic contributions to ride on the separate vehicles dictated these scale changes.
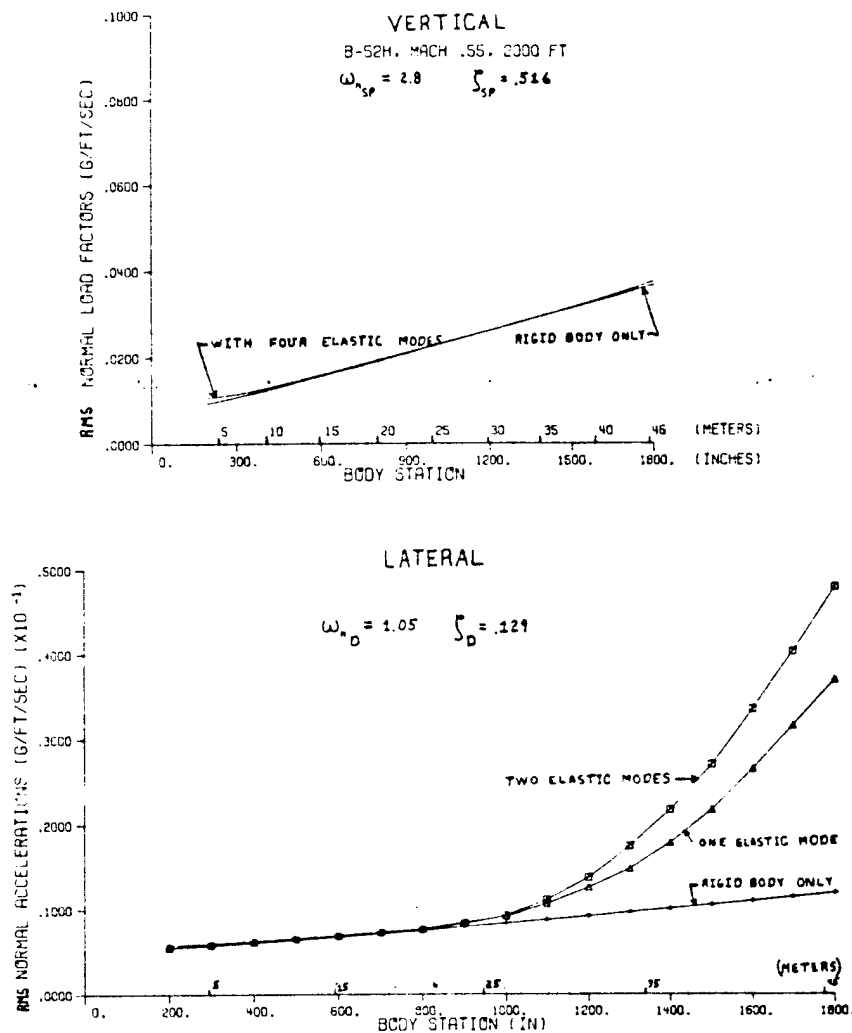
Figure 4: B-52H Unaugmented Loadfactors

RQ SENSITIVITY TO HANDLING CHARACTERISTICS

Under each control law studied, the gains were changed so that a range of handling characteristics and their resulting loadfactors could be cataloged. The values used for the handling characteristics were restricted to the acceptable ranges given in MIL SPEC 8785B. Hence the following boundaries:
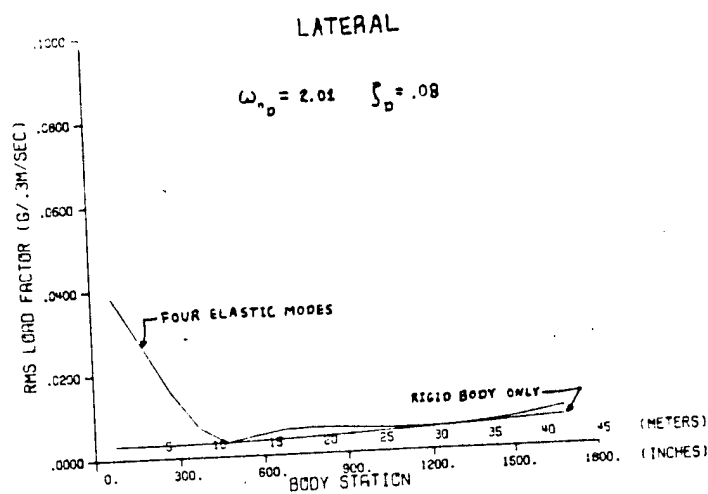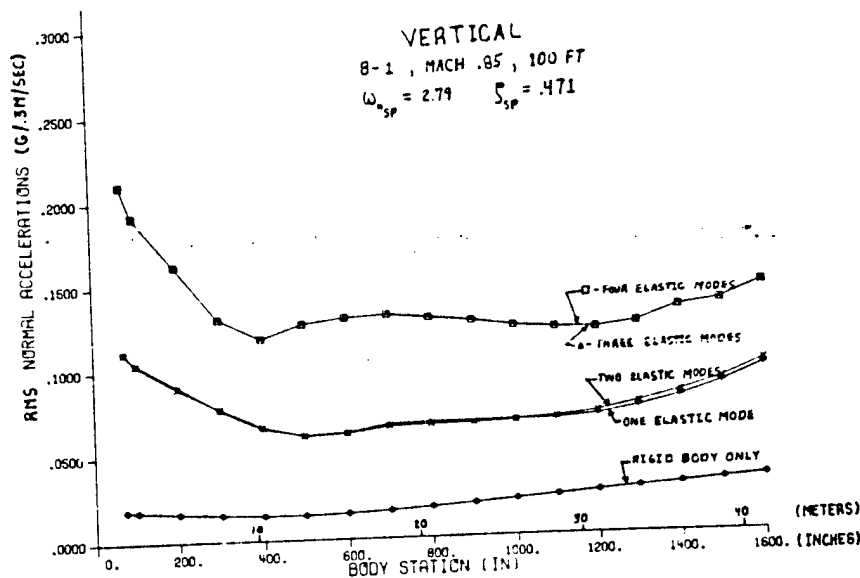
Figure 5: B-1 Unaugmented Loadfactors

Longitudinal Short Period $\left\{ \begin{array}{l} .3 \leq \zeta_{sp} \leq 2.0 \\ 2.0 \leq \omega_n^{sp} \leq 10.0 \end{array} \right.$

Lateral Dutch Roll $\left\{ \begin{array}{l} .08 \leq \zeta_D \\ .40 \leq \omega_n \end{array} \right.$

It is important to reiterate at this juncture that the study goal was RQ sensitivity to feasible controls, not the design of an optimal control for either vehicle.

Pitch Rate Feedback (B-52H)

Figure 6 shows the percentage change in loadfactor for various handling characteristics. The baseline in all these cases is the unaugmented vehicle loadfactors from figures 4 or 5, whichever is appropriate. As shown, the increase of damping and frequency for higher stabilizing feedback gains produced better RQ.
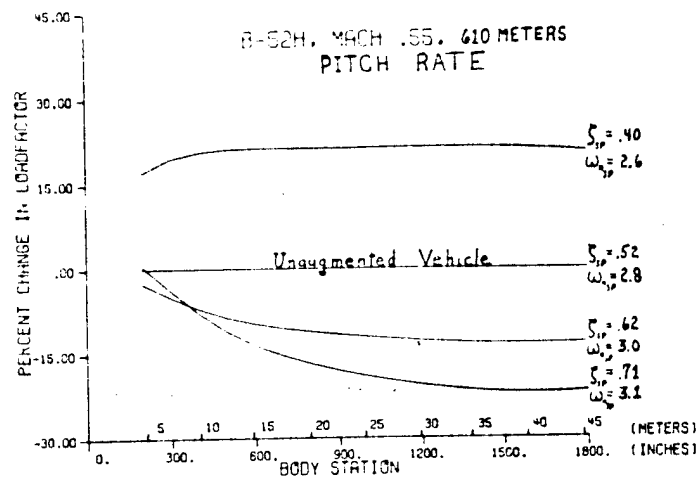
Figure 6: Pitch Rate SAS Changes

Yaw Rate Feedback (B-1)

Figure 7 shows the loadfactor curves for the B-1 lateral dynamics. Notice the effect is similar; increased damping produces better RQ.

536

Figure 7: B-1 Yaw Rate SAS Loadfactors

Blended Pitch Rate and Acceleration (C*) (B-1)

Figure 8 shows the percentage changes in loadfactor under the C* control policy with variations in handling characteristics. Again the same general trends appear.

Figure 8: B-1 C* SAS

Full State Feedback (B-52H)

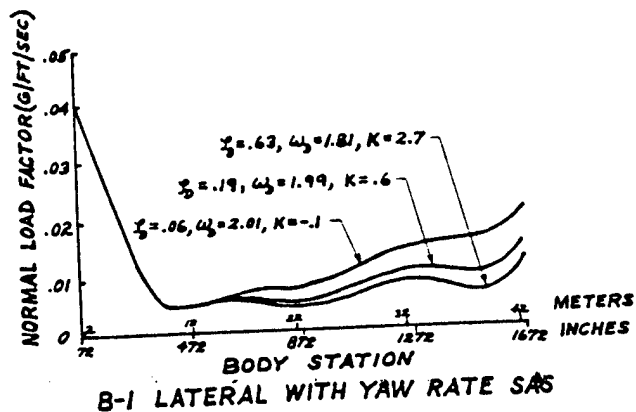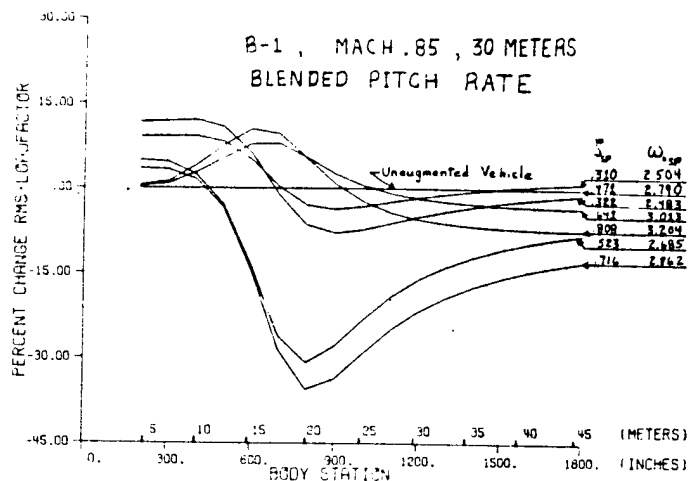The trend expected by control experts would show that higher frequency and higher damping beget better RQ. This expectation was validated using full state feedback pole placing capability. Figure 9 shows the results as percentage changes in loadfactor compared to the unaugmented vehicle. The forward fuselage percentage changes were distorted by relatively low baseline loadfactor values. Hence the higher damping/frequency loadfactor curves represent better rides overall. The asterisk cases in figure 9 deserve special mention. In these two cases the elastic mode damping was artificially increased through the elevator feedback control policy. Note that both cases generated appreciably worse RQ. This occurred because of the increased elevator excitation of the rigid body parameters in equations (2). Breakdowns of the elastic contributions to the loadfactors showed the three elastic modes chosen for increased damping actually did contribute less to the rms loadfactor.
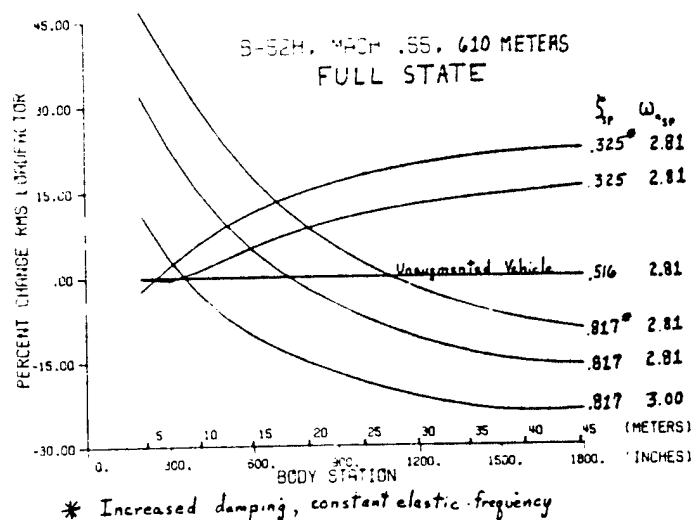
Figure 9: B-52 Full State SAS

This result prompted a theoretical attempt to parametrically plot loadfactor versus frequency and damping. Using a transfer function approach and the Dryden power spectral density for vertical gusts, the loadfactor mean square value was computed as an integral over the frequency domain. The results support the numerical analysis shown in figure 9.

As frequency increases, the RQ gets better. Likewise damping value excursions from the coupled elastic mode eigenvalue at constant frequency will adversely affect the loadfactors. A numerical example was run for the B-52H and is shown in figure 10 for two increased short period frequency cases. The elastic mode increased damping was not included in these cases.

Figure 10: B-52H Increased Short Period Frequency Effect
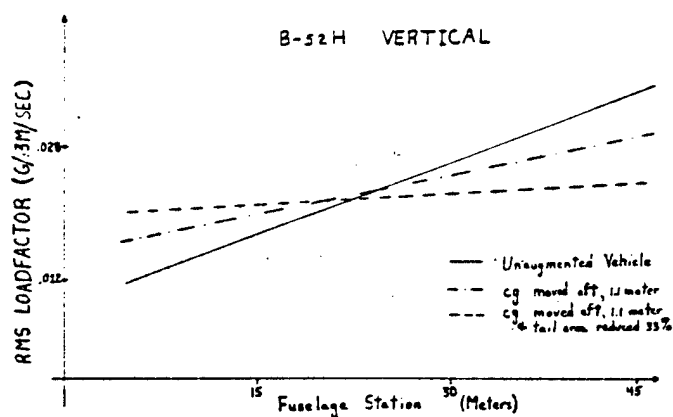
Figure 11: B-52H Rigid Body Relaxed Static Stability

539

RELAXED STATIC STABILITY (RSS)

Two methods were used to simulate this effect on the study vehicles. First the tail volume coefficient, $\bar{V}$, was reduced.

$$\bar{V} = \frac{\bar{l}_t \, S_t}{\bar{c} \, S} \tag{5}$$
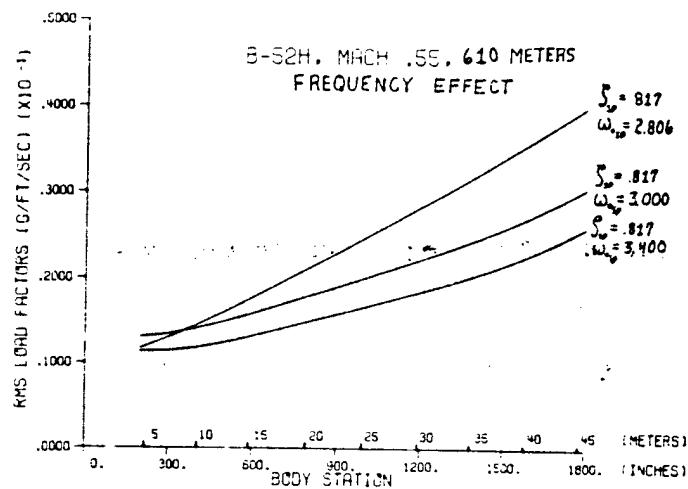
This has the effect of shifting the vehicle aerodynamic center toward the center of gravity. Static stability is thereby reduced. The second method involves an artificial cg shift toward the tail. This is the more practical of the two methods, as it has already been incorporated as a fuel transfer or management activity on a test vehicle (CCV B-52).

Figure 11 shows the effect of RSS on vertical ride for the rigid body B-52H vehicle. Essentially pitching moment effects are reduced until at neutral stability the loadfactors are constant and due only to the vertical accelerations. This would logically follow from the definition of the neutral point. The question now arises, what rides are induced by restoring the original handling characteristics of the unaugmented vehicle with an active control system? Figure 12 shows these results in terms of percent loadfactor change. In general the restoration resulted in degraded RQ.
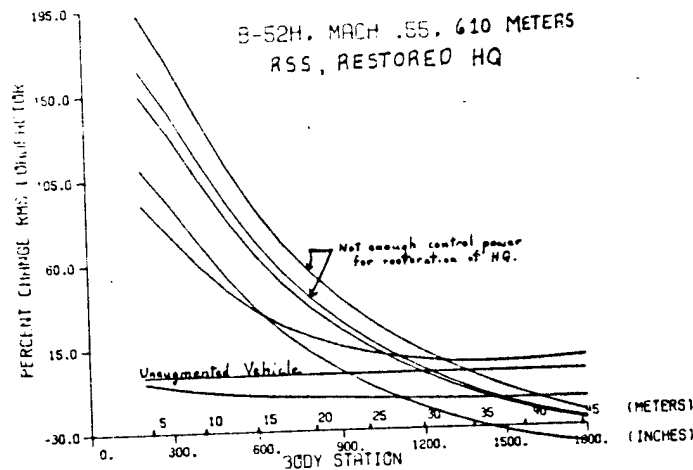
Figure 12: B-52H RSS, Restored Handling Qualities

CONCLUSIONS

1. Ride quality is particularly sensitive to the handling characteristics specifications.

2. Except in optimizing a particular vehicle's control capabilities, ride quality is not dependent on the type of control law chosen.

3. Relaxed Static Stability has a favorable effect on B-1 ride quality in that less pitch acceleration and/or velocity contribute to the loadfactor.

4. Relaxed Static Stability with restored handling qualities generates higher loadfactors on the B-52H and B-1 at the flight conditions studied.

REFERENCES

1. Heath, Robert E., II: State Variable Model of Wind Gusts, Air Force Flight Dynamics Laboratory Technical Memorandum, AFFDL-FGC-TM-72-12, Wright-Patterson AFB, Ohio, July 1972.

2. Gelb, Arthur, et al.: Applied Optimal Estimation, MIT Press, Cambridge, Mass., 1974.

3. Swaim, R. L., et al.: An Analytical Method for Ride Quality of Flexible Airplanes, Proceedings of the 3rd AIAA Atmospheric Flight Mechanics Conference, Arlington, Texas, June 1976.

A UNIFIED THEORY

FOR

PILOT OPINION RATING

By Ralph H. Smith
Vantage Engineering
Frenchtown, NJ

SUMMARY

This paper presents theory for understanding and predicting pilot opinion rating (POR) in closed loop, precision control tasks. The general implementation of the theory requires a unified model for pilot dynamics that is hypothesized to be multiple loop in form with essential nonlinearities. A search for such a model was unsuccessful. However, the apparent self-adaptive nature of the postulated model with respect to controlled element dynamics and system input suggests that, for single axis tracking tasks, a simple POR metric can be estimated using state-of-the-art pilot models. The POR theory was successfully demonstrated using available single axis tracking data. The proposed metric was shown to be a consistent, sensitive measure of POR for these data. Certain of these data were used to calibrate the variation of POR with the POR metric. This calibration, together with a suitable model for pilot-vehicle dynamics, can be used for the prediction of POR. It is suggested, however, that state-of-the-art models for pilot dynamics are generally unsuited for the precision estimation of the postulated POR metric in multiple loop or multiple axis tracking tasks; otherwise the POR theory has no obvious limitations of the sort that bound the validity of available pilot models. A generalized Paper Pilot method is proposed in a form consistent with this theory.

SYMBOLS

J	Cost functional for the optimal pilot model.
K_c	Controlled element gain
K_{D_θ}, K_{D_q}	Describing function approximations for display gains in θ and q loops
K_{F_θ}, K_{F_q}	Equivalent Kalman filter gains in θ and q loops
K_p	Pilot gain in the Servo model representation
K_θ, K_q	Controller gains in the optimal pilot model for the θ and q loops

POR	Pilot Opinion Rating (Cooper-Harper)
q	Pitch attitude rate, deg/sec
q_c	Pitch attitude rate command, deg/sec
q_p	Pitch attitude rate perceived by the human pilot, deg/sec
R	Cost functional weighting on $\sigma^2_{\dot{\delta}e}$
r	Cost functional weighting on $\sigma^2_{\beta q}$
s	Laplace transform variable, $s = \sigma+j\omega$
T_L	Pilot lead time constant in the servo model representation, secs
t	Time, secs
u	Forward speed, m/sec
W_θ, W_q	Cost functional weightings on σ^2_θ and σ^2_q
$Y_c(s)$	Controlled element transfer function
$Y_p(j\omega)$	Pilot describing function (servo model)
β_q	Central nervous system signal from central processor functions to the neuromuscular system
δ_e	Elevator deflection, deg
$\dot{\delta}_e$	$d\delta e/_{dt}$
θ	Pitch attitude, deg
θ_e	Pitch attitude tracking error, deg
θ_p	Pitch attitude perceived by the human pilot, deg
σ_q	Standard deviation of q, degs/sec
σ_{q_p}	Standard deviation of q_p, degs/sec
$\sigma_{\beta q}$	Standard deviation of βq, degs
σ_{θ_p}	Standard deviation of θ_p, degs

INTRODUCTION

The present state-of-the-art of handling qualities is fundamentally empirical. Available theories for handling qualities are all based upon a network of empirical data, experiences with classical airframe dynamics, servomechanisms analogies, and conjectural hypotheses which attempt to establish a connection between handling qualities and available models for human pilot dynamics. All these have some demonstrated value for the codification of experimental data or for the design of experiments; none has provided significant insight into the physics of handling qualities or has a demonstrated, general capability for a priori prediction of handling qualities. We have no better physical understanding now of the dynamics of human subjective response than we had prior to development of the servomechanisms model for human pilot dynamics.

The elusive, intangible nature of handling qualities has presented a formidible obstacle to the development of a physical theory for the subject. We haven't even successfully defined what we mean by "handling qualities". Attempts to do so are inevitably either personalized and vehicle-centered or general, vague and practically useless. The entire concept of "quality" is involved. Reference 1 is recommended for a discourse on quality and what it can mean to our technology.

The lack of a suitable definition for handling qualities does not prevent us from recognizing degrees of handling qualities in practice. We attempt to systematically code these in terms of airframe and control system parameters as a means for evaluating system design. It is here that the lack of a physical and philosophical understanding of handling qualities has its real impact on research. We arbitrarily invent handling quality metrics and proceed to devote valuable resources to their study. This is all too often done without concern for whether our inventions are capable of bringing unity of understanding to a chaotic subject. This tangential approach has produced no real payoff to research or systems design.

The sad fact is that handling qualities is not entirely credible as a mature design technology; it remains a handbook art. This field differs from other technology areas involved in aircraft design in one fundamental respect: it is without foundation on physical principles such as exist for other fields. Handling qualities has no counterpart to the equations of Navier-Stokes, Maxwell, or Euler-Lagrange. Accordingly, we are unable to quantify the benefits of handling qualities to systems design except on the most primitive level.

The handling qualities discipline originated with the pilot's subjective opinion of ease of aircraft control. Opinion scales were invented to quantify the pilot's subjective response. Pilot opinion rating (POR) is a widely used and poorly understood metric for handling qualities. It has almost become a de facto substitute for handling qualities through familiarity.

POR data often appear to be highly variable and to exhibit unpredictable, systematic biases among the pilot population and random variations for a given pilot. A major tenet of the present work is that anomalies in POR data may be illusory. Without a physical theory for handling qualities (and, therefore, for POR) one should not assume that all the factors parameterizing POR are known for a given experimental configuration. Given the typical handling quality experiment, it is a logical error to classify POR data as inconsistent or variable merely because the same numerical rating was not obtained for multiple runs with the same configurations of vehicle dynamics and system input or because the variation of POR with vehicle response parameters does not obey the analyst's preconceived theory.

As a practical matter we must expect that POR data obtained from a carefully designed, realistic experiment will exhibit a certain amount of variability. What we need to do is develop methods for ensuring that the variability is not the systematic result of applying faulty theory or inadequate metrics for the correlation and assessment of POR data. Unexplained variations in POR would not, in fact, be random if the pilot subjectively responds to a particular system property; in that case POR data might be almost perfectly consistent with a suitable, but unknown, metric--in other words it is conceivable that it is the engineering analyst and not the pilot who establishes the level of variability in POR data!

Of course the pilot is not a machine; run-to-run variability of a genuinely random nature probably must be expected. The Cooper-Harper scale for POR is not perfect and must be selectively interpreted by the evaluation pilot. The present state-of-the-art requires that such effects be minimized by averaging sufficient POR data. We should insist, however, that such data be uncontaminated by effects that are within our capabilities to understand and control. This is not easily accomplished.

The research summarized in this paper is based on the hypothesis that:
(1) a pilot's subjective response originates from a particular point, or area, within his central nervous system, and
(2) POR is directly and uniquely related to the strength of the neural signal at this location. If the validity of this hypothesis can be established, then handling qualities can eventually be quantified by direct measurement; also, handling qualities can be predicted given a satisfactory model for pilot dynamics.

A UNIFIED MODEL FOR PILOT DYNAMICS

There exist only two state-of-the-art models for pilot-vehicle system dynamics and performance that have received general acceptance for analysis of single loop, continuous tracking tasks. The servomechanisms model (reference 3) was developed to parameterize pilot dynamics for a wide range of controlled elements. The Kleinman optimal control model (reference 4) was devised as a formal tool for the prediction of pilot-vehicle system performance. Both models are fundamentally empirical. One must depend upon the

existence of baseline data for their parameterization; they are, in a sense, interpolative. Neither model offers real hope for understanding the fine-grain character of pilot dynamics (e.g. the variations of phase margin or crossover frequency with controlled element dynamics, the source of pilot remnant, crossover frequency regression, control stick "pulsing", control stick "pumping", the basis for pilot-generated dynamic equalization, etc.). If we are to develop a general theory for handling qualities, then a more refined and physically oriented model for pilot dynamics is a necessity.

Reference 2 offers two hypotheses which define the scope and nature of the model sought:

HYPOTHESIS 1:

The servo and the optimal control models for human pilot dynamics are linearizations of a more fundamental (and physically acceptable) nonlinear model.

HYPOTHESIS 2:

A model for human pilot dynamics that structurally matches the human physiology in the tracking process will lead to a natural and physical measure for POR.

The pilot model shown in figure 1 was investigated in reference 2 and is proposed to be such a model. It is believed that—when properly parameterized—it will exhibit most of the known response properties of the human pilot. The model of figure 1 is intended to subsume the servo and the optimal control models. Note that figure 1 applies for a pitch attitude tracking task. This is the only case that will be considered in this paper. The model is applicable to any single axis task, however.

The model of figure 1 is nonlinear and multiple loop in form. It has, to this date, not been successfully parameterized in the fashion desired. It is demonstrated in reference 2, however, that the nonlinear model is a very plausible explanation for the parametric variations required by the servo model as a function of controlled element dynamics. This is illustrated in figure 2 for the three familiar controlled element forms: $Y_c(s)=K_c$, K_c/s & K_c/s^2. A highly simplified, linear version of the proposed nonlinear pilot model is shown on figure 2. It may be directly compared with the servo model $Y_p(j\omega)$ following closure of the q-loop; the resulting closed loop model connecting θ_c with δe is then formally the same as $Y_p(j\omega)$ from the servo model representation. The approximate forms for $Y_p(j\omega)$ predicted by the nonlinear model are shown in figure 2 for each of the three elementary controlled elements. The model in figure 2 is assumed to result from combinations of model nonlinearities and closed loop dynamics which create the situation shown where q_c is negligible with respect to q.

The nonlinear model suggests that low frequency approximations to $Y_p(j\omega)$ should resemble

1. a pure gain for $Y_c(s) = K_c/s$
2. a gain and a low frequency lag for $Y_c(s) = K_c$, and
3. a gain with a low frequency lead for $Y_c(s) = K_c/s^2$.

These results are consistent with measured human dynamics as embodied in the servo model. The fact that rate feedback in the nonlinear model (figure 1) can conceivably produce an apparent low frequency lag in measurements of $Y_p(j\omega)$ for pure-gain controlled elements is a remarkable result. When the effects of q_c are not neglibible in comparison with those of q the nonlinear model will predict a gain plus first order lead for $Y_c(s) = K_c/s^2$ rather than the gain with pure lead shown.

Another startling implication of the nonlinear model is that it can exhibit considerable rate feedback without creating an apparent low frequency lead in measurements of $Y_p(j\omega)$--see figure 2 for $Y_c(s) = K_c/s$. In general, the nonlinear model indicates that the level of pilot control of system rate need not be directly reflected in low frequency lead or lag equalization as measured in the describing function $Y_p(j\omega)$--the servo model for pilot dynamics. In contrast, this author's experience with the Kleinman optimal control model indicates that it too can produce a sizable rate feedback gain with a K_c/s-like controlled element. Thus, there is a formal similarity between the Kleinman model and the nonlinear model of figure 1.

A THEORY FOR PILOT OPINION RATING

The qualitative nature of the handling quality tasks posed by each of the three elementary controlled elements is noted on figure 2. It might appear that increasing task difficulty (as reflected in POR) can be associated with an increase in the pilot model's rate gain K_q. This is not entirely true. A more appropriate indication of task difficulty should be expected in measures of closed loop signals since it is these which ultimately determine the linearized forms for the pilot model and its components. It is therefore tempting to speculate that βq, the q-channel response of the nonlinear pilot model, will parameterize POR regardless of system input or controlled element dynamics since βq will depend on both K_q and the closed loop response.

As an illustration of the possible connection between system rate and handling qualities consider that for easily controlled vehicles system rate is seldom large, whereas a vehicle that is difficult to control will demand that the pilot devote considerable effort to the stabilization of rate errors. It should be apparent that if rate cannot be readily controlled then neither can attitude and the handling will suffer. Thus, good rate control is very nearly a necessary and sufficient condition for good handling qualities. The closed loop signal βq would, in the human pilot, consist of a series of neural potentials (or electrical pulses) within a certain region of the central nervous system. These conjectures are formalized in the following

547

hypothesis.

HYPOTHESIS:

A physiological measure for POR is the rate of nerve impulses (or an equivalent measure) at the point within the central nervous system where all signals originating due to rate control are summed or operated upon by a decision process of some sort. The neuromuscular system is postulated to provide a component to this hypothesized signal junction; this component is dependent upon the feel system characteristics and will affect POR. The relation between POR and the nerve impulse rate is fixed for each pilot. It may depend upon his piloting experiences, training and his personal interpretation of the rating scale. It is independent of controlled element dynamics, input and task.

The postulated output from the human pilot "central processor's" rate channel βq (as depicted in figures 1 & 2) is not directly accessible for measurement. It is internal to the central nervous system. In its simplest form βq probably consists of a series of nerve pulses with the pulse frequency proportional to the neural excitation at the point of impulse generation. For present purposes it is probably sufficient to assume that, in continuous tracking tasks with random inputs, βq can be parameterized by its standard deviation $\sigma_{\beta q}$. Given a high fidelity pilot-vehicle system model, $\sigma_{\beta q}$ can be estimated; perhaps $\beta q(t)$ can eventually be directly monitored given advances in medical technology.

By the above hypothesis and the assumption that βq can be represented by $\sigma_{\beta q}$, we may expect that POR will vary with $\sigma_{\beta q}$ in the manner illustrated in figure 3.

Observe that, by hypothesis, POR is a function of only $\sigma_{\beta q}$ for a given pilot. However, $\sigma_{\beta q}$ is dependent upon anything that affects the signal strength of $\beta q(t)$. This includes controlled element dynamics, input spectrum, display properties (since these affect the signal transmission of rate error) the task and feel system. It may include various vehicle motion cues available to the pilot in a flight test or moving base simulation.

At the present time no model for neuromuscular system dynamics is known to this author which will permit the estimation of feel system effect on $\sigma_{\beta q}$. Many past experiments have confirmed the importance to POR of the feel system. As a result, our present theory for the correlation or prediction of POR appears to be restricted to consideration of only those pilot-vehicle data for which the control system was optimized with respect to POR.

VALIDATION OF THE RATING METRIC
IN SINGLE AXIS TRACKING

The hypothesized POR metric $\sigma_{\beta q}$ can be correlated with rating data from

any handling quality experiment provided sufficient data are available to permit the estimation of $\sigma_{\beta q}$ (given a satisfactory model for pilot dynamics), provided that the control feel system was optimized with respect to POR prior to each data run, and given sufficient POR data to permit the estimation of statistically valid POR averages for each tested configuration. Few such data sources exist.

Note that the servo and the optimal control models for pilot dynamics are suitable only for the estimation of <u>average</u> system properties. This will constitute a source for systematic error in any attempts to correlate POR with $\sigma_{\beta q}$ using these pilot models since it is likely that $\sigma_{\beta q}$ will vary from run-to-run with the same configuration due to pilot nonlinearities. It is reasonable to suspect that the run-to-run variance of $\sigma_{\beta q}$ will be greatest for those configurations that are the most difficult to control. Until $\sigma_{\beta q}$ can be directly measured by experiment, there is no way to eliminate this error component from correlations of POR with $\sigma_{\beta q}$; hopefully, its effects will be small relative to the basic trends. If present theory is basically correct, then the run-to-run variation of $\sigma_{\beta q}$ is responsible for much of the so-called pilot variability that pervades the handling qualities data base. It also explains why more data runs are required for the valid estimation of average POR when the vehicle dynamics are poor (reference 5).

It has already been noted that the servo model will not always correctly reflect the level of rate control predicted by the nonlinear or optimal control models for pilot dynamics. When $Y_c(s) = K_c/s$ the servo model requires no low frequency equalization (and therefore no rate control) whereas the nonlinear model indicates that considerable rate control may exist. As a rule-of-thumb, when the servo model would require either a lead time constant less than 0.5 seconds or a lag then it should not be used for the estimation of $\sigma_{\beta q}$.

The nonlinear model of figure 1 has not yet been successfully parameterized and therefore cannot be used for the estimation of $\sigma_{\beta q}$. However, there is no objection to use of the optimal control model. A version of this is shown in figure 4 for the pitch attitude control example. This model differs significantly from the conventional Kleinman model. It incorporates describing function representations for the visual threshold nonlinearities in the rate and attitude channels (K_{Dq} & $K_{D\theta}$, respectively); the cost functional is stated in terms of the state variables perceived by the human pilot. A discussion of this model can be found in reference 6 where it was introduced. The cost functional weights shown in figure 4 were selected in reference 6 to optimize the fit between measured and predicted closed loop system performance for Arnold's tracking data (reference 7). Arnold's data are entirely satisfactory for testing the proposed POR metric.

Note that for the Kleinman-Dillow model,

$$\sigma_{\beta q} = K_{Dq} \, K_{Fq} \, K_q \, \sigma_q = K_q \, \sigma_{q_p}$$

The Kalman filter gain K_{Fq} is describing function approximation to the actual filter operation. The model shown in figure 4 is strictly applicable only after convergence of the optimization routine.

The Kleinman-Dillow model was applied to the Arnold tracking data to estimate $\sigma_{\beta q}$ for each of his dynamic configurations. The Arnold POR measurements were obtained using values of pitch control effectiveness that were approximately optimum with respect to POR, and sufficient data were collected to permit the reasonable determination of average POR for each configuration. Arnold also published measured σ_q; thus the Kleinman-Dillow model was required only for the prediction of rate loop gain $K_{Dq} K_{Fq} K_q$. The resulting correlation between Arnold's averaged POR data and the model-predicted $\sigma_{\beta q}$ (shown on figure 5) is seen to be quite good; the hash marks represent plus and minus one-half rating unit (Cooper-Harper scale) about the mean curve.

The Arnold-derived correlation shown on figure 5 was obtained from POR data averaged over several pilot subjects. Thus, if present theory is correct the variation of $\sigma_{\beta q}$ with the nominal fit to Arnold's POR data should constitute a model for the _prediction_ of POR, averaged over many pilots, provided only that a satisfactory model for pilot dynamics is available to enable the estimation of $\sigma_{\beta q}$. In other words, the function POR $(\sigma_{\beta q})$ shown in figure 5 should be constant over a wide range of experimental conditions.

The optimal control model of figure 4 was applied _without change_ to McDonnell's data (reference 5). Unfortunately reference 5 did not publish measured σ_q; thus it was necessary that the Kleinman-Dillow model be used for the prediction of the rate loop gains and σ_q. Also, the McDonnell data were very sparse; in order to extend his data base it was necessary to average his POR data for a given configuration without regard for control system gain. The resulting correlation is shown on figure 5; the correlation is supportive of the present theory to a degree that is better than might be expected in view of the data's shortcomings.

Two additional data points were obtained from Johnson (reference 8) who applied the Paper Pilot theory to moving base simulator data published by Onstott, et al (reference 9). The servo model was used to represent pilot dynamics. Of the 35 configurations examine by Johnson only two resulted in non-zero estimates for the pilot lead time constant; thus, these are the only two cases for which the servo model can be used to estimate $\sigma_{\beta q}$. (Time did not permit the application of the Kleinman-Dillow model to these 35 cases). For these two points $\sigma_{\beta q} = K_p T_L \sigma_q$ where $K_p T_L$ are the servo model gain and lead time constant, respectively. Onstott did not publish σ_q and his control system was not optimized relative to POR. Johnson's published values of σ_q, estimated from the Paper Pilot analysis, were used here for the esti-

mation of $\sigma_{\beta q}$. The two Onstott-based data points, shown in figure 5, completely support the present theory.

The three data sets shown on figure 5 represent a wide range of controlled element dynamics, input intensities, manipulator characteristics and piloting backgrounds. The Onstott data were from a motion simualtion. McDonnell's data were for a command input tracking task.

There are no other acceptable data sources known to this author for further testing of the present theory. Based on the correlations obtained, the hypothesis that POR is parameterized by $\sigma_{\beta q}$ is considered as tentatively confirmed under the cited restrictions.

IN-FLIGHT VS. FIXED-BASE POR DIFFERENCES

Arnold compared his fixed-base simulation measurements of POR with those of Neal and Smith obtained from flight test for the same aircraft dynamics (reference 10). This comparison, shown in figure 6, is generally good. Arnold's three best-tested configurations were significantly down-rated in flight, however. He attributed this to task differences between the two experiments.

These three configurations were re-examined using present theory. The Kleinman-Dillow model was modified to simulate the probable display characteristics of the Neal-Smith flight tests. This was done simply by removing the large display threshold present in Arnold's simulation. Predictions were then made of $\sigma_{\beta q}$ for these three cases. The predicted in-flight POR were estimated from the nominal curve fit to Arnold's data shown in figure 5. These revised predictions of in-flight POR are spotted on figure 6.

The good agreement between the predicted and measured in-flight POR for these cases suggests that Arnold's display threshold was a major source for the in-flight vs. fixed-base POR differences. Display threshold effects on the other configurations would be comparatively small. Motion cue effects may be important for explaining the differences between the more poorly rated configurations. These do not appear to be explainable with the Kleinman-Dillow model in the form shown in figure 4.

RATING PREDICTION IN MULTIPLE LOOP TRACKING

Estimates of $\sigma_{\beta q}$ were made for the precision VTOL hover configurations of Miller and Vinje (reference 11) using data supplied to the author by James Dillow of the Air Force Institute of Technology. These were made using the Kleinman model configured to match the measured system performance data. This was the data base used by Anderson in his original Paper Pilot study (reference 12). The Miller-Vinje data were obtained with optimized control

551

effectiveness. The POR were based on the Cooper scale; these were converted to the Cooper-Harper scale using conversion equations suggested by McDonnell (reference 5).

The Miller-Vinje simulation task was to hover a VTOL aircraft over a ground reference in turbulence. The longitudinal control problem was to create or arrest a forward velocity with pitch attitude control. The pilot was therefore required to control forward position, speed u, pitch attitude θ, and pitch attitude rate q.

The variation of predicted $\sigma_{\beta q}$, with measured POR is shown in figure 7. It appears that $\sigma_{\beta q}$ is not unreasonable as a correlating metric for POR; however, the data do not support the Arnold results except in the region where POR is less than about 3.

Part of the correlation problem is that it isn't clear what we should use as a measure for system rate in a multiple loop system with the Kleinman model. If both u and q are superimposed to form an augmented rate then a somewhat better fit can be obtained as shown in figure 7.

A conclusion of reference 2, however, was that no state-of-the-art pilot model is entirely suited for the estimation of the handling quality metric. It was further concluded that a switching model was a likely candidate for explaining pilot dynamics in multiple loop/axis tracking.

It is interesting that both metrics shown in figure 7 yield POR correlations that are asymptotic to the Arnold data in the region of good handling qualities. This suggests that, in this region, outer loop control of speed or position has little effect on handling qualities.

A GENERALIZED PAPER PILOT METHOD

Dillow and Picha, in reference 6, propose a generalized Paper Pilot method for formalizing the prediction or correlation of POR. They suggest using the Kleinman model for pilot dynamics--incorporating provisions for display or visual thresholds--and a cost functional based on pilot-perceived system states as illustrated in figure 4. By replacing the servo model with the Kleinman model and its attendant cost functional they hoped to eliminate the troublesome Paper Pilot rating functional which has been a principal weakness in the theory. Their rationale for doing this was that it may be easier to select appropriate weights for the Kleinman model cost functional than to find a general rating functional for the Paper Pilot theory.

Their approach to the estimation of POR is empirical. They assume that POR=$\sqrt{J}$, provided that the weights of J (the cost functional) are selected to optimize the model-predicted and measured match of system performance and POR. This rating predictor was totally inaccurate for the McDonnell data when the cost functional was weighted using Arnold's data as a base.

It is suggested in reference 2 that the Dillow-Picha revisions to Paper Pilot have merit provided that J is augmented by a term representing POR (in keeping with the spirit of the original Paper Pilot theory); the POR estimate must then be determined using this component of J and not the total value. For the pitch tracking cases discussed in this paper a suitable cost functional should be

$$J = W_\theta \sigma_p^2 + [W_q + rK_q^2] \sigma_{q_p}^2 + R\sigma_{\delta_e}^2$$
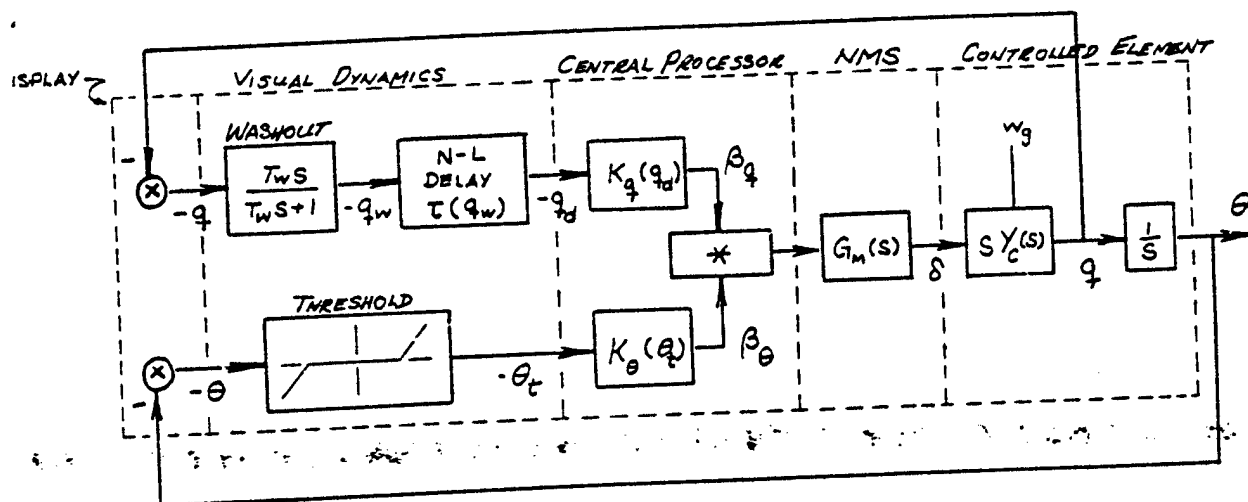
$$POR = fcn\ (\sigma_{\beta q})$$

Note that J is now a function of the optimal control gain K_q.

REFERENCES

1. Pirsig, Robert M.: Zen and the Art of Motorcycle Maintenance. Bantam Books, April 1975.

2. Smith, Ralph H.: A Theory for Handling Qualities With Applications to MIL-F-8785B. AFFDL-TR-75-119.

3. McRuer, Duane; Dunstan Graham; Ezra Krendel; William Reisener, Jr.: Human Pilot Dynamics in Compensatory Systems: Theory, Models and Experiments With Controlled Elements and Forcing Function Variations. AFFDL-TR-65-15, July 1965.

4. Baron, Sheldon; David L. Kleinman; Duncan C. Miller; William H. Levison; and Jerome I. Elkind: Application of Optimal Control Theory to the Pre-Diction of Human Performance in a Complex Task. AFFDL-TR-69-81, March 1970.

5. McDonnell, John D.: Pilot Rating Techniques for the Estimation and Evaluation of Handling Qualities. AFFDL-TR-68-76, December 1968.

6. Dillow, James D.; Douglas G. Picha: Application of the Optimal Pilot Model to the Analysis of Aircraft Handling Qualities. Air Force Institute of Technology, Wright-Patterson AFB, Ohio, AFIT-TR-75-4, August 1975.

7. Arnold, John D.: An Improved Method for Predicting Aircraft Longitudinal Handling Qualities Based on the Minimum Pilot Rating Concept. Air Force Institute of Technology, Wright-Patterson AFB, Ohio, GGC/MA/73-1, June 1973.

8. Johnson, Robert B.: Predicting Pitch Task Flying Qualities Using Paper Pilot. Air Force Institute of Technology, Wright-Patterson AFB, Ohio, GGC/MA/73-2, June 1973.

9. Onstott, E.D.; E.P. Salmon; R.L. McCormick: Prediction and Evaluation of Flying Qualities in Turbulence. AFFDL-TR-71-162, February 1972.

10. Neal, T.P.; R.E. Smith: An In-Flight Investigation to Develop Control System Design Criteria for Fighter Airplanes. Vol. I and II, AFFDL-TR-70-74, June 1970.

11. Miller, David P.; Edward W. Vinje: Fixed-Base Flight Simulation Studies of VTOL Aircraft Handling Qualities in Hovering and Low Speed Flight, AFFDL-TR-67-152, January 1968.

12. Anderson, R.O.: A New Approach to the Specification and Evaluation of Flying Qualities. AFFDL-TR-69-120, May 1970.

* A SUMMER OR A NONLINEAR SWITCH

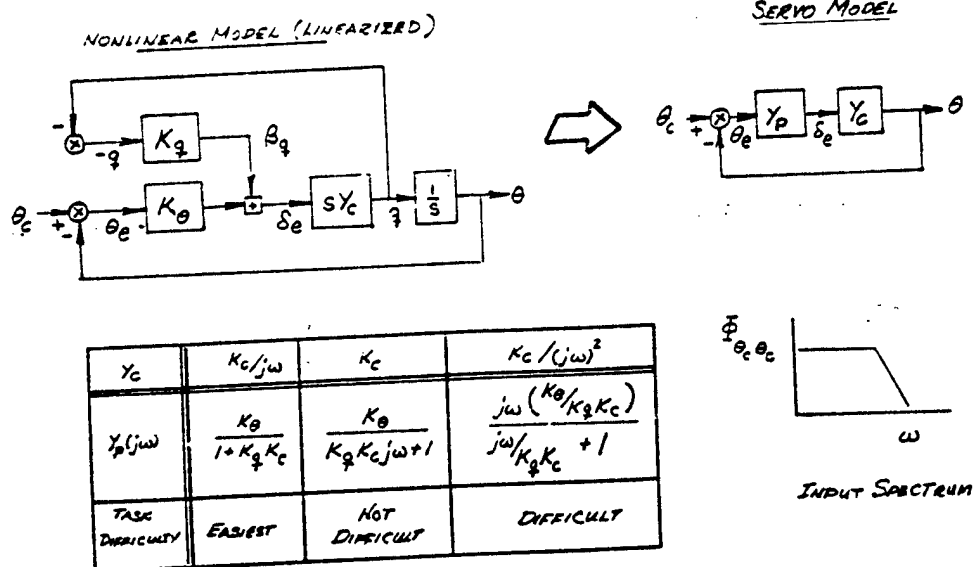Figure 1....Nonlinear Model for Pilot-Vehicle System

Figure 2....Linear vs. Nonlinear Model Comparisons

555
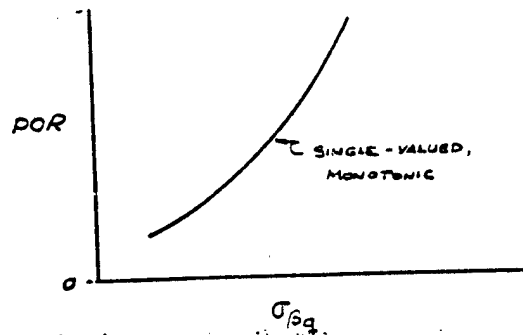
POR= fcn(σ_{β_q} , pilot...experience, background, etc.)

σ_{β_q} = fcn($Y_c(s)$, input, display, task, manipulator)

Figure 3....Hypothetical Variation of σ_{β_q} with POR
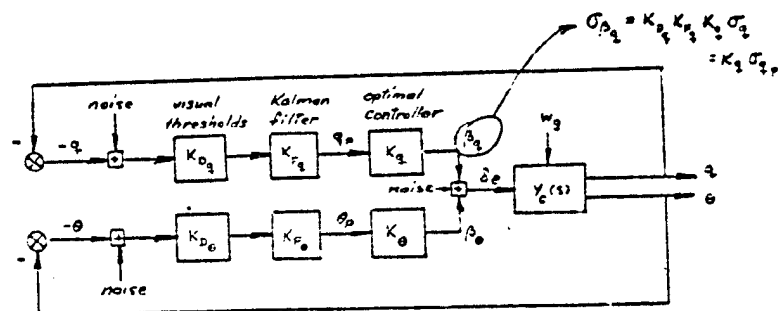
$q = \frac{d\theta}{dt}$

$K_{D_q} \, \& \, K_{D_\theta}$.- VISUAL THRESHOLD DESCRIBING FUNCTIONS

$K_{F_q} \, \& \, K_{F_\theta}$ - EQUIVALENT KALMAN FILTER GAINS

$K_q \, \& \, K_\theta$ - FEEDBACK GAINS CHOSEN TO MINIMIZE

$$ J = 70\,\sigma_{\theta_p}^2 + 7\sigma_{q_p}^2 + R\sigma_{\delta_e}^2 $$

$q_p \, \& \, \theta_p$ - OPERATOR PERCEIVED STATE VARIABLES

Figure 4....Equivalent Kleinman-Dillow Model for Pitch Attitude Tracking

Figure 5....Data Correlations

Figure 6....In-Flight vs. Fixed-Base POR Data

Figure 7....Correlations of Multiple Loop POR Data

LONGITUDINAL FLYING QUALITIES IN THE LANDING APPROACH

By William W. Rickard

McDonnell Douglas Corporation, Douglas Aircraft Company
Long Beach, California 90846

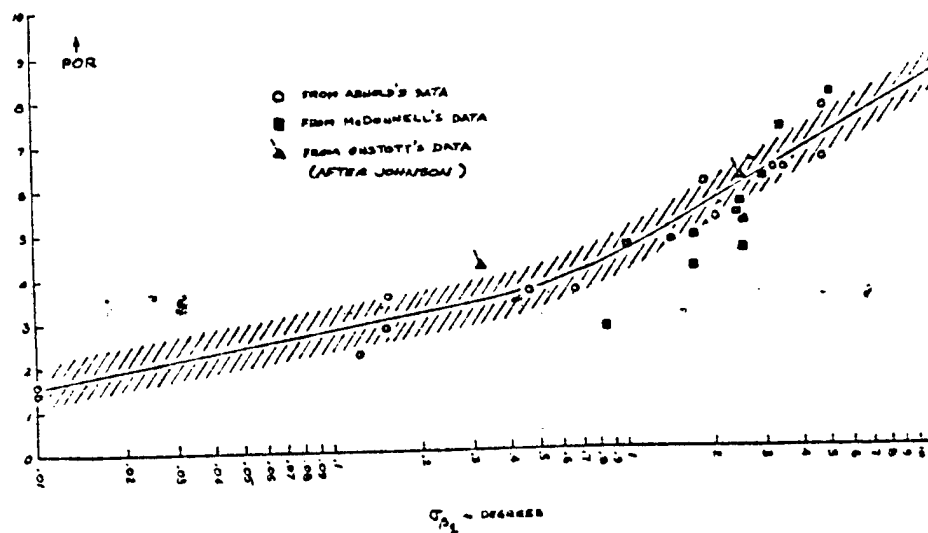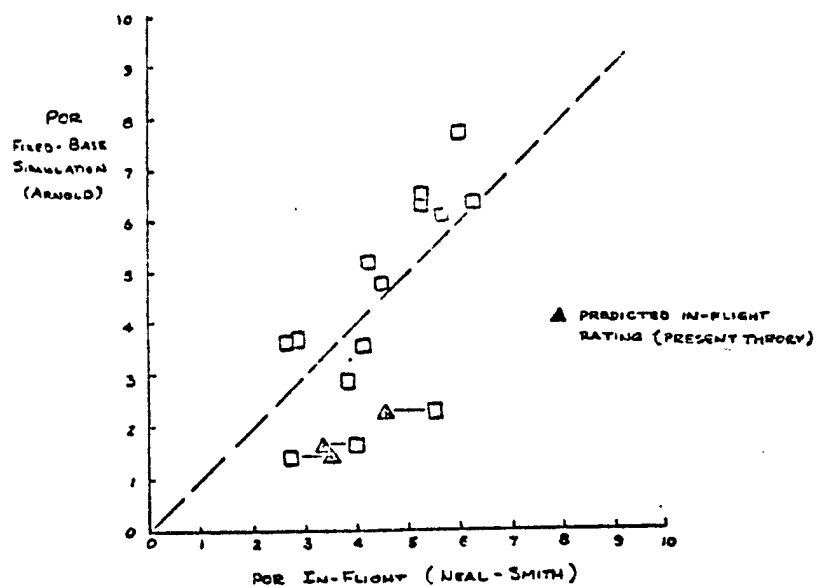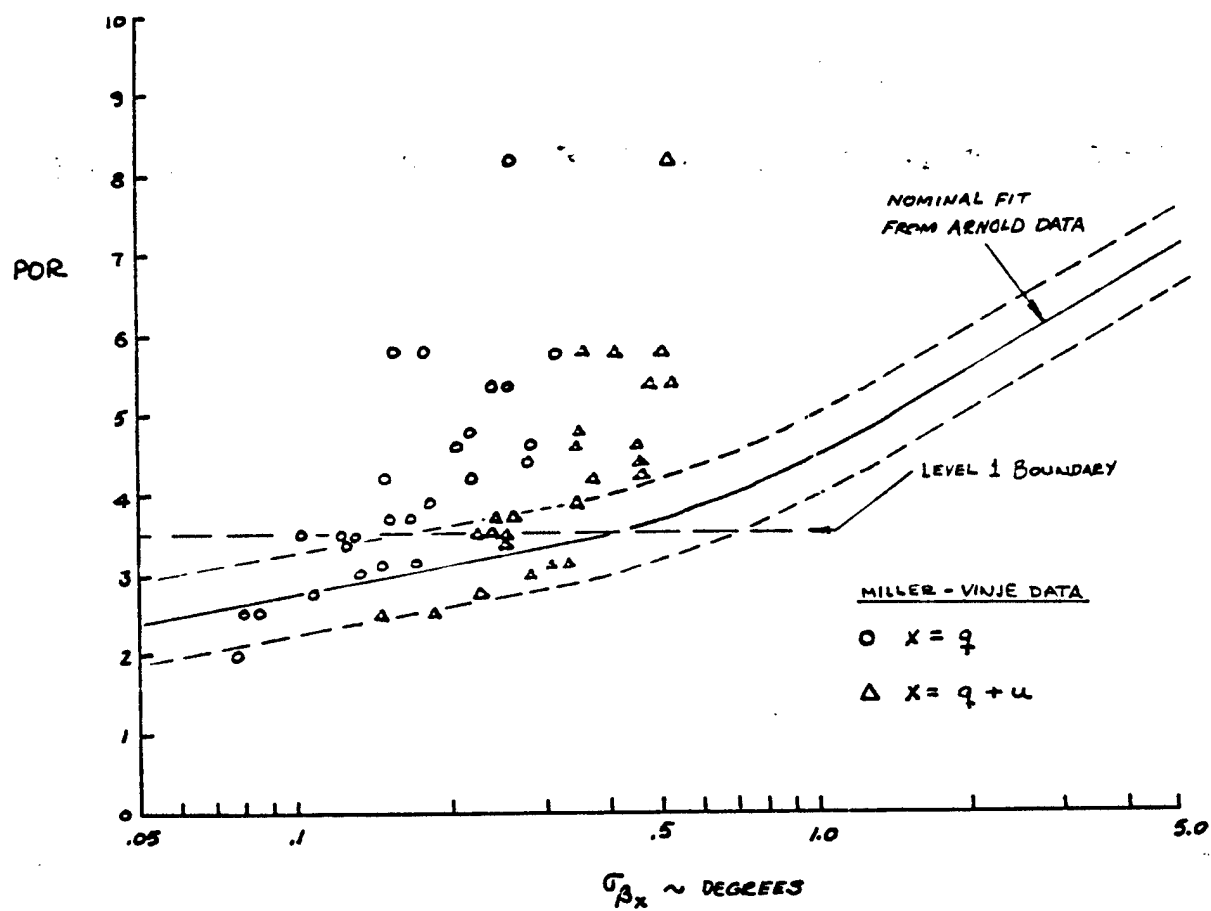## ABSTRACT

An investigation of the longitudinal flying qualities of large transport aircraft in the landing approach was performed as a portion of a long-range flying qualities independent research and development program at the Douglas Aircraft Company. A literature study was performed to gather all criteria which showed promise as estimators[1] of flying qualities. Then a piloted motion base simulator experiment was conducted to produce data which could be used to evaluate the selected criteria. Each criterion was evaluated by comparing the estimated flying qualities it produced for each configuration with the Cooper-Harper ratings given by the pilots. An appraisal was then made of each criterion based on its performance in this study. The criteria evaluated included several from MIL-F-8785B (Reference 1) (flight path stability, short period frequency, short period damping ratio, phugoid stability, and static stability), the short period criterion of SAE ARP 842B (Reference 2), the short period criterion of Reference 3, and a pitch tracking task criterion (References 4,5,6). The best results were obtained by combining the information contained in the flight path stability and pitch tracking task criteria.

INTRODUCTION

The ability to accurately estimate the flying qualities of an airplane which exists only on paper is essential to the aerodynamic, control system, and autopilot design processes. Many criteria exist for estimating flying qualities, of which the best example is the MIL-F-8785B. Unfortunately, this is a military flying qualities specification, containing criteria developed primarily on the basis of research and design experience on military aircraft. The criteria in the MIL-F-8785B can be applied to all types of aircraft, from the smallest trainer to the largest transport. However, there is much less data to support the criteria for large transport (Class III) airplanes than there is for fighter/attack/interceptor (Class IV) airplanes. Designers of civil transport aircraft tend to doubt or even disbelieve the validity of some of the criteria (e.g., the lower limit on short period frequency). Further, civil aircraft tend to have missions which are quite different from those of military aircraft, which suggests that different performance standards would apply. This is not to say that the military criteria are not used; however, they have certain shortcomings when applied to civil transport design.

[1]The term "estimators" is used because the criteria produce quantitative estimate of flying qualities (i.e., pilot ratings or flying qualities levels).

A more serious criticism of most existing criteria is rooted in the fact that they are based on approximations to the response of an airplane. Examples of this are seen in the MIL-F-8785B criteria for the short period. These criteria are based on experimental data for which the short period is well damped and well separated from the phugoid. The current trend toward relaxed static stability airplanes with stability and control augmentation is gradually eroding the ability of such criteria to accurately predict flying qualities, especially for failure cases. There is a trend towards the use of pilot-model-in-the-loop criteria which place performance standards on the pilot plus airplane system, rather than on the airplane alone. At this time, however, no closed loop criteria have been accepted for inclusion in the MIL-F-8785B.

For these reasons, the Douglas Aircraft Company has undertaken a program of research in the area of transport aircraft flying qualities. The goal of this research program is the determination of flying qualities criteria for the design of conventional as well as relaxed static stability airplanes. This paper is a description of the work being done to develop longitudinal flying qualities criteria for large transport aircraft in the landing approach. This description of the research program will be broken down into the following sections: (1) discussion of criteria selected for investigation, (2) design of the experiment, (3) performance of the experiment, and (4) analysis of the results. Each phase will be discussed in detail below.

DISCUSSION OF LONGITUDINAL FLYING QUALITIES CRITERIA SELECTED FOR INVESTIGATION

The first stage of the program of research was a wide-ranging review of the literature for longitudinal flying qualities criteria. There are far too many criteria in existence to be tested in an experimental program or to be discussed in detail here. A relatively small number which showed promise or which are generally accepted, were selected for inclusion in this flying qualities experiment. The criteria of the MIL-F-8785B were included because they are "accepted" criteria. The short period criterion of the ARP 842B was included as an "accepted" criterion in civil aircraft design. The short period criterion of Reference 3 was included because it contains, in a single criterion, the information provided by several other criteria. Finally, a pilot-model-in-the-loop pitch tracking task criterion which had shown promise in earlier studies was included. These criteria will be discussed below for large airplanes (Classes II and III) in the landing approach (Category C phase of flight).

The MIL-F-8785B criteria which were evaluated were: flight path stability ($d\gamma/dV$), short period frequency (ω_{nSP} vs n/α), short period damping (ζ_{SP}), phugoid stability (ζ_{Ph} or T_2), and static stability. All of these criteria, except static stability, are stated in terms of levels of flying qualities. Table 1 shows the relation of the flying qualities levels to pilot ratings and to a set of descriptors. The static stability criterion requires that an airplane exhibit positive static stability at all times. The advent of relaxed static stability airplanes has called this criterion into question, and the question was addressed. The flight path stability criterion limits backside operation by placing limits on the parameter $d\gamma/dV$.

Limiting values are given in Table 2. The short period frequency criterion places upper and lower limits on short period frequency as a function of n/α. Experience with the large transport aircraft (e.g., C-5, DC-10, etc.) indicates that the lower limit is too restrictive. This criterion, when combined with the short period damping ratio criterion, places limits on the short term pitch response. Since n/α is related to $T_{\theta 2}$, all parameters except gain have been specified for the short period pitch transfer function. The short period damping ratio limits are given in Table 3, and the short period frequency requirement in Figure 1. The phugoid stability criterion places limits on long period airspeed oscillations. This criterion, like the static stability criterion, is considered unrealistically restrictive, especially for relaxed static stability airplanes. The phugoid stability limits are given in Table 4.

The ARP 842B short period criterion is based on a presumption that for transport aircraft, the desired ranges of values ω_{nSP} and ζ_{SP} are invariant with flight condition. It is similar to the CAL "thumbprint" which was well accepted in the past, but has lost popularity as it is not in the MIL-F-8785B. The criterion limits are illustrated in Figure 2. The short period criterion of Reference 3 is similar to the MIL-F-8785B short period criterion, combining frequency and damping ratio limits in a single criteria. The parameter n_α was replaced with the closely related variable L_α, as shown in Figure 12.

The pilot-model-in-the-loop pitch tracking task models the pilot task of compensatory tracking of pitch attitude in the presence of random disturbances. It is in some respects similar to the Crossover Model (References 7,8) and to the Paper Pilot (References 9,10). The criterion places the following performance requirements on the closed loop system: (1) no more than 3db droop in the decade below the bandwidth frequency, (2) bandwidth of 1.2 radians per second, (3) closed loop phase angle of $-90°$ at the bandwidth frequency, and (4) minimum closed loop resonance at any frequency greater than the bandwidth frequency divided by 10. The pilot model has a gain, a transport delay (generally taken to be 0.3 seconds), a lead, and a lag. Inclusion of a low frequency lag ($e^{-\alpha/s}$) was found to have at best no positive effect on the criterion, though the theory indicates that a low frequency lag should be included for very slow controlled elements (see, e.g., Reference 8). The pilot lead, lag, and gain must be adjusted to satisfy the performance requirements, as the pilot transport delay and the airplane model are fixed. The flying qualities are then estimated as a function of pilot phase compensation (exclusive of the transport delay) and system resonance. The phase compensation is represented by the phase angle of the pilot model lead-lag network at the bandwidth frequency. Figure 3 illustrates the boundaries for this criterion. This criterion will be referred to as the Bandwidth Model.

DESIGN OF THE EXPERIMENT

A flying qualities experiment was designed to provide data for evaluation of the selected flying qualities criteria. The proper approach to designing such an experiment is first to collect all the parameters involved in the criteria to be evaluated. They are as follows: static stability, $d\gamma/dV$, ω_{nSP}, ζ_{SP}, n/α, ω_{nPH}, ζ_{PH}, phase compensation, and resonance. A set of configurations should then be designed which vary each parameter independently,

so that the effects of each parameter may be isolated. Assuming that four values of each parameter will cover the region of interest, and that static stability is not independent, there will be 4^8 or 65536 configurations. The pilots would probably get bored evaluating so many configurations, so a balanced fractional factorial design could be used to reduce the matrix by a factor of perhaps eight, leaving only 8192 configurations.

Since this proper approach yields impractical results, two other approaches were used to design two groups of configurations. The twenty-six configurations of the first group are either typical wide-body airplanes with cg location varied from far forward to far aft of the neutral point, or such airplanes with a single stability derivative varied to change the flying qualities. The characteristics of these configurations are given in Table 5. The configurations of Group II, on the other hand, were obtained by specifying the characteristics given in Table 6; and solving for the equations of motion coefficients. The solution to this transformation is not unique, as there are more than twice as many unknowns as there are conditions. A computer program was written to solve this transformation on the basis of minimizing a weighted sum of squared errors between the specified values of the parameters and the values calculated for a trial set of equations of motion constants. The algorithm exhibited poor convergence properties in general, and in particular for $|\zeta_{ph}| < 0.04$. However, several hundred configurations were calculated for which the algorithm converged. The sixteen configurations of Group II were selected from these.

PERFORMANCE OF THE EXPERIMENT

The configurations were rated by pilots flying the McDonnell Douglas six-axis motion base simulator located at Long Beach. The simulator, shown in Figure 4, is supported by six hydraulic jacks arranged in a configuration developed by the Franklin Institute. The limits of linear and rotary motion of this system are given in Table 7. Interior and exterior views of the simulator cockpit are shown in Figures 4 and 5. The airplane equations of motion are programmed on a hybrid computer system, of which the major elements are a Xerox Sigma Five digital computer and a Comcor Astrodata Ci-5000 analog computer. Cockpit motion commands are generated in the hybrid system and transmitted to a DEC PDP 11/40 minicomputer. The minicomputer computes the geometric transformations and controls the hydraulic jacks in a closed loop fashion, using LVDT transducer feedback from the jacks. Figure 6 is a schematic of the elements of the motion base simulator facility. The visual display is generated by a Redifon II system, using a detailed terrain model for landing approaches. Figure 7 is a layout of the System Simulation Laboratory, of which the motion base simulator is a part.

Five Douglas Aircraft Company test pilots performed 154 evaluations of the forty-two configurations over a period of two weeks. Each evaluation consisted of one to three ILS approaches, at the pilot's discretion, after which the pilot gave the configuration a pilot rating on the Cooper-Harper scale. The ILS approach began at a range of 13.7 kilometers (7.4 n.mi.) from the threshold, at an altitude of 457 meters (1500 feet), and on the extended runway centerline. The three-degree glide slope was intercepted at a range of about 8.7 kilometers (4.7 n.mi.). The pilot then flew down the

glide slope in a turbulent atmosphere. Lateral-directional dynamics typical of a wide-body transport were simulated but held constant throughout the experiment. After breakout at an altitude of 213 meters (700 feet), the pilot transitioned to the visual display for flare and touchdown. The simulation permitted the pilot to stop, turn, and taxi the airplane on the ground, but this was not part of the evaluation task. The test engineer, who rode in the copilot seat, recorded the pilot rating and pilot comments. Figure 8 is a typical evaluation record. Every variable of interest (and many of no interest) was recorded on half-inch-wide nine-track tape on 760 meter (2500 feet) reels at a rate of four hertz, while the simulation computer cycle rate was twenty hertz. The configurations were presented to the pilots in random order, with a different random order for each pilot.

RESULTS AND ANALYSIS

The evaluation of the flying qualities criteria was performed by comparing the level of flying qualities predicted for a given configuration with the actual, or true, level of flying qualities for that configuration. The true level of flying qualities for each configuration was assumed to be represented by the average of the ratings that the pilots gave that configuration. The Cooper-Harper pilot rating scale used in this experiment is repeated here as Figure 9. The results of this experiment are given in Tables 8 and 9 for the Group I and Group II configurations, respectively. The first column in each of these tables lists the configurations by number. The next column gives the mean pilot rating for each configuration. The third column, labeled R_0, is the actual, or true, level of flying qualities for each configuration, based on the mean pilot rating. Every configuration in Group I was rated by at least three different pilots, some by four, and some by all five pilots. In Group II, one configuration was rated by one pilot, one by two pilots, and the rest by three, four, or five pilots. The average number of ratings per configuration was 3-2/3 for both groups.

While the criteria generally do not have half levels, a configuration that falls near a level boundary probably is indistinguishable from a configuration just across the boundary. Therefore, half levels were created for most of the criteria by the rules given in Table 10. Some of the criteria do not have a boundary for every level. The MIL-F-8785B short period frequency criterion, for example, has a common lower boundary for levels 2 and 3. A level 2 boundary was added midway between the level 1 and level 3 boundaries, as shown in Figure 10, to facilitate evaluation of this criterion. The ARP 842B short period criterion is stated, not in terms of levels, but by the terms "acceptable augmented," "acceptable unaugmented," and "unacceptable." These terms bear a similarity to the definitions of the flying qualities levels, so were equated to levels 1, 2, and 3, respectively, as shown on Figure 11.

The fourth column, labeled R_1, is the level of flying qualities predicted for each configuration using the Bandwidth Model criterion. The name Bandwidth Model is used to refer to the pilot-model-in-the-loop pitch tracking task criterion. The number at the bottom of the column (23 for Group I and 23 for Group II) is the total error (in half levels) of these predictions.

Inspection of the totals for all criteria reveals that the Bandwidth Model criterion is the best performer for the Group I configurations and is second to $d\gamma/dV$ for Group II.

The flight path stability criterion (R_2) is the second best performer for the forty-two configurations. This is an indication that pilots are more sensitive to bad flight path response than they are to bad pitch response. The MIL-F-8785B short-period-frequency criterion (R_3) was the poorest performer overall and also for Group II, but was slightly better than the worst for Group I. The short-period-damping-ratio criterion (R_4) performed better than R_3, though pilot opinion should be insensitive to it over a wide range. Even the phugoid stability criterion (R_5) outperformed R_3. The static stability criterion (R_6) was evaluated, but not on the basis of levels. The positive answer was considered an estimate of level 1 to 2-1/2, and a negative answer as level 3 to 4. On this basis, R_6 was wrong for eight of the twenty-six configurations of Group I. A more meaningful observation is that only half of the statically unstable configurations are level 3 or worse. This means that in half the cases, a requirement for positive static stability was not needed to achieve level 2 flying qualities. The performance of R_6 with Group II is not mentioned because it was not varied in Group II.

There is not any methodology in the MIL-F-8785B for combining the estimates for several criteria to get an overall airplane level of flying qualities. One can only guess that the overall flying qualities will be as bad as the worst rating or perhaps worse. Criterion R_{10} is an overall predicted level of flying qualities based on the MIL-F-8785B criteria. It is equal to the worst of R_2 to R_6, and turns out to be a poorer performer than any other criteria except R_3 and R_5. The prediction of R_{10} was better than actual in six cases, and worse than actual in twenty-eight cases. While it is better to err on the conservative side, this performance is too conservative.

The last two criteria evaluated, the short period criteria of ARP 842B (R_8) and of Reference 3 (R_9) performed well, being third and fourth best out of eight when both groups are considered. They both performed better than the MIL-F-8785B short-period criteria.

Inspection of the data for R_1 and R_2 shows that when R_1 is better than R_0, R_2 is worse than R_1, and thus probably closer to R_0, in 85% of the cases. When R_1 is worse than R_0, R_2 is better than R_1 in 78% of the cases. But, when R_1 is the same as R_0, R_2 is better than R_1 in 77% of the cases. Thus, when R_2 is worse than R_1, R_0 is generally worse than R_1. But when R_2 is better than R_1, the odds are even that R_0 is the same as R_1 or better than R_1. This suggests a combination criterion, R_{13}, which is defined by the equations:

$$R_{13} = R_1 \qquad \text{when} \qquad R_1 > R_2$$

$$= \frac{1}{2} (R_1 + R_2) \qquad \text{when} \qquad R_1 < R_2$$

The results show that this combination criterion is better than any of the other criteria evaluated. The sum of the errors is thirty half-levels for forty-two configurations. Further, when the characteristics covered by the various criteria are taken into account, such a criterion makes more

sense. The Bandwidth Model criterion is sensitive to all parameters varied in this experiment, except $d\gamma/dV$. Thus, a criterion which takes both the Bandwidth Model and $d\gamma/dV$ criteria into account, is sensitive to all the parameters varied in this experiment.

RECOMMENDATIONS FOR FURTHER WORK

1. Since there was enough data collected in the simulator experiment to permit the evaluation of virtually any longitudinal criterion, it is recommended that some additional criteria be evaluated. Obvious candidates are the Crossover Model (Reference 8) and the Pitch Paper Pilot (Reference 10). The Crossover Model will be difficult to evaluate on two counts. First, one must decide how to model the task. The performance of a landing approach appears to be a two-input, two-output task longitudinally, which the Crossover Model cannot handle. Second, assuming that a suitable system model can be determined, and the required pilot model adjustments made, one must then have a rule for estimating flying qualities. The information available in the literature indicates that the estimated flying qualities depend on the amount of pilot compensation required and on the nature of the controlled system. Further candidates for evaluation include the following: (a) McPilot (Reference 11), (b) c^* (Reference 12), (c) $\dot\theta/\dot\theta_{SS}$ and $n_z/n_{z_{SS}}$ (Reference 13), (d) c_{θ}^* (Reference 14), and (5) maneuvering stability (F_S/n_z) (Reference 1).

2. Another line of further work would be identification of the parameters of a model of the human pilots. This was attempted briefly, but abandoned when the algorithm failed to converge. The computer program used was Program Newton, a modified Newton-Raphson technique documented in Reference 15.

3. While the combined criterion, R_{13}, performed quite well for the present study, it should be tested against other longitudinal flying qualities data for large transport aircraft in the landing approach. A source of such data is Reference 6, an in-flight simulation of a large delta wing transport in the landing approach.

SUMMARY AND CONCLUSIONS

A number of longitudinal flying qualities criteria were evaluated against the results of a motion base simulation of large transport aircraft in the landing approach. The criteria of MIL-F-8785B performed poorly overall. Two short-period criteria, from ARP 842B and Reference 3, performed adequately. The best performance was exhibited by a criterion combining the results of a pitch tracking task and the flight-path-stability criterion.

REFERENCES

1. Anon.: Flying Qualities of Piloted Airplanes. MIL-F-8785B(ASG), Aeronautical Systems Division, 1969.

2. Anon.: Design Objectives for Flying Qualities of Civil Transport Aircraft. ARP 842B, Society of Automotive Engineers, 1970.

3. Shomber, H.A., and Gertsen, W.M.: Longitudinal Handling Qualities Criteria: An Evaluation. AIAA Paper 65-78, 1965.

4. Neal, T.P., and Smith, R.E.: An In-Flight Investigation to Develop Control System Design Criteria for Fighter Airplanes. AFFDL-TR-70-74, Volumes I and II, 1970.

5. Wasserman, R., Mitchell, J.F., Rickard, W.W., Huber, R.W., and Schelhorn, A.E.: In-Flight Investigation of Minimum Longitudinal Stability for Large Delta-Wing Transports in Landing Approach and Touchdown. AFFDL-TR-72-143, Volume 2, 1973.

6. Rickard, W.W.: A Review of Flying Qualities Estimation and Flying Qualities Estimators. Douglas Memorandum C1-250-Aero-75-399, 10 July 1975.

7. McRuer, D., Graham, D., Krendel, E., and Reisener, W., Jr.: Human Pilot Dynamics in Compensatory Systems. AFFDL-TR-65-15, 1965.

8. McRuer, D.T., et al.: New Approaches to Human-Pilot/Vehicle Dynamic Analysis. AFFDL-TR-67-150, 1968.

9. Anderson, R.O.: A New Approach to the Specification and Evaluation of Flying Qualities. AFFDL-TR-69-120, 1970.

10. Anderson, R.O., Connors, A.J., and Dillow, J.D.: Paper Pilot Ponders Pitch. AFFDL/FGC-TM-70-1, 1970.

11. Bruelle, R.V., and Anderson, D.C.: Design Methods for Specifying Handling Qualities for Control Configured Vehicles. AFFDL-TR-73-142, 1973.

12. Tobie, H.N., Elliot, E.M., and Malcolm, L.B.: A New Longitudinal Handling Qualities Criterion. National Aerospace Electronics Conference, Dayton, Ohio, 16-18 May 1966.

13. Sudderth, R.W., Bohn, J.G., Caniff, M.A., and Bennett, G.R.: Development Of Longitudinal Handling Qualities Criteria for Large Advanced Supersonic Aircraft. NASA CR-137635, 1975.

14. Kisslinger, R.L., and Wendl, M.J.: Survivable Flight Control System Interim Report No. 1, AFFDL-TR-71-20 Supplement 1, 1971.

15. Taylor, L.W., Jr., and Iliff, K.W.: Systems Identification Using a Modified Newton-Raphson Method — A Fortran Program. NASA TN D-6734, 1972.

TABLE 1. FLYING QUALITIES LEVELS

Level	Cooper-Harper Pilot Rating	Description of Flying Qualities
1	1 - 3.5	Clearly adequate for mission.
2	3.5 - 6.5	Adequate to accomplish mission but with reduced performance or increased pilot workload.
3	6.5 - 9$^+$	Safely controllable but excessive workload or inadequate performance.
>3	9$^+$ - 10	Loss of control probable.

TABLE 2. FLIGHT PATH STABILITY CRITERION (MIL-F-8785B)

Level	$d\gamma/dV$ Less Than
1	0.06 deg/kt
2	0.15 deg/kt
3	0.24 deg/kt

TABLE 3. SHORT PERIOD DAMPING RATIO LIMITS (MIL-F-8785B)

Level	ζ_{SP} Min	Max
1	0.35	1.3
2	0.25	2.0
3	0.15	- -

TABLE 4. PHUGOID STABILITY LIMITS (MIL-F-8785B)

Level	ζ_{Ph} or T_2 (sec)
1	0.04
2	0
3	55 (sec)

TABLE 5. GROUP I CONFIGURATION CHARACTERISTICS

$$V = 140 \text{ kts} \qquad \gamma = -3° \qquad W = 350{,}000 \text{ lb}$$

	$\omega_{n_{SP}}$	ζ_{SP}	$\omega_{n_{Ph}}$	ζ_{Ph}	n/α	$d\gamma/dV$	$1/T_{\theta_1}$	$1/T_{\theta_2}$
1	0.846	0.628	0.186	0.072	3.80	-0.0399	-0.084	-0.506
2	0.732	0.708	0.169	0.063	3.94	-0.0432	-0.083	-0.528
3	(-0.633)	(-0.307)[1]	0.086	0.318	4.14	-0.0491	-0.082	-0.556
4	(-0.811)	(+0.090)[2]*	0.200[+]	0.636[+]	4.20	-0.0511	-0.082	-0.564
5	(-0.909)	(+0.158)[3]*	0.184[+]	0.210[+]	4.24	-0.0530	-0.082	-0.568
6	0.828	0.645	0.190	0.057	3.80	0.148	-0.013	-0.577
7	0.819	0.653	0.192	0.049	3.80	0.236	+0.015	-0.605
8	0.811	0.662	0.194	0.041	3.80	0.324	+0.041	-0.631
9	0.804	0.565	0.188	0.084	2.75	0.0054	-0.102	-0.339
10	0.795	0.502	0.191	0.099	1.78	0.095	[0.166]	[0.917]
11	0.723	0.431	0.194	0.117	0.82	0.400	[0.143]	[0.587]
12	0.853	0.888	0.184	0.080	3.80	-0.0399	-0.084	-0.531
13	0.836	0.337	0.188	0.066	3.80	-0.0399	-0.084	-0.481
14	0.829	0.149	0.189	0.064	3.80	-0.0399	-0.084	-0.466
15	(-0.991)	(+0.225)[4]*	0.211[+]	0.388[+]	4.29	-0.0551	-0.082	-0.575
16	(-1.061)	(+0.291)[5]*	0.210[+]	0.331[+]	4.35	-0.0572	-0.082	-0.583
17	(-1.125)	(+0.358)[6]*	0.209[+]	0.295[+]	4.43	-0.0593	-0.081	-0.595
18	0.953	0.570	0.165	0.107	3.65	-0.0360	-0.087	-0.484
19	0.596	0.841	0.141	0.073	4.06	-0.0465	-0.082	-0.544
20	0.843	0.395	0.187	0.106	0.71	0.498	[0.141]	[0.545]
21	0.441	0.665	0.170	0.043	1.05	0.285	[0.149]	[0.676]
22	(-0.577)	(+0.152)[7]*	0.190[+]	0.347[+]	1.22	0.222	[0.154]	[0.731]
23	(-0.767)	(+0.341)[8]*	0.196[+]	0.240[+]	1.37	0.173	[0.158]	[0.776]
24	(-0.904)	(+0.499)[9]*	0.196[+]	0.207[+]	1.54	0.133	[0.163]	[0.828]
25	0.833	0.263	0.188	0.065	3.80	-0.0340	-0.084	-0.475
26	0.831	0.197	0.189	0.064	3.80	-0.0340	-0.084	-0.470

( ) First-order factor $\qquad\qquad\qquad\qquad\qquad [\omega] \qquad [\zeta]$

[1] $\omega = 0.441, \quad \zeta = 1.07$ $\qquad$ [4] $T_2 = 3.08$ $\qquad$ [7] $T_2 = 4.56$

[2] $T_2 = 7.70$ $\qquad\qquad\qquad$ [5] $T_2 = 2.38$ $\qquad$ [8] $T_2 = 2.03$

[3] $T_2 = 4.39$ $\qquad\qquad\qquad$ [6] $T_2 = 1.94$ $\qquad$ [9] $T_2 = 1.39$

*Tested against phugoid criterion

[+]Tested against short period criterion

TABLE 6. GROUP II CONFIGURATION CHARACTERISTICS

$V = 140$ kts $\quad \gamma = -3°$ $\quad W = 350,000$ lb

Config	ω_{SP}	ζ_{SP}	ω_{Ph}	ζ_{Ph}	n/α (g/rad)	dγ/dV (deg/kt)	$1/T_{\theta_1}$	$1/T_{\theta_2}$
27	1.39	0.50	0.16	0.12	3.5	0.1	−0.0607	−0.325
30	1.05	0.85	0.16	0.12	2.0	0.1	−0.334	−0.179
39	$(-0.744)^1$	$(-2.585)^1$	0.16	0.28	3.5	0.1	−0.0372	−0.484
40	1.05	0.85	0.16	0.12	2.0	0.1	−0.119	0.0435
43	1.39	0.5	0.08	0.12	3.5	−0.05	−0.0534	−0.293
49	1.05	0.5	0.08	0.12	2.0	0.1	−0.0397	−0.221
61	1.39	0.85	0.08	0.28	3.5	0.1	−0.0428	−0.555
62	1.05	0.85	0.08	0.12	2.0	0.1	−0.0408	−0.218
66	0.592	0.85	0.08	0.12	3.5	0.1	−0.0681	−0.380
75	$(-0.318)^2$	$(-1.10)^2$	0.16	0.28	3.5	0.1	−0.0471	−0.608
76	0.592	0.85	0.08	0.28	3.5	−0.05	−0.0767	−0.430
84	0.447	0.85	0.16	0.12	2.0	−0.05	−0.171	0.0595
85	0.447	0.5	0.16	0.12	2.0	0.1	−0.0494	−0.272
90	0.592	0.5	0.08	0.12	3.5	−0.05	−0.0761	−0.400
91	0.447	0.5	0.08	0.12	2.0	−0.05	−0.0860	−0.458
96	1.05	0.5	0.08	0.12	2.0	0.1	−0.186	0.0667

^{1}Equivalent $\omega_{n_{SP}} = 1.39$, $\zeta = 1.2$

^{2}Equivalent $\omega_{n_{SP}} = 0.592$, $\zeta = 1.2$

TABLE 7. MOTION LIMITS FOR THE MOTION BASE

Motion	Excursion	Velocity	Acceleration
Heave	±116 cm (±46 in.)	(±81 cm/sec (±32 in./sec)	±1.75 G
Sway	±147 cm (±58 in.)	±98 cm/sec (±38.5 in./sec)	±1.45 G
Surge	±152 cm (±60 in.)	±98 cm/sec (±38.5 in./sec)	±1.45 G
Roll	±30°	±23°/sec	6.9 rad/sec^2
Pitch	±30°	±23°/sec	6.9 rad/sec^2
Yaw	±30°	±30°/sec	8.1 rad/sec^2

TABLE 8. GROUP I — COMPARISON OF CRITERIA

		R_0	R_1	R_2	R_3	R_4	R_5	R_6	R_8	R_9	R_{10}	R_{13}
				MIL-F-8785B					ARP-842			
Config	PR	PR Level	Bandwidth Model	$dγ/dV$ Level	$ω_{nSP}$ vs $n/α$ Level	$ζ_{SP}$ Level	$ζ_{Ph}$ or T_2 Level	Static Stab.	$ω_{nSP}$ vs $ζ_{SP}$	$L_α/ω_{nSP}$ vs $ζ_{SP}$ Level	Worst of R_2-R_6	
1	2.50	1	1	1	2	1	1	Yes	1	1½	1	1
2	2.20	1	1½	1	2	1	1	Yes	2	2	2	1
3	4.30	2	2	1	4	1	2	Yes	3	3	4	1½
4	3.93	1½	2½	1	4	1	4	No	3	3	4	2
5	5.17	2	2½	1	4	3	4	No	3	3	4	2
6	5.00	2	1	2½	1	1	1	Yes	1	2	2½	2½
7	4.25	2	1	3½	1	1	1	Yes	1	2	3½	2
8	8.33	3	1½	4	1	1	1	Yes	1	2	4	2½
9	5.00	2	1	1½	1	1	1	Yes	1	1	1½	1½
10	5.67	2	1	2	1	1	1	Yes	2	1	2	1½
11	7.33	3	2½	4	3	1	1	Yes	2	1	4	3½
12	4.00	2	1	1	1	1	1	Yes	3	2	1	1
13	4.00	2	1½	1	1	2	1	Yes	2	2	2	1½
14	7.00	3	5	1	1	3½	1	Yes	3	3	3½	3
15	6.67	2½	2½	1	4	1	4	No	3	3	4	2½
16	7.67	3	3	1	4	2	4	No	3	3	4	3
17	9.00	3	3	1	4	2	4	No	3	3	4	3
18	3.75	1½	1	1	1	1	1	Yes	1	1	1	1
19	4.00	2	2	1	4	1	1	Yes	2	3	4	2
20	8.00	3	3½	4	3	1	1	Yes	2	3	4	4
21	6.17	2½	2	4	2	1½	1	Yes	2	1	4	3
22	6.33	2½	2	3	4	1½	4	No	3	3	4	2½
23	9.33	3½	3	3	4	3	4	No	3	3	4	3
24	9.33	3½	3	2	4	3	4	No	3	3	4	2½
25	5.00	2	2	1	1	2	1	Yes	2½	3	2	1½
26	5.67	2	2½	1	1	3	1	Yes	3	3	3	2
			25	50	57	47	59		34	34	51	18

TABLE 9. GROUP II — COMPARISON OF CRITERIA

			R_1	R_2	R_3	R_4	R_5	R_6	R_8	R_9	R_10	R_13
					← MIL-F-8785B →					L_α/ω_{nSP}	Worst	
			Bandwidth	$d\gamma/dV$	ω_{nSP}	ζ_{SP}	ζ_{Ph} or T_2	Static		vs ζ_{SP}	of	
Config	PR	PR Level	Model	Level	vs n/α	Level	Level	Stab.	ARP-842B	Level	R_2-R_6	
27	7.00	3	1½	2	1	1	1	Yes	1	3	2	2
30	4.75	2	1	2	1	1	1	Yes	2½	3	2	1½
39	5.75	2	1	2	1	1	1	Yes	3	3	2	1½
40	4.63	2	1	2	1	1	1	Yes	2½	3	2	1½
43	3.75	1½	2	1	1	1	1	Yes	1	3	1	2
49	3.50	1½	2	2	1	1	1	Yes	1	3	2	2
61	5.00	2	1	2	1	1	1	Yes	2½	3	2	1½
62	3.63	1½	1	2	1	1	1	Yes	2½	3	2	1½
66	4.00	2	1½	2	3	1	1	Yes	2½	3	3	2
75	4.50	2	1½	2	3	1	1	Yes	3	3	3	2
76	3.33	1½	1½	1	3	1	1	Yes	2½	3	3	1½
84	3.25	1½	2	1	3	1	1	Yes	2½	3	3	2
85	5.50	2	2	2	3	1	1	Yes	3	3	3	2
90	3.00	1	2	1	3	1	1	Yes	2	3	3	2
91	5.60	2	2	1	3	1	1	Yes	3	3	3	1½
96	7.25	3	1	2	1	1	1	Yes	1	3	2	2
			23	11	37	29	29		30	35	25	14
			48	61	94	76	88		64	69	76	32

571

TABLE 10. SOME NOTES ON THE APPLICATION OF THE FLYING QUALITIES CRITERIA

1. PR Levels:

PR	1-3	3.01-3.99	4-6	6.01-6.99	7-9	9.01-9.49	9.50-10
Level	1	$1\frac{1}{2}$	2	$2\frac{1}{2}$	3	$3\frac{1}{2}$	4

2. Bandwidth Model: Half levels were created by saying that any configuration within 0.7 dB or 3.5° of a boundary would be rated as an average of the adjacent levels.

3. $d\gamma/dV$:

Level	1	$1\frac{1}{2}$	2	$2\frac{1}{2}$	3	$3\frac{1}{2}$	4
$d\gamma/dV$	+0.045	0.0451- 0.0749	0.075- 0.135	0.1351- 0.1649	0.165- 0.225	0.2251- 0.2549	0.255 & Up

4. ωn_{SP} vs n/α: See Figure 10 — No half levels for lower boundaries.

5. Half Levels for Other Criteria: When parameter falls on or very close to boundary, it is considered half way between levels.

6. R_{10}: The standard way of applying MIL-F-8785B is to compute flying qualities of an airplane for a number of criteria. The only way to estimate the overall flying qualities of the airplane is the let it be the same as the worst estimate.

7. R_{13}: This criterion is a combination of the Droop-Bandwidth criterion and the $d\gamma/dV$ criterion. If the level for $d\gamma/dV$ is worse than the level for bandwidth, the two are averaged. If not, the bandwidth level is taken.
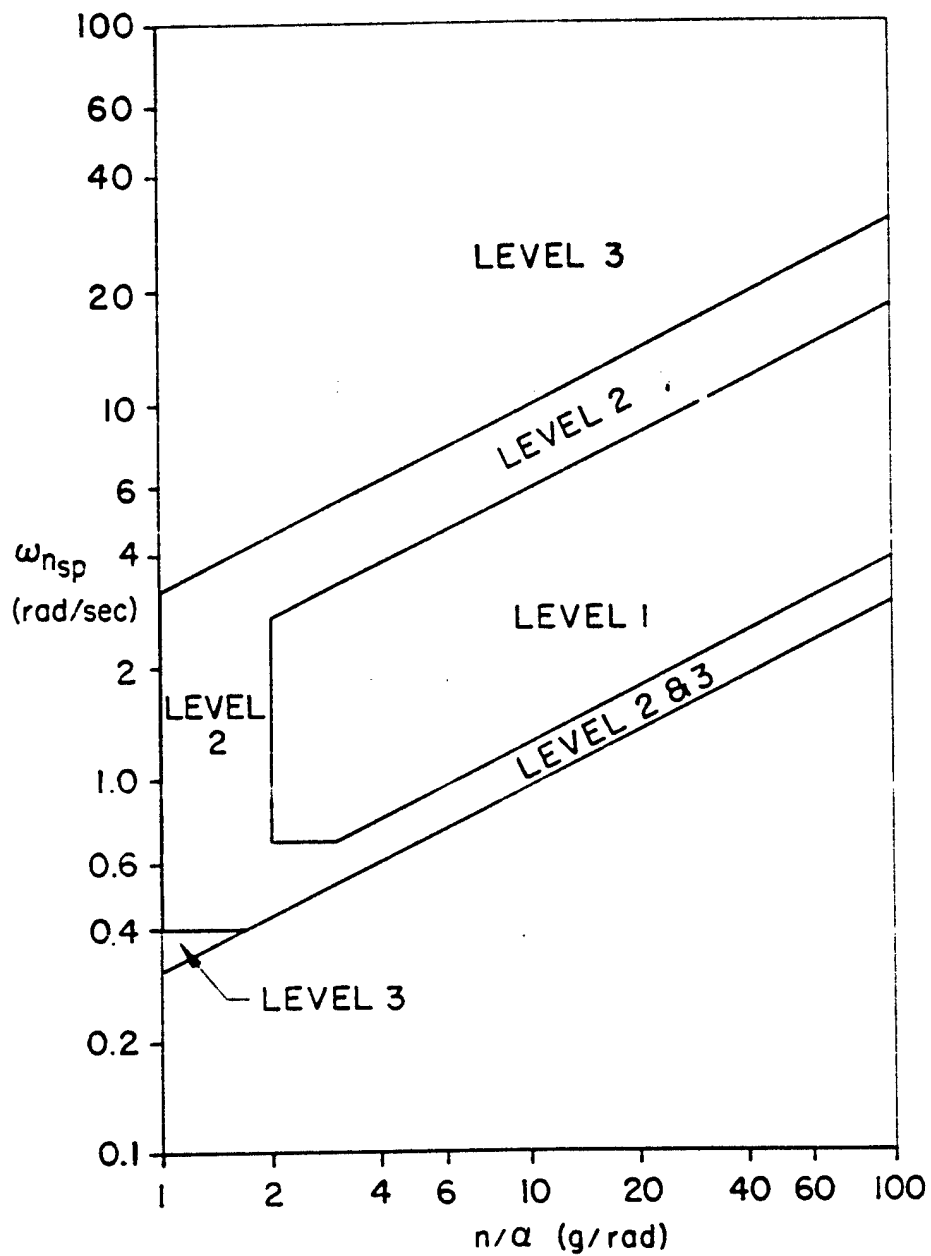
FIGURE I. MIL-F-8785B SHORT PERIOD
FREQUENCY CRITERION
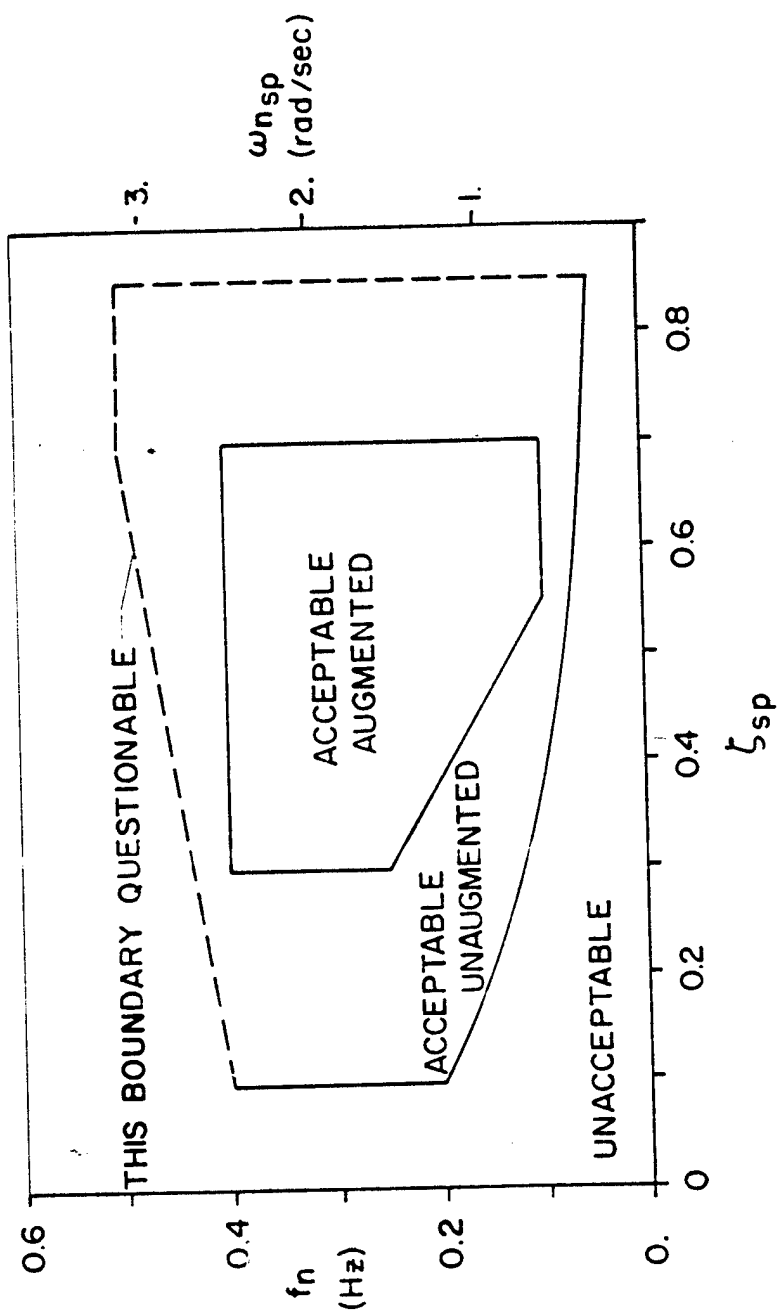
FIGURE 2. ARP 842B SHORT PERIOD CRITERION
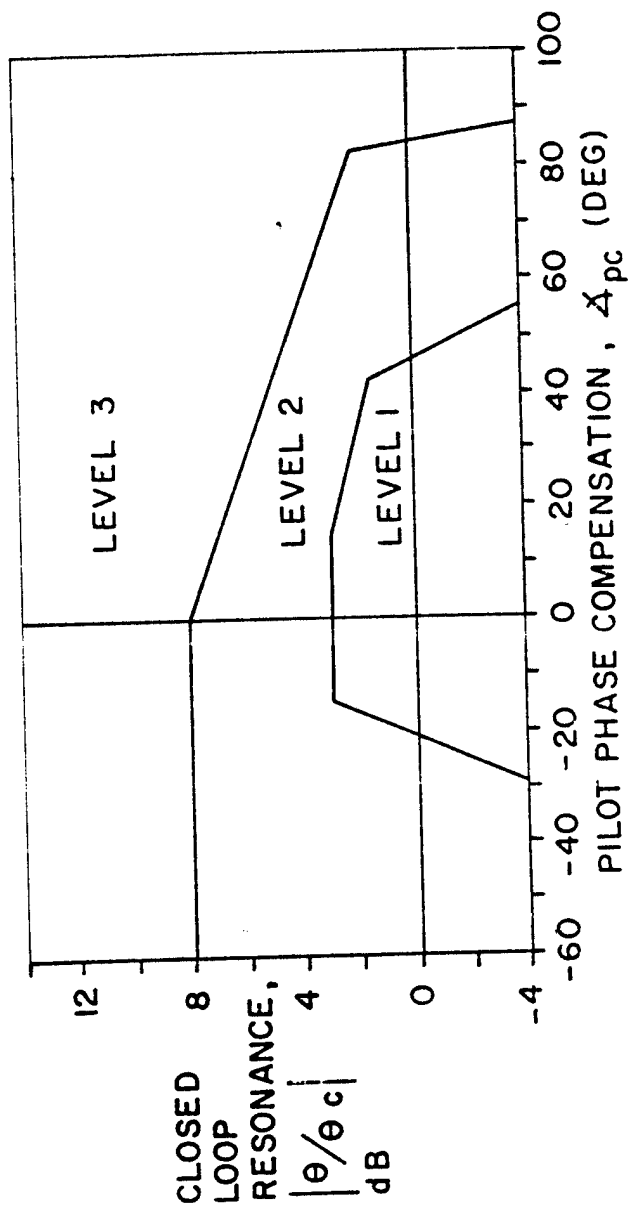
FIGURE 3. BANDWIDTH MODEL CRITERION
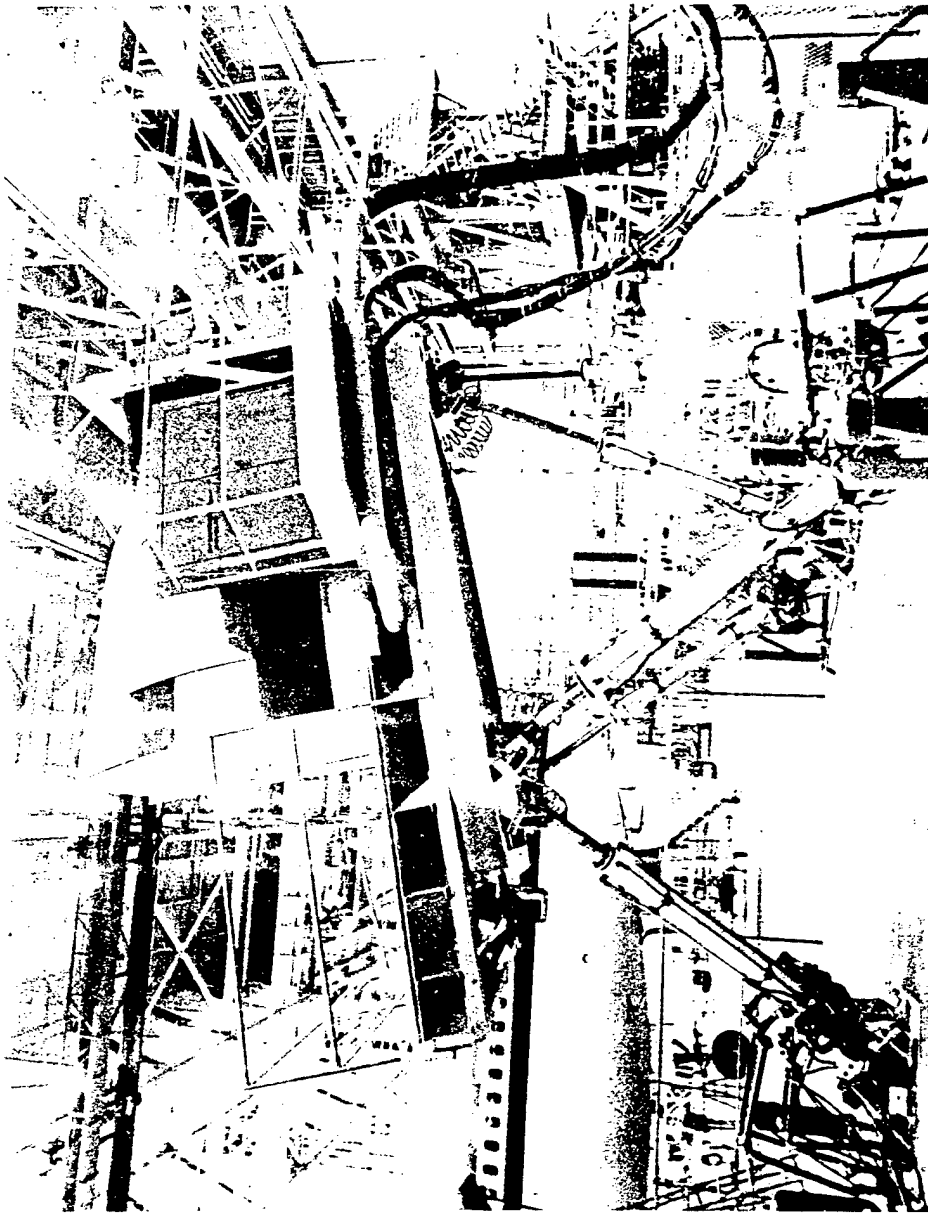
FIGURE 4. MOTION BASE SIMULATOR.
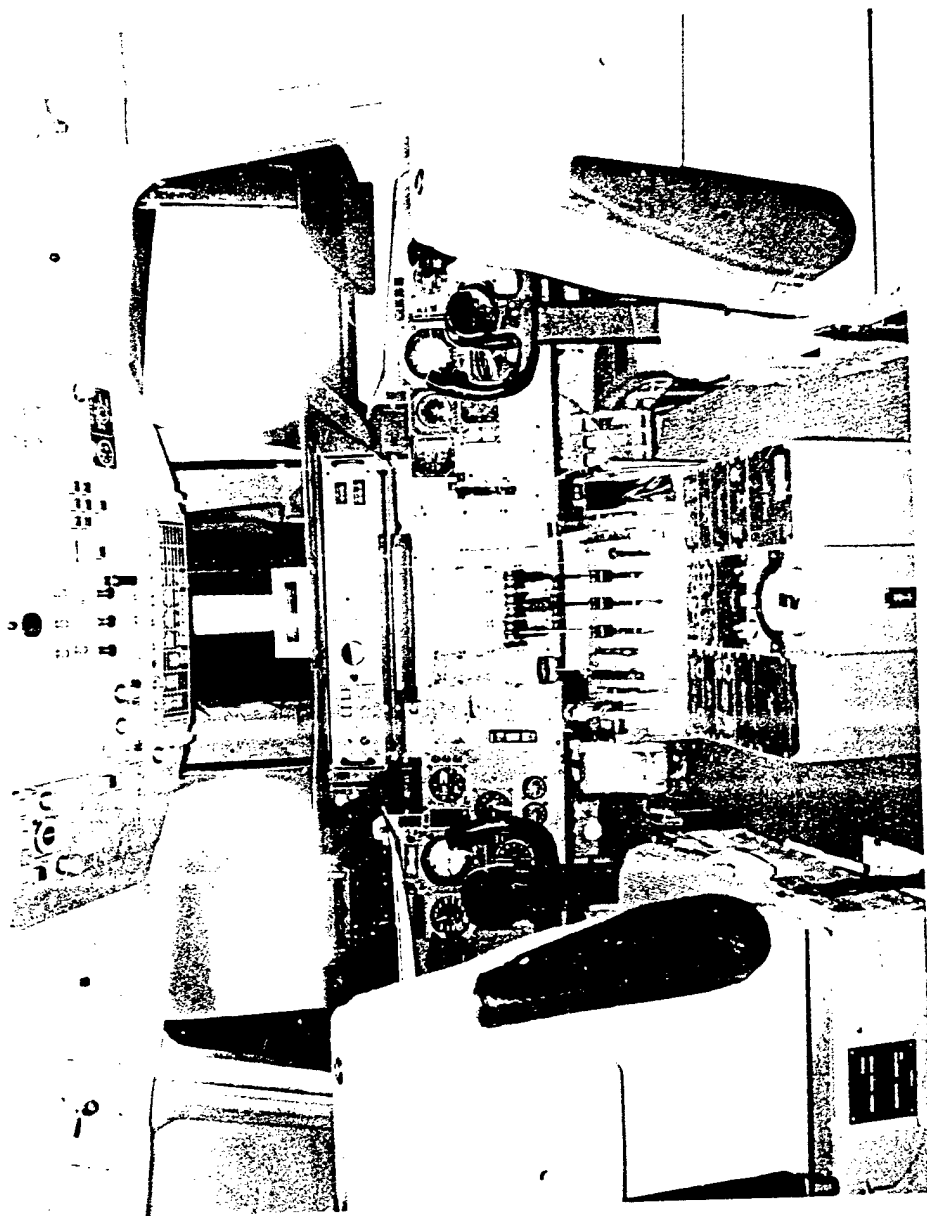
FIGURE 5. MOTION BASE SIMULATOR COCKPIT.
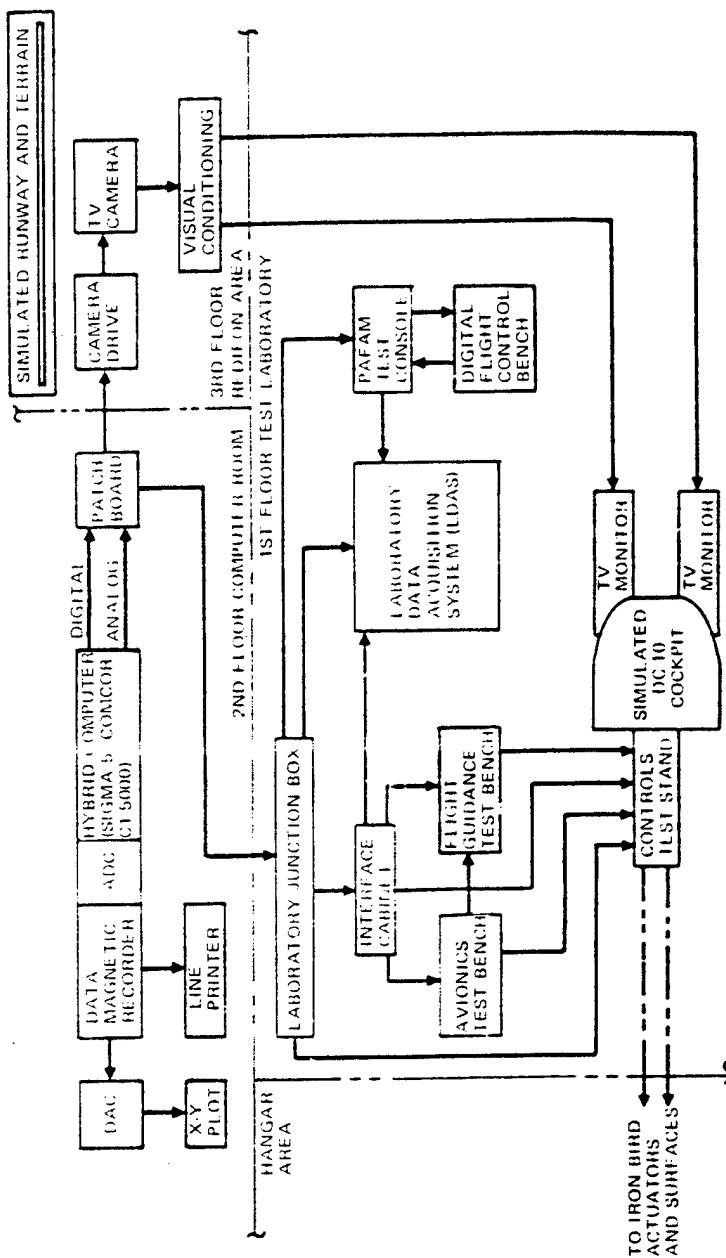
FIGURE 6. FIXED BASE SIMULATOR.
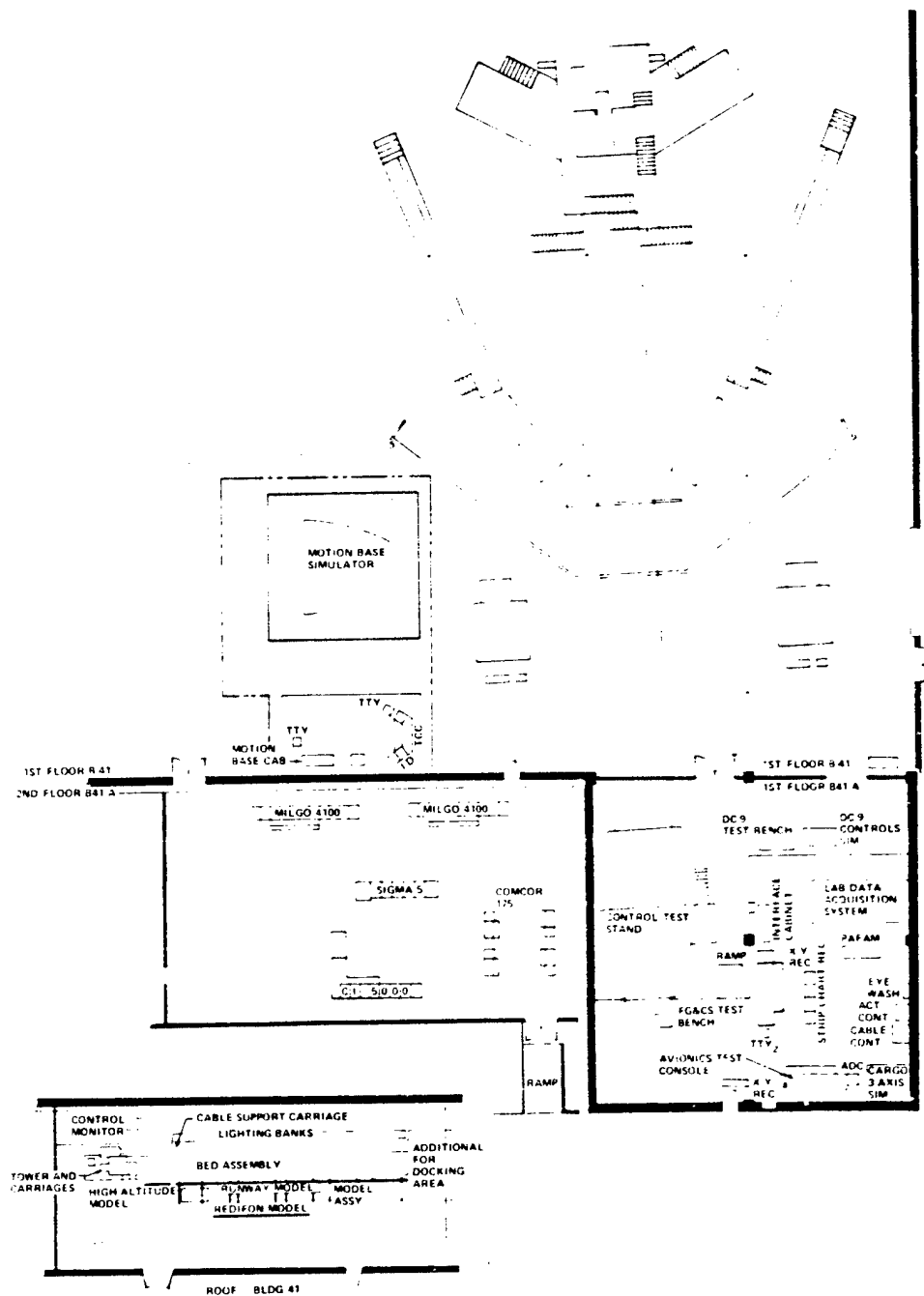
FIGURE 7. SYSTEM SIMULATION LABORATORY.

PiLOT DEBRIEFING FORM

Date: 12-3-75

Name: Pilot A

Run No. 1

Configuration No. 5

Turbulence Level: Moderate

Time of Day (Start):
a) 11:55:3)
b) 11:59:46

Ability to control flight path:

Good

Ability to control airspeed:

Satisfactory — good

Pitch response:

Damping on weak side

Other:

Requires considerable attention because of weak pitch damping. Tends to overshoot slightly in pitch.

Pilot Rating:

4

Main reason for rating, if adverse:

FIGURE 8. TYPICAL EVALUATION RECORD.
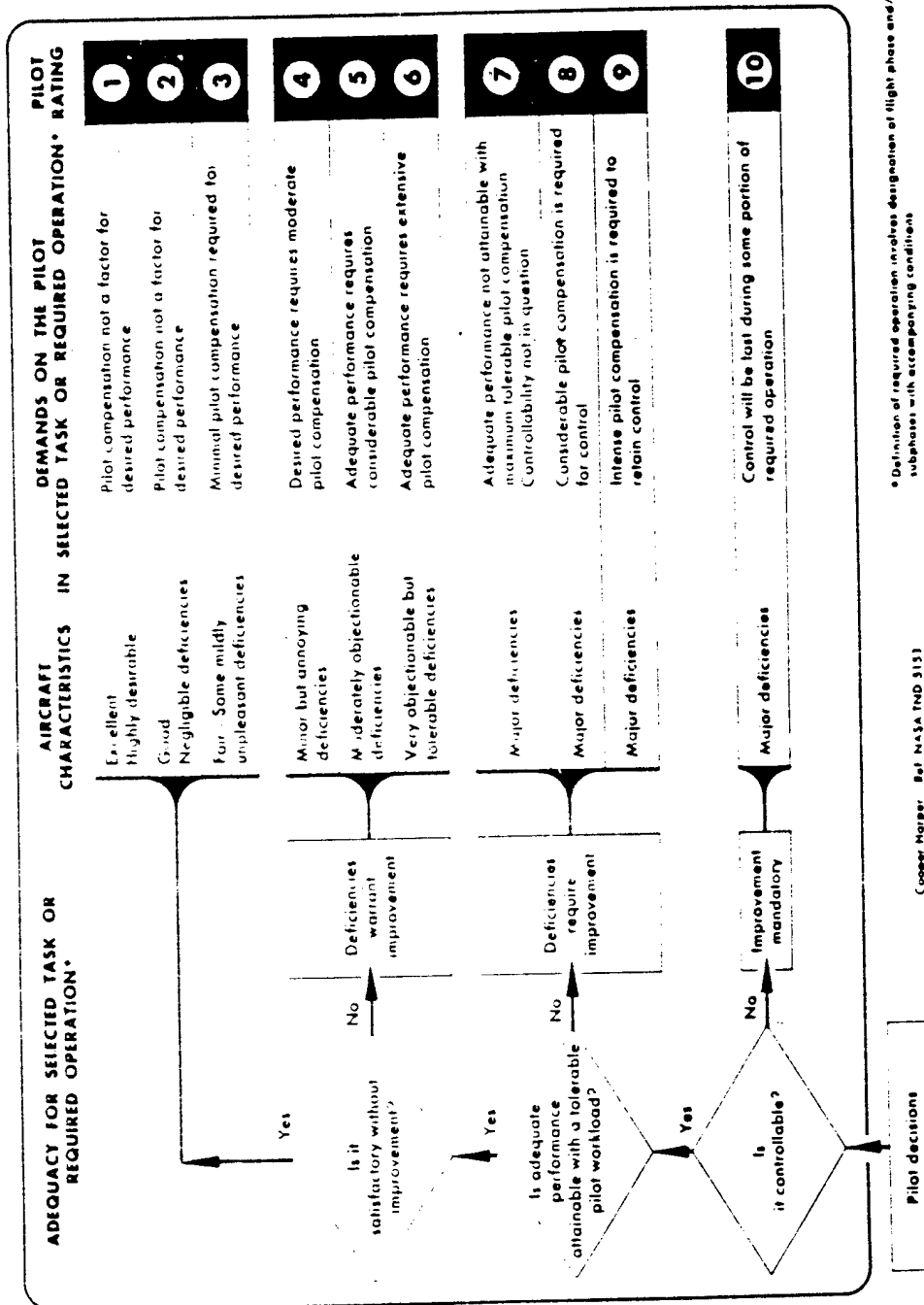
FIGURE 9. COOPER—HARPER PILOT RATING SCALE.
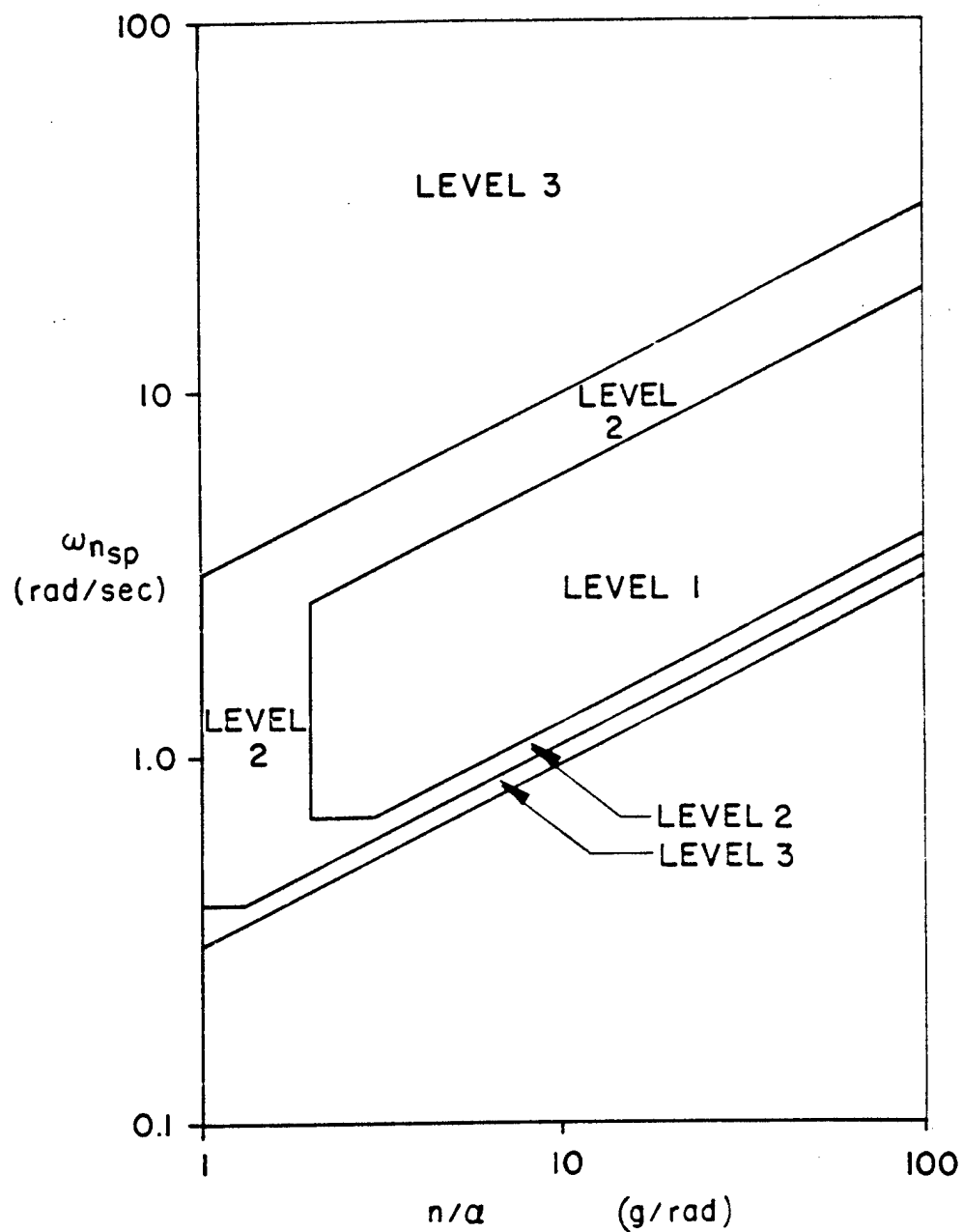
FIGURE 10. MiL-F-8785B SHORT PERIOD FREQUENCY CRITERION

582
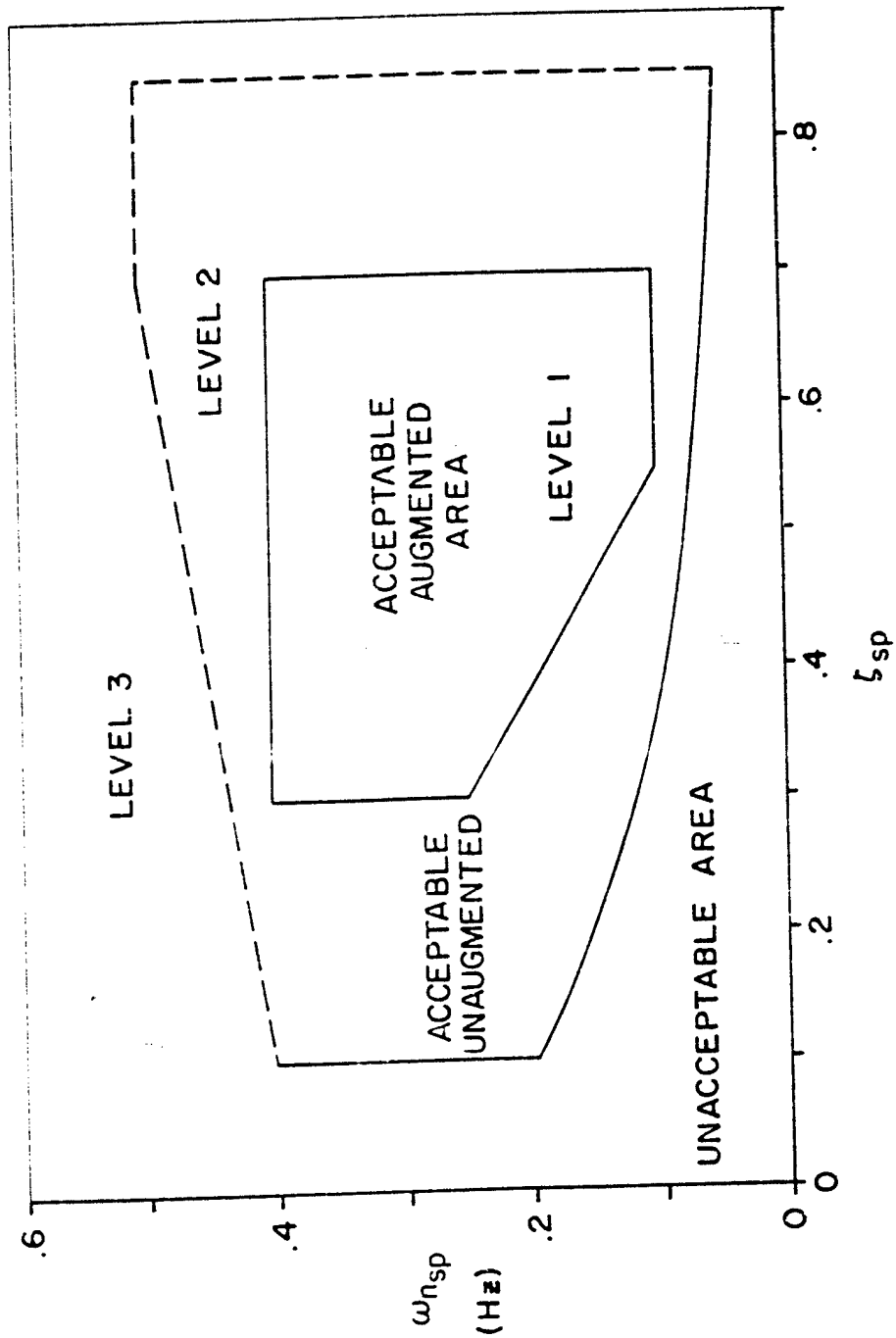
FIGURE II ARP 842B SHORT PERIOD CRITERION
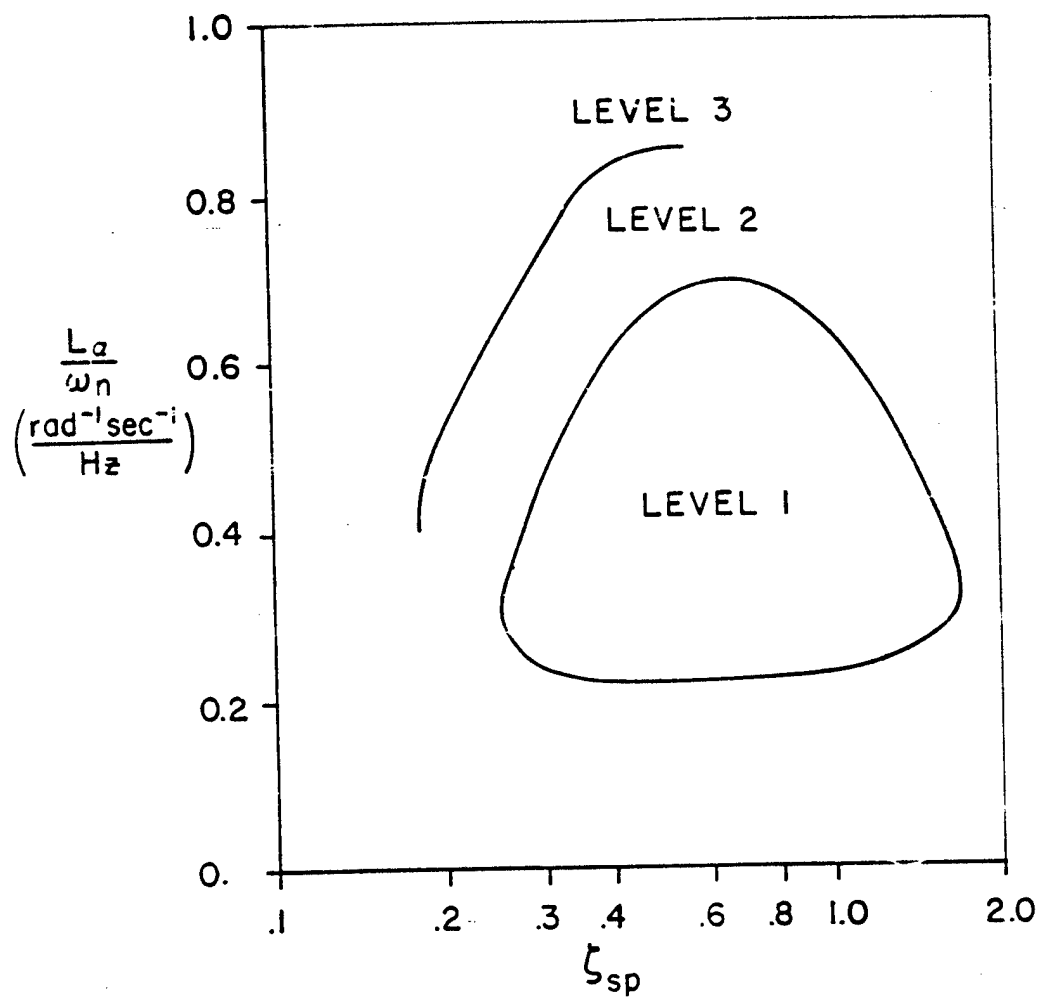
FIGURE 12. SHORT PERIOD CRITERION OF
REFERENCE 3

WORTH ASSESSMENTS OF APPROACH TO LANDING

Renwick E. Curry

Man Vehicle Laboratory
Massachusetts Institute of Technology
Cambridge, Mass. 02139

ABSTRACT

The objective of worth assessment is to determine the relative importance of attributes in the overall preference of objects, i.e., to determine the functional relationship between preference and the known, physical attributes of a set of objects. This technique is described below and is applied to the assessment of worth functions in approach to landing for general aviation and air carrier pilots.

INTRODUCTION

The objective of the worth assessment technique is to determine a functional relationship between preference in a set of objects and their known attributes (say) x_1, x_2, x_3 ... . In other words, we wish to be able to create a function $W(x_1, x_2,...)$ which can be used to determine the relative importance of the attributes as well as determining the preference between any pair of objects with those attributes. As we will show, the technique is identical to the regression point of view in the analysis variance, and we will further show how one can obtain essentially interval scale data from ordinal, ranked preference for objects.

Applications of this technique have been used primarily in marketing research (Green and Wind, 1973). There are many possibile applications within the man-machine systems area as well; for example , in display evaluation (with attributes of displayed variables, resolution, etc.) and in handling qualities, where the Cooper rating is known to depend on the dynamic element being controlled, the disturbance level, the RMS error, etc.

WORTH MODELS

Suppose we have a set of objects or stimuli (S_i) with attributes limited to, for illustrative purposes, three variables x_1, x_2, x_3. In this section we will discuss the techniques for obtaining a worth function for this set of objects under two conditions: in the first case magnitude estimates of worth are available from the subject, i.e., numerical values for preference; in the

585

second case, a rank ordering of all objects in a set is used to obtain the worth function.

Magnitude Estimation

There are many situations where the only feasible way of measuring preferences is by numerical estimate provided by the subject. This is the well-known magnitude estimation technique, known to have many pitfalls (Poulton, 1968), but is a useful way to gather data when treated with caution. If, in the example above, we have three attributes with various levels along each, we can assume various forms for the worth function. Perhaps the most common form is the additive worth function given by

$$W(X_1, X_2, X_3) = W_1(X_1) + W_2(X_2) + W_3(X_3)$$

Denoting the numerical responses to the stimuli by y_{ijk}, we may express these responses in the traditional main-effects analysis of variance format.

$$y_{ijk} = \mu + A_i + B_j + C_k + e_{ijk}$$

There are many analysis of variance programs, for example, BMD10V (from the UCLA Biomedical Package), which treat analysis of variances as regression problems. In this case, the vector of the responses can be expressed in terms of the design matrix and of unknown parameters in the form

$$y \approx \hat{y} = Z\hat{\beta}$$

Treating the numerical representations for preference in this way, one is able to reconstruct the additive partial worth functions W_1, W_2, W_3 from the coefficients $\hat{\beta}$.

Assuming additive worth functions of the type described above allows for complete freedom in the shape of the individual or partial worth functions. For example, we may still have a non-monotonic worth function as would be true of someone who prefers one teaspoon of sugar in coffee: cups with one teaspoon of sugar are preferred to cups with zero teaspoons or two teaspoons of sugar, leading to an inverted U-shaped partial worth function for sugar.

On the other hand, there are many worth functions where it is known a priori that the worth functions are monotonic with the attribute, e.g., money. For such worth functions, it is not unreasonable to assume a linear/interaction (LINT) form for the worth functions as given by equation

$$W(X_1, X_2, X_3) = \beta_1 X_1 + \beta_2 X_2 + \beta_3 X_3 + \beta_4 X_1 X_2 + \beta_5 X_1 X_3 + \beta_6 X_2 X_3$$

Whether the additive worth functions or the LINT worth function models are used, the number of objects to be evaluated, i.e., cases to be evaluated, will depend on the requirement for the regression to be non-singular. Certainly the factorial presentation will suffice in both of the above cases.

Rank Ordering of Preferences

In many cases it is feasible, and, from a psychological scaling point of view, more desirable to obtain the rank order preferences of the objects within the set. To obtain the worth functions from these rankings, we assumed that these rankings are related to the (internal) worth by the following

$$r_{ijk} = M(A_i + B_j + C_k)$$

where $M(\cdot)$ is any monotonic function of the apparent worth provided by the model, i.e., $A_i + B_j + C_k$. This worth can be formulated in the same form as equation 3, with the coefficients β adjusted to minimize some suitable statistical criterion. In our work, we have used the Spearman rank-order correlation coefficient, which is equivalent to minimizing the RMS rank error between the ranks provided by the model and the ranks provided by the subject. A reasonable initial value for these β is to do a least squares fit, assuming that the ranks are in fact the scale values. That is, we assume all objects are at equal distances along the interval scale, an assumption which is no doubt untrue. However, this is a reasonable starting point for the βs to be further iterated to minimize the RMS rank error. In all of the cases we have tried to date, we have not found any coefficients β that could improve the RMS rank error below that obtained by the least square procedure. Thus it seems reasonable, although it should always be checked, that the assumption of equal-intervals along the interval scale is in practice a good one.

WORTH OF APPROACH TO LANDING

We have applied the worth assessment techniques to evaluation of different landing conditions by general aviation and air carrier pilots. In the first experiment, we placed all possible combinations of a limited set of wind direction, wind strength, runway surface conditions, and turbulence level on 36 computer cards. These computer cards were rank ordered by a general aviation pilot and a DC-9 first officer. The two wind directions (340° and 090°) were symmetrical about the runway heading of 035°. The additive worth functions obtained from these two pilots are shown in Figure 1, where it can be seen that both pilots had no preference for wind direction, and essentially the same preference to the effect of turbulence. The major differences occur in the attributes of wind strength and runway surface conditions, where it can be seen that the general aviation pilot is more sensitive to wind strength, whereas the DC-9 first officer is much more sensitive to the runway surface conditions. Presumably these results reflect the concerns of both of these pilots of the relative importance of these attributes during the landing operation.

We continued this experiment by providing 36 computer cards containing the factorial combinations of attributes shown in Figure 2 to seven air carrier pilots; the results for six of these are shown in Figure 2. It can be seen that there is a wide variety in individual responses to the day/night condition, the wind strength condition, and the braking conditions. Most pilots had essentially the same response to the visibility condition (RVR), the dominant attribute.

After these pilots had ranked the approaches, the instructions continued as follows:

"You have just finished ranking the approaches in the order of preference of which you would like to make them. Some are good, some are bad, so bad, in fact, that you would never attempt an

approach under those conditions. Assume the following situation
holds. You have had a good night's sleep and now you are about
to make the first landing of the day. Your alternate is 200
miles away. Place the colored card between those approaches
you would attempt (the top group) and those approaches you would
not attempt (the bottom group)."

The results of this are shown in Figure 3 which displays the number of
approaches that the pilots would attempt as a function of age and total flight
time. Besides showing correlation between age and total flight time, there is
a surprising consistency across all pilots with one exception. It cannot be
inferred from this procedure that this one pilot really would attempt 24 of
the approaches because of possible misinterpretation of instructions, nonethe-
less it appears that this might be a reasonable way to assess risk taking
tendencies.

THE WORTH OF WORTH ASSESSMENT

The approaches of worth assessment outlined here appear to be a convenient
method to determine the relative importance of various attributes from object
preferences, whether these preferences be expressed in numerical terms (magni-
tude estimates) or in terms of rank ordering various objects in a set. These
techniques have the advantage that standard ANOVA programs can be used to pro-
cess the data if they provide regression coefficients as part of the output.
We have found in our experience that ranks seem to be a good approximation to
the actual scale value when processing the rank-order data. This is particu-
larly useful since it allows one to obtain essentially interval scales from
ordinal responses. We suggest using models incorporating both additive worth
functions and those with interactions, since the latter may be important under
some conditions. (For six out of the seven air carrier pilots in the evalua-
tion of landing approaches, additive worth functions gave better agreement to
the actual responses than any of the LINT models.)

We have also found that the card sorting procedure may yield artifacts,
since subjects seem to sort the cards based on the one or two most important
attributes, and then sort cards within the major attributes according to some
algorithm which does not truly reflect preference. It also may be an indica-
tion that the attributes beyond the first two are ignored (Shepard, 1964) and
perhaps may not be important relative to other attributes.

All in all, the worth assessment techniques outlined here should prove to
be a very useful analytical tool in man-machine system studies.

REFERENCES

1. Green, P.; Wind, Y.: Multiattribute Decisions in Marketing, Hinsdale,
      Ill.: The Dryden Press, 1973.

2. Poulton, C.: The New Psychophysics: Six Models for Magnitude Estimation,
      Psychol. Bull., 64, 1-18, 1968.

3. Shepard, R.: On Subjectively Optimum Selection Among Multiattribute Alt-
      ernatives, in Shelly and Bryan (Eds.), Human Judgements of Optimality,
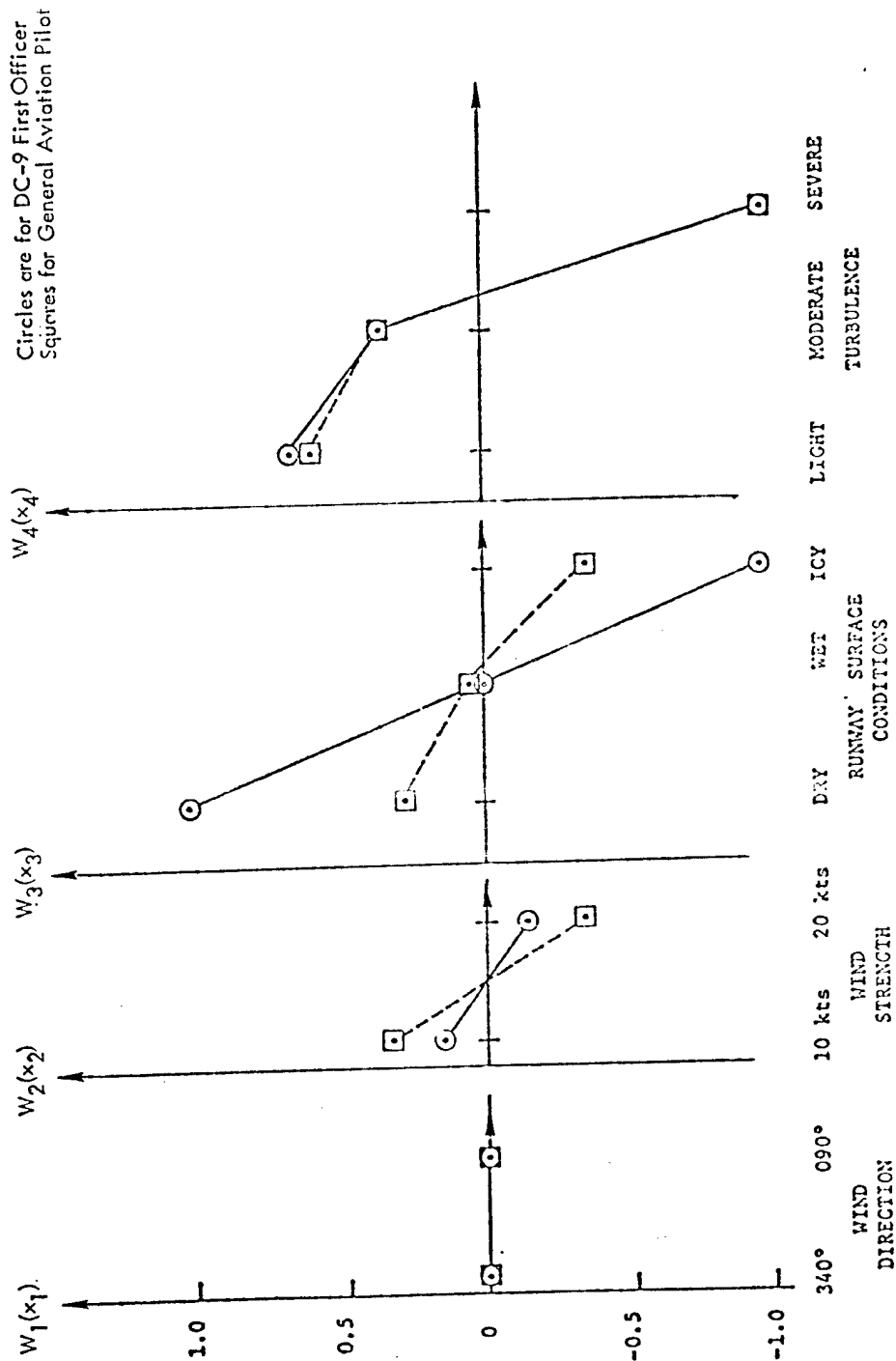   New York: Wiley, 1964.

Figure 1: Partial Worth Functions for Approach to Landing – General Aviation Pilot and DC-9 First Officer
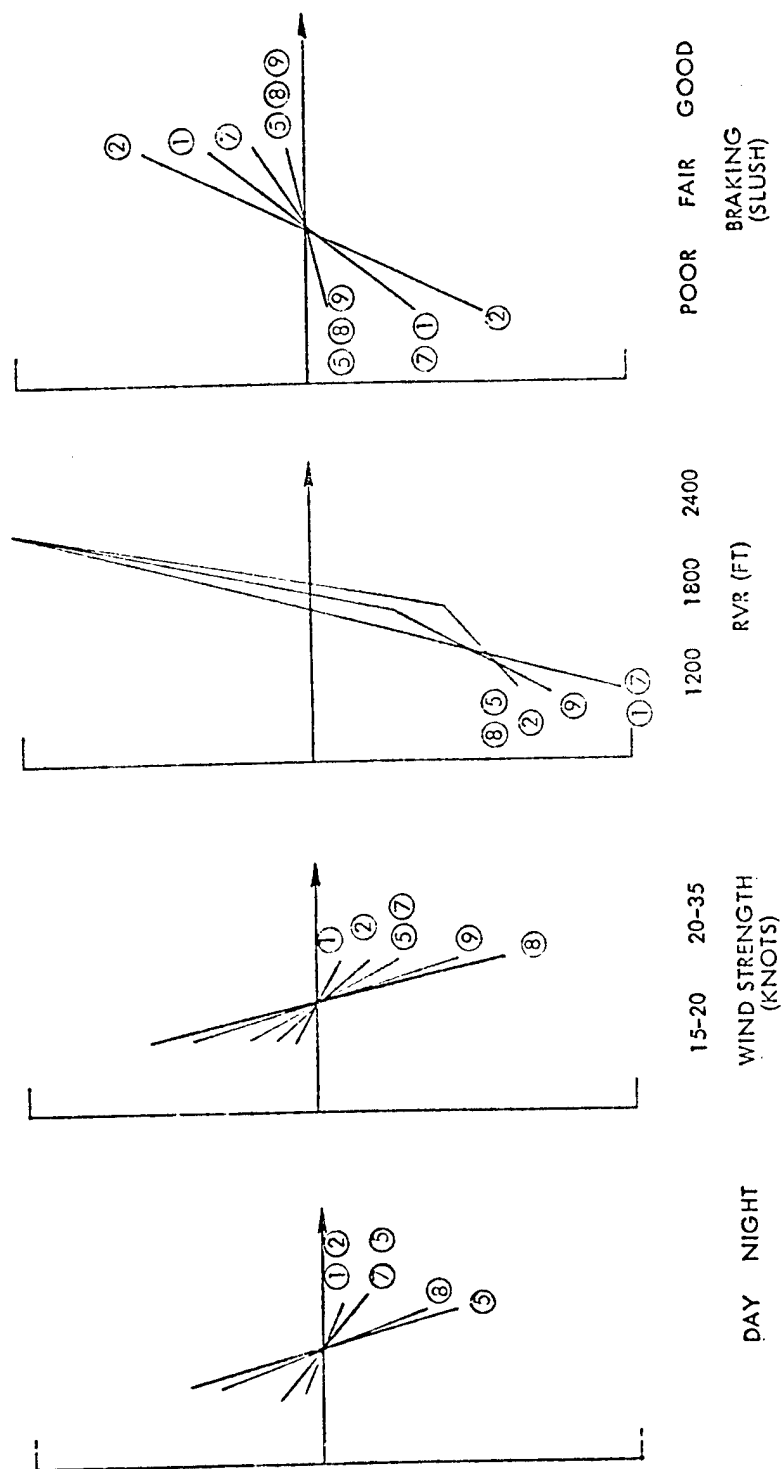
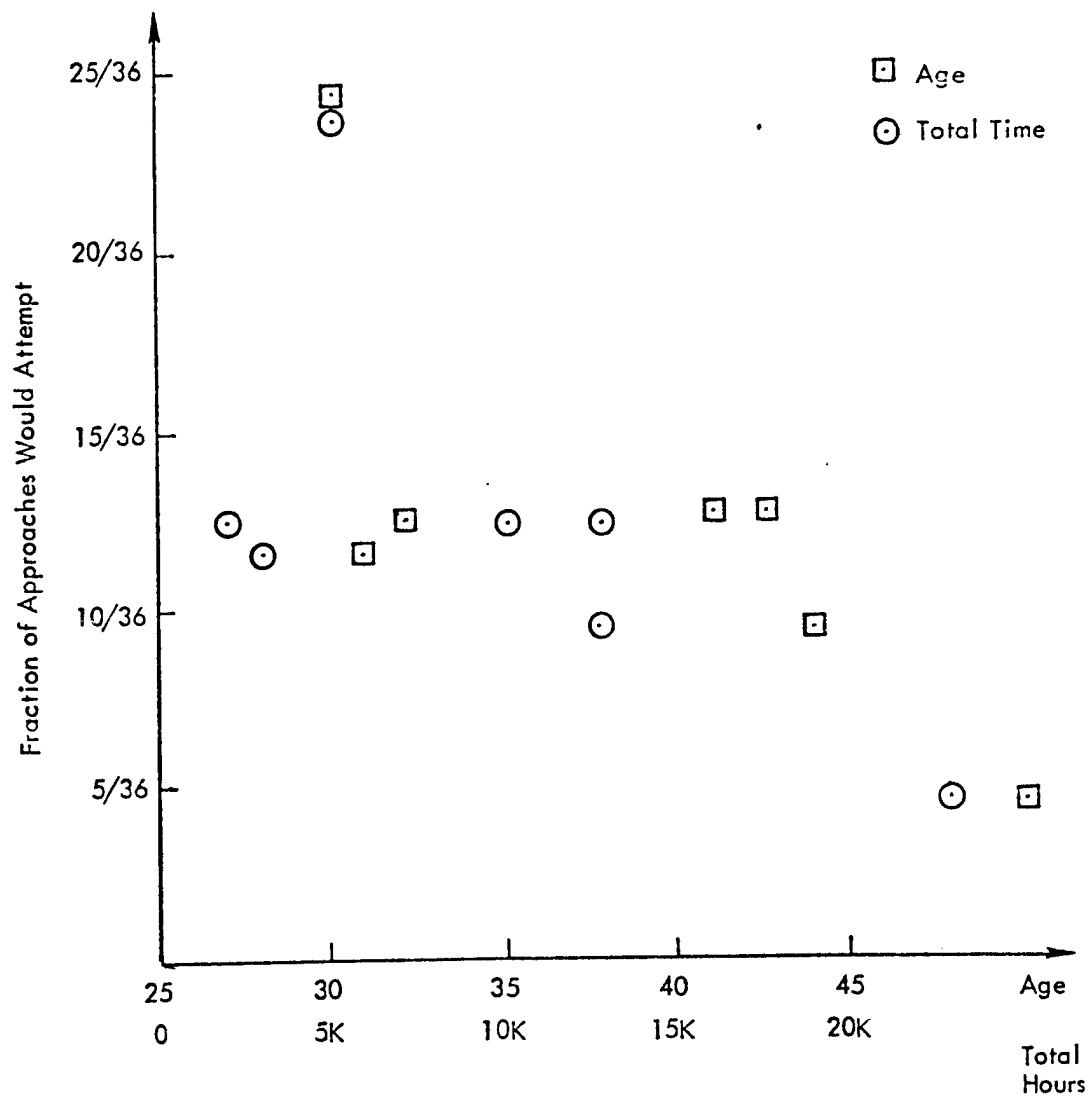Figure 2: Partial Worth Functions for 6 Air Carrier Pilots

Figure 3: Fraction of Approaches Pilots Would Attempt vs. Total Time and Age.

SESSION VIII

REMOTE MANIPULATION

Chairman: T. B. Sheridan

A COMPUTER-CONTROLLED MACHINING AND MANIPULATING DEVICE

By Tony C. Woo and John M. Paul

Coordinated Science Laboratory

University of Illinois

Urbana, Illinois

SUMMARY

This paper concerns the control of a laboratory scale machining and manipulating device for automatic fabrication of three-dimensional mechanical parts. The device performs the function of pickup of stock, setup and clamping of stock, cutting, and transfer under the control of a time-sharing DEC-10 system.

INTRODUCTION

As part of the Advanced Automation Research Group in the Coordinated Science Laboratory, the manufacturing automation project has embarked on the goal of automatic fabrication of discreet mechanical components from designs. There have been three tasks defined within the present scope--the design and description of parts, automatic interpretation of designs, and automatic fabrication. This paper describes the hardware and control aspects of a device for fabrication.

Three-dimensional parts are designed with volumetric primitives [1, 6]. The primitives are unit solids such as cubes, cylinders, and fillets. In addition to such conventional operations as translation, rotation, and scaling, the primitives can be glued together graphically via an ADD command or negated and then intersected with other volumes via a REMOVE command. The logic involved in ADD and REMOVE of solids is quite different than the conventional Boolean logic.

Before a design can be realized by cutting a piece of stock, certain procedural information must be obtained from the design. Among the information to be derived are the cutting tools required, the cutter paths, stock size, and manipulation and clamping information. The difficulty in arriving at these information lies in the fact that the geometry of the volumetric designs are locally simple yet globally complex. To combat this difficulty, the concept of a cavity is employed as an intermediate description between design and fabrication. The automatic interpretation process is reported elsewhere[7].

One way of creating three-dimensional objects from derived data is via cutting. Though paper tape driven numerical controlled machines have long been available, the idea of treating a milling machine as a computer peripheral device in conjunction with computer graphics has only been explored recently [3]. One of the advantages of having a three-dimensional model made from graphical data is the enhancement of visualization. A user, for example, does not need to integrate multiple views in order to appreciate the subtleties often not detectable in graphical form.

The device reported in this paper has a modest manipulating capability as well as cutting capability. Our interest in the manipulation aspect relates strongly to productivity in manufacturing and programmable automation. According to one recent study [4], over 95 percent of the time a part spends in a factory is in transfer, positioning, loading, etc. This motivates our implementation of programmable transfer and fixture capabilities as an integral part of the reported device.

The combined machining and manipulating capabilities enable us to automate the fabrication process without human assistance. A typical scenario involving our device is as follows. After initialization, a piece of stock is picked up and placed on a worktable. Pneumatic clamps are positioned around the stock and are tightened to the worktable. A cutter is then selected and the cutting proceeds. The entire process is reversed after cutting is finished.

The computer controlled machining and manipulating device is interfaced to a DEC-10 KI processor via a 7 megabaud I/O bus . The device was originally designed as a robot for hand-eye coordination studies [2]. It has a gantry configuration, capable of reaching anywhere in a five

by five by five foot volume. The arm can be moved in the x,y and z directions. The arm contains a shaft with an 11/16 chuck which can be rotated in the theta direction by means of either a high or low speed motor.

| DEC-10 | I/O | Computer | | Machining and |
| Processor | Bus | Interface | | Manipulating Device |
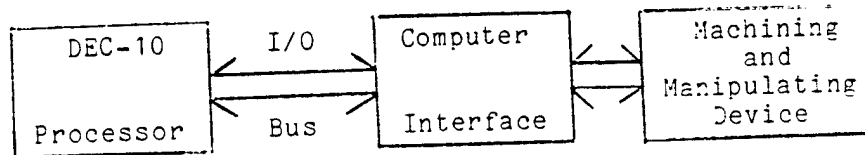
A work table in the form of a raised platform in the work space is constructed so as to minimize the bending moment of the z-axis under cutting force. The table top is an aluminum plate with an array of half inch threaded holes spaced two inches apart. The holes serve a dual purpose. Small chips can be vacuumed through the holes to a vacuum cleaner under the work table. Blocks can also be fastened to the worktable for automatic clamping and set up. A tool rack rests on one side of the worktable. The tools include cutters for drilling, milling, facing, and a socket for tightening the bolts on the programmable blocks.
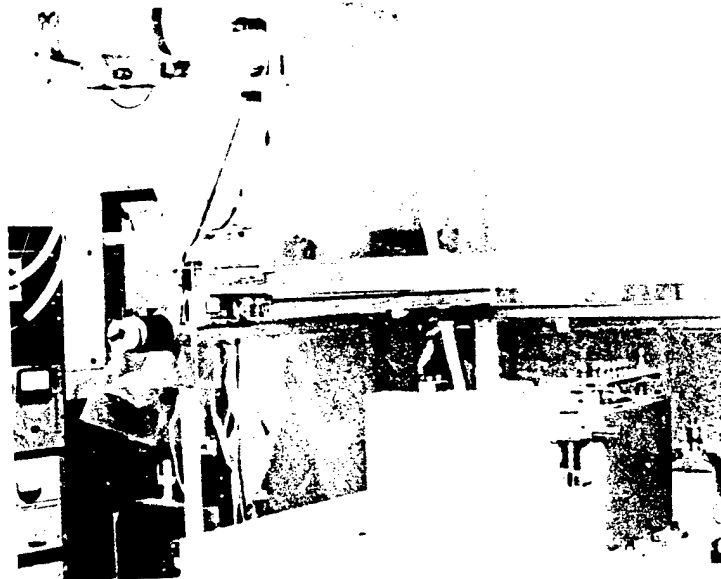
Machining and Manipulating Device

FEATURES

X,Y and Z Movement

Movement of the arm in the three translational directions is accomplished with computer controlled stepping motors. The X and Y axis have 120 steps per inch and the Z direction has 96.4 steps per inch. Scaling can be done with software and will be discussed later. The control of the stepping motors is open loop, therefore if a stepping motor stalls for any reason the arm will have to be reset. The speed of movement in any direction is under computer control with a maximum rate of 1 inch per second.

Quick Change

For computer controlled changing of tools on the wrist shaft a solenoid actuated quick change mechanism with a 11/16 inch chuck is used. All the tools, including cutters, sockets and the hand can be placed on the rotary shaft of the arm under computer control. Then either the low speed stepping motor or the high speed cutting motor can be used to rotate the arms shaft.

Pneumatic Clamp

Automatic clamping of materials to be machined is accomplished with an air vise. Two blocks are positioned with the hand and bolted down with the socket tool. Then through computer control one of the blocks slides under air pressure to clamp the work piece in place. The pressure created by the vise is also under computer control.

Hand with fingers

As mentioned earlier a hand may be placed on the rotary shaft of the arm. Then by means of the low speed stepping motor the hand may be rotated in the + and - theta direction. The hand has two fingers which can be used to grasp objects and can also apply varying amounts of pressure through the fingers. The hand can be attached and detached from the arm completely under computer control.

High Speed Shaft Rotation

The shaft may be rotated at high speeds (70-25,000 RPM) with an AC motor. There are 256 increments in the speed control and this motor can only engaged if tne low speed stepping motor is disengaged.

Low speed shaft rotation

The low speed stepping motor can be used to rotate the shaft in increments of 4 degrees. The maximum rotational velocity with this motor is approximately 120 RPM. However torque is greater at a low speed.

HARDWARE CONTROLLER

The DEC-10 has a 36 bit word format. All hardware is interfaced to the I/O bus through a 36 bit parallel word. Three different I/O instructions can be used to communicate with the device:

DATAO <address>, <accumulator>

CONO <address>, <accumulator>

CONI <address>, <accumulator>

where <address> is the devices address on the I/O bus (424) and <accumulator> contains the appropriate 36 bit word or in the case of CONI will contain tne 36 bit word read. The DATAO instruction writes the contents of the accumulator to the device as data. The CONO instruction writes tne contents of the accumulator to the device as condition information. The CONI reads a 36 bit word from tne sensors of the device. Appendix A contains the bit assignments for each of the 3 different instructions. For example by executing a DATAO instruction witn bit 35 of the accumulator a "1" the arm will move one step in the +x direction. Executing 10 consecutive DATAO'S will step the arm 10 steps in the +x direction. It can be seen that speed and feed control is strictly done with software. A CONI instruction that returns a "1" in bit 35 will indicate that the +x limit switch has been depressed. It can be seen that the majority

of the actual hardware is just 36 bit data latches, along
with a high speed motor controller, AC solenoid drivers, an
air pressure controller, stepping motor drivers, and
interrupt handling hardware. Software is responsible for
the majority of control.

SOFTWARE CONTROL

The control program for the device is called
Robhnd.exe[5,736] and can be run interactively with the
DEC-10 monitor command:

.ru robhnd[5,736]

After typing the above monitor command the program will
respond with:

ROBOT READY, GIVE RESET FIRST
OR DETACH

If DETACH is typed, the robot-handler program is ready to
accept calls from programs written in higher level
languages. If RESET is typed, the device is ready to accept
commands. The following commands are valid:

RESET

>Used to initialize the device or to recover from
"HARD" errors. A reset leaves the arm at the
absolute position, X=-3240 Y=-3240 Z=1400 and W=0,
where W represents the wrist. All pressure
registers are cleared.

SENSE

>Returns current status of the arm which includes X
position, Y position, Z position, and W position.

XREL N

>Move N steps in the x direction relative to its
current location. -3241 < N < 3241.

XABS N

>Moves to location N on the X axis. Again, -3241 <
N < 3241.

600

YREL N

> Moves N steps in the y direction.

YABS N

> Moves to the y coordinate position N.

ZREL N

> Moves N steps in the z direction (N may be negative).

ZABS N

> Moves to the z coordinate position N.

SETVEL N

> where N is a number between 0 and 1, and is used as a scale factor for velocity (feed) when moving in the X,Y,Z, or W direction.

SETVC N

> this set the hand pressure control power source.
>
> 0 for current
>
> 1 for voltage
>
> It should be set to 0 with the hand attached.

SETPR N

> where N is between 0 and 1777. A number greater than 1777 is loaded as 1777 and any number less than 0 is loaded as 0. This controls the D/A controlled power supply to either current magnitude of 0-5 amps, or voltage magnitude of 0-15 volts.

HAND N

> if N equals 1 the hand opens
>
> N equals -1 the hand closes
>
> N equals 0 no power will be delivered to the hand.

SETHS N

where N is between 0 and 255. This sets the speed
for the high speed motor controller between 0 and
25,000 RPM with 100 RPM increments.

SETAP N

where N is between 0 and 255. This set the air
pressure for the air vise to between 0 and 60 PSI.

HIGHS N

a 0 turns off the high speed motor, a 1 turns on
the motor. This is interlocked with engaging the
low speed motor by hardware.

LOWSP N

a 0 disengages the low speed motor, a 1 engages
the low speed motor. This is interlocked with the
high speed motor in hardware.

AIR N

a 0 turns off the pneumatic clamp, and a 1 turns
it on.

QUICK N

a 0 disengages the quick change, and a 1 engages
the quick change.

ACKNOWLEDGEMENT

REFERENCES

[1] Briad, I. C. Designing with Volumes, Cantab Press,
Cambridge, England, 1975.

[2] Jones, V. C. A simple robot arm, CSL AI Technical Note
1, University of Illinois, 1973.

[3] Lang, C. A. A three-dimensional model making machine,
in Computer Languages for Numerical Control (J. Hatvany,
ed.), pp.109-119, North Holland Publishing Company, 1973.

[4] Merchant, M. E. The future of CAM systems, Proceedings of 1975 National Computer Conference, pp.793-799.

[5] Snyder, W. E. and Jones, V. C. A user's guide to the CSL vision system, CSL Report R-714, University of Illinois, 1976.

[6] Voelcker, H. B. et. al. Part and assembly description language, Report TM-20a, University of Rochester, 1974.

[7] Woo, T. C. Computer understanding of designs, CSL Report R-695, University of Illinois, 1975.

APPENDIX A

bit	meaning	notes

DATO bits

0-2	3 bit field for Priority Interrupt Channel	i
3-6	4 bit field for AC solenoid control	s
	0000 not used	
	0001 quick change on	
	0010 quick change off	
	0011 not used	
	0100 not used	
	0101 high speed motor on	
	0110 high speed motor off	
	0111 low speed motor engaged	
	1000 low speed motor disengaged	
	1001 air pressure off	
	1010 air pressure on	
	1011 not used	
	1100 not used	
	1101 not used	
	1110 not used	
	1111 set all functions off	
7-8	2 bit field to determine which register is loaded with bits 21-29	s
	00 not used	
	01 set air pressure	
	10 set high speed motor register	
	11 clear all above register	
9	load hand pressure register flag	j
10	set slow wrist if wrist busy	j
11	start timer	s
12	move -z	s
13	move -y	s
14	turn off hand solenoid	s
15	open jaw	s
16	move -w if not slow wrist	s
17	move -x	s
21-29	8 bit data field for air pressure register	

```
                  high speed motor register
                  hand pressure register
                  depending on bits 7,8 or 9
30        move +z                                           s
31        move +y                                           s
32        turn on hand solenoid                             s
33        close jaw                                         s
34        move +w if not slow wrist                         s
35        move +x                                           s


CONO control bits


18-26     load "page register"                             c
          (these bits specify the upper 9 bits
          of the address to which interrupts will
          vector)
27        clear "change interrupt"                          s
28        clear "slow wrist and wrist busy                  s
29        clear "time interrupt"                            s
30        clear "time enable"                               c
          (enable timer interrupts)
31        set "time enable"                                 c
32        set "time interrupt" if  "time enable
          and timer not running
33-35     load PI channel                                   c


CONO bits


0         slow wrist flip flop                              a
1         jaw open                                          b
2         finger 1 touching                                 b
3         finger 2 touching                                 b
4         not used
5         jaw closed                                        b
6         hand down (soft)                                  c
7         hand down (hard)                                  d
8         extra switch                                      d
9         hand code                                         e
10        -z limit switch                                   d
11        -y limit switch                                   d
12        hand locked                                       e
15        hand energized                                    e
16        wrist home                                        e
17        -x limit switch                                   d
```

```
27      change interrupt
28      wrist busy                                          e
29      time interrupt
30      +z limit switch                                     d
31      +y limit switch                                     d
35      +x limit switch                                     d


notes:
        a: set by DATAO bit 10, if wrist busy
           "change interrupt" is also set
        b: the first jaw switch "on" sets interrupt
        c: this switch sets "interrupt" when it changes state
        d: this group of seven switches sets "interrupt"
           when the first switch turns "on"
        e: no interrupt
        i: occurs during interrupt sequence
        j: occurs during CONO CLR or DATAO CLR time
        s: occurs during CONO SET or DATAO SET time
```

MECHANICAL DESIGN AND COMPUTER CONFIGURATION IN THE

COMPUTER-AIDED MANIPULATOR CONTROL PROBLEM

By Philippe Coiffet[1], Jean Vertut[2], and Etienne Dombre[3]

SUMMARY

Use of a computer-aided manipulator for performing a given task implies that the computer keeps in memory a mathematical model of the manipulator in order to periodically generate control signals. Interesting dynamical performances may be obtained if the computer works very rapidly or the model is simple enough.

The algorithms necessary for control of an articulated system depend on the complexity of its dynamic equations. A study of the French AEC-MA23 manipulator considers the effects of changes in the mechanical design on this relationship.

For a given control algorithm, methods which allow one to propose computer configurations able to generate this algorithm are also presented. Time minimization, memory size and eventual cost are taken into account.

These previous elements are of most interest in the design of new manipulators since they would lead to a suboptimal control system from the standpoint of performance-cost relationship.

INTRODUCTION

In the design of robots which are not provided with refined algorithms of an artificial intelligence type, manual control is necessary since man has to interact with them at different levels. However, the purpose is to decrease the psychological and muscular cost to the human operator who is required until the robot can be driven without the help of man.

Since the end of World War II, the evolution of manipulators corroborates this previous trend: since Goertz' sophisticated mechanical grasping device, manipulators are now provided with electrical servo-systems and are coupled with computers. The physical duty of the operator has then been removed and now becomes more psychological.

[1]Laboratoire d'Automatique de Montpellier, USTL, Place E. Bataillon, 34060 Montpellier, Cedex, France.
[2]Centre d'Etudes Nucléaires de Saclay, France.
[3]Laboratoire d'Automatique de Montpellier, France. Currently at Rancho Los Amigos Hospital, Downey, California.

However, these improvements have been done in an empirical manner and it appears that a general theory of robot synthesis, manipulators especially, is still lacking.

Our purpose in what follows is to make propositions regarding some aspects of the synthesis of manipulators, mainly to point out the linkages between the mechanical structures and different methods of control, as well as a means to define these controls according to a cost-performance criterion. A French manipulator, the MA-23, designed by the CEA-Saclay, will be put forward as an example when required.

DIFFICULTIES OF THE SYNTHESIS PROBLEM

A manipulator is no more than a kind of sophisticated tool. Therefore, it is an interface between man and tasks to be performed. In order to support man, this interface has to be provided with helpful characteristics such as:

- versatility; i.e., the ability to perform various tasks

- adaptability; i.e., the ability to execute a given task despite environmental modifications

The major problem encountered in the synthesis of a manipulator is the definition of an interface when the two systems to be coupled are not fully defined (systems which are evolutionary and interactive with the interface).

For this reason the synthesis is generally done taking into account specifications required by the customer (or by the builder who has made a survey of some specific application). There are three steps:

a) Generation of a mechanical structure which will execute the specified tasks

b) Setting up of control algorithms. There are two classes:

    (1) Elementary task type algorithms; i.e., those which link the control variables to the variations of the manipulator variables (degrees of freedom, applied forces, etc.)

    (2) Algorithms of strategy; i.e., the arrangement of the elementary task sequence according to a goal and/or to a determined criterion.

c) Implementation of the control methods which makes the execution of those algorithms possible.

The result, that is to say, the final realization is intended to satisfy several requirements such as:

- the actual execution of the desired tasks under the desired conditions.

- the minimization of the cost of realization in order that the manipulator can be actually used.

This cost-performance criterion is present in all the steps of the synthesis as well as in all their interconnections.

INFLUENCE OF THE MECHANICAL STRUCTURE ON THE CONTROL COST IN ELEMENTARY TASK TYPE ALGORITHMS

The specifications give the necessary conditions but usually, they are not sufficient to provide a unique mechanical structure. Indeed, the predicted tasks have to be executed, but they must be executed under certain constraints and the simplification of the control algorithms must be facilitated. (As a matter of fact, the simplification is connected with the cost of the implementation and, therefore, with the cost of the manipulator.)

The MA-23 will help us to show the connection between structure and complexity of the algorithms. The MA-23 (references 1 and 2) is the most recent of a series of telemanipulators which have been designed by the "Centre d'Etudes Nucléaires" in Saclay (France). Manipulation of radioactive elements and operations in hot environments were the first goal. The MA-23 possesses 6 degrees of freedom (θ_i) shown in figure 1, plus the closing up of the terminal device. It is activated by electrical torque-motors secured on the fixed frame of the manipulator (fig. 2). The transmissions and reductions are performed by cable systems and metallic tape systems. Gears are used only for the wrist. The benefit of metallic tapes with respect to gear transmission systems is to reduce markedly static friction and backlash. Moving counterweights enables one to obtain a neutral equilibrium, whatever the configuration of the unloaded manipulator. Three patterns of load are available, 60, 100 and 250 Newtons respectively.

Kinematic Model and Position Control Coupling

The kinematic modeling consists in relating the generalized variables Θ_i (or degrees of freedom of the manipulator) to the coordinates of the different lever extremities, especially the coordinates of the terminal device X_j. These coordinates are located in a fixed tridimensional reference system, related to the manipulator holding frame. Therefore, the motor control voltage is related to the previous coordinates. This can be described as below:

| Motor Voltages | A → | Motor Rotations | B → | Values of Θi | C → , C^{-1} | Values of the terminal device coordinates |

(1)   (2)   (3)   (4)
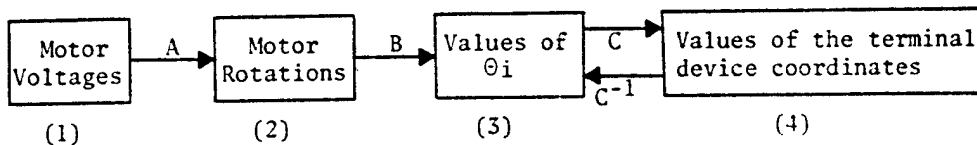
The system can be position-controlled if the terminal device coordinates can be predicted from the command Θ_i and vice versa (since generally, the displacements are fixed and the corresponding command is generated).

Therefore, the complexity of the control depends on:

    a) The complexity of A, B and C

    b) The fact that it may happen that A, B and C are
       not reversible.

The connections A and B concern the means of control to implement in order to enable the transformation C and C^{-1}. Those are nothing more than the kinematic model of the manipulator, which by the way, has to be simplified in an important manner.

The complexity of the kinematic control is due to many characteristics such as:

    a) The number of degrees of freedom (however, the minimal number
       depends on the type of tasks to be performed.)

    b) The geometrical complexity of the manipulator which affects
       the nature of the transformation formulas between the fixed
       reference system and the generalized variables.

    c) The minimal number of variables which have to be known about
       the terminal device in order to elicit clearly the actual
       values of the generalized variables. This is the problem of
       the manipulator <u>realizability</u>.

The MA-23 does not exhibit any translational degree of freedom. There-fore, the transformations from one coordinate system to another may be represented by rotation matrices. Their product becomes more complex when the fixed reference system is transformed into a terminal device coordinate system.

The realizability of the MA-23, that is to say the analytical description of C^{-1}, is possible only if the points C and E and the angle Θ_6 (fig. 1) are known, or if the coordinates of C and the terminal device orientation are known.

In other words, for a given manipulator, the structure interacts with the position control in the kinematic mode. The complexity of the control depends on the solution to the realizability problem.

Kinematic Model and Rate Control Coupling

The kinematic model for rate control consists of relating the generalized variables (Θ) to variations $\Delta\Theta$ and ΔX of the terminal device rather than to its coordinates (X).

The new connection is established from C by appropriate derivation. Therefore, the existence of the command depends on the issue of realiz-ability. The complexity of this rate control is consequently directly related to the complexity of the position control but the problem becomes more serious considering the existence of singularities.

A singular point corresponds to a specific configuration where it is impossible to get a given ΔX from any $\Delta\Theta$. (This problem occurs usually when a determinant is zero.) If these singularities occur in configurations which are used often during the execution of tasks, the implementation of the control is made more difficult since the singularities must be detected and the algorithm must be consequently modified. Therefore, the cost increases.

For the MA-23, the main singularities happen when a lever axis (for instance, the axis Z_7 of the terminal device in fig. 1) goes through another joint. Thus, the ranges of each degree of freedom have been computed in order to avoid those configurations during actual motion. It can be noticed, in Table 1, that despite this constraint, the amplitudes of motion remain significant.

Dynamic Model and Dynamic Control Coupling

The equations describing the manipulator dynamics have to account for inertia and acceleration of each generalized variable. They are then generally very complicated. For the MA-23, the set of equations can be written as follows:

$$(1) \quad \begin{cases} \sum_{j=1}^{6} \{ A(i,j)\, \ddot{\theta}_j + C(i,j)\, \dot{\theta}_j^2 + \sum_{k=j+1}^{6} B(i,j,k)\, \dot{\theta}_j \dot{\theta}_k \} = Q(i) + \Gamma_{\theta_i} \\ i = 1,6 \end{cases}$$

The $A(i,j)$, $B(i,j,k)$ and $C(i,j)$ coefficients are, for the most part, functions of the generalized variables θ_i of the inertias and the masses of the manipulator and of its geometry. They are not explicitly dependent upon time. The terms $Q(i)$ represent the torques due to gravity and are functions of the configuration and of the masses of the system. The terms Γ_{θ_i} are the motor-torques which act about the different degrees of freedom.

Looking for a command consists in searching the Γ_{θ_i} to be applied in order that the manipulator be driven with the required characteristics and following equations (1). Any control algorithm refers to equations (1) which are then to be simplified to a great extent.

In the case of the MA-23, provided with 4 levers and 6 degrees of freedom (not accounting for the closing of the terminal device) there are 36, 90 and 36 terms for $A(i,j)$, $B(i,j,k)$ and $C(i,j)$ which means a total of 162 terms. Most of them need several lines of writing.

To decrease the cost of the control, the expression of Γ_{θ_i} has to be simplified. The solution is to void or make negligible as many terms of A, B or C as possible.

Three possibilities are available:

a) The general theorems of the theory of mechanics with which it may be written for instance:

$$A(i,j) = A(j,i)$$

$$C(i,i) = 0 \qquad \text{etc . . .}$$

b) The mechanical structure design as for instance the cutting out of θ_6 with respect to the other angles, the parallelism between certain axis of rotation, etc. . .

c) The maximal rates admissible, which leads one to neglect some centrifugal force terms or Corriolis' force terms. This point can only be verified by simulation.

Table 2 gives the number of coefficients which can be neglected by simplifications specific to the MA-23 (reference 1). Those simplifications can be done if the maximal rate of the terminal device and the maximal load do not go beyond 1 m./s. and 50N respectively. Equations (1) are written as:

$$\begin{cases} \sum_{j=1}^{6} A(i,j)\, \ddot{\theta}_j = Q(i) + \Gamma_{\theta_i} \\ \\ i = 1,6 \end{cases}$$

(The $A(i,j)$ coefficients represent a symmetrical matrix with 6 zeros. There are only 15 <u>different</u> terms left.)

Therefore, the connection between control cost and mechanical structure has been established. However, it must be noticed that in order to define a structure on which the previous simplifications are possible, it is necessary to write the overall equations of the system. Furthermore, the behavior must be simulated for several structures, the outcomes of mechanical modifications on the behavior must be forecast, etc. . . It is then obvious that the writing of the equations by hand is not only tedious but difficult to get through without any mistake.

This is the reason why a computer program has been prepared (reference 3), using the PL1 language. From heuristic data on a tree-like network, such as number of levers, number of degrees of freedom, relation order, etc., the program yields <u>literally</u>:

* the different coordinate transformation matrices

* the coordinates of each lever end point in a fixed reference system

* the gravity torques

* the dynamic coefficients $A(i,j)$, $B(i,j,k)$ and $C(i,j)$

To date, this program is restricted to systems with only rotational degrees of freedom (the extension to translational motions is in progress). It needs 2 minutes (CPU) on an IBM 360-65 to give the results corresponding to the MA-23. Another computer program, making use of the standard Runge-Kutta method, simulates the manipulator behavior from the results of the first program.

These results form an interesting and efficient tool for the determination of a structure which decreases the control cost.

613

INFLUENCE OF THE MECHANICAL STRUCTURE ON THE
CONTROL COST IN THE STRATEGY TYPE ALGORITHMS

Since the strategy type algorithms use a sequence of elementary task type algorithms according to a given criterion of execution (reference 4), it can be said that the connection between mechanical structure and strategy type algorithms is relatively flexible. The connection operates only if the transducers which are necessary to the criterion elaboration introduce a modification of the structure by means of their physical presence. For instance, if visual information is desired, the TV camera which could be put on a light lever of the manipulator would modify the masses and inertias in an important manner. Likewise, changes in the shape of the terminal device would be necessary if a sonar was supposed to be set up.

Usually, mechanical structure and algorithm are supposed to be completely unrelated. With this hypothesis, researchers have been able to propose complex artificial intelligence type algorithms but they are not concerned with the mechanical structure to be controlled. Likewise, the computer which is supposed to generate the algorithms is seldom specified. This, then, is another problem from the standpoint of cost-performance criterion.

IMPLEMENTATION OF A CONTROL ALGORITHM

So far, we have discussed the specifications required for a mechanical structure to minimize the complexity of the elementary task type algorithm in order to decrease the system cost (references 5 and 6). Those algorithms being established, as well as the strategy type algorithms, we are now concerned with the implementation in order that their efficiency and their cost be optimized.

Practically this means that the motions of the manipulators must be fast enough (usually with a rate near that the man uses to carry over a load) but that the "computer" and the manipulator must cost about the same.

The hypotheses of references 7, 8 and 9 are recalled below:

a) The algorithm is assumed to be given with a fixed mathematical formulation

b) The mathematical methods used in the processing (for instance, to get the inverse matrix) are given

c) The computer structure is given as well. It is, at the present time, a multiprocessor structure with unique memory (figure 3)

The problem is to define the number of processors to be used and the respective minimal memory size in order to execute the algorithm in a given time (this time is imposed by the expected performances of the manipulator).

For this purpose, the execution of the algorithm is described by a state transition graph with nodes and arcs. The arcs represent the crossing conditions from one node to another. Computation times and memory sizes are associated with nodes (figure 4).

The application of the "critical path method" (references 10, 11, 12 and 13) to the state transition graph gives the minimal time of execution for the algorithm if sufficient resources (number of processors and memory size) are allocated to it. In this way, it is possible to determine an upper limit for these resources. The purpose is to minimize the resources accounting for the time constraint.

Two algorithms have been studied, with which it is possible to minimize the memory size when the number of processors is given.

- The first one is of an heuristic type and the distance between its solution and the optimum is unknown.

- The second one gives the optimum but all the possible configurations of the task have to be specified.

Finally, a method allowing one to obtain the configuration which minimizes the cost of the hardware (the cost is defined as a linear function of the number of processors and of the memory size) and avoiding the specification of all the possible configurations has been developed with a progressive evaluation and separation procedure (PSEP) (reference 14).

Research is currently in progress in order to extend the hypothesis. The possibility of conflict between several processors, from the standpoint of memory access, is taken into account. Besides, it is assumed that an addition of large but slow access memories, such as disks, is provided.

Currently in progress as well, is the realization of the control of the MA-23 with microprocessors. (To date, this control is made with a T-1600 type of computer from "Télémécanique" (France) with a memory size extended by a disk unit.)

615

CONCLUSION

The present robots or manipulators used in industry are all controlled in a kinematic mode and without adaptive characteristics (in other words, without closed loop strategy type of algorithms). It might be thought that the implementation of control algorithms in the dynamic mode and of adaptive algorithms costs too much if the efficiency of open loop controlled robots is considered. However, the robots are supposed to perform tasks which are mainly those bringing out the versatility and the adaptability of the human operator (assembly tasks, transfers of load, etc. . .).

The research presented in this paper is a contribution to the synthesis of modern manipulators. The criteria of realistic cost and of performance of the system are emphasized.

REFERENCES

1. Vertut, J.; and Coiffet, P.: Bilateral Servo Manipulator in Direct Mode and Via Computer Optimized Control. Second Conference on Remotely Manned Systems, Los Angeles, June 1975.

2. Vertut, J.; Charles, J.; Coiffet, P.; and Petit, M.: Advance of the New MA-23 Force Reflexive Manipulator System. 2nd Int. Symp. on Ro. Man. Sy., Warsaw (Poland), Sept. 1976.

3. Liegeois, A.; and Coiffet, P.: Le Projet Pilote SPARTACUS. Institut de Recherche en Informatique et Automatique, Rocquencourt (France) March 1976.

4. Liegeois, A.; and Renaud, M.: A Method for the Dynamic Control of Redundant Manipulators. Proc. of 5th Int. Symp. on External Control of Human Extremities. Dubrovnik, August, 1975.

5. Coiffet, P.; Liegeois, A.; Fournier, A.; Khalil, W.; Molinier, P.; and Vertut, J.: Computer Aided Control of Force Reflective Manipulators. Symposium IFAC, Automatic Control in Space, Rottach-Egern, May 1976.

6. Liegeois, A.; Khalil, W.; Dumas, J. M.; and Renaud, M.: Mathematical and Computer Models of Interconnected Mechanical Systems. 2nd Int. Symp. on Theory and Practice of Robots and Manipulators, (Ro. Man. Sy.) Warsaw (Poland), Sept. 1976.

7. Dumas, J.M.; and Prunet, F.: A Method for Local and Reduced Studies in Parallel and Processes Models. Digital Processes, 1976.

8. Prunet, F.; Floutier, D. and Dumas, J.M.: Computer Aided Design of Industrial Control Systems. 12th Design Automation Conference, Boston, 1975.

9. Dumas, J.M.; and Prunet, F.: Searching for Properties on a Parallel Processes Model. Proceedings of the Int. Workshop of Real Time Processes, Boston, August, 1975.

10. Cerf, V.G.: Multiprocessors, Semaphores and a Graph Model of Computation. Ph.D. Thesis, University of California (1972).

11. Parent, M.R.: The Control Graph Models: A Unified Approach to Performance Evaluation. Case Western Reserve University, June, 1974.

12. Fernandez, E.,et al.: Bounds on the Number of Processors and Time for Multiprocessor Optimal Schedules. IEEE Tran. on Computers. C-22,8,August 1973.

13. Serlin,O.: Scheduling of Time Critical Processes. Spring Joint Computer Conference, 1972.

14. Roy,B.: Algebre moderne et theorie des graphes. 2 tomes, Dunod, Paris, 1969.

15. Proceedings of the 3e CIRT, Nottingham, March, 1976.

Ranges of motion and lengths of the different
levers for the MA-23 (see Figure 1)

OA = 320 mm

AB = 400 mm

BD = 650 mm

$$- 60^{\circ} < \theta_1 < + 60^{\circ}$$

$$- 70^{\circ} < \theta_2 < + 57^{\circ}$$

$$- 135^{\circ} < \theta_3 < - 30^{\circ}$$

$$- 179^{\circ} < \theta_4 < 179^{\circ}$$

$$- 81^{\circ} < \theta_5 < + 57^{\circ}$$

$$- 180^{\circ} < \theta_6 < 180^{\circ}$$

$$BCD = 128^{\circ}$$

Table 1

618

Table of simplifications to calculate the dynamic
coefficients of the MA-23 type of manipulator

Dynamic Coefficients	Number to be evaluated	Decrease in the number to be evaluated		Number of Coefficients Remaining
		Due to	Number	
A_{ij}	$n^2 = 36$	General Theorems of the Theory of Mechanics $\frac{n(n-1)}{2} = 15$		21
		Mechanical Design	6	15
		Maximal Rates Admissible	0	15
B_{ijk}	$\frac{n^2(n-1)}{2}$	General Theorems of the Theory of Mechanics $\frac{n(n-1)}{2} = 15$		75
		Mechanical Design	Disjunction of $\theta_6 = 35$	40
			Parallel Axis = 11	29
		Minimal Rates Admissible	29	0
C_{ij}	$n^2 = 36$	General Theorems of the Theory of Mechanics $n = 6$		30
		Mechanical Design	15	15
		Maximal Rates Admissible	15	0
Total	$\frac{n^3 + 3n^2}{2}$ $= 162$		147	15

Table 2

<u>Captions</u>

Figure 1: Skeletal of the MA-23

θ_1 and θ_4 are zero when O.A.B.C and D are in the OYZ plane

θ_6 is zero when the terminal device is in an orthogonal plane with respect to OYZ

Figure 2: A view of the MA-23

(1) Motors
(2) Servo - Systems
(3) Cable Reducers
(4) Counterweights

Figure 3: General architecture of the computer

MC = central memory
P_i = processors

Figure 4: Example of graph associated to the calculation of two commands V_1 and V_2

$$V_1 = \sqrt{sinS_1} + sinS_2$$
$$V_2 = cosS_1 + \sqrt{cosS_2}$$

A computation time and a memory size are associated to each mode
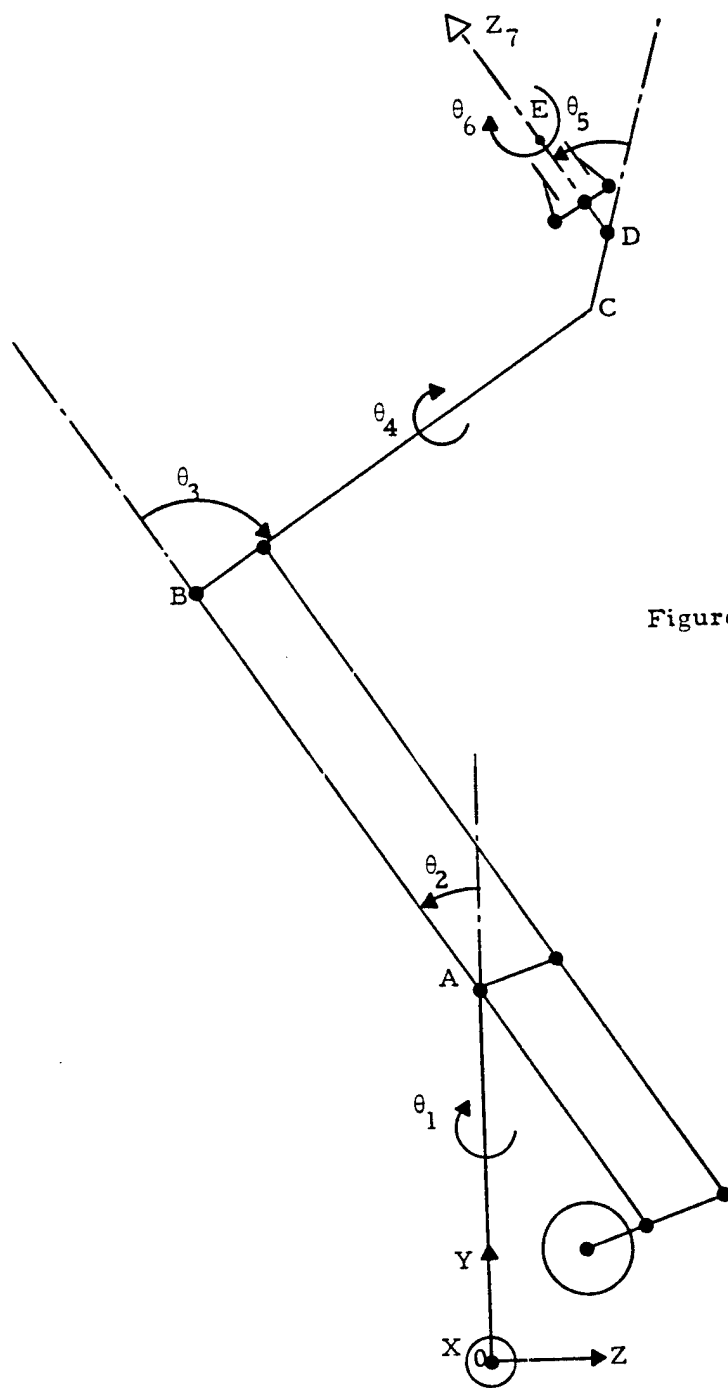
Figure 1
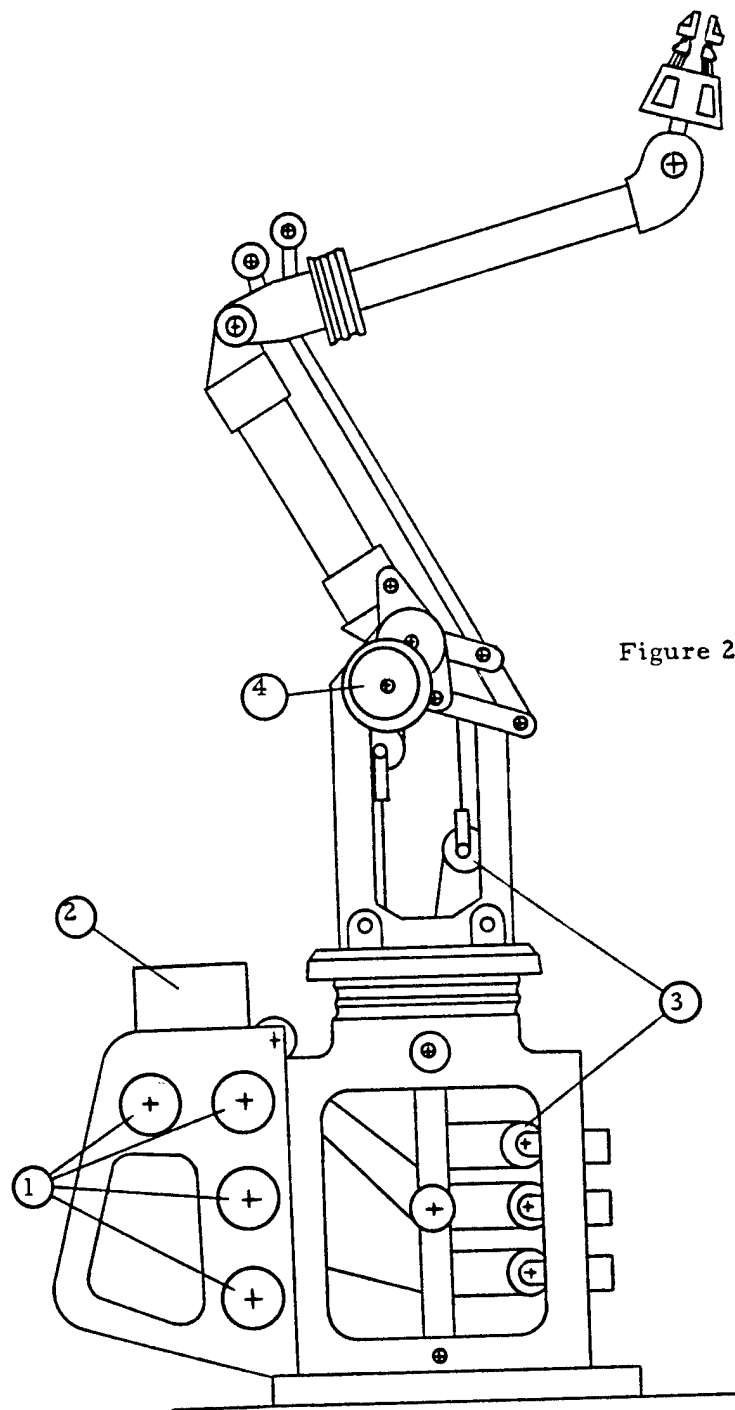
Figure 2
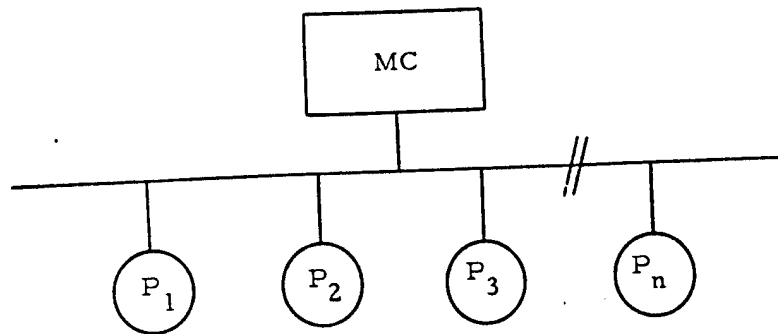
Figure 3
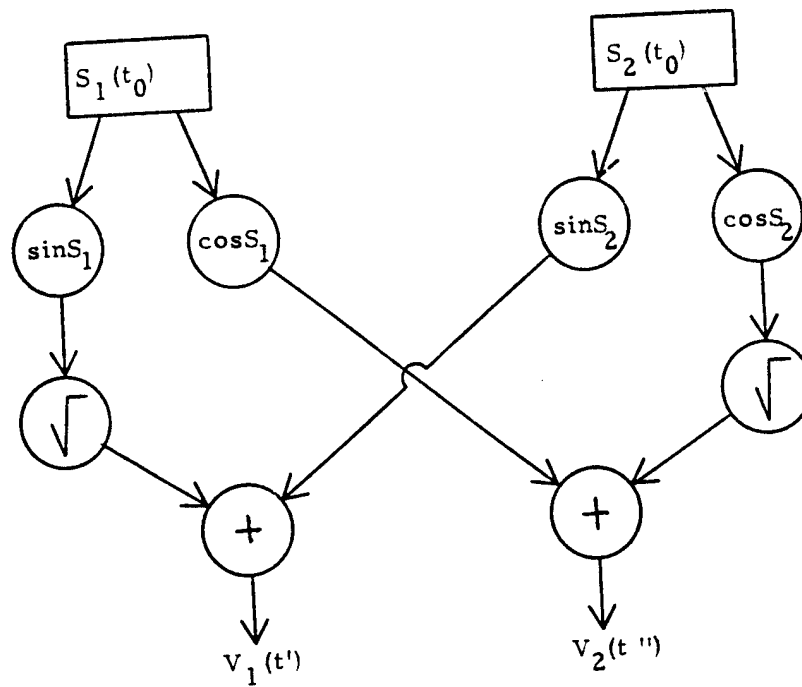
Figure 4

A PRELIMINARY EVALUATION OF MANUAL CONTROL TASKS

ASSOCIATED WITH THE SPACE SHUTTLE REMOTE MANIPULATOR SYSTEM*

Lloyd D. Reid

University of Toronto
Institute for Aerospace Studies

SUMMARY

A major hardware component in the Space Shuttle cargo handling system is a large (50' long) remote manipulator arm. This arm is employed in the zero-g space environment to load and unload cargo while in orbit. Due to weight restrictions this arm must be of light construction and consequently care must be taken to ensure that flexibility induced problems do not arise while it is under the control of human operators.

The purpose of the present project was to perform a preliminary investigation of the ability of human operators to control the arm. In particular attention was focused on the human's ability to damp out structural oscillations of the system. This was achieved by implementing the system equations of motion on an analog computer and employing a pictorial display on a CRT driven by a digital computer. The simulation was based on a single-degree-of-freedom model.

Both arm stiffness and display update were varied in order to assess their impact on system performance. Phase plane plots and tracking precision measures were obtained as part of the study. It was found that the system was best controlled by a form of open loop response and that the structural oscillations could be successfully damped out.

INTRODUCTION

At the present time a group of Canadian firms is developing a Remote Manipulator System (RMS) for the space shuttle. This arm will be used to move payloads into and out of the cargo hold. It is approximately 15.2m (50 ft.) in length with a shoulder joint, elbow joint, wrist joint, and end effector. One mode of operation involves three axes rate control by a human operator while viewing the arm either directly out a window or on a closed-circuit TV monitor.

In order to minimize the system weight design trade-offs must be made against arm rigidity. This in turn can lead to significant structural

oscillations when the system is operated. The present study was intended to investigate the ability of human operators to damp out structural oscillations in the arm when a massive payload is held by the end effector. A secondary goal was the evaluation of the influence of computer induced time delays and display update lags in order to assess their importance in future RMS simulations.

OVERALL SYSTEM DESCRIPTION

The task to be simulated was a simplified single-degree-of-freedom version of the real task (see Fig. 1). Our laboratory was provided with the appropriate equations of motion at the start of the project. These described a single joint arm system. The human operator's task was to damp out vertical oscillations (relative to the space shuttle body axes) of a 29,030 kg (32 ton) payload at the end of a 15.2m (50 ft.) flexible arm.

Working in from the payload, the simulated system consists of:

(1) The 15.2m (50 ft.) arm, described by its first mode of oscillation (the cantilever mode). Arm stiffness values employed ranged from 0.57 to 13.7 mm deflection per Newton force applied at the tip. Structural damping ratios employed ranged from 1% to 2.4%.

(2) The shoulder joint servo generates a relative angle γ between the root of the arm and the space shuttle horizontal body axis. This servo system is rate limited and torque limited such that the nominal maximum arm tip vertical speed is less than 7.6 cm/s (neglecting structural oscillations) and the nominal maximum tip force that can be applied to a payload by the shoulder joint servo system is 129 N.

(3) The space shuttle was free to roll and translate in the transverse body axes plane. An automatic roll attitude control system was employed to attempt to maintain $\theta = 0$ referenced to an inertial frame. This involved a rather limited pulsing rocket thruster.

VISUAL DISPLAY

The visual display employed was a mini-computer generated simulation of a closed circuit vision monitor. It depicted a 3 x 3 x 6m rectangular payload on the end of a 15.2m arm (see Fig. 2). For the simple task studied here a close-up picture of the payload was employed. The inverted V is a screen fixed reference mark (see Fig. 3). The display is generated by a high-speed digital-to-analog converter and is based on a 256 x 256 dot matrix presentation on a 20 x 28 cm screen.

HARDWARE

The system equations of motion were programmed on a TR-48 analog computer and the visual display generated by an HP 2100 mini-computer. The work station contained the display and the controller. The latter was hand held and finger operated and does not represent anticipated flight hardware.

TASK DETAILS

In the present study the payload was assumed to be already attached to the end of the arm with the arm flexed and at rest. The task begins with the release of the system from these initial conditions.

The primary recording device employed was an X-Y plotter. This was used to generate phase plane plots of payload vertical speed vs. payload vertical position (positive upwards) (see Fig. 4). This figure depicts the nature of these phase plane plots when no human control is present. It is seen that the overall system behaves much like a second order system despite the presence of nonlinearities. In this plot the time in seconds following system release is indicated by the flagged numbers located at the horizontal axis crossings.

The overall system period and damping ratio as measured from phase plane plots have been used to identify the various cases in Fig. 5. Four different systems have been studied and two different display update rates employed. The subjects were selected from a group of 8 volunteers on the basis of good performance on the present task. A total of 272 final runs were analyzed.

As can be seen in Fig. 5, the system's period of oscillation was quite long and the damping modest. As a result it was found that in order for the subjects to damp out the oscillation an intermittent form of control activity was required. Attempts at continuous closed-loop control on the part of the subjects almost always led to an instability.

Figure 6 can be used to illustrate the problem. Here all the elastic properties of the arm are concentrated in a spring at its root. The human operator is assumed to control the angle γ through the integrated effects of his rate command inputs. Structural damping is absent.

In order to damp out the structural oscillation of this system the energy contained in the elastic deflection of the spring and the motion of the payload must be dissipated. When the system is released from position (1) all the energy is contained in the spring. By the time the payload passes through $Z = 0$ (provided that γ still is zero) all the energy resides in the kinetic energy of the payload. Attempting to oppose this motion is not very effective because this tends to simply shift the energy of the oscillation from kinetic energy to strain energy of the spring. The simplest

626

way to dissipate the energy is to rapidly release the spring by appropriate control over γ at some point where $\dot{Z} = 0$.

In addition, since we wish to bring the payload to rest at $Z = 0$ the net change in γ during these operations must also be zero. A possible sequence to achieve this is to release half the strain energy at (1) by commanding down γ and half at (2) by commanding up γ. Note that in order to release strain energy from the spring up control is applied when the deflection is upward, etc.

This approach can be applied to the present system. Typical results are shown in the plot of the elastic deflection of the arm tip in Fig. 7. The upper trace shows the response following the release from an initial downward deflection when no control is applied. The middle trace shows the effect of up command when the deflection is still downward. The bottom trace shows the influence of applying up command at the upward deflection peak in the cycle.

HUMAN OPERATOR CONTROL

The actual control technique adopted by the subjects was similar to that outlined above. They were instructed to damp out the structural oscillation which resulted when the arm plus payload was released from an initial deflection and to bring the payload to rest at the centre of the display (marked by the inverted V symbol). The latter corresponds to $\gamma = 0$. The task was allowed to run for 2 min.

Figure 8 illustrates the control activity of our best subject. He employed strain energy relieving commands at the peak deflections and generally followed an up command by a down in order to maintain γ near zero. The latter technique was necessary because the simulated system gives the operator no indication of the arm root angle γ. Thus with a rate command system he must keep track of the integrated effect of his inputs to the system in order to bring the payload to rest at $\gamma = 0$.

Figure 9 illustrates an actual phase plane plot for the system under human control. It was found that quite effective control could be exercised over the system after a reasonable period of training (8 hrs). The rectangle drawn around the origin represents an artificial target zone used to assess the time taken to achieve effective control over the system. Its dimensions are $Z = \pm 14$ cm and $\dot{Z} = \pm 1$ cm per sec. The time taken to enter this zone of the phase plane was termed "time to capture". (Note that the display resolution represents 6 cm full scale with the present configuration.)

EXPERIMENTAL MEASUREMENTS

Performance was judged by the residual energy in the structural oscilla-

tion at the end of 2 min. of human control and by the final value of γ (see Fig. 10). The residual energy was indicated by the peak-to-peak amplitude of the structural oscillation and the final value of γ by $|Z|$ steady state. The time to capture was also recorded. Only the detailed results for the runs performed by the group of 4 subjects are presented here.

An analysis of variance performed on the data indicated that subject and stiffness effects were significant at the 5% level while update interval effects were not. This applied to all three sets of data.

CONCLUSIONS

The following conclusions are based on the results for the systems with periods of oscillation of 27 and 51 sec.

(1) Flexibility is more important than display update rate in determining system performance. Stiffer arms result in better performance.

(2) Update rates (along with system time delays) of up to 2 sec. have no significant influence on the performance measures employed in this study.

(3) Performance in some cases approached the resolution limit of the display.

(4) The tasks performed were quite complex in nature and the individual subjects showed significant interaction effects with flexibility.

(5) An indication to the human operator of shoulder joint position would probably have simplified the tasks considerably.

The results for the systems with periods of oscillation of 11 and 22 sec. were too limited to allow the formation of firm conclusions. However, it appeared that the stiffer arm was marginally better and that increased display update intervals tended to cause poorer performance.
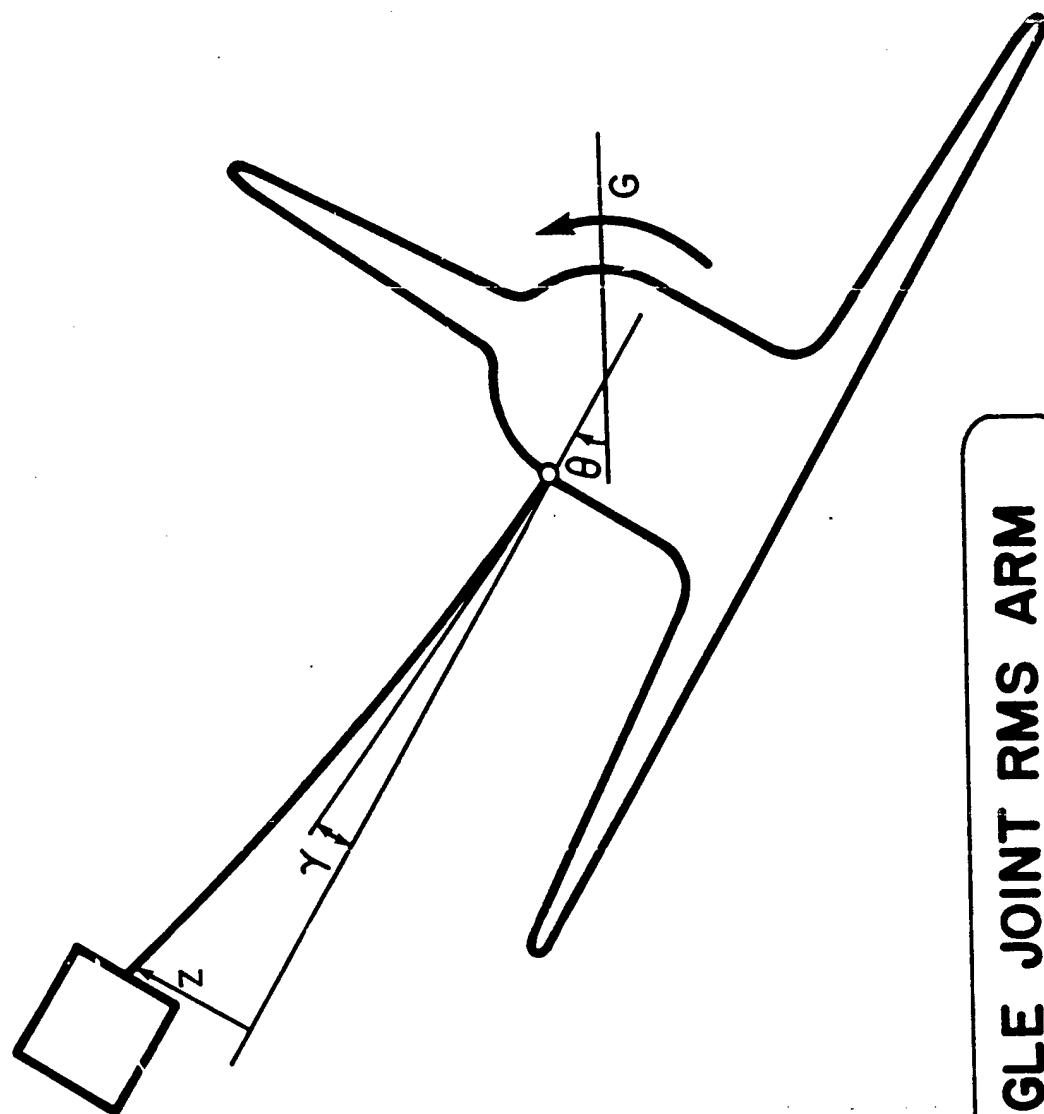
JOINT SERVO
   RATE COMMAND
   SATURATION
   RATE LIMITER
GEAR BOX
   BACKLASH
ATTITUDE CONTROLLER
   DEAD BAND
   SATURATION
   PULSE RATE
ARM DYNAMICS
   FIRST MODE

SINGLE JOINT RMS ARM

FIGURE 1

FIGURE 2

630
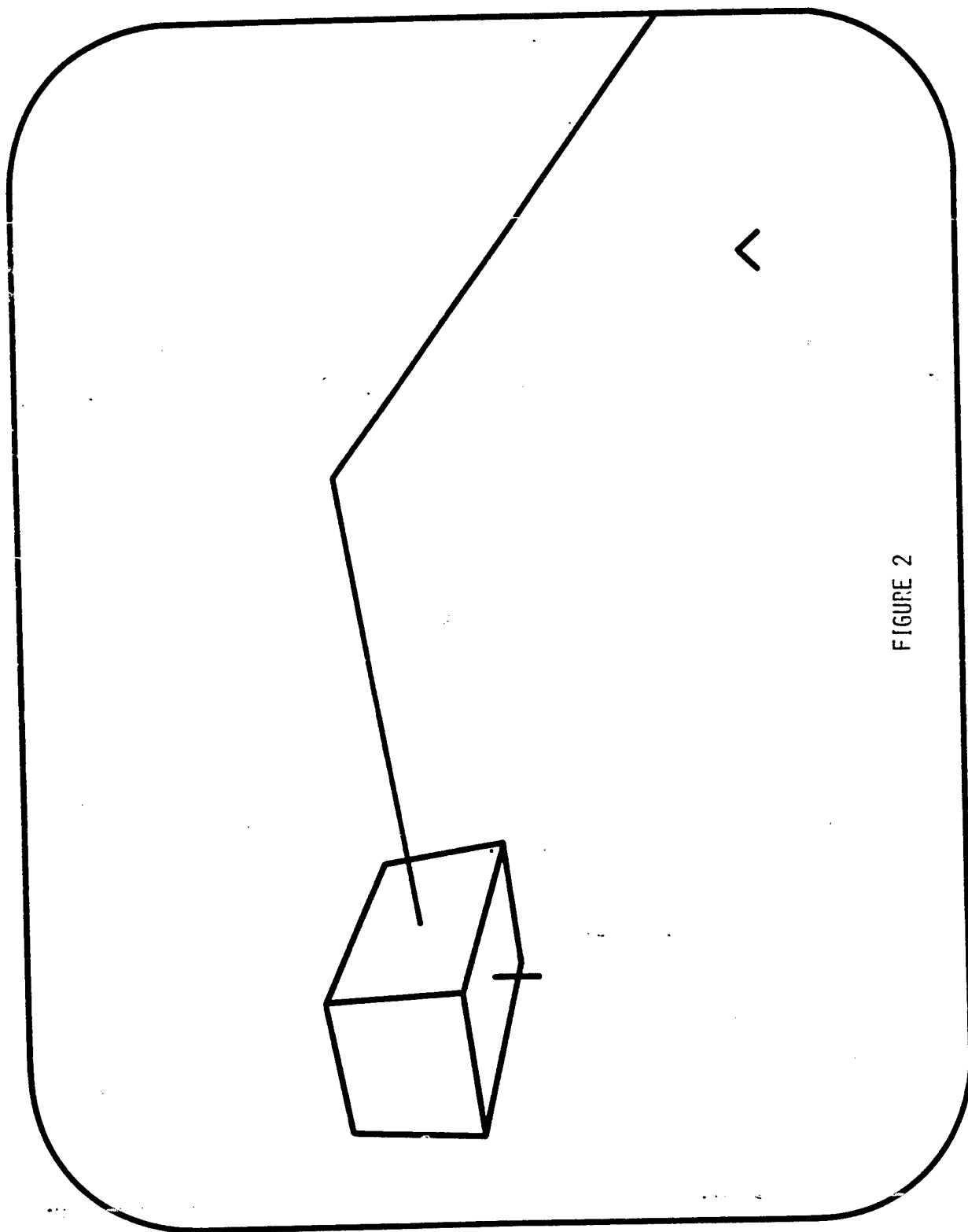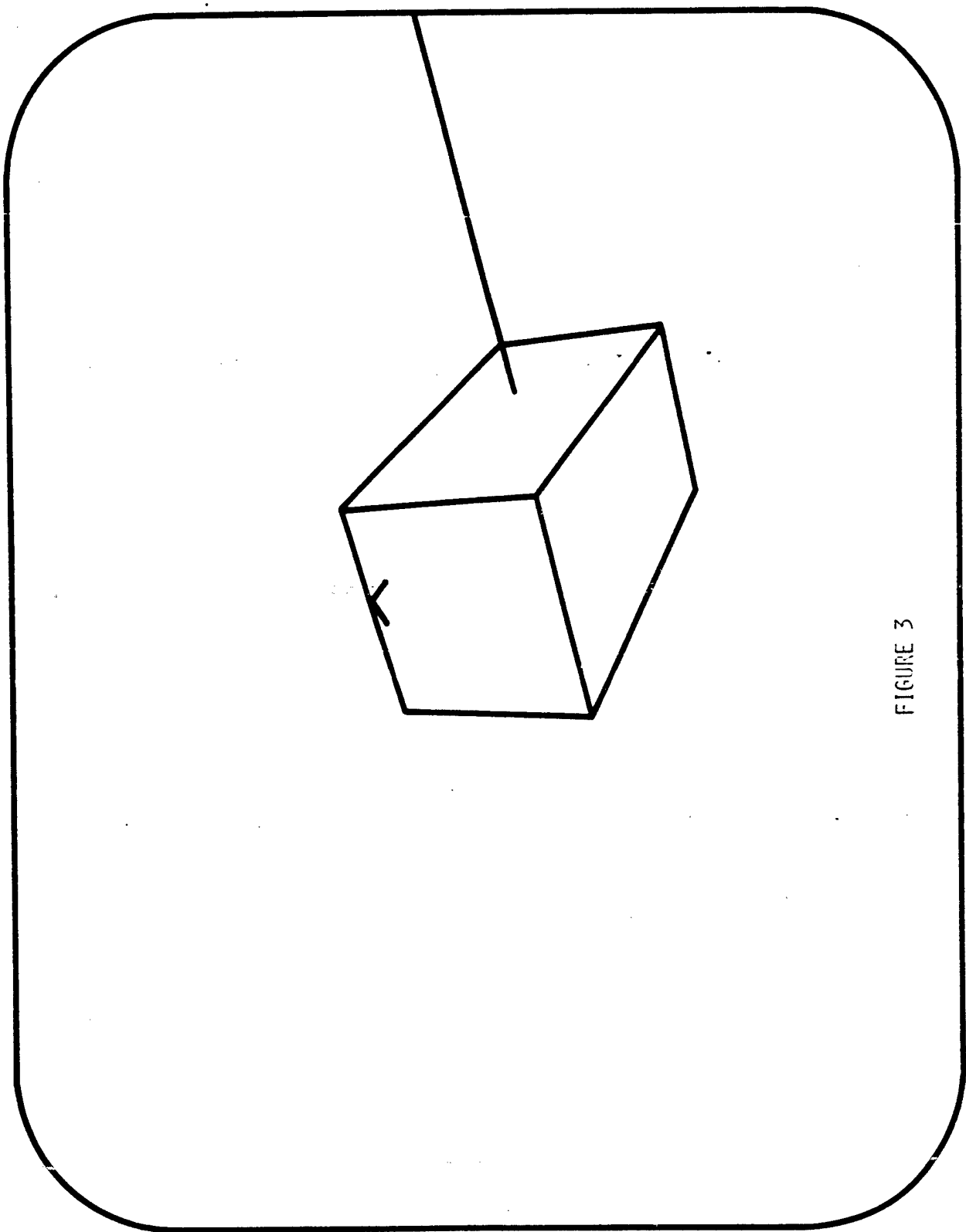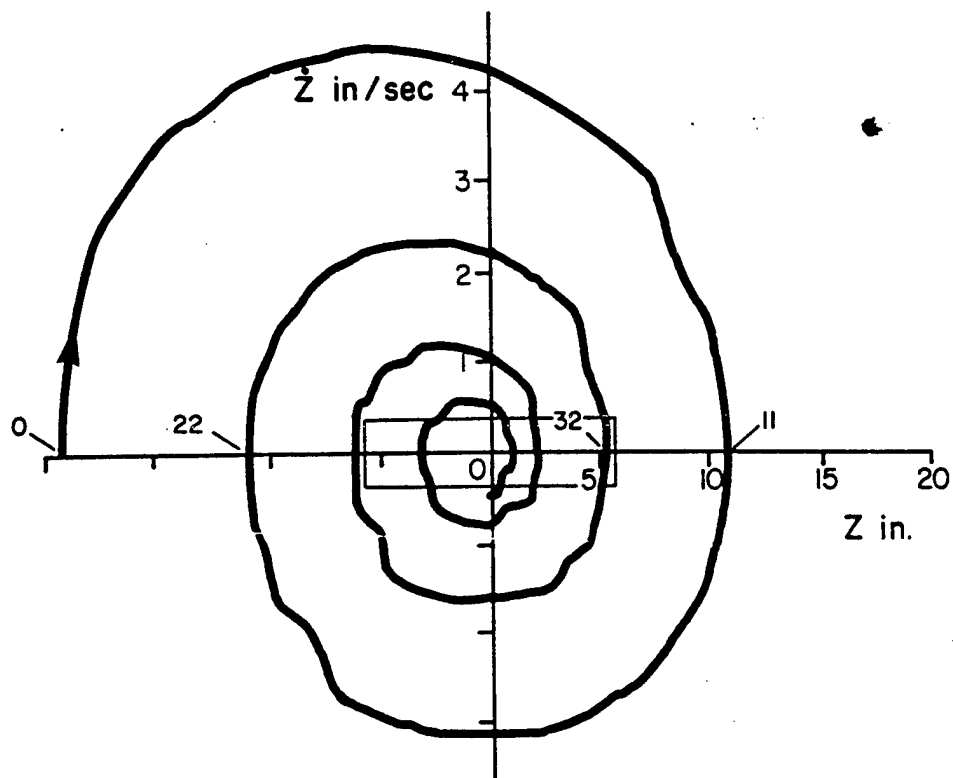
FIGURE 3

PHASE PLANE PLOT
PAYLOAD DISPLACEMENT

PERIOD = 22 SEC., ζ = 0.08

FIGURE 4

632

TASK	PERIOD	ζ	UPDATE INTERVAL	INITIAL DEFLECTION	NUMBER OF SUBJECTS	NUMBER OF FINAL RUNS
	SEC		MS	FT		
1	51	.019	50	2.67	4	48
2	27	.018	50	2.67	4	48
3	51	.019	2000	2.67	4	48
4	27	.018	2000	2.67	4	48
C	22	.080	50	1.60	2	20
D	11	.146	50	1.60	2	20
E	22	.080	2000	1.60	2	20
F	11	.146	2000	1.60	2	20

FIGURE 5

FLAT SPRING

RIGID ARM
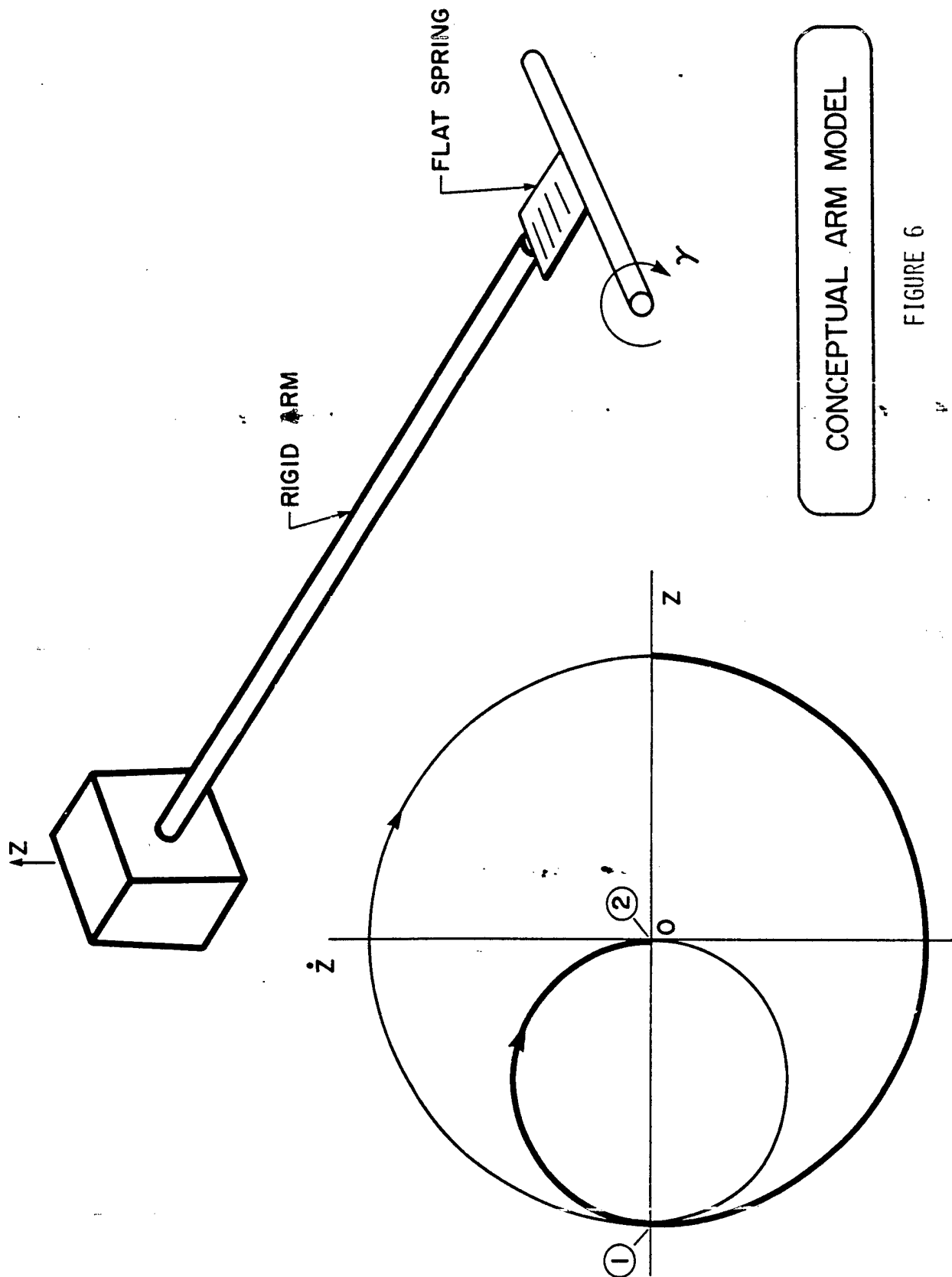
CONCEPTUAL ARM MODEL

FIGURE 6

634
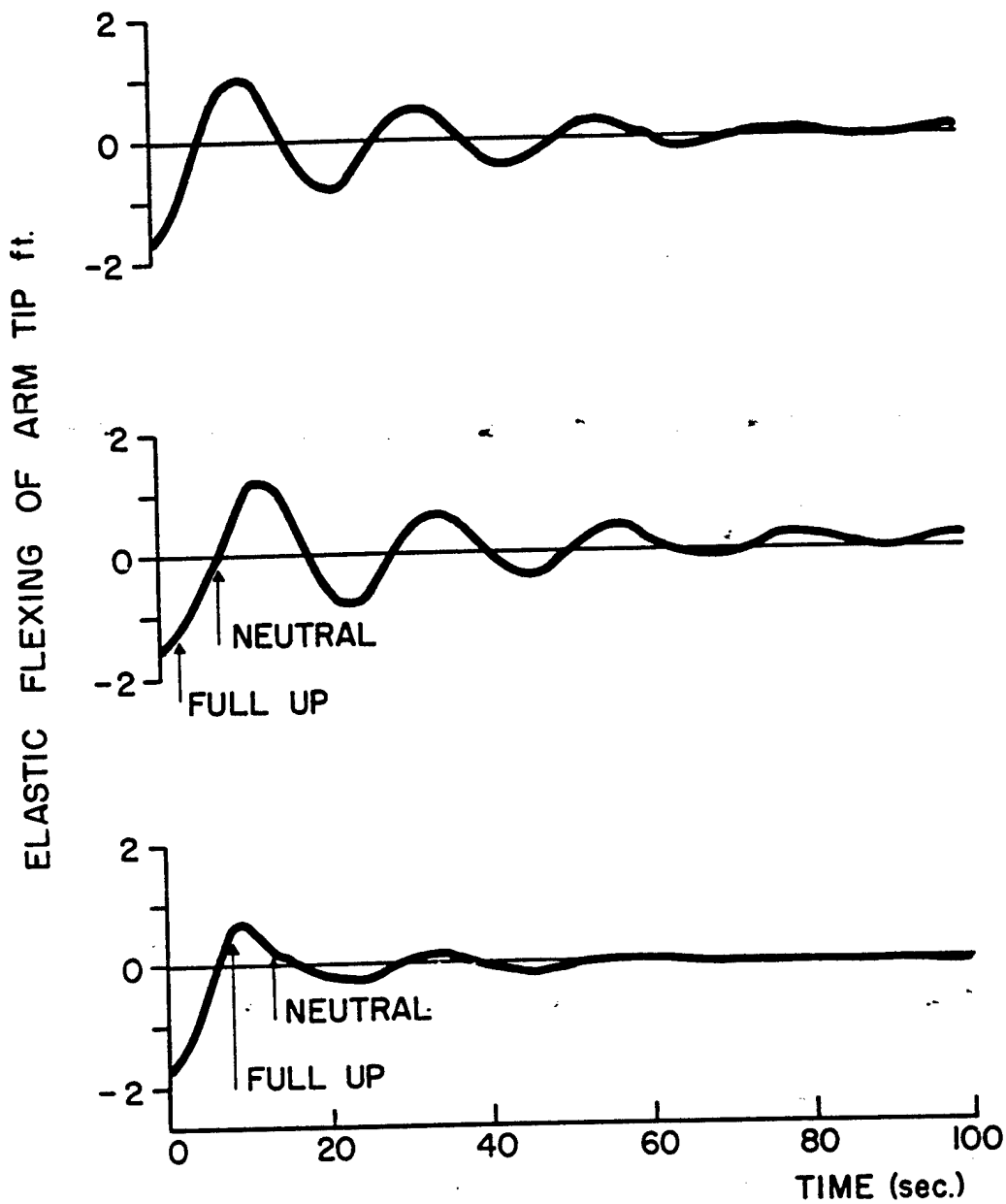
CONTROL EFFECT ON FLEXING OF ARM
PERIOD = 22 SEC., ζ = .08
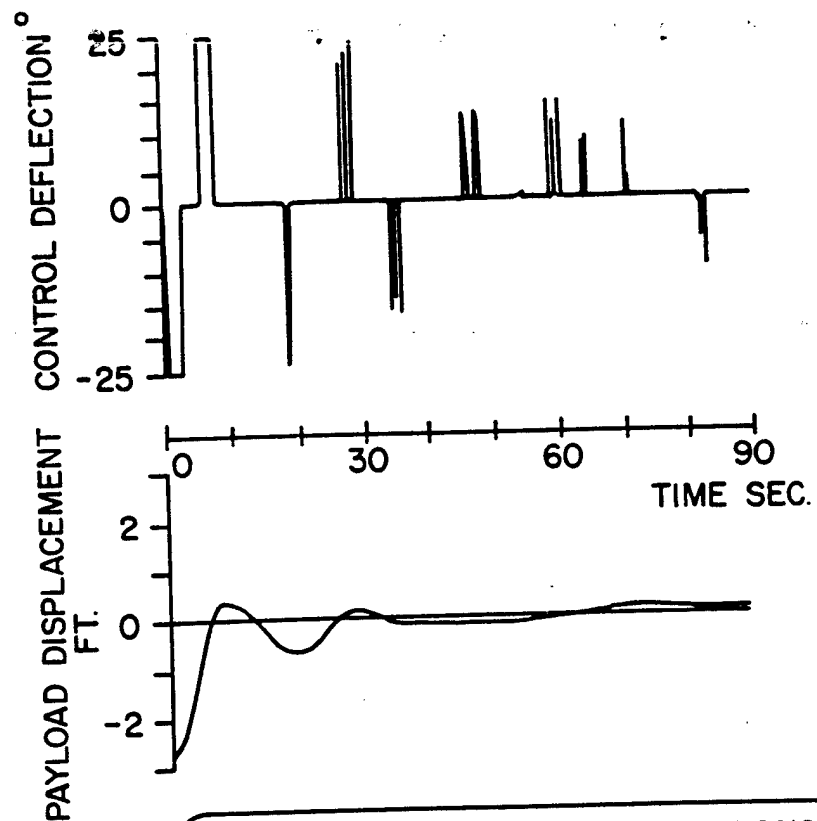
FIGURE 7
635

TYPICAL HUMAN CONTROL RESPONSE

PERIOD = 27 SEC., ζ = .018

UPDATE INTERVAL = 50 ms

FIGURE 8
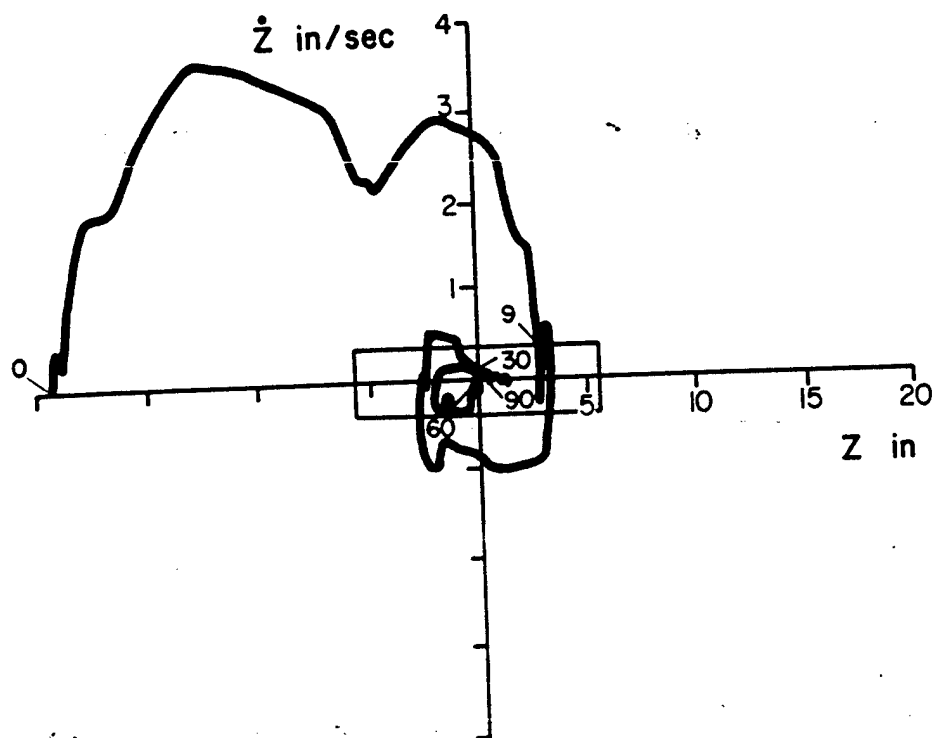
PHASE PLANE PLOT
PAYLOAD DISPLACEMENT
UNDER HUMAN CONTROL

PERIOD = 22 SEC., ζ = 0.08
DISPLAY UPDATE INTERVAL = 50 ms

FIGURE 9
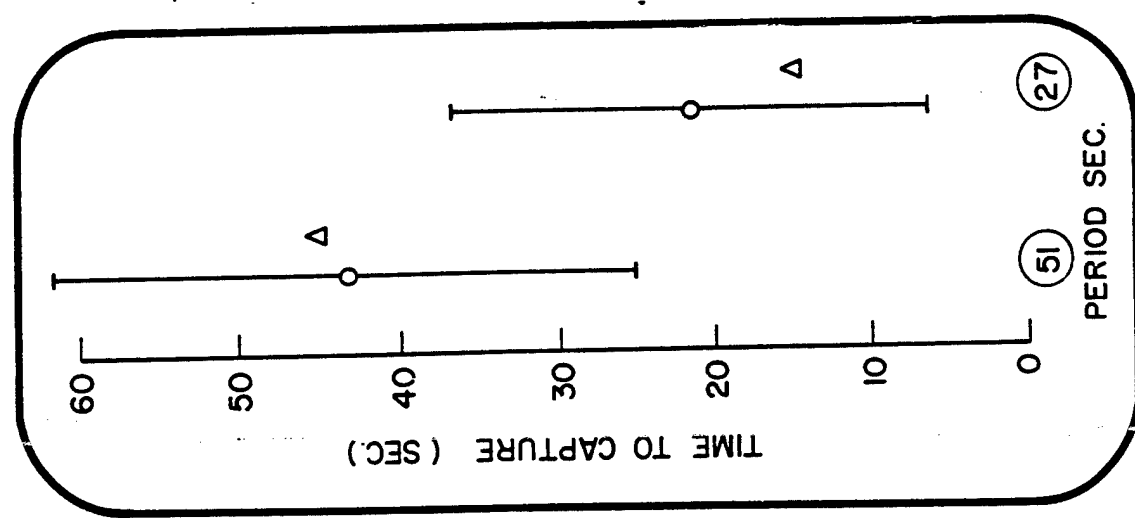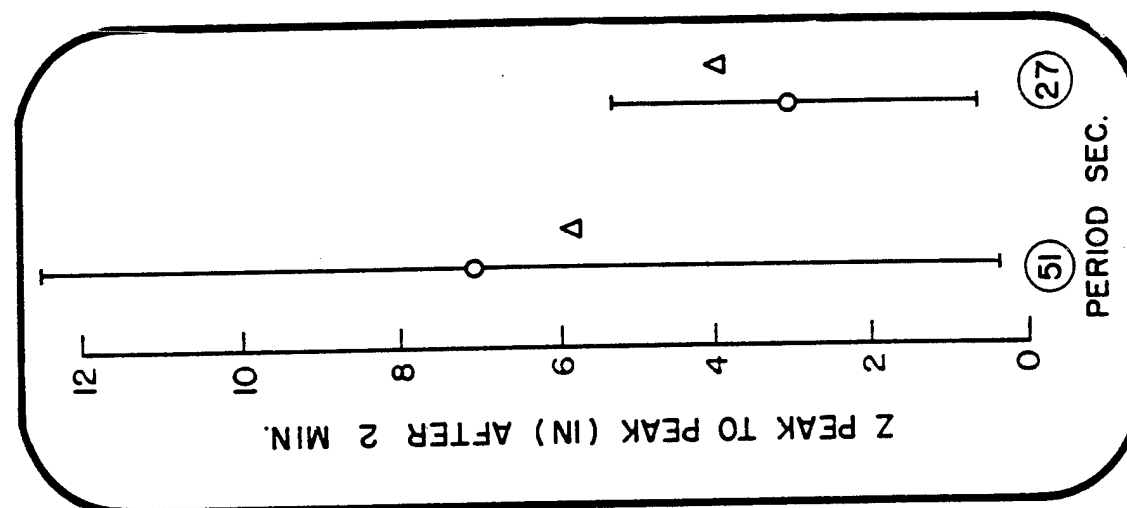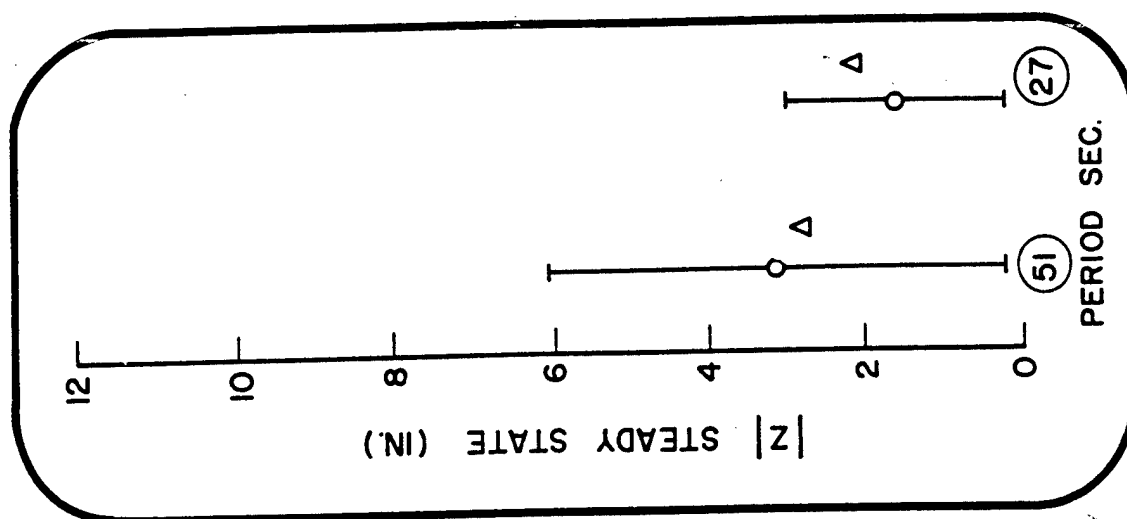
UPDATE INTERVAL 50 ms ○ ; 2000 ms △
40 REPLICATES

FIGURE 10

MODELING A MANIPULATION TASK OF VARIABLE DIFFICULTY

John W. Hill
Stephen J. Matthews

Stanford Research Institute

SUMMARY

In this paper we describe a manipulation experiment of variable difficulty carried out with an Ames manipulator, Rancho manipulator, and the unencumbered human hand. The difficulty of the task is changed not by varying the precision in the usual manner but by varying the number of degrees of freedom (or constraints) of a fitting operation. The goal of this work is to model human performance with real-world tasks.

The preliminary model developed to describe the experimental results requires that the tasks be broken down into consecutive phases or therbligs similar to the units used in industrial time and motion analyses. This model has several advantages over the information-theory model (Fitts' law) proposed in reference 1. For example, the index of difficulty for nonprecise tasks is zero. In Fitts' approach, the index of difficulty for such tasks remains large, and his original model cannot be easily extended to predict the manipulator results from the hand results as can the consecutive-phases model. We also develop an explanation for the failure of Fitts' law in high-precision tasks where the task time increases abruptly as the precision exceeds a certain limit.

INTRODUCTION

Previous experiments have examined manipulation tasks such as placing a peg in a hole where the difficulty was controlled by the precision of fit (references 1 through 6). In this study, we describe a manipulation task where the difficulty is controlled by varying the degrees of freedom; the translational and rotational degrees of freedom of the task are constrained one by one, and the real-time trajectories are recorded and analyzed. The constraints will be measured as degrees of constraint (DOC) after the system introduced in reference 7. As the number of degrees of freedom are reduced, the DOCs increase from 0 to 6. This approach allows us to extend the results of the previous laboratory studies to real-world tasks which seldom fit the positioning and peg-in-hole tasks often used.

639

Fitts has shown that the completion time for a number of different tasks is proportional to the task difficulty expressed in bits,

$$\text{movement time} = a + b \ (\text{index of difficulty}). \qquad (1)$$

This relation is commonly referred to as Fitts' law. Neither intercept a nor slope b are the same, however, for a complex task, such as placing a peg in a hole, or for a simple task, such as touching the inside of a rectangular bar with a pencil point. These constants also change by a large amount (10 to 1) with different manipulators.

The usefulness of Fitts' law in describing actual manipulation data is limited to a moderate range of difficulties, between 5 and 10 bits. When difficulties are less than 5 bits, time is required for the trajectory and does not go to 0 with zero difficulty. An offset, proposed in reference 3, assumes that the subject is aiming for the far side of the target rather than at the center. Another failure is with very precise tasks having difficulties greater than 10 bits; here, time increases disproportionately as the difficulty is increased. After a point, such tasks take so long that they effectively cannot be done.

Another problem with Fitts' law is in calculating the index of difficulty (I_d) of the task. For example, consider Task A in figure 1. The difficulty in touching the inside of a rectangle of height H and width W, from distance d, with a pointed tool is (reference 1)

$$I_d = \log_2 \left(\frac{2d}{W} \right) . \qquad (2)$$

The question is to determine how the difficulty changes as the height of the rectangle is decreased (Task B in figure 1). If movements on the two axes are independent, the difficulties could be summed on the two axes. In Task B, this leads to the solution,

$$I_d = \log_2 \left(\frac{2d}{W} \right) + \log_2 \left(\frac{0}{H} \right) . \qquad (3)$$

The 0 in the numerator of the second term is the distance on the vertical axis corresponding to d on the horizontal axis of the task. The second term
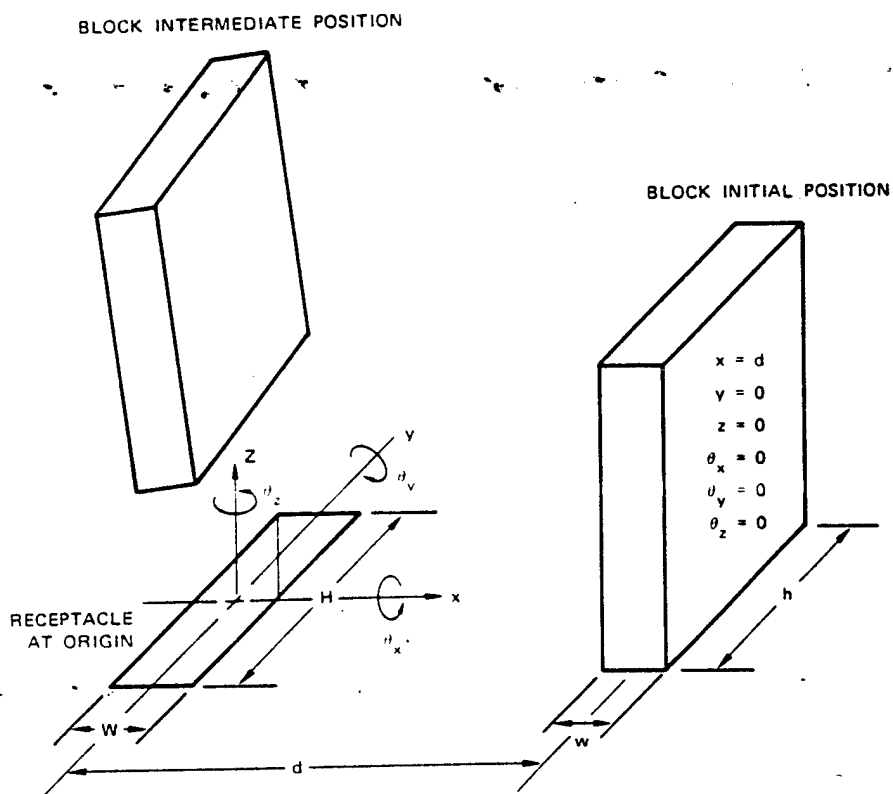
TASK A

TASK B
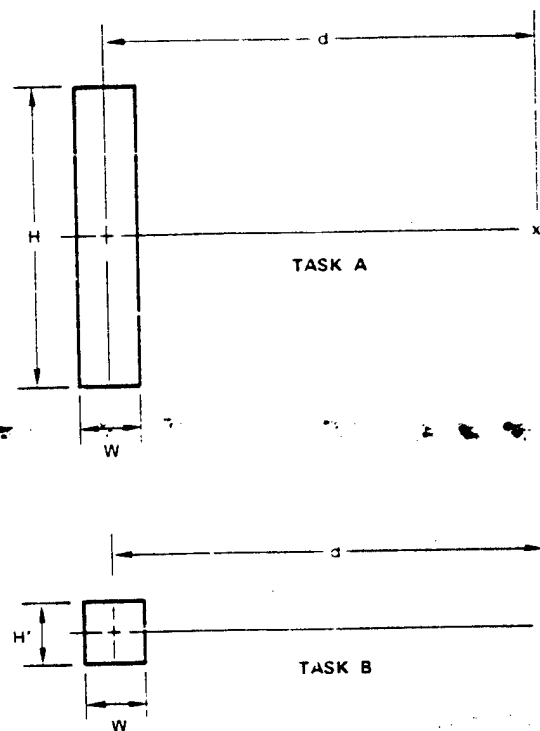
SA-4055-17

FIGURE 1   TWO SIMPLIFIED TASKS

evaluates to minus infinity, and it is impossible to assign a physical meaning to this result.
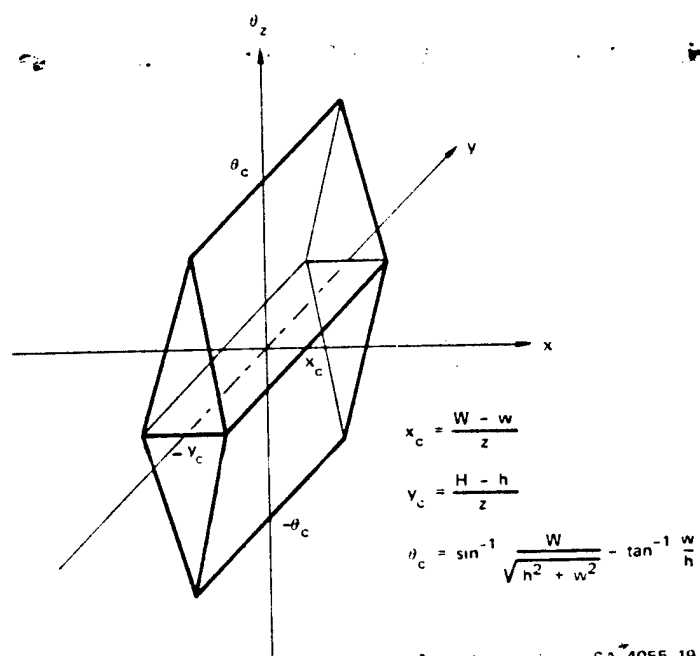
This example is just a simple case showing the difficulties that arise when we try to apply Fitts' approach to fitting real objects together. If the tool in the above example were not a point but a rectangular bar (figure 2), the task would be even more difficult to quantize. To enter the hole, not only must the tolerances on the x- and y-axes be within the tolerances (W-w) and (H-h), but the rotational orientation around the z-axis must be within certain limits. These limits are described by the three-dimensional volume illustrated in figure 3. Outside these limits, the block will not enter.

Furthermore, if the block is to descend into the hole, tolerances on the two additional angles (θ_x and θ_y defined in figure 2) must also be within certain limits. If the receptacle or the manipulator have adequate compliance, the object need only be inserted into the hole; the full insertion will be no more difficult than the entry. If, however, the receptacle and manipulator are rigid, the θ_x and θ_y tolerances will increase the difficulty of the insertion task.

641

BLOCK INTERMEDIATE POSITION

BLOCK INITIAL POSITION

$x = d$
$y = 0$
$z = 0$
$\theta_x = 0$
$\theta_y = 0$
$\theta_z = 0$

RECEPTACLE
AT ORIGIN

SA-4055-18

FIGURE 2   REALISTIC TASK TO BE ANALYZED

The equations shown in the figure:

$$x_c = \frac{W - w}{z}$$

$$y_c = \frac{H - h}{z}$$

$$\theta_c = \sin^{-1}\frac{W}{\sqrt{h^2 + w^2}} - \tan^{-1}\frac{w}{h}$$

SA-4055-19

FIGURE 3   ENTRANCE VOLUME

The parallelopiped describes the coordinates of the base of a rectangular block permitting entrance into a rectangular hole.

We know intuitively that, even when the tolerances are the same, inserting a bar into a hole will be more difficult than inserting a pencil point, but it is not easy to extend the formulation used in reference 1 to such a realistic case. In figure 2, only motion along the x-axis contributes a finite difficulty; alignments on the other four axes require no motion and all evaluate to minus infinity. We could begin immediately to speculate about different means for measuring the difficulty of such real-life tasks; however, we have decided to conduct a practical experiment to obtain a data base to test such hypotheses. The experiment requires the fitting of a tool into a receptacle where the DOCs of the task are increased one by one.

MULTIPLE DEGREES OF CONSTRAINT EXPERIMENT

Our experiment was performed with a multiple-DOC task board. The task consisted of moving a previously grasped tool to a given receptacle and inserting it into the receptacle. Tool trajectories were recorded on magnetic tapes as a function of time, using the minicomputer-based data-acquisition system described in reference 8. The variables of interest were generated by off-line computer analysis of these data tapes.

Apparatus

The multiple-DOC task board is shown in figure 4. Initially, a tool was held over the liftoff switch so that the switch was depressed until the experimenter signaled "go." The tool was then moved to the specified receptacle on the left portion of the task board and was inserted. The matching of receptacles and tools for the six tasks is illustrated in figure 5. In the 0-DOC and 1-DOC tasks, a microswitch signaled the completion of the task by lighting a lamp. In the other tasks, a linear potentiometer measured progress into the hole and triggered the lamp after a certain distance (38.1 mm) was reached.

Based on the dimensions of the tools and receptacles, the tolerances for each of the six placement tasks (0-DOC to 5-DOC) are listed in table 1. Tolerances are the total translational or rotational motion on each axis, as indicated by the dimension (W-w) in figure 2 or twice the critical distances in figure 3. In table 2, the total distances moved are those traversed by the end point of the manipulator, not the end point of the tool. When the Rancho arm was used, the initial angles (θ_{xi} and θ_{zi} in figure 4) were -20° and 0°, respectively; for the Ames arm, they were 10° and -30°. These angles were chosen for convenience in holding the tools over the liftoff switch.
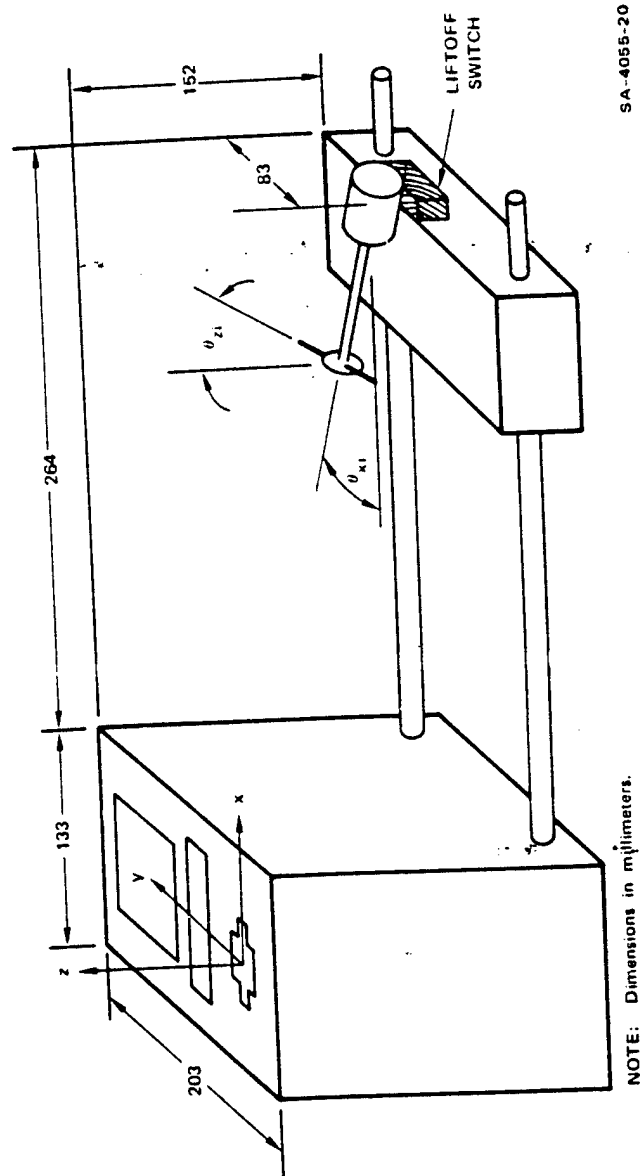
NOTE: Dimensions in millimeters.

FIGURE 4   6 DOC TASK BOARD

SA-4055-20

645

0-DOC TASK

1-DOC TASK

2-DOC TASK

3-DOC TASK

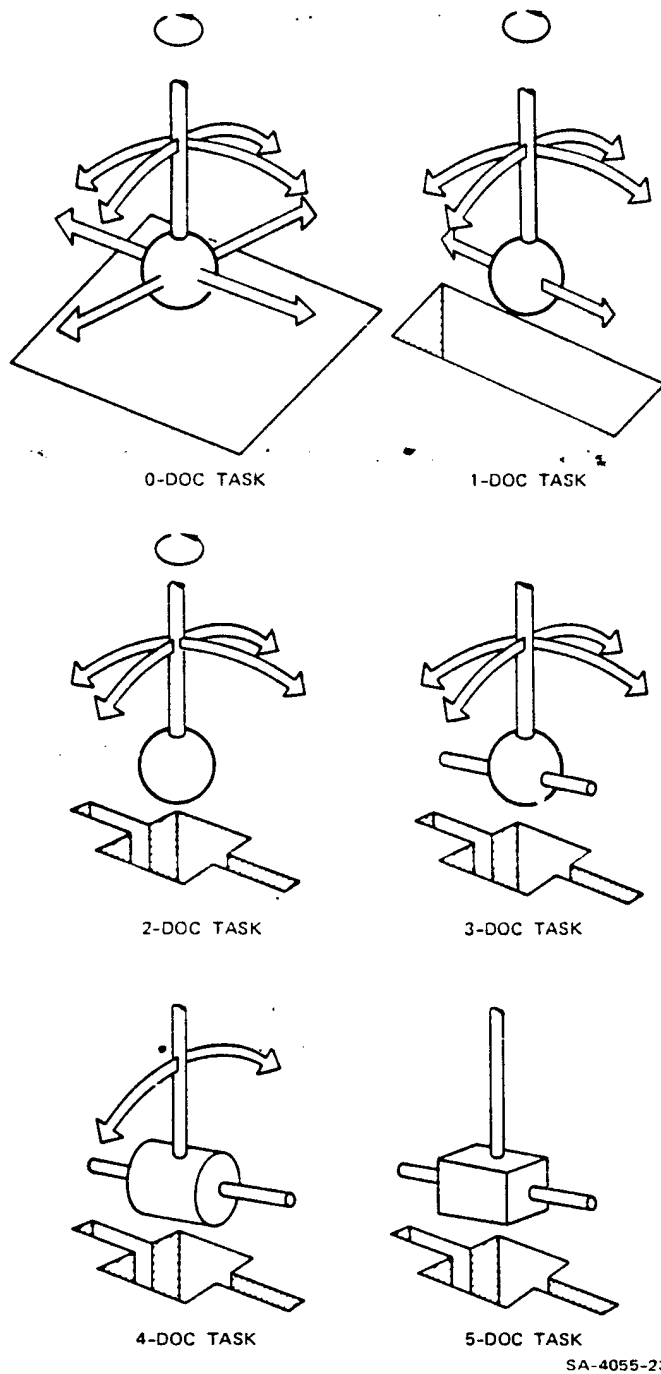4-DOC TASK

5-DOC TASK

SA-4055-23

FIGURE 5   FITTING TOOLS INTO SPECIAL HOLE
Arrows indicate free angular alignments.

646

Table 1

TOLERANCES OF THE MULTIPLE
DEGREES OF CONSTRAINT TASK BOARD

Task	ΔX (mm)	ΔY (mm)	$\Delta\theta_x$ (degrees)	$\Delta\theta_y$ (degrees)	$\Delta\theta_z$ (degrees)
0-DOC	71.4	76.2	180	180	360
1-DOC	76.2	3.2	76	150	360
2-DOC	3.2	3.2	42	47	360
3-DOC	2.4	3.2	42	47	3.0
4-DOC	2.4	3.2	48	18	3.0
5-DOC	3.2	3.2	18	20	3.0

Table 2

BASIC DISTANCES AND ANGLES MOVED IN THE DOC TASKS
(distances in mm; angles in degrees)

Task	X	Y	Z	Straight-Line Distance	θ_x	θ_y	θ_z
0-DOC	322	48	-373	495	0	90	0
1-DOC	319	-10	-373	490	0	90	0
2-DOC	319	-59	-373	494	0	90	0
3-DOC	319	-59	-373	494	0	90	0
4-DOC	319	-59	-373	494	0	90	0
5-DOC	319	-59	-373	494	0	90	0

Procedure

The three manipulating means used in this experiment were the Rancho arm, Ames arm, and an unencumbered hand. Two male subjects participated in all three parts of the experiment.

Each experimental run consisted of one trial with each of the DOC tasks. Runs were repeated ten times for each subject. The order of presentation of

the different DOC tasks was randomized for each run. Several practice trials were performed prior to data collection. The subject and experimenter exchanged roles to provide rest periods. Continuous operation was limited to less than 30 minutes without rest.

Contour pads fitted to the manipulator jaws (on both the Rancho and Ames arms) ensured proper tool location in the jaws. The pads also served to eliminate any possible slipping of the tools in the jaws during final positioning.

Results

The mean times for the two subjects during ten repetitions of the tasks are plotted in figure 6. The results obtained from the two manipulators and the hand indicate a general increase in the task time as the constraints of the task are increased. The task times with the human hand and Ames manipulator were particularly linear with the number of DOCs; the linear trend accounted for at least 95 percent of the variance, and the nonlinear components were not statistically significant. The task times with the Rancho manipulator was not linear, and the cubic or S-shaped component was statistically significant $[F(1,90) = 5.25, p < 0.05]$. Completion times for the tasks varied greatly among the manipulators; the Ames was approximately four times slower and the Rancho was approximately 20 times slower than the hand.

The normalized task times plotted in figure 7 were obtained by dividing each time by the time for the 0-DOC task. The resulting spread between the three manipulators indicates that this simple scaling does not account for the differences observed; in particular, as the rotational constraints of the 3-DOC and 4-DOC tasks are added, a disproportionately longer time is required compared to the simpler tasks. In other words, the DOC measure does not produce an index of difficulty that satisfactorily unifies the human and manipulation results.

BREAKDOWN INTO SUBTASKS

We wish to determine whether there is a natural breakdown of the manipulation tasks into the therbligs traditionally used in time and motion studies (reference 8). The therbligs for this task are transport loaded and position. The first therblig describes the motion between the liftoff switch and a close proximity to the hold, and the second indicates the alignment or orientation of the tool to the receptacle.
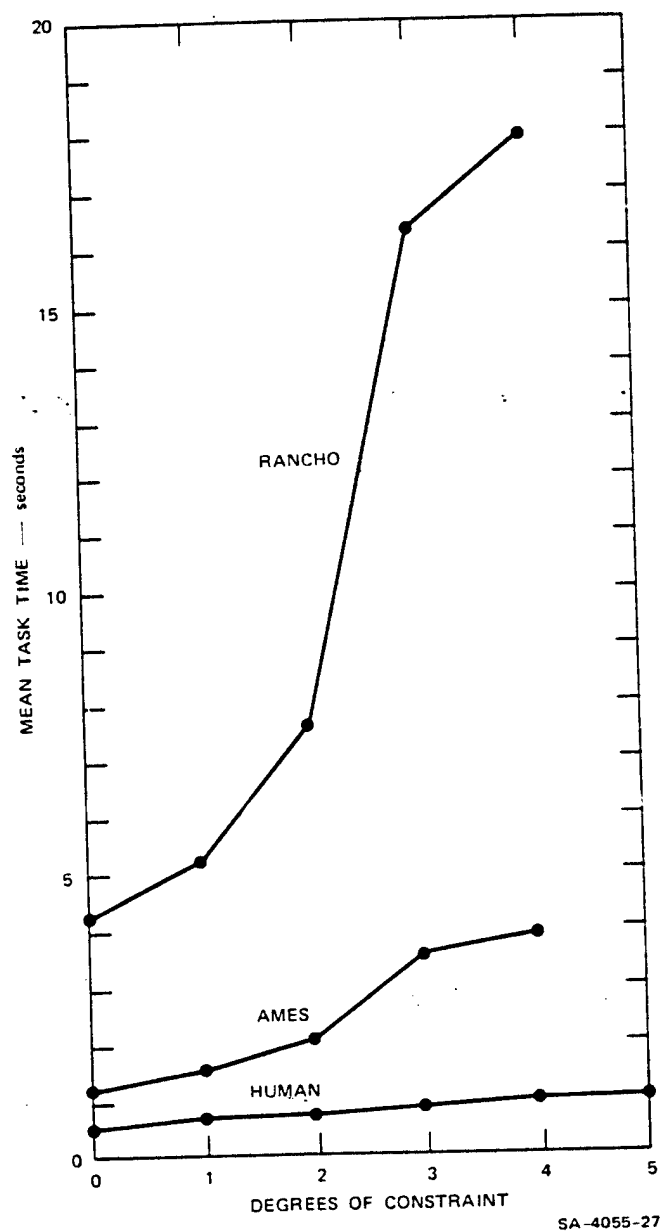
MEAN TASK TIME — seconds

RANCHO

AMES

HUMAN

DEGREES OF CONSTRAINT

SA-4055-27

FIGURE 6   COMPARISON OF THE THREE MANIPULATORS

$$T_D/T_O$$
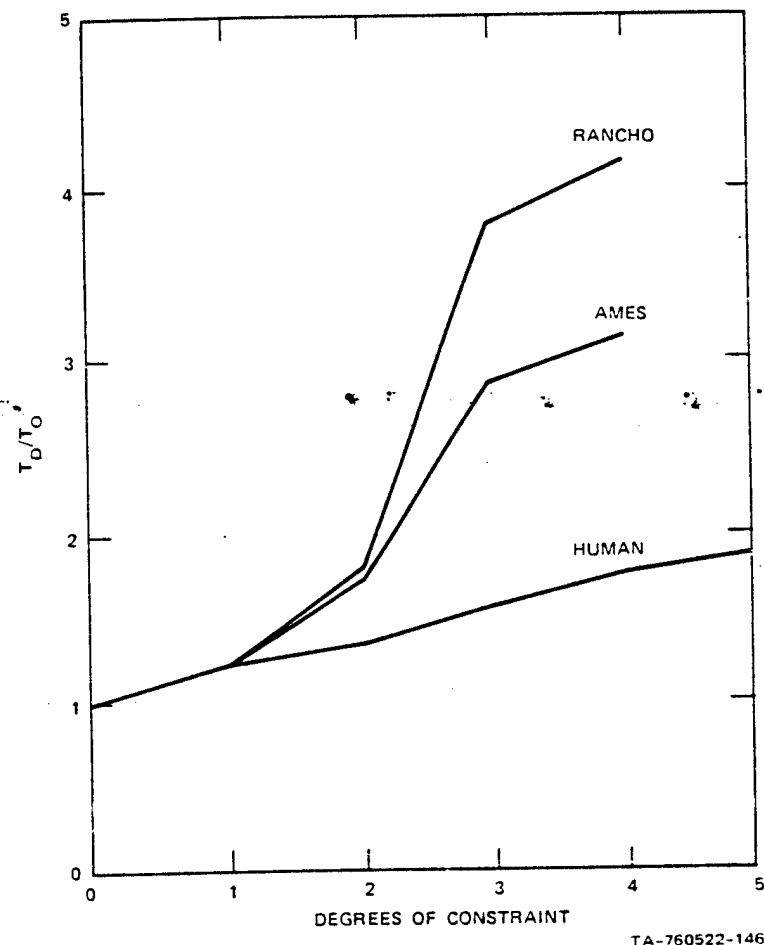
DEGREES OF CONSTRAINT

TA-760522-146

FIGURE 7   NORMALIZED RESULTS OF THE
THREE MANIPULATORS

Using the digitized trajectories recorded on magnetic tape, the x, y, and z coordinates of the tool at the first contact with the hole were obtained. By comparing x, y, and z coordinates measured at previous points on the trajectory, the times to a given distance from the contact position were obtained. Times from two intermediate distances from the receptacle to the end of the trajectory are plotted in figure 8 for the three manipulators of the experiment.

Time for the first part of the trajectories from liftoff to a distance of 25 or 50 mm from the hole (corresponding to the transport therblig) is relatively independent of the DOCs. This is evidenced by the nearly

650
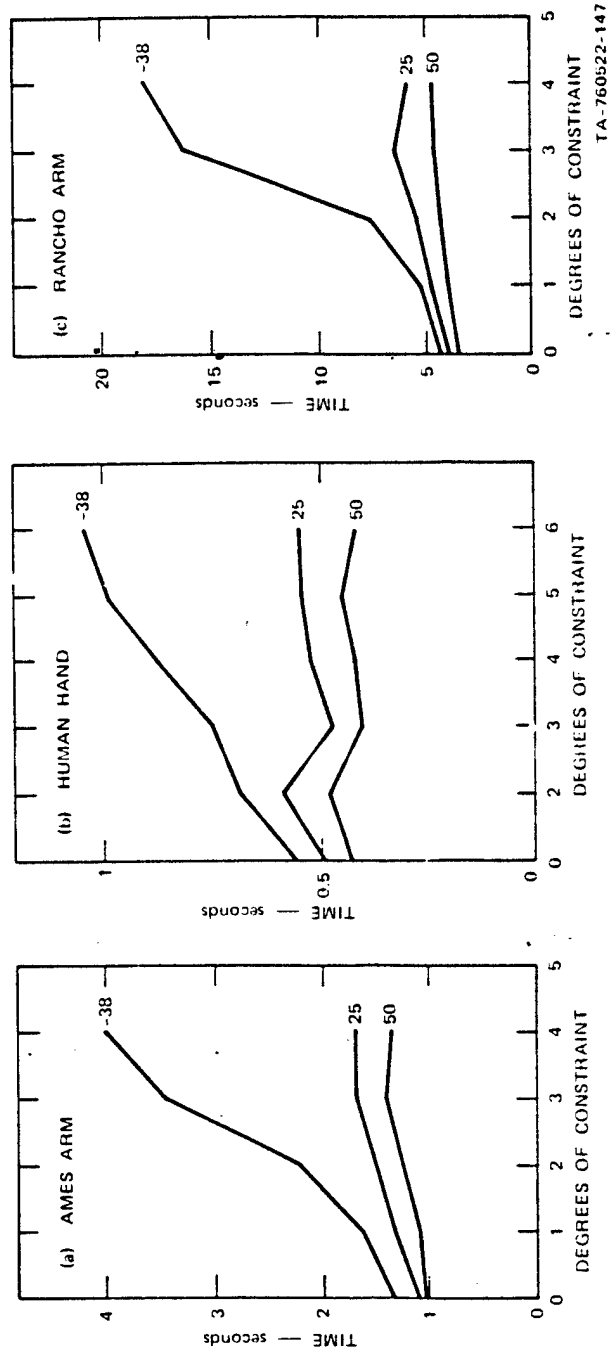
FIGURE 8   COMPARISON OF THE THREE DIFFERENT MANIPULATIONS. Task times are shown as a function of distance in millimeters from first contact with the hole: -38 mm corresponds to full insertion, 0 to first contact, and 25 mm and 50 mm to the first time those distances were obtained from the contact point.

651

horizontal lines in the lower part of the figure. For the human hand, these results are horizontal; however, for the two manipulators, there is a slight upward slope which indicates a more conservative strategy as the DOCs increase. These results are similar to those described in references 2 and 5 where the transport times were found to be independent of task difficulty. The second phase of the trajectories, between 25 to 50 mm of the receptacle to full insertion (corresponding to the position therblig), depends greatly on the DOCs.

There are several major differences between the unencumbered-hand and manipulator therbligs. For both manipulators, the transport time (time to 25 mm of first contact) increases approximately 10 percent per DOC instead of remaining constant as it does for the human hand. The position therblig for the manipulators is more time-consuming than that for the hand.

MODELING EXPERIMENTAL RESULTS

The DOC measure does not take into account the tolerance of the task. In a task with a fixed number of DOCs, time is proportional to an index of difficulty. In many tasks, this takes the logarithmic form previously given in equation 2. The problem here is to extend the approach originated in reference 1 and subsequently used by others to realistic tasks with constraints on several axes.

Using an information-theory approach, Fitts proposed that the decrease in uncertainty of the task be calculated by subtracting the uncertainty of the final position from the uncertainty of the initial position. For these uncertainties, he used

$$H_{final} = \log_2 \Delta x \qquad (4)$$

$$H_{initial} = \log_2 2x, \qquad (5)$$

and the resulting difficulty index is

$$I_d = H_{initial} - H_{final} = \log_2 \left(\frac{2x}{\Delta x}\right) . \qquad (6)$$

In this case, the initial uncertainty of the object is twice the reach distance, and Fitts' formulation inherently assumes that the initial position of the object is uniformly distributed between +x and -x from the final position. This approach is incorrect because. in most cases, the initial position is well known. For example, if the object is held in a fixture, all its coordinates and angles are known exactly and its initial uncertainty is zero.

A new approach to the analysis of the task combines the results of the time and motion studies and the information-theory approach. We assume that the motion is composed of two parts, an initial but uncertain open-loop trajectory between the initial and final positions, followed by a corrective-positioning motion. This approach is supported by references 2 and 6 in which it was observed that, in the first part of the manipulation tasks, the trajectory time from initial to final position is independent of task difficulty. All variability in the task time with difficulty must occur in the final positioning phase.

To determine the feasibility of this two-phase model, we conducted a simple experiment, using the same unencumbered hand and the Ames and Rancho manipulators. The standard deviation of the open-loop positioning error was measured by having two subjects make 20 moves each from a fixed initial point toward a final point separated by 500 mm. They were instructed to shut their eyes as the move began and not to open them until after the move was finished. For the translation measurements, a string tensioner was attached to the tip of a pencil-like tool to measure the position after each move. Angular motions were measured by having the subjects turn a potentiometer fitted with a pointer and graduated scale between two fixed angles. The results of these experiments are listed in table 3.

Table 3

STANDARD DEVIATIONS FOR SINGLE-AXIS MOVES

Manipulator	σ_x (mm)	σ_θ (degrees)
Human hand	7.5	5.4
Ames	28	3.7
Rancho	29	4.7

In this two-phase approach, the initial uncertainty is zero because the position of the tool is known. The intermediate uncertainty of the normal distribution of errors after the open-loop move is

$$H_{intermediate} = \log_2 \sqrt{2\pi e} \; \sigma \doteq 2.05 + \log_2 \sigma, \qquad (7)$$

where σ is the standard deviation of the normal distribution. We assume that the shape of the distribution after final positioning is the clipped distribution shown in figure 9. Its uncertainty is approximately that of a rectangular distribution if Δx is small,

$$H_{final} \doteq \log_2 \Delta_x \qquad \Delta_x < 2\sigma, \qquad (8)$$

and is approximately that of the original distribution if Δx is large,

$$H_{final} \doteq H_{initial} \quad , \qquad \Delta x > 5\sigma. \qquad (9)$$

The reduction in uncertainty ($H_{initial} - H_{final}$) for intermediate values of Δx obtained by numerical integration are plotted in figure 10.

If the translational and rotational errors given in table 3, which are measured on only one axis, are assumed valid for all axes, then the uncertainty after the open-loop move can be calculated. Using the dimensional tolerances for the task board in table 1, the standard deviations in table 3, and the formulation in figure 10, we obtained the indices of difficulty for each manipulator, as plotted in figure 11.

One of the surprising results of this analysis is that there is very little difference in difficulty between the 2-, 3-, and 4-DOC tasks. The orientational constraints introduced by these tasks are much less than the open-loop positioning ability of the subjects. The round-bottomed tools employed in the first four tasks may also have less than the calculated difficulty because of their self-guiding behavior when inserted into the hole.
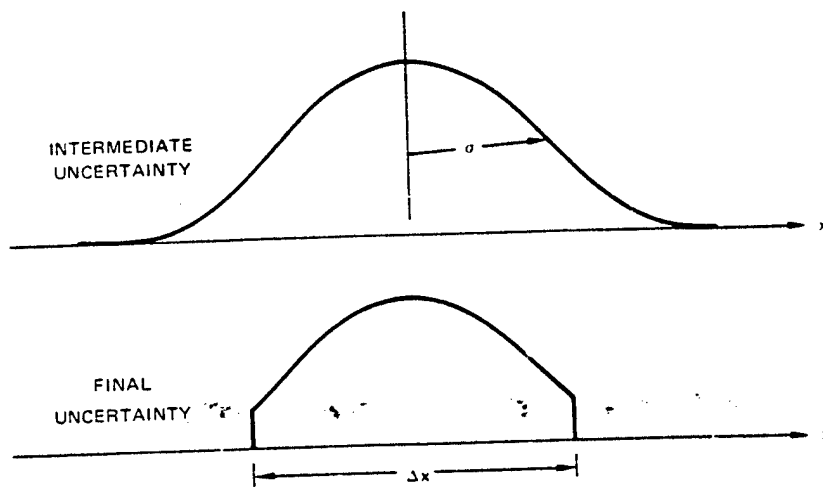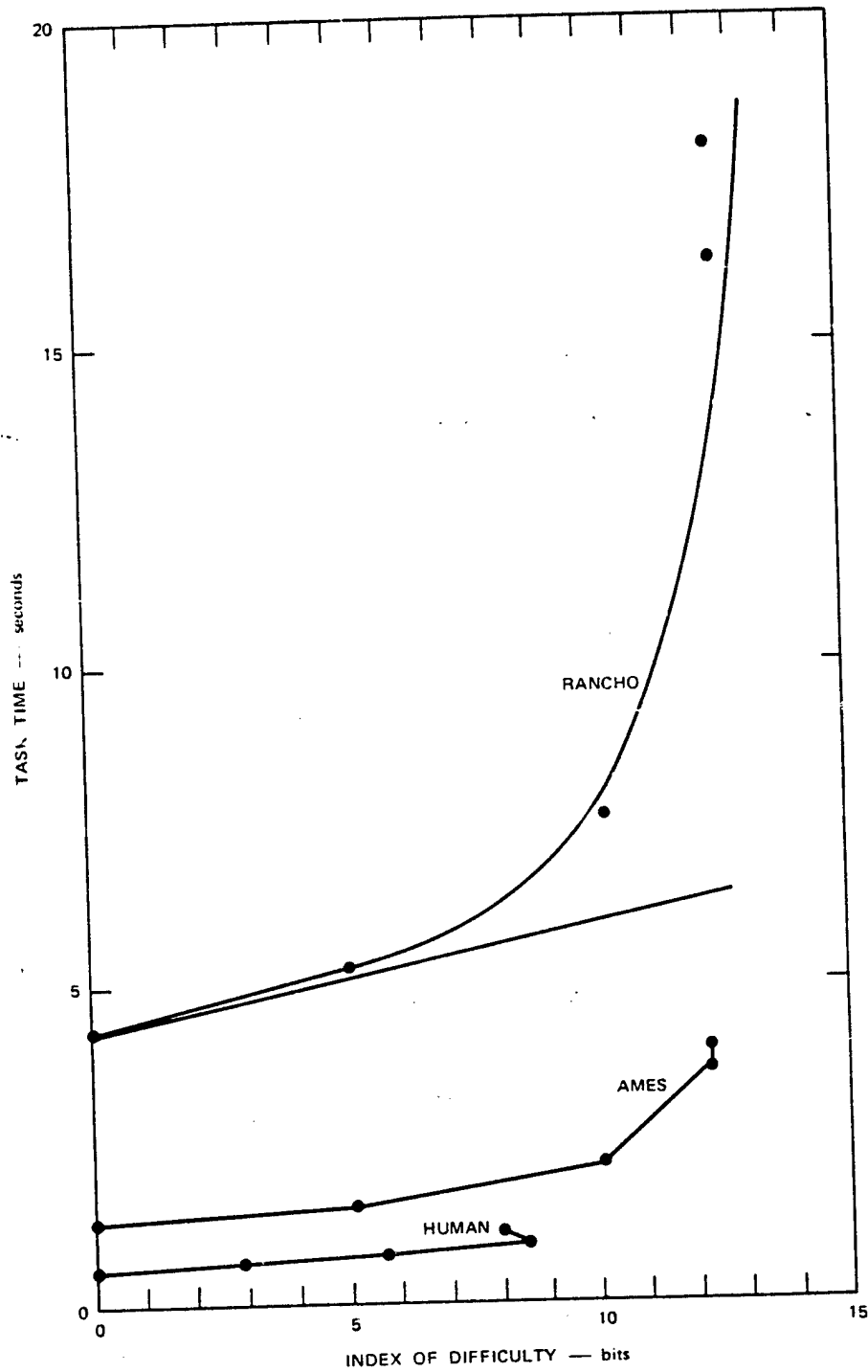
FIGURE 9 CLIPPING OF NORMAL DISTRIBUTION
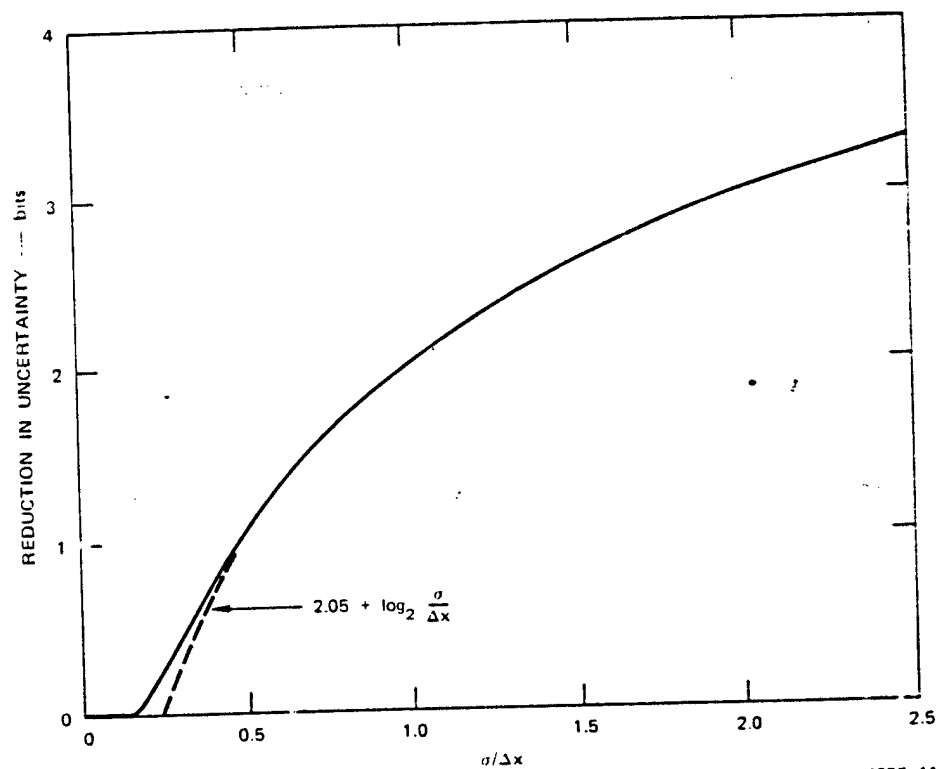
FIGURE 10 NUMERICAL INTEGRATION RESULTS

655

FIGURE 11   EXPERIMENTAL RESULTS WITH NEW INDEX OF DIFFICULTY

SA-4055-37

656

One advantage of the task model is that the 0-DOC task has practically zero difficulty because the receptacle is large enough for the tool to be inserted with the eyes closed. In contrast, Fitts' formulation [equation (2)] yields a task difficulty of 3.8 bits. The time we measure for the 0-DOC task is then the time for the transport therblig which is assumed constant for all the tasks. A second advantage of the model is that the difference between manipulators may be largely resolved into different time factors. When the task times of each manipulator are normalized by dividing by the 0-DOC task time, the curves superimpose as shown in figure 12. This attributes one portion of the time to the task--the part that changes with the index of difficulty--and a second that multiplies the first--a constant for each manipulator.

The disadvantage of the model is that the results are not linear at high difficulties. This may be caused by underestimating the difficulties on the 3-, 4-, and 5-DOC tasks. For example, the 4- and 5-DOC tasks have the same difficulty, but the 5-DOC task always takes a longer time. A possible explanation for the upward curving lines of figure 11 may be the limited accuracy of even the smallest moves. The small moves of the Rancho manipulator approach a limit cycle with a standard deviation of 3 mm and 1.2°. In this limit cycling, there is only a fixed probability of entering the receptacle within the correct positions and angles for each move. With each added bit of difficulty, the probability of being in the correct positions and angles reduces by one-half. For example, consider the probability of being inside the parallelopiped in figure 3 when the uncertainty of the tool is described as a sphere around it. With each added bit of difficulty (or uncertainty), the probability of entering the parallelopiped decreases by half and the number of moves or time to enter doubles. The curve in figure 11 describes this phenomenon for the Rancho results. The mathematical form of the curve is

$$T = 0.20 \ I_d + 2^{(I_d - 10.0)} , \tag{10}$$

where the first term denotes a slope (the portion where Fitts' law applies), and the second term represents the limited positioning ability of the arm.

A real-time explanation of this behavior is plotted in figure 13. The first phase of motion is the open-loop move toward the target. The accuracy at the termination of this phase is roughly that required by the 0-DOC task. This is followed by an exponential decrease in position error, the exponential-alignment phase in which the accuracy increases by a factor of 2 every 0.20 seconds (for the Rancho arm, see equation 10). The 1- and 2-DOC tasks fall in this region for the Rancho. After the uncertainty has been reduced by

657
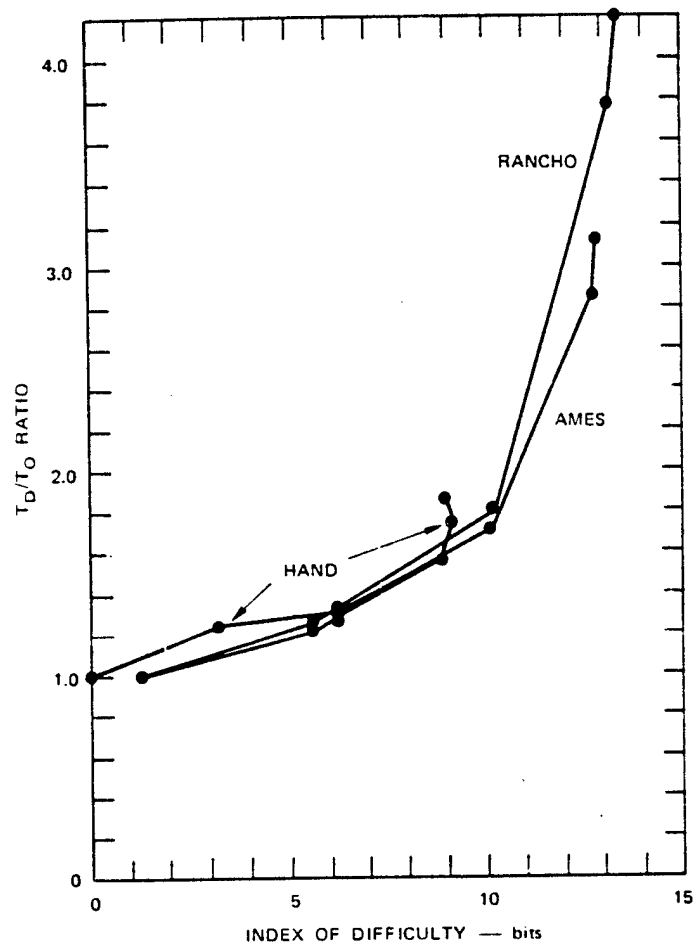
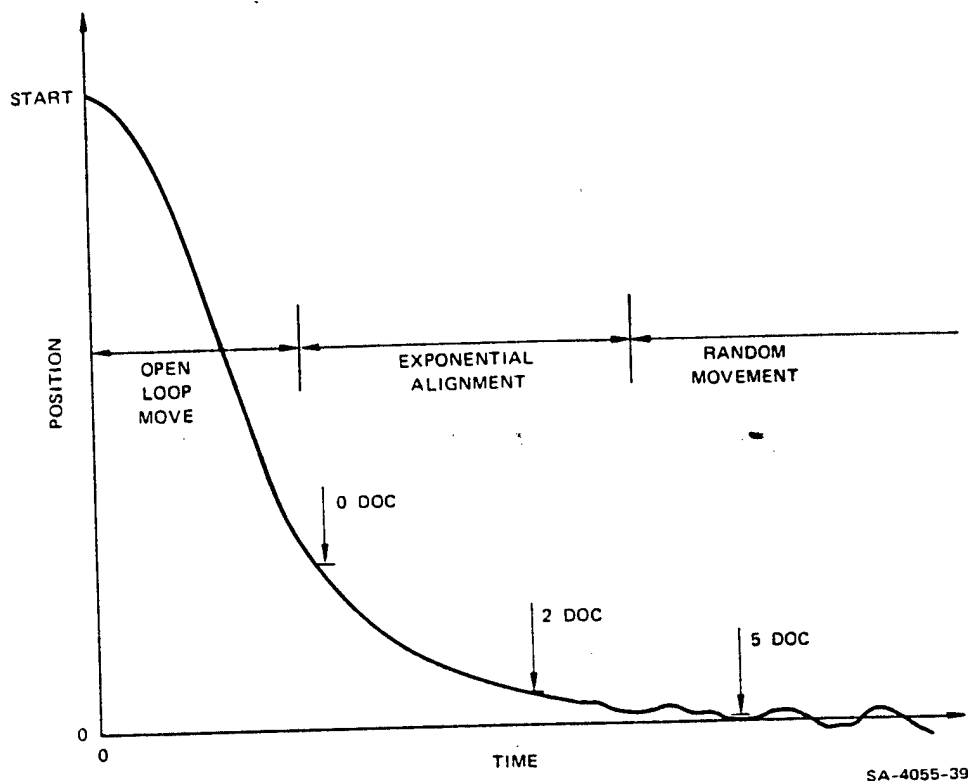FIGURE 12   NORMALIZED EXPERIMENTAL RESULTS

SA-4055-38

FIGURE 13   PHASES OF MANIPULATION ACTIVITY

10.0 bits (again for the Rancho arm), the random-movement phase begins, corresponding to the 4- and 5-DOC tasks. During this last phase, there is only a fixed probability of completing the task per unit time.

REFERENCES

1.   Fitts, P. M.:   The Information Capacity of the Human Motor System in Controlling Amplitude of Movement. J. Exp. Psychol., Vol. 47, (1954) pp. 381-391.

2.   Annett, J.; Golby, C. W.; and Kay, H.:   The Measurement of Elements in an Assembly Task - The Information Output of the Human Motor System. Q. J. Exp. Psychol., Vol. 10 (1958), pp. 1-11.

3.   Welford, A. T.:   The Measurement of Sensory Motor Performance: Survey and Reappraisal of Twelve Years Progress. Ergonomics, Vol. 3, 1960, pp. 189-230.

659

4. Fitts, P. M.; and Peterson, J. R.: Information Capacity of Discrete Motor Responses. _J. Exp. Psychol._, Vol. 67, No. 2, 1964, pp. 103-111.

5. McGovern, D. E.: Factors Affecting Control Allocation for Augmented Remote Manipulation. Ph.D. dissertation, Stanford University, Stanford, California. November 1954.

6. McGovern, D. E.: Comparison of Two Manipulators Using a Standard Task of Varying Difficulty. Paper 74-WA/Bio-4, presented at the Annual Meeting of the ASME, New York, November 1974.

7. Mundel, M. E.; and Lazarus, I. P.: Predetermined Time Standards in the Army Ordinance Corps. J. Ind. Eng., November 1954, pp. 13-20.

8. Hill, J. W.: McGovern, D. E; and Sword, A. J: Study To Design and Develop Remote Manipulator System. Final Report, NAS 2-7507, Stanford Research Institute, Menlo Park, California, May 1974.

9. Niebel, B. W.: _Motion and Time Study_. 5th edition, R. D. Irwin, Inc., Homewood, Illinois, 1972.

NOTES

A COMPARISON OF MASTER-SLAVE AND RATE CONTROL IN THE
PRESENCE OF A TRANSMISSION TIME DELAY

By Gregory P. Starr

Stanford University

SUMMARY

When a time delay is inserted into the feedback loop of a manual control
system, in this case a remote manipulator system, certain characteristics of
the control system may change in importance. We conducted a one-dimensional
discrete tracking experiment to simulate manipulation and compared three
controllers. Performance using a joystick rate controller degraded less with
increasing time delay than that using the same joystick as a position con-
troller. The results indicate the need for a comparison using a manipulator
system.

INTRODUCTION

When a time delay is inserted into the feedback loop of a man-manipula-
tor system as occurs when the manipulator is very distant, the normal tem-
poral organization of stimulus and response is disrupted. This disruption
has been shown (references 1, 2, 3) to be very detrimental to performance.

Ferrell (reference 1) found that his subjects used one of two strategies
to deal with the time delay. The first strategy that of moving slowly, re-
quires the operator to keep track of his movements for one full delay period
in the past to predict the position of the manipulator. This is very diffi-
cult to do with delays of several seconds and operator frustration often
occurs.

The second strategy, which was called "move-and-wait" by Ferrell, was
spontaneously adopted by seven of his eight subjects. In the move-and-wait
strategy, moves are made open-loop, i.e. without visual feedback, then the
control is held stationary until the manipulator "catches up." Ferrell's
results were obtained using a simple two degree-of-freedom manipulator. In
subsequent experiments Blackmer (reference 2) and Black (reference 3) both
observed the move-and-wait strategy being followed using a six degree-of-
freedom manipulator. Although all of these studies were carried out using
master-slave position control, Ferrell believed that the move-and-wait stra-
tegy would be used with rate control as well.

Both Blackmer and Black noted a problem in using the move-and-wait

strategy: the subjects often had trouble holding the master control motion-
less while waiting for the manipulator to respond. Undesired "drifting" of
the control made it more difficult for them to use the move-and-wait strategy.

A master controller with an operator-actuated brake which would provide
positive locking of the master, a completely counterbalanced master, or a
spring-centered rate controller are controllers which would make it easier for
the operator to hold the manipulator motionless while waiting for feedback.

Tracking and Manipulation

Some aspects of manipulation resemble pursuit or compensatory tracking.
Many of the motions involved in manipulation have as their goal the minimi-
zation of a visually perceived error, which is the definition of tracking.

The manipulation task differs from continuous tracking tasks in that
all of its elements except the manipulator are usually motionless, and there-
fore the manipulation task is a self-paced task. In contrast, a continuous
tracking task requires the operator to follow a constantly moving target.
Discrete tracking provides a situation similar to manipulation, since the
target is not moving during the positioning task.

Perhaps the main difference between tracking and manipulation is the
number of degrees of freedom of the controlled element. Tracking usually
involves one or occasionally two degrees of freedom, while manipulation
ordinarily requires control of six.

Taking into account the differences between tracking and manipulation,
we feel that a sufficient degree of commonality exists between them to justify
the use of a discrete tracking task as a preliminary experiment in an inves-
tigation of position versus rate control of a manipulator.

EXPERIMENT

We performed a discrete tracking experiment with controller, target
distance, and time delay as the variables. The task was to bring a dot,
the controlled element, into the target as quickly as possible. The target
was represented by two vertical lines. The dot and target were both dis-
played on a closed circuit TV monitor. The target lines were three cm. in
length and were 0.88 cm. apart. The dot was one mm. in diameter. The task
was completed when the subject kept the dot continuously inside the target
for two seconds. After the completion of the task, the target then appeared
at a new location on the TV monitor, signifying the beginning of another task.

Generation of the target lines and dot as well as data acquisition was
done by an IBM 1800 digital computer. The computer program which generated
the display used a sampling rate of 120 samples per second to insure a
flicker-free image. The positions of the dot and target were recorded on
magnetic tape during each sample frame. This provided an accurate recording
of the subjects' performance. These tapes were the data base from which all

of the results were extracted.

The dynamics of the dot were either zeroth order, corresponding to position control, or first order, corresponding to rate control. In neither case were effects such as inertia, damping, or static friction simulated.

Controllers

Three controllers were used in the experiment; two for position control and one for rate control. The controllers were a joystick for position control, the same joystick for rate control, and a linear displacement position control. These controllers were respectively analogous to the following manipulator controllers: master-slave control, spring-centered rate control, and counterbalanced or lockable master-slave control.

The joystick position controller was originally a three-axis joystick. We physically locked out the yaw axis and used the roll axis as the command axis. Position of the dot was proportional to stick deflection about this axis. The joystick was spring centered but there was no detent at the center position. The torque/deflection ratio of the joystick was 1.16 newton-meter/radian.

The second position controller is termed a linear displacement control. The position of the dot was proportional to the position of the controller handle along its axis. The primary reason this controller was included for study is that no force need be applied to the controller to hold it stationary at an arbitrary position. This was true of the joystick. A subject could remove his hand from the linear position control and the control would remain in position. We felt that this would prove advantageous when using the move-and-wait strategy.

The third controller was the same joystick previously described, but this time used as a rate controller. The characteristics of the joystick were the same as before, with one important difference, which was the use of a centering detent. This provided a positive indication of the center position. The velocity of the dot was proportional to the deflection from center of the joystick. When the operator removed his hand from the joystick, the center detent insured that the velocity of the dot would be zero.

Controller Gains

One characteristic of the tracking system which has not been mentioned is the controller gain, i.e. the amount of dot motion produced by a unit displacement of each controller. The gain for both position controllers was dictated partially by hardware considerations. The optimal rate gain was determined experimentally.

Gibbs (reference 4) investigated the choice of gain in a position control tracking system using thumb, hand, and forearm controlled joysticks. He found that best results were obtained with the lowest controller gains. We decided on the basis of Gibbs' findings to set the position controller

gains as low as possible. Considering the range of motion of the joystick position controller and the necessary range of motion of the dot, the resulting gain for this controller was 33.8 cm. of dot motion per radian of stick rotation. In terms of stick tip translation the gain of the joystick was 2.65 cm. of dot motion per one cm. of joystick tip translation. We wished to set the gain of both position controllers at the same value, so dissimilar gains would not be the cause of differences between them. The gain for the linear position control was therefore also set at 2.65 cm. of dot motion per one cm. of handle motion.

We conducted an experiment to determine the optimum gain for our rate controller. Two subjects, both right-handed and with good vision, participated in the experiment. We investigated six rate gains. The gains, expressed as ratios of dot velocity in radians/second at the subject's eye divided by joystick deflection in radians, were 0.20, 0.30, 0.40, 0.50, 0.60, and 0.70 seconds^{-1}. The corresponding maximum dot velocities were 9.85, 14.72, 19.73, 24.66, 29.89, and 34.01 cm/second measured at the display. Data were taken at no delay and with a 1.5 second time delay.

Each subject made one run at each of the twelve conditions of rate gain and time delay. One run consisted of a sequence of 100 tasks. When the subject completed one task, the target jumped to a new position, and the next task was begun. The distance from one target to the next was randomized by using a computer subroutine to generate random numbers. The "seed" number for the subroutine was the same on each run, so the resulting random sequences were identical for all of the runs.

We obtained two performance measures: the sum of completion times for the 100 tasks and the sum of the distances moved by the dot for the 100 tasks. The completion time was defined as the time interval from the beginning of the subject's first move to the time when the dot entered the target for the last time, plus one delay time. This last delay time was added because the task cannot be considered as completed until the operator knows it is completed.

With no time delay, increasing the gain beyond 0.30 seconds^{-1} did not improve performance in terms of completion time or distance moved. With the 1.5 second time delay, the 0.30 seconds^{-1} gain was the best in terms of both measures. Therefore the 0.30 seconds^{-1} gain was selected as the optimum gain for the rate controller.

Method

We used a factorial experimental design. The factors were controller (C), time delay (T), target distance (D), and subjects (S). The controllers were the joystick position control, linear position control, and joystick rate control. The time delays were 0, 0.33, 1.0, and 3.0 seconds. Five target distances were used, 1.766 cm., 5.297 cm., 8.828 cm., 12.359 cm., and 15.890 cm., all distances measured on the screen of the display. Four subjects participated in the experiment, all were right-handed with good vision.

Each subject performed in two sessions, held on separate days. A session consisted of 12 runs, one at every condition of controller and time

delay. One run consisted of the sequential presentation of 50 targets. The course of 50 targets was pseudo-randomized over the five task distances. Constraints on the course were:

1) 10 tasks at each of the 5 distances must be presented

2) Of these 10 tasks, 5 must require dot motion from right to left and 5 from left to right.

These constraints, when combined with the magnitudes of the target distances and the width of the display, ruled out a true randomized course. The width of the display, about 25 cm., prevented certain distances and directions of the tasks from following one another. For example, a left-to-right task of 15.890 cm. could not follow a left-to-right task of 12.359 cm. In all, 4800 individual positioning tasks were completed.

RESULTS

Analysis of Variance

We performed an analysis of variance on the completion times and found all of the main effects (C, D, T, S) to be significant at the .01 level, as were all but one of the interactions. Since the CxDxT interaction was significant, it is not valid to test any of the lower order terms containing the C, D, or T factors against the residual. We will therefore examine the results at each condition of C, D, and T.

Figure 1 shows mean completion time vs. target distance for each controller at each time delay. Breakdown analyses of variance were done at each condition of C, D, and T, and the results are shown in Table 1. As time delay increased, performance with the joystick rate controller degraded less than with the joystick position controller at the 5.297 cm. and 8.828 cm. target distances. At the 12.359 cm. and 15.890 cm. distances the rate control system's maximum attainable velocity of 14.72 cm/second became a limitation, and at these distances the rate controller did not compare as favorably with the joystick position controller. The linear position controller, however, became the most effective controller of the three as time delay increased. These results indicate that the suitability of the controller to the move-and-wait strategy becomes increasingly important as the time delay increases.

Move Analysis

To examine the accuracy of individual moves, as well as to determine if the move-and-wait strategy was being employed by the subjects, we broke down the position vs. time record into periods of moving and waiting. The first step was development of move criteria, i.e. the conditions under which the subject would be considered to be moving. We wanted to distinguish between moves which were separated by at least one delay time and those which were not. The former were called "move-and-wait" moves, since the subject had seen the results of the previous move before making the current move, while
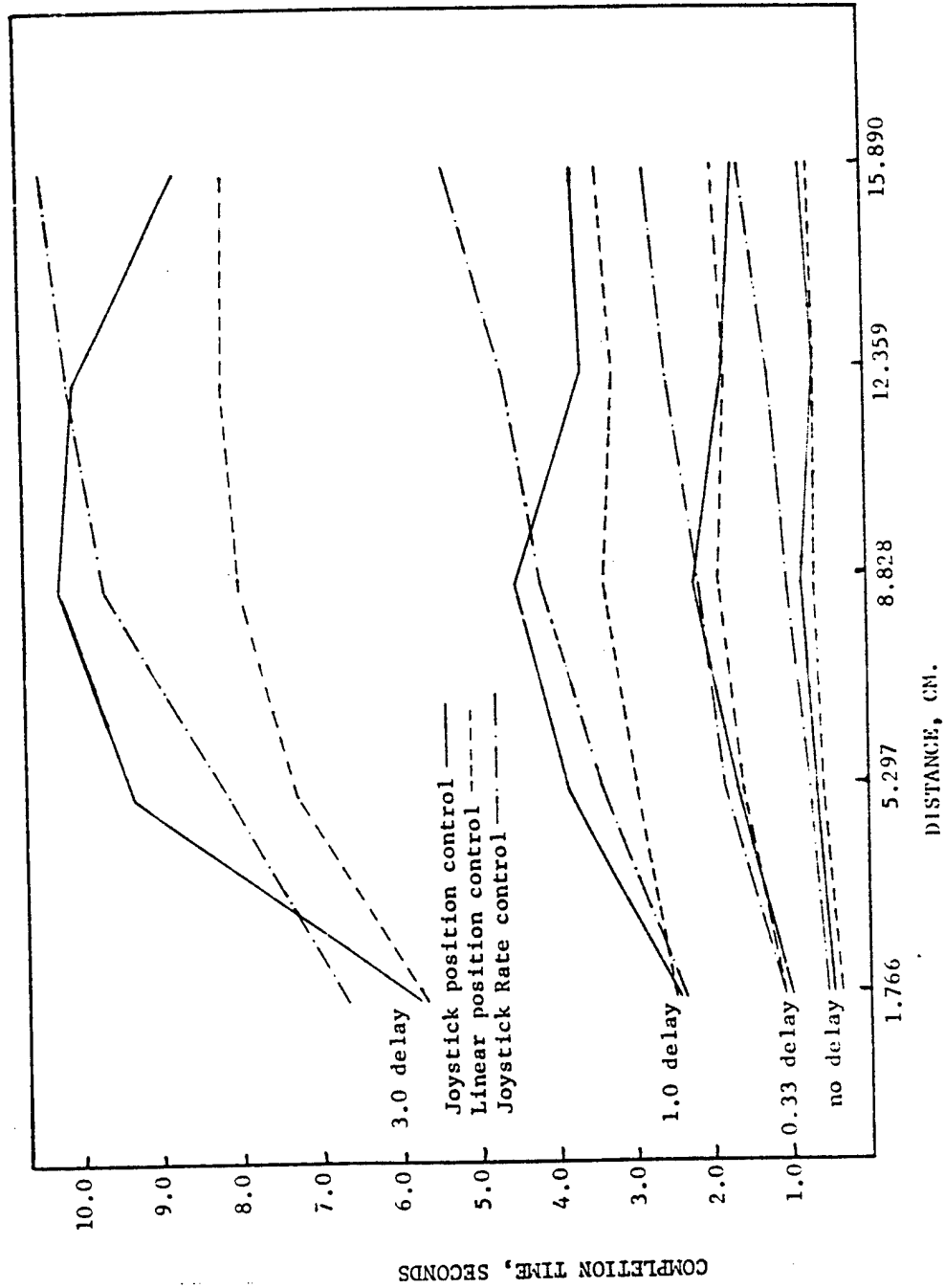
DISTANCE, CM.

Figure 1. Completion time vs. distance at all time delays

P denotes joystick position control
L denotes linear position control
R denotes joystick rate control

Time Delay	Distance	F	sig. level %	Means			Least Significant Difference
				P	L	R	
0.0	1.766	3.96	2.5	0.297	0.283	0.405	L P R
	5.297	4.61	1	0.558	0.497	0.654	L P R
	8.828	17.15	1	0.775	0.591	0.941	L P R
	12.359	125.9	1	0.576	0.594	1.178	P L R
	15.890	139.3	1	0.730	0.635	1.548	L P R
0.33	1.766	.491	-	0.955	1.056	1.023	P R L
	5.297	.786	-	1.683	1.580	1.759	L P R
	8.828	2.40	-	2.203	1.883	2.113	L R P
	12.359	19.42	1	1.768	1.737	2.531	L P R
	15.890	30.75	1	1.601	1.840	2.746	P L R
1.0	1.766	.043	-	2.386	2.439	2.377	R P L
	5.297	5.34	1	3.769	2.912	3.340	L R P
	8.828	6.84	1	4.436	3.255	4.137	L R P
	12.359	15.83	1	3.590	3.115	4.570	L P R
	15.890	20.43	1	3.688	3.352	5.282	L P R
3.0	1.766	2.234	-	5.657	5.603	6.538	L P R
	5.297	5.431	1	9.123	7.132	8.004	L R P
	8.828	6.218	1	10.019	7.798	9.464	L R P
	12.359	5.042	1	9.829	8.032	9.881	L P R
	15.890	6.596	1	8.489	7.972	10.198	L P R

Table 1. Results of breakdown analyses of variance at each condition of distance and time delay.

the latter were designated "non move-and-wait" moves, since the results of the last move had not yet been seen when the current move was initiated. The move criteria in their final form consist of two velocity-time thresholds plus a time criterion and a distance criterion. They were the following (all distances were measured on the display):

(1) Beginning of move: velocity greater than 1.24 cm/second continuously for 0.042 seconds.

(2) End of move: velocity less than 0.52 cm/second continuously for 0.042 seconds.

(3) Moves shorter than 0.172 cm. were disregarded.

(4) If the elapsed time between the end of the previous move and the beginning of the current move were equal to or greater than the delay time, the current move was classified as a "move-and-wait" move; if not, then it was classified as a "non move-and-wait" move.

The normalized task completion time, broken down into periods of time spend executing "move-and-wait" moves, "non move-and-wait" moves, and time spend waiting, is shown in Figure 2. The percentage of time spent waiting increases with time delay, as expected from the move-and wait strategy. The most interesting aspect of Figure 2 is the comparatively large percentage of time spent in the execution of "non move-and-wait" moves with the joystick position control. At the 3.0 second time delay, the time spent executing "non move-and-wait" moves is one-fourth the time spent executing "move-and-wait" moves. This indicates a substantial departure from the pure move-and-wait strategy with the joystick position control. The linear position control exhibits less time spent in "non move-and-wait" moving and the joystick rate controller shows the least time spent executing "non move-and-wait" moves.

It appears that the move-and-wait strategy was adhered to most rigidly by subjects when they were using the joystick rate control, and least when they were using the joystick position control. Greater adherence to the move-and-wait strategy does not necessarily correspond to better performance, but in this experiment they were correlated.

FUTURE RESEARCH

The next step is comparison of position control and rate control in controlling a multi-degree-of-freedom manipulator. The manipulator control situation is obviously much more complex than the one-dimensional task we have considered here. The difficulty of coordinating manipulator joint motions using a rate control system may more than compensate for the ease in holding the manipulator stationary during waiting periods. We are currently comparing master-slave position control and resolved motion rate control (reference 5) using the seven degree-of-freedom Ames manipulator (reference 6).
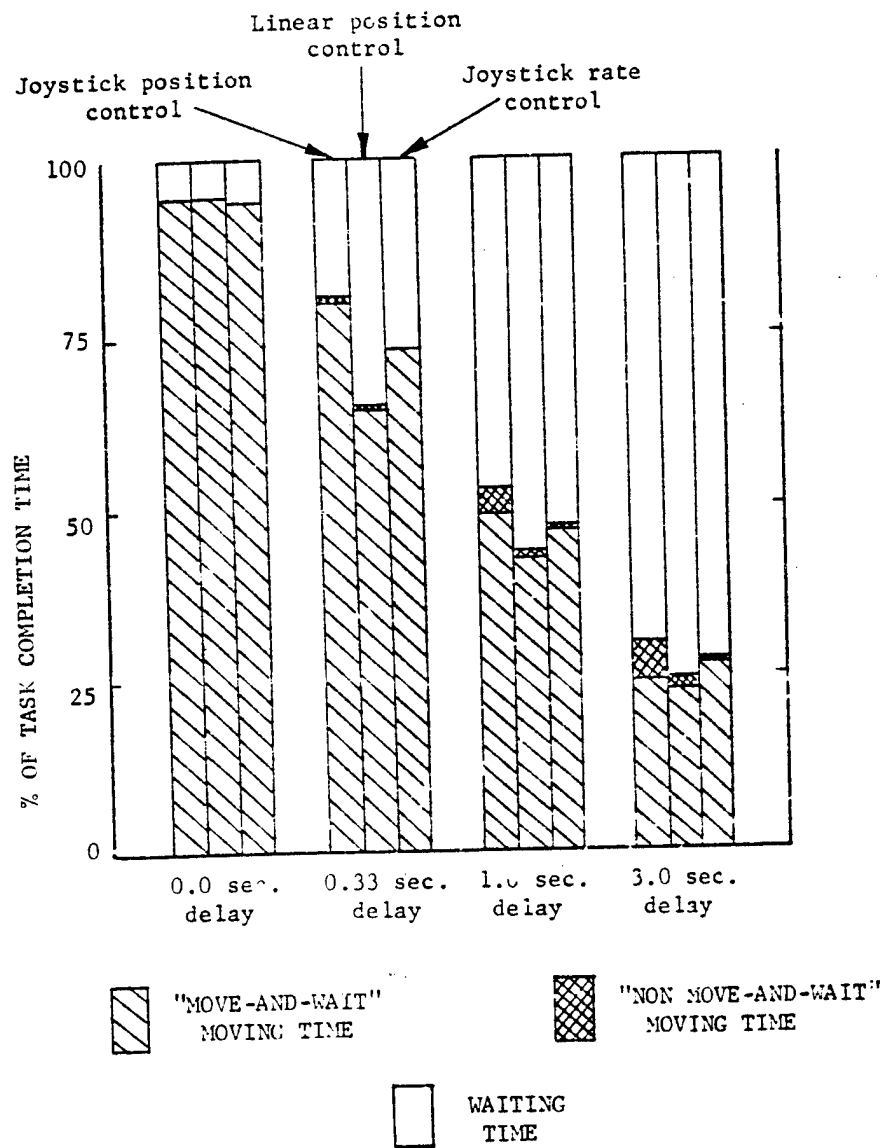
Figure 2. Breakdown of normalized completion
time into periods of moving and waiting.

CONCLUDING REMARKS

In this one-dimensional discrete tracking experiment with a transmission time delay we have shown that the level of performance was correlated with the subjects' adherence to the move-and-wait strategy. Since manipulation bears substantial similarity to discrete tracking, controllers for manipulator systems in which there is a time delay should be chosen with this in mind. The particular characteristic of the controller which determines its suitability is the extent to which human operator input is required to maintain a stationary position of the controlled element, or manipulator. By this criterion, center-off rate controllers and fully counterbalanced (or equivalent system) position controller. are the best choice.

REFERENCES

1. Ferrell, W. R.: Remote Manipulation with Transmission Delay, NASA TN D-2665, 1965.

2. Blackmer, R. H.: Remote Manipulators and Mass Transfer Study, AFAPL-TR-68-75, Wright-Patterson AFB, 1968.

3. Black, J. H., Jr.: Factorial Study of Remote Manipulation with Transmission Time Delay, M.S. Thesis, Mech. Engr. Dept., MIT, 1970.

4. Gibbs, C. B.: Controller Design: Interaction of Controlling Limbs, Time Lags, and Gains, in Positional and Velocity Systems, Ergonomics, v. 5, n.2, 385-402, 1962.

5. Whitney, D. E.: Resolved Motion Rate Control of Manipulators and Human Prostheses, IEEE Trans. on Man-Machine Systems, MMS-10, n.2, 47-53, 1969.

6. Vykukal, H. C. et al: An Anthropomorphic Master-Slave Manipulator System, Proc. of the First National Conf. on Remotely Manned Systems, E. Heer, ed., 189-198, Sept. 1972.

SESSION IX

SYSTEM IDENTIFICATION

Chairman: L. Reid

A COMPARISON OF TECHNIQUES FOR IDENTIFYING HUMAN OPERATOR DYNAMICS UTILIZING TIME SERIES ANALYSIS

by

Keiji Tanaka*, Norihiro Goto**, Kyuichiro Washizu***

*Instrumentation and Control Division, National Aerospace Laboratory, Tokyo, **Department of Aeronautical Engineering, Kyushu University, Fukuoka, ***Department of Aeronautics, University of Tokyo, Tokyo

ABSTRACT

Several human operator models were identified utilizing the current spectral analysis technique and the time domain analysis techniques based on the Akaike's Minimum Final Prediction Error (MFPE) method. Evaluation of the time domain techniques is aimed at in this report. Analyses were made of the data obtained from compensatory tracking tasks involving a human operator and from digital simulations using a human model.

The results of the time domain techniques are generally in good accordance with each other. Moreover one of the techniques can offer the remnant shaping filter, the controlled element dynamics and the impulse response of the human operator.

Some preliminary consideration of the correlation between the human lead operation and the human function to forecast the system output has been made through the analysis of the human operator dynamics in control of unstable second order systems.

SYMBOLS

$\underline{A}_M(m)$	m-th autoregressive coefficient matrix when the order is M
B	backward shift operator
$c(t), c(n)$	human operator output
dB	decibel
$\underline{d}_M$	estimated variance matrix of noise source when the order is M

$e(t)$, $e(n)$	displayed error
$F\{x(t)\}$	Fourier-transform of $x(t)$
j	$\sqrt{-1}$
MFPE(M)	Multiple Final Prediction Error when the order is M
$m(t)$, $m(n)$	controlled element output
N	data length
n	sampling time ($= n\Delta$)
$r(t)$, $r(n)$	remnant
s	Laplace operator
t	time, seconds
$Y_c(j\omega)$	controlled element
$Y_p(j\omega)$	describing function of a human operator
$y_p(n)$, $y_p(\tau)$	impulse response of a human operator
Δ	sampling interval, seconds
τ	time shift, seconds
$\Phi_{xy}(j\omega)$	cross power spectrum between $x(t)$ and $y(t)$
ω	frequency, rad/sec

INTRODUCTION

Recent progress in aircraft size, variety, and automation of flight control has greatly changed the role of the human pilot in aircraft control. The change causes more complex man-machine system problems than ever, and to solve them requires essential knowledges about the human operator dynamic characteristics. In most cases human operator dynamics have been investigated on the basis of the describing functions, such as the crossover model, in tracking tasks. The obtained human operator dynamics, however, usually show a large variety according to the objects or circumstances of the experiments. This is mainly because of his inherent adaptive dynamics, which include threshold, memory, and learning characteristics. For this reason precise and general techniques for identifying the human operator dynamics have been

674

required.

Confining ourselves to the approaches to identify the human operator dynamics, we may say that there are several techniques which have been fully discussed and put in order in literatures. In this paper, existing techniques are briefly summerized in the next section, followed by the introduction of several new techniques utilizing Akaike's MFPE method, which takes advantage of the recent development of the time series analysis and the statistical system identification. Results of the new techniques are compared with those obtained by the existing well-developed closed-loop spectral method. They indicate that the structure of the human operator dynamics can be distinctly expressed by employing the techniques of the MFPE method, and elucidate the superiority of the new techniques to the existing ones.

REVIEW OF EXISTING IDENTIFICATION TECHNIQUES

The man-machine system treated in this paper is confined to the simple compensatory tracking system as Fig.1, where the human operator output, $c(t)$, is the sum of the linear response to the displayed error, $e(t)$, and the remnant, $r(t)$. The objective of the identification is to determine the linear portion of the operator model, Y_p; namely the describing function of the human operator. Also, the term "identification" is sometimes used to mean the determination of the model structure and the parameters in that linear model.

The existing techniques for identifying the human operator dynamics may be calssified roughly into the following five kinds; the first three are in the frequency domain, while the last two are in the time domain:

(A) Closed-Loop Spectral Method [Refs.1 ∿ 4]

Let the portion irrelevant to the input in the human operator output $c(t)$ be $p(t)$. Then, $p(t)$ can be

$$p(t) = c(t) - \int_0^\infty g(\tau)i(t-\tau)d\tau , \qquad (1)$$

where $g(\tau)$ is the closed-loop impulse response function from $i(t)$ to $c(t)$. The impulse response function $g(\tau)$ may be determined in such a way that it minimizes the variance of $p(t)$. By using a few other relationships and the Fourier-transform, we obtain the well known result as to the estimate of the unknown human operator dynamics, as;

$$\hat{Y}_{pa}(j\omega) = \frac{\Phi_{ic}(j\omega)}{\Phi_{ie}(j\omega)} . \qquad (2)$$

It is generally admitted that this method can offer less fluctuant estimate than the following two methods.

(B) Open-Loop Spectral Method [Ref.3]
   If we minimize the variance of

$$r(t) = c(t) - \int_0^\infty y_p(\tau)e(t-\tau)d\tau \quad ,$$

we obtain the second estimate of the describing function as follows;

$$\hat{Y}_{pb}(j\omega) = \frac{\Phi_{ec}(j\omega)}{\Phi_{ee}(j\omega)} \quad . \tag{3}$$

It is generally admitted that cares should be taken of the fact that if

$$\Phi_{ii}(\omega) \ll \Phi_{rr}(\omega)$$

then

$$\hat{Y}_{pb}(j\omega) = - \frac{1}{Y_c(j\omega)} \quad . \tag{4}$$

(C) Direct Fourier-Transform Method [Ref.3]
   Direct Fourier-transform of the signals, $e(t)$ and $c(t)$, can offer the estimate;

$$\hat{Y}_{pc}(j\omega) = \frac{F\{c(t)\}}{F\{e(t)\}} \quad . \tag{5}$$

The describing functions obtained from the three methods mentioned above have inevitable fluctuations in the frequency domain; therefore it is a common practice to derive from these describing functions a human operator model with a small number of parameters by the use of additional criteria.

(D) Impulse Response Function Method [Refs.2,5,6]
   The human impulse response function can be estimated by applying the least squares algorithm, the criterion of which is the same as that of the method B. In the sampled data form the estimate $\hat{\underline{Y}}_{pd}$ is given by

$$\hat{\underline{Y}}_{pd} = [\ \underline{E}^T\underline{E}\ ]^{-1}\underline{E}^T\underline{c} \tag{6}$$

where

$$\hat{\underline{Y}}_{pd} = [\hat{y}_{pd}(1),\hat{y}_{pd}(2),\cdots,\hat{y}_{pd}(M)]^T$$

$$\underline{c} = [c(M),c(M+1),\cdots,c(N)]^T$$

$$\underline{E} = \begin{pmatrix} e(M) & e(M-1)\cdots & e(2) & e(1) \\ \vdots & & & \vdots \\ e(N) & \cdots\cdots\cdots & & e(N-M+1) \end{pmatrix} \quad ,$$

and hereafter any $x(n)$ $(n=1,2,\cdots)$ denotes the time series which is assumed to be sampled from the corresponding continuous signal $x(t)$ with the sampling interval Δ. M is the length of the human operator impulse response, and N is the data length. A describing function can easily be estimated by carrying out the Fourier-transform of $\hat{y}_{pd}$. This method has an advantage of the physical realizability of the estimate, but it should be noted that the same caution as in Y_{pb} must be paid to this method. It has also been pointed out that in the case of estimating an element in a feedback loop, it is not possible to obtain an unbiased estimate unless the remnant is white [Ref.7]. Also note that the orthogonal filter method uses the basically same criterion as this method [Ref.5].

(E) Improved Impulse Response Function Method
   The second named author has succeeded in obviating the difficulty existing in the preceding method by pre-whitening the remnant [Ref.8]. He assumes the remnant to be a shaped output of a white noise and to be given in a discrete autoregressive form by

$$r(n) = \sum_{\ell=1}^{L} h(\ell)r(n-\ell) + \varepsilon(n) \quad , \tag{7}$$

where $\varepsilon(n)$ $(n=1,2,\cdots,N)$ is a white noise process, and $h(\ell)$ $(\ell=1,2,\cdots,L)$ are autoregressive coefficients of $r(n)$. Then, $h(\ell)$ $(\ell=1,2,\cdots,L)$, and $y_p(m)$ $(m=1,2,\cdots,M)$ are estimated by applying the least squares algorithm, the criterion of which is the minimization of the variance of $\varepsilon(n)$. This procedure gives a good estimate regardless of the existence of feedback links.

AKAIKE'S MFPE METHOD

The method E in the preceding section is essentially different from the others, A to D, in that it estimates the remnant parameters and the system (human operator) parameters. It, however, has a difficulty in determining the number of parameters to be estimated. Namely, though the model may improve the fidelity to reproduce the experimental data with an increase of the number of parameters, the value of each estimated parameter possibly loses its accuracy. Recently a very practical criterion to determine the order of the model has been proposed by Akaike [Ref.7], and a brief account of the method is introduced here.
   We consider the case of model identification when the data are of k-dimensions. According to a properly selected regression order L, the following k-dimensional autoregressive model can be fitted to the data vector $\underline{x}(n)$, which is assumed stationary and zero-mean:

$$\underline{x}(n) = \sum_{m=1}^{L} \underline{A}_L(m)\underline{x}(n-m) + \underline{\varepsilon}(n) \quad , \tag{8}$$

where

$$\underline{x}(n) = [x_1(n), x_2(n), \cdots, x_k(n)]^T \quad ,$$

and $\underline{\varepsilon}(n)$ is a k-dimensional white noise vector given by

$$\underline{\varepsilon}(n) = [\varepsilon_1(n), \varepsilon_2(n), \cdots, \varepsilon_k(n)]^T \quad ,$$

the elements of which are assumed to be mutually independent. Also, in Eq.(8)

$$\underline{A}_L(m) = \begin{bmatrix} a_{L11}(m) & a_{L12}(m) & \cdots & a_{L1k}(m) \\ a_{L21}(m) & a_{L22}(m) & & \vdots \\ \vdots & & & \vdots \\ a_{Lk1}(m) & \cdots\cdots\cdots & a_{Lkk}(m) \end{bmatrix} \quad , \quad (m=1,2,\cdots,L)$$

denoting the m-th k×k-dimensional autoregressive coefficient matrix when the order of regression is selected to be L. Values of $\underline{A}_L(m)$ and the estimated variance matrix of $\underline{\varepsilon}(n)$, denoted by $\underline{d}_L$, are determined by making use of the estimated variance matrix of $\underline{x}(n)$, denoted by $\underline{C}(\ell)$ ($\ell=1,2,\cdots,L$) as follows: where

$$\underline{d}_L = \begin{bmatrix} \sigma_{11}^2 & \sigma_{12}^2 & \cdots & \sigma_{1k}^2 \\ \sigma_{21}^2 & \sigma_{22}^2 & & \vdots \\ \vdots & & & \vdots \\ \sigma_{k1}^2 & \cdots\cdots\cdots & \sigma_{kk}^2 \end{bmatrix}$$

and

$$\underline{C}(\ell) = \begin{bmatrix} c_{11}(\ell) & c_{12}(\ell) & \cdots & c_{1k}(\ell) \\ c_{21}(\ell) & c_{22}(\ell) & & \vdots \\ \vdots & & & \vdots \\ c_{k1}(\ell) & \cdots\cdots\cdots & c_{kk}(\ell) \end{bmatrix} \quad , \quad (\ell=1,2,\cdots,L),$$

also

$$c_{ij}(\ell) = \frac{1}{N} \sum_{n=1}^{N-\ell} x_i(n+\ell) x_j(n) \quad , \quad (\ell=1,2,\cdots,L) \quad . \quad (9)$$

Upon multiplying the i-th equation of Eq.(8) by $x_h(n-\ell)$, we obtain

$$x_i(n) x_h(n-\ell) = \sum_{m=1}^{L} \sum_{j=1}^{k} a_{Lij}(m) x_j(n-m) x_h(n-\ell) + \varepsilon_i(n) x_h(n-\ell) \quad . \quad (10)$$

On taking the expectation of the both sides of Eq.(10), we obtain the following k-dimensional Yule-Walker equations;

$$\gamma_{ih}(\ell) = \sum_{m=1}^{L} \sum_{j=1}^{k} a_{Lij}(m) \gamma_{jh}(\ell-m) \quad , \quad (h=1,2,\cdots,k; \ell=1,2,\cdots,L) \quad , \quad (11)$$

678

where $\gamma_{ih}(\ell)$ denotes the covariance between x_i and x_h. Note that the expectation $E[\varepsilon_i(n), x_h(n-\ell)]$ vanishes when $\ell > 0$. By substituting the estimate $c_{ij}(\ell)$ for $\gamma_{ij}(\ell)$, we can solve Eq.(11) for $\underline{A}_L(m)$ $(m=1,2,\cdots,L)$. At the same time, from Eq.(8), $\underline{d}_L$ is obtained by using $\underline{A}_L(m)$ as;

$$\underline{d}_L = \underline{c}(0) - \sum_{m=1}^{L} \underline{A}_L(m)\underline{c}^T(m) \quad . \tag{12}$$

The calculation can be performed by an iterative procedure, where it is to be noted that the lower order coefficients $\underline{A}_{L-1}(m)$ $(m=1,2,\cdots,L-1)$, $\underline{A}_{L-2}(m)$ $(m=1,2,\cdots,L-2),\cdots$, $\underline{A}_1(m)$ $(m=1)$ are also obtained during the iterative process of determining $\underline{A}_L(m)$ $(m=1,2,\cdots,L)$. Then, the Akaike's method proposes to determine the order M as the value of L which minimizes the following criterion

$$MFPE(L) = (1 + \frac{Lk + 1}{N})^k (1 - \frac{Lk + 1}{N})^{-k} |\underline{d}_L| \quad . \tag{13}$$

This is called the multiple final prediction error, which means the mean-square error of the one-step-ahead prediction obtained by using the estimated coefficients $\underline{A}_L(m)$ $(m=1,2,\cdots,L)$. In Eq.(13), $|\underline{d}_L|$ denotes the determinant of $\underline{d}_L$, and N is the number of data points.

The present method, which will be called Akaike's MFPE method hereafter, has been applied by the first named author to identifying the human operator dynamics in the control system shown in Fig.1. By the use of the MFPE method, the following techniques have been developed:

(1) The MFPE Method Utilizing Data of $e(t)$ and $c(t)$

A two-dimensional autoregressive model by the use of $e(t)$ and $c(t)$ is determined first. Then, after checking the model appropriateness by the values of the off-diagonal elements of $\underline{d}_M$, (namely, the estimated cross-covariance of the white noises be very small compared with the diagonal elements,) we obtain from Eq.(8) the autoregressive equations of $e(n)$ and $c(n)$ in a matrix form as

$$\begin{vmatrix} c(n) \\ e(n) \end{vmatrix} = \begin{vmatrix} A_{11}(B) & A_{12}(B) \\ A_{21}(B) & A_{22}(B) \end{vmatrix} \begin{vmatrix} c(n) \\ e(n) \end{vmatrix} + \begin{vmatrix} \sigma_{11} & 0 \\ 0 & \sigma_{22} \end{vmatrix} \begin{vmatrix} \xi_1(n) \\ \xi_2(n) \end{vmatrix}, \tag{14}$$

where

$$A_{ij}(B) = a_{ij}(1)B + a_{ij}(2)B^2 + \cdots + a_{ij}(M)B^M, \quad (i,j=1,2)$$

$$Bx(n) = x(n-1) \quad [\text{Refs.9 and 10}] \quad .$$

M is the order of the model determined by MFPE, and $\xi_i(n)$ $(i=1,2)$ denote white noise process of unit variance, which are independent of each other. It should be noted that $\varepsilon_1(n)$ $[= \sigma_{11}\xi_1(n)]$ and $\varepsilon_2(n)$ $[= \sigma_{22}\xi_2(n)]$ are the estimated noise sources of the remnant $r(n)$ and the external forcing function $i(n)$, respectively, as shown in Fig.2.

Then, we obtain from the first equation of Eq.(14),

$$\{1 - A_{11}(B)\}c(n) = A_{12}(B)e(n) + \sigma_{11}\xi_1(n)$$

and consequently

$$c(n) = \frac{A_{12}(B)}{1 - A_{11}(B)} e(n) + \frac{\sigma_{11}}{1 - A_{11}(B)} \xi_1(n) \quad . \quad (15)$$

Therefore an estimate of the human impulse response function is given by

$$\hat{y}_{p1}(B) = \frac{A_{12}(B)}{1 - A_{11}(B)} \quad . \quad (16)$$

The operator B can be replaced by $\exp(-j\omega\Delta m)$ to get the frequency response function as;

$$\hat{Y}_{p1}(j\omega) = \frac{A_{12}(j\omega)}{1 - A_{11}(j\omega)} \quad (17)$$

where

$$A_{ij}(j\omega) = \sum_{m=1}^{M} a_{ij}(m) e^{-j\omega\Delta m} \quad .$$

Eq.(17) will be called the first estimate of the describing function. Moreover, an estimated shaping filter of the remnant is given by

$$\hat{F}_r(j\omega) = \frac{\sigma_{11}}{1 - A_{11}(j\omega)} \quad . \quad (18)$$

From the second equation in Eq.(14), an estimate of the controlled element frequency response and the shaping filter of the forcing function are also given by

$$-\hat{Y}_c(j\omega) = \frac{A_{21}(j\omega)}{1 - A_{22}(j\omega)} \quad , \quad (19)$$

and

$$\hat{F}_i(j\omega) = \frac{\sigma_{22}}{1 - A_{22}(j\omega)} \quad , \quad (20)$$

respectively.

(2) The MFPE Method Utilizing i(t) and c(t)
    An estimate of the closed-loop frequency response, $\hat{Y}_{ic}(j\omega)$ is calculated as before. Making use of $\hat{Y}_{ic}(j\omega)$ and the known $Y_c(j\omega)$ gives the second estimate of the describing function as;

$$\hat{Y}_{p2}(j\omega) = \frac{\hat{Y}_{ic}(j\omega)}{1 - Y_c(j\omega)\hat{Y}_{ic}(j\omega)} \quad . \quad (21)$$

(3) The MFPE Method Utilizing $e(t)$ and $m(t)$

An estimate of the open-loop frequency response from $e(n)$ to $m(n)$, $\hat{Y}_{em}(j\omega)$ is calculated. By making use of $\hat{Y}_{em}(j\omega)$ and the known $Y_c(j\omega)$, the third estimate is given by

$$\hat{Y}_{p3}(j\omega) = \frac{\hat{Y}_{em}(j\omega)}{Y_c(j\omega)} \qquad . \tag{22}$$

DIGITAL SIMULATIONS

Before proceeding to the identification of a human operator dynamics, digital simulations were carried out to check the validity of the MFPE method. The block diagram of the simulations is shown in Fig.1, where the controlled element dynamics and the known filter corresponding to the human operator dynamics were

$$Y_c(s) = \frac{9}{s^2 + 2s + 9} \cdot e^{-0.05s} \tag{23}$$

and

$$Y_p(s) = \frac{0.5}{1 + 0.2s} e^{-0.25s} \qquad , \tag{24}$$

respectively. The simulated system was driven by two random number series: one was for the simulated input and the other for the simulated remnant.

Data analyses were carried out to obtain $\hat{Y}_{pa}$, $\hat{Y}_{p1}$, $\hat{Y}_{p2}$ and $\hat{Y}_{p3}$. These were compared with the theoretical results. Examples are shown in Figs.3 ～ 6. It is found that:

(1) $\hat{Y}_{pa}$, $\hat{Y}_{p1}$ and $\hat{Y}_{p2}$ prove to be correct, while $\hat{Y}_{p3}$ to be nearly correct.

(2) The order of the extent of independency from the influence of the remnant is, from small to large, $\hat{Y}_{p1}$, $\hat{Y}_{p2}$ and $\hat{Y}_{pa}$.

HUMAN TRACKING DATA AND THEIR REDUCTIONS

Next, single-loop compensatory tracking experiments involving a human operator as shown in Fig.7 were carried out. Three male subjects participated in the experiments, and the following twelve kinds of controlled elements were mechanized by an analogue computer:

$$Y_c(s) = 1, \quad \frac{1}{s} , \quad \frac{2}{s \pm 2} \tag{25}$$

and

$$Y_c(s) = \frac{\omega_n^2}{s^2 + 2\zeta\omega_n s + \omega_n^2} \qquad (26)$$

with $\omega_n = 3$, 5 [rad/sec], and $\zeta = 0.167$, 0, -0.167, -0.333.
The forcing function was generated by shaping a white noise by the filter,

$$F_i(s) = \frac{22.5}{(s + 1.5)^2} + \frac{100}{(s + 10)^2} \qquad (27)$$

Data reductions were implemented on NAL magnetic-tape-data reduction system and FACOM 230-75 computer.

RESULTS OF HUMAN TRACKING DATA ANALYSIS

The techniques investigated were $\hat{Y}_{pa}$, $\hat{Y}_{p1}$, $\hat{Y}_{p2}$ and $\hat{Y}_{p3}$. It was chosen that $\Delta = 0.1$ [sec]. The number of the data points, N, was 1200 (ten minutes), and the number of variance functions used was 100 (ten seconds). Also for $\hat{Y}_{pa}$, Hamming-window was used.

Examples of the human operator describing functions of $\hat{Y}_{p1}$, $\hat{Y}_{p2}$ and $\hat{Y}_{p3}$ are shown in Fig.8 ∿ 11 for $Y_c = 1$, $1/s$, $9/(s^2-s+9)$ and $9/(s^2-2s+9)$, respectively. They show good accordance with each other. In order to compare the identified models with the describing function based on the spectral analysis, $\hat{Y}_{p1}$ and $\hat{Y}_{pa}$ are plotted one over the other. Examples are shown in Figs.12 and 13, where it can be observed that $\hat{Y}_{p1}$ and $\hat{Y}_{pa}$ are in good agreement.

It is noted, however, that the off-diagonal element of d_M of the autoregressive model of $\hat{Y}_{p3}$ takes a relatively high value; therefore the modeling of $\hat{Y}_{p3}$ is not always successful. Also caution has to be paid to the values of the relative noise contribution to confirm the effectiveness of the identified models: the relative noise contribution $R_{ij}(\omega)$ is defined under the assumption of the mutual independence of $\epsilon_i(n)$'s in Eq.(8) as

$$R_{ij}(\omega) = \frac{q_{ij}(\omega)}{p_{ii}(\omega)} \qquad (28)$$

where $p_{ii}(\omega)$ is the power spectrum of $x_i(n)$, and $q_{ij}(\omega) = |[A(\omega)^{-1}]_{ij}|^2 \sigma_{jj}^2$, the contribution from each noise source to the total power of $x_i(n)$. $[A(\omega)]_{ij}^{-1}$ is the (i,j)-element of $[A(\omega)]^{-1}$,

$$A(\omega) = \sum_{m=0}^{M} A_M(m)\exp(-j\omega\Delta m)$$

where $A_M(0) = -I$, and σ_{jj}^2 is the variance of $\epsilon_j(n)$. The relative noise contribution of the noise source of $i(n)$ to $c(n)$ is often in low level when Y_c is unstable; this may suggest that in this case the human operator is in Pilot-Induced-Oscillation.

An example of the comparison between the model output $c^*(n)$, which is

computed through the convolution of $\hat{y}_{p1}(s)$ and $e(n)$ of the data, and the human operator actual output data, $c(n)$, is shown in Fig.14. It is indicated that the linear model of $\hat{y}_{p1}$ accounts for a considerable portion of the human output.

SOME OBSERVATIONS OBTAINED FROM IDENTIFIED HUMAN OPERATOR MODELS

Several observations obtained from the identified human operator models may be summarized as follows:

(1) It is fairly clear that the describing functions of the human operators in controlling the elements;

$$Y_c(s) = 1, \frac{1}{s}, \frac{2}{s+1} \quad ,$$

can be expressed by the crossover model, whereas those in controlling an unstable second-order system can be approximated by

$$Y_p(s) = K_p \frac{1 + T_L s + T_L' s^2}{1 + T_I s} e^{-\tau_e s} \quad . \tag{29}$$

(2) Examples of $\hat{g}_{pe}(\tau)$, shown for $Y_c = 1$ and $9/(s^2-s+9)$ in Figs.15 and 16 respectively, indicate that the net time delay, which is the dead time in the impulse response of the human operator, τ_0, seems to be about $0.1 \sim 0.2$ [sec] and is relatively smaller than the effective time delay, τ_e in Eq.(29).

(3) It is often observed that when the controlled element is unstable, there exists a human lead operation which is expressed by the lead terms in the human operator describing function. It is quite natural to presume that when a human operator becomes familiar with the system dynamics, he can grasp the characteristics of the controlled element and predict the output of the controlled element [Ref.6]. This leads us to consider that the first- and the second-order lead terms in human models may indicate the human operator's function to forecast the output of the controlled element.

(4) The describing functions $-\hat{Y}_c$ and $\hat{F}_r$ have proved to be nearly correct in the frequency range between 0 and 10 [rad/sec]. Also, the describing function F_r seems to be correct. However, it has no tendency of depending on Y_c.

FINAL REMARKS

The linear models of a human operator controlling unstable systems, which have been considered so far to be hard to estimate, have been precisely identified by the MFPE method. These models have proved to be successful in

expressing a considerable part of the human operation.

The identification techniques utilizing the recently developed time series analysis can offer very evident results. It may be concluded that these techniques are effective tools to analyze the man-machine systems with, and that $\hat{Y}_{p1}$ offers the most information among the three. Yet, it should be noted that in order to validate the model, full attention must be paid to the variance matrix of noise sources, the coherency and the relative noise contribution. As this MFPE method is primarily quite effective when applied to multi-variable systems, it is expected to become one of indispensable tools for multi-variable system analyses.

ACKNOWLEDGMENT

REFERENCES

1. McRuer,D.T.; and Krendel,E.S.: The Human Operator as a Servo System Element. Rept. from Journal of Franklin Institute, Vol.267, No.5 and No.6, 1959.

2. Shirley,R.S.: A Comparison of Techniques for Measuring Human Operator Frequency Response. Sixth Annual Conference on Manual Control, 1970, pp.803-869.

3. Frostell,C.E.: A Comparison of Pilot Describing Function Measurement Techniques. UTIAS TN No.167, 1971.

4. McRuer,D.T.; and Krendel,E.S.: Mathematical Models of Human Pilot Behavior. AGARD-AG-188, 1974.

5. Wingrove,R.C.: Comparison of Methods for Identifying Pilot Describing Functions from Closed-Loop Operating Records. NASA TN D-6235, 1971.

6. Taylor,L.W.Jr.: A Comparison of Human Response Modeling in the Time and Frequency Domain. Third NASA-University Conference on Manual Control, NASA SP-144, 1967, pp.137-153.

7. Akaike,H.; and Nakagawa,T.: Statistical Analysis and Control of Dynamic Systems. 1972, Science Co., (in Japanese).

8. Goto,N.; and Washizu,K.: On the Dynamics of Human Pilots in Marginally Controllable Systems. AIAA Journal, Vol.12, No.3, 1974.

9. Shinners,S.M.: Modeling of Human Operator Performance Utilizing Time Series Analysis. IEEE Trans. on Systems, Man and Cybernetics, Vol. SMC-4, No.5, 1974.

10. Box,G.E.P.; and Jenkins,G.M.: Time Series Analysis Forecasting and Control. 1970, Holden Day.

11. FACOM 230 TAFT [Time series Analysis in Frequency and Time Domain] Manual. 1974, Fujitsu Co., (in Japanese).

12. Akaike,H.: Autoregressive Model Fitting for Control. Ann. Inst. Statist. Math., Vol.23, 1971, pp.163-180.
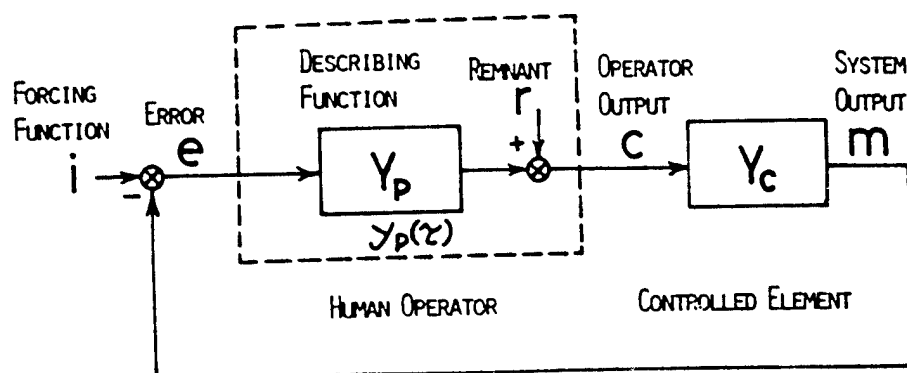
Figure 1. Equivalent Block Diagram of Compensatory System
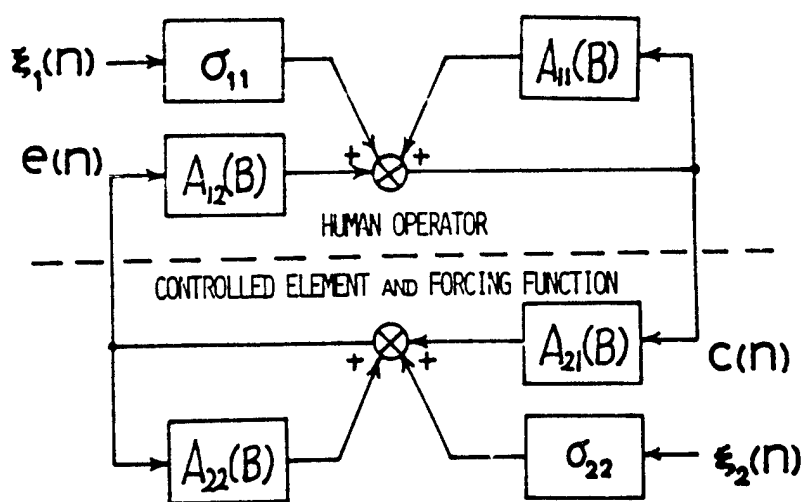
Figure 2. Block Diagram of Compensatory System by MFPE Method

Figure 4. Estimated Frequency Response of a
Known Filter by Spectral Analysis

Figure 3. Estimated Frequency Responses of a
Known Filter by MFPE Method

687

Figure 6. Estimated Frequency Response of a
Known Filter by Spectral Analysis
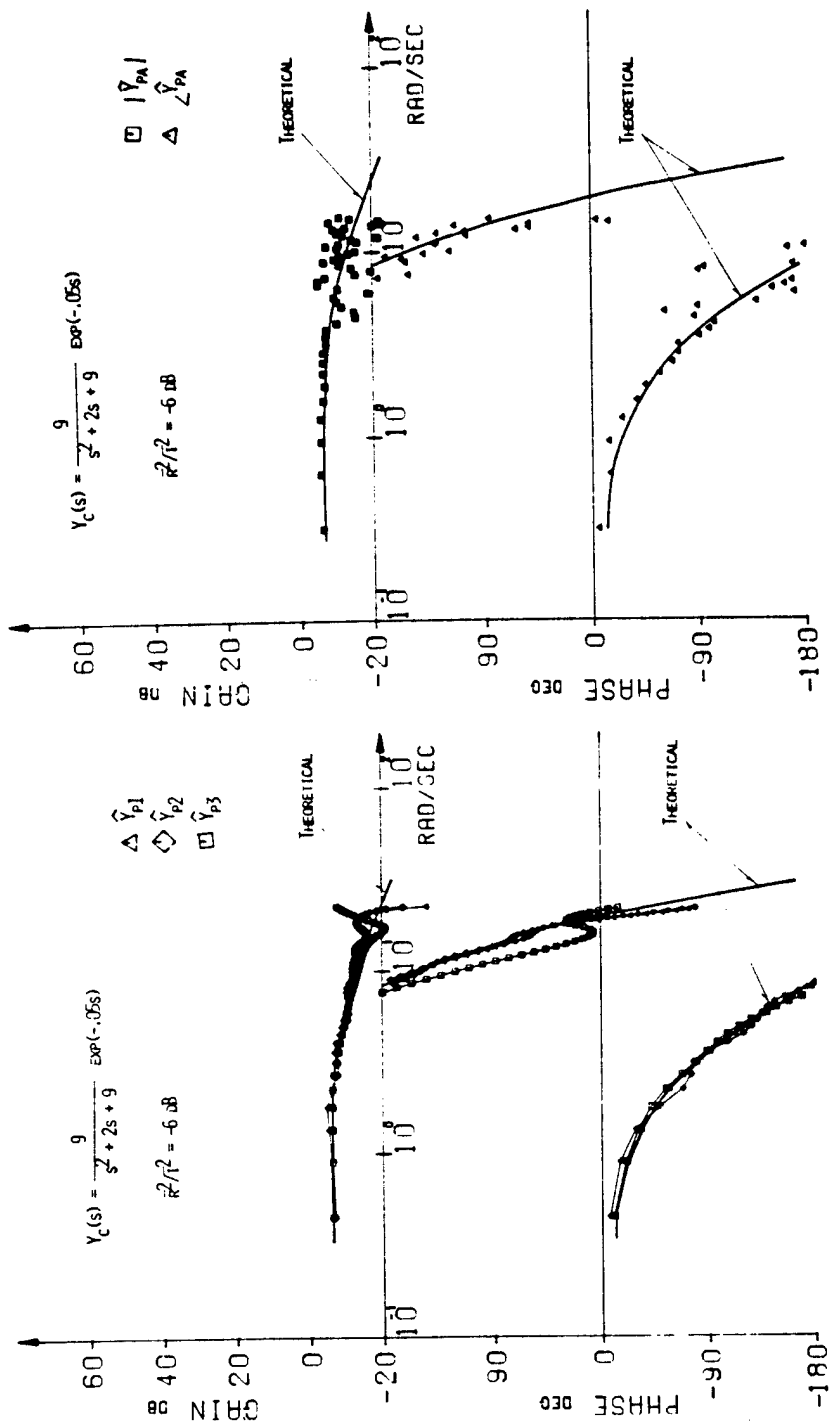
Figure 5. Estimated Frequency Responses of a
Known Filter by MFPE Method
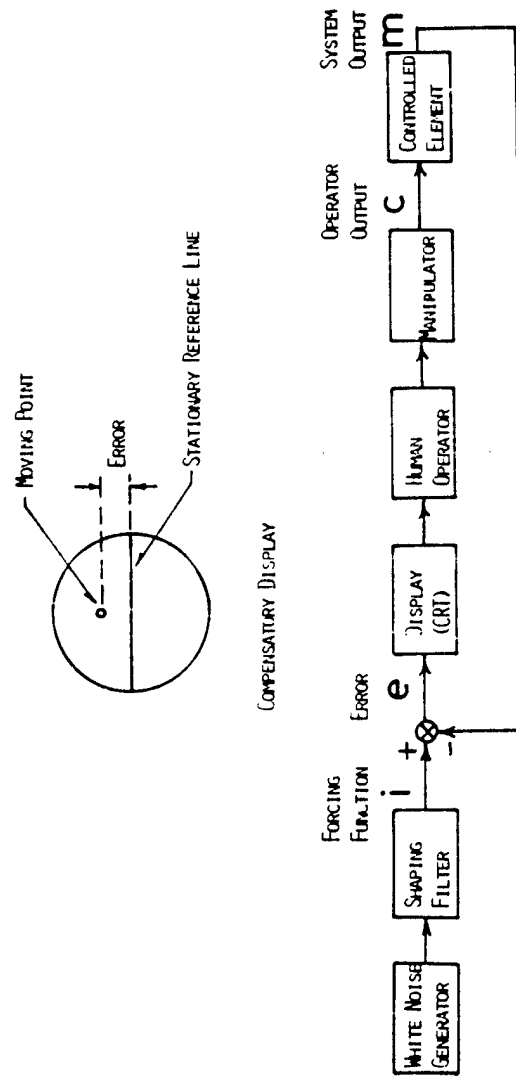
Figure 7. Block Diagram of Simple Compensatory Manual Control System

689

Figure 8. $\hat{Y}_p(j\omega)$

Figure 9. $\hat{Y}_p(j\omega)$

$\hat{Y}_{P1}$
$\hat{Y}_{P2}$
$\hat{Y}_{P3}$

RAD/SEC

$Y_c(s) = \dfrac{9}{s^2 - 2s + 9}$

GAIN DB

PHASE DEG

Figure 11. $\hat{Y}_p(j\omega)$

$\hat{Y}_{P1}$
$\hat{Y}_{P2}$
$\hat{Y}_{P3}$

RAD/SEC

$Y_c(s) = \dfrac{9}{s^2 - s + 9}$

GAIN DB

PHASE DEG
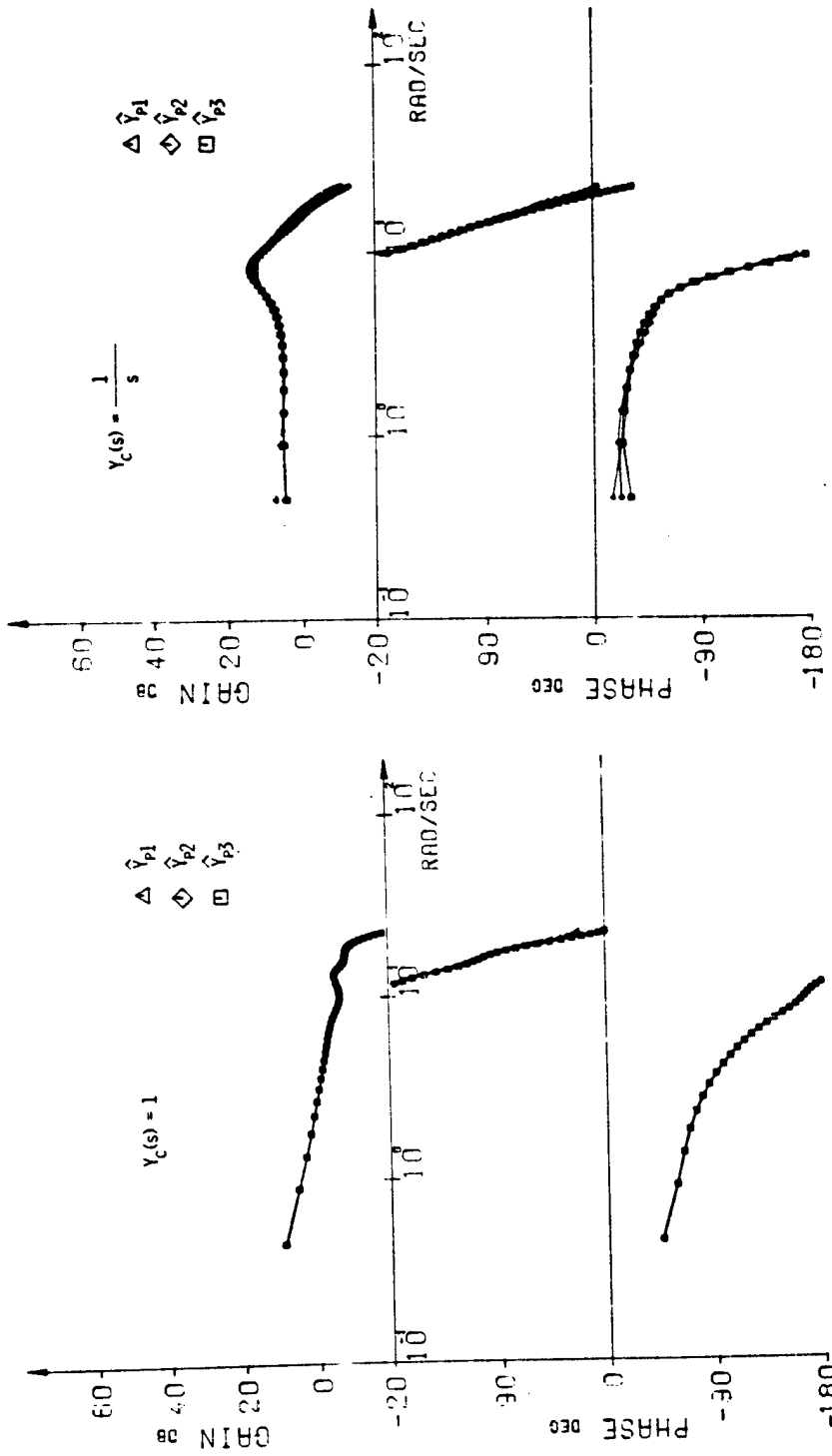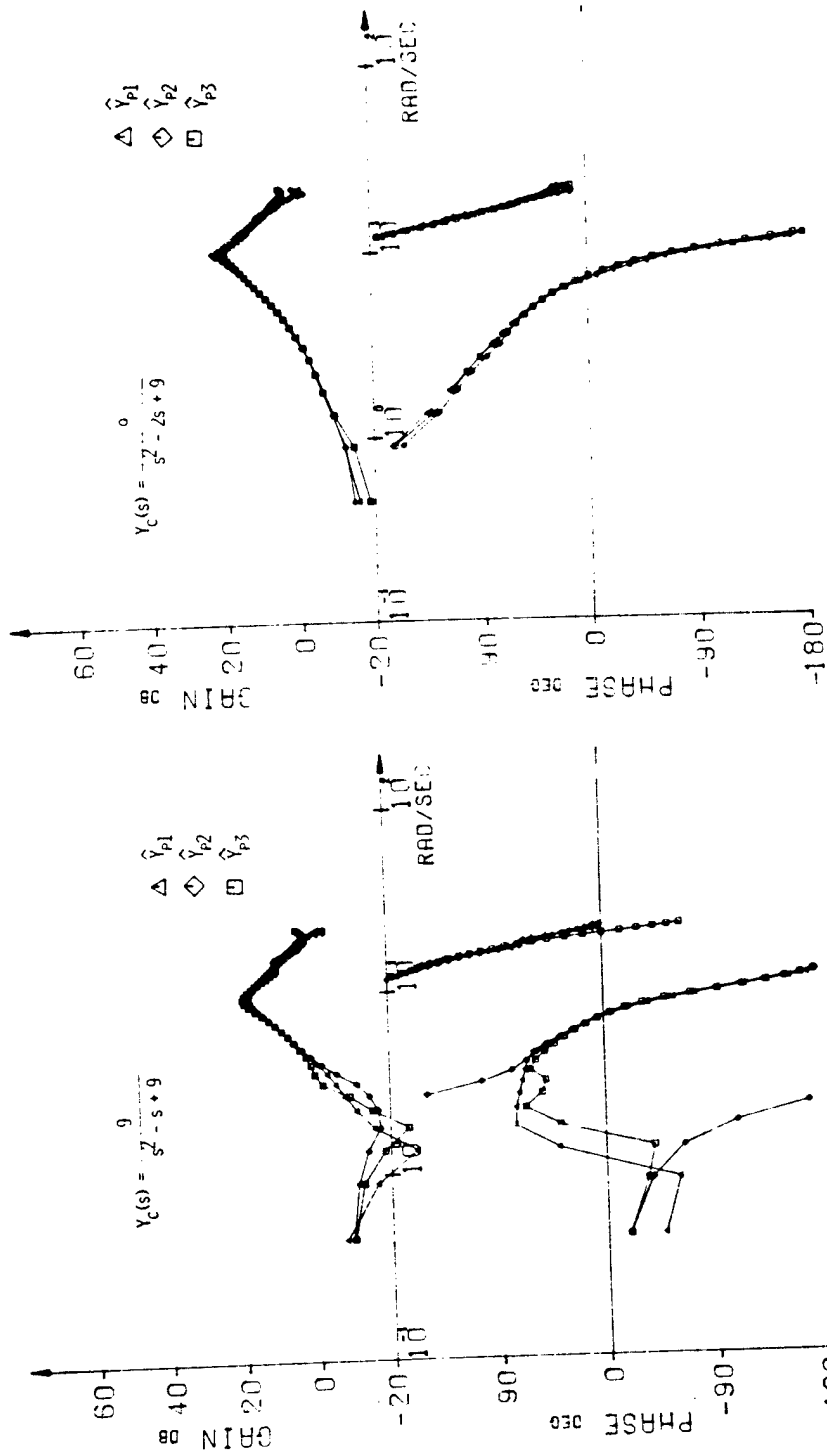
Figure 10. $\hat{Y}_p(j\omega)$

Figure 13. $\hat{Y}_{pa}(j\omega)$ and $\hat{Y}_{pl}(j\omega)$
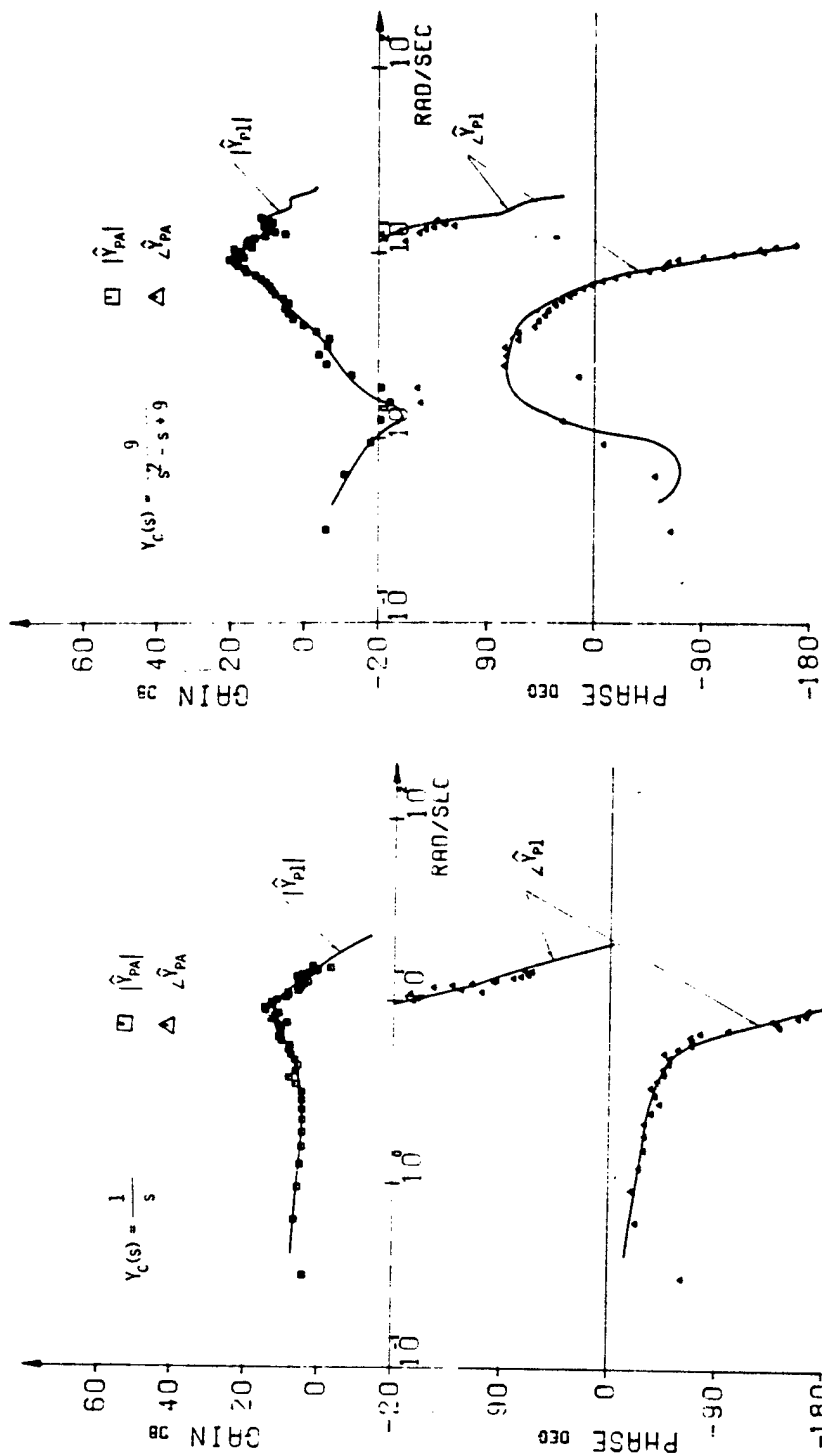
Figure 12. $\hat{Y}_{pa}(j\omega)$ and $\hat{Y}_{pl}(j\omega)$
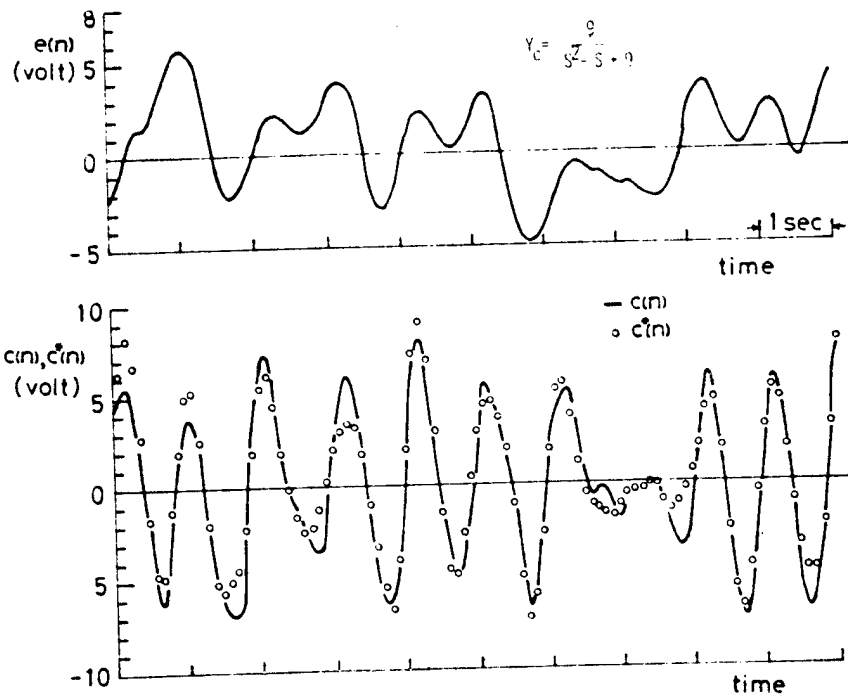
Figure 14. A Comparison between Human Output (c(n)) and Model Output (c*(n)) Computed through Error (e(n)) and Identified Human Impulse Response ($\hat{y}_{p1}$)
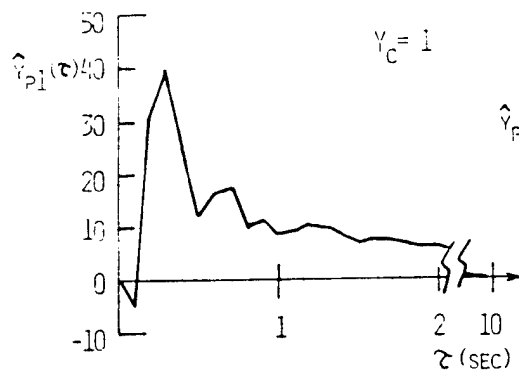
Figure 15. $\hat{y}_{p1}(\tau)$
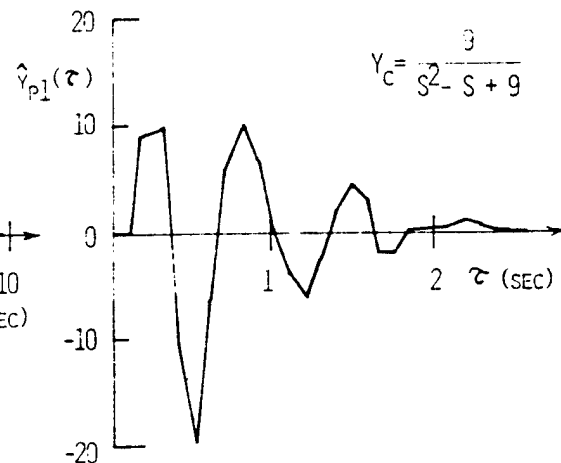
Figure 16. $\hat{y}_{p1}(\tau)$

SYSTEM IDENTIFICATION VIA A MICROCOMPUTER

Ralph Mekel and Avtar Singh

The City College of The City University of New York
New York, N. Y. 10031

SUMMARY

The purpose of this paper is twofold. The first part describes an adaptive identification technique for updating the parameters of a mathematical model and in the second part it is shown how the identification process may be implemented through a microcomputer system consisting of a microprocessor (CPU unit), RAMs, ROMs, I/O devices, a clock generator and other interfaces.

INTRODUCTION

The identification technique is formulated using a model-reference system approach in conjunction with Liapunov's direct method to insure the convergence of the identification process. An appropriate Liapunov function is chosen whose time derivative provides the identification law equations. An important feature is the simplicity of the system adaptive laws which are decomposed into primitive forms for easier implementation on the microcomputer. These adaptive laws depend explicitly on the model-reference system state variables and input. Therefore, in this identification technique it is assumed that the entire state vector is known or accessible for measurement.

The dotted block in Fig. 1. shows the part of the identification process which is to be realized by the microcomputer. Figure 2. describes the sequence of operations performed by the microcomputer in the process of identification. The identification process is a program on 8 ROMs each serving a specific purpose. The RAMs contain the initial, intermediate and final identified model as well as the system input, state vectors and various matrices used in the process of identification. The RAMs are also used for intermediate steps of calculations which need to be stored.

DERIVATION OF THE IDENTIFICATION LAW EQUATIONS

A block diagram depicting the identification process is given in Fig. 1. Let the reference system be described by

$$\dot{\underline{z}} = A\underline{z} + H\underline{r} \tag{1}$$

and the model to be identified by

$$\dot{\underline{x}} = K\underline{x} + (B - K)\ \underline{z} + C\underline{r} \tag{2}$$

where $\underline{z}$, $\underline{x}$ are the state vectors each of order n, K is a stable n x n matrix, $\underline{r}$ is the input vector of order m. Matrices A, B, C and H are initially different. The objective of the identification process is to generate a scheme that dynamically adjusts the elements of matrices B and C so that

$$\lim_{t \to \infty} B = A \tag{3}$$

$$\lim_{t \to \infty} C = H \tag{4}$$

$$\lim_{t \to \infty} (\underline{x} - \underline{z}) = \lim_{t \to \infty} \underline{e} = 0 \tag{5}$$

Define the misalignment of the matrices as

$$(B - A) = \sum_{i=1}^{n} \underline{b}_i\ \underline{u}_i^T \tag{6}$$

and

$$(C - H) = \sum_{i=1}^{n} \underline{d}_i\ \underline{w}_i^T \tag{7}$$

where $\underline{b}_i$ and $\underline{d}_i$ are constant column vectors with i-th row as 1 and all other rows being zero and $\underline{u}_i$ and $\underline{w}_i$ are the misalignment vectors. Next, define the model-reference system error as

$$\underline{e} = (\underline{x} - \underline{z}) \tag{8}$$

The time derivative of (8) yields

$$\dot{\underline{e}} = \dot{\underline{x}} - \dot{\underline{z}} \tag{9}$$

Substitution of (1) and (2) into (9) yields the following differential equation for the error

$$\dot{\underline{e}} = K(\underline{x} - \underline{z}) + (B - A)\ \underline{z} + (C - H)\ \underline{r} \tag{10}$$

Using (6), (7) and (8), Eq. (10) can be rewritten as

$$\dot{\underline{e}} = K\underline{e} + \left[\sum_{i=1}^{n} \underline{b}_i \underline{u}_i^T \right] \underline{z} + \left[\sum_{i=1}^{n} \underline{d}_i \underline{w}_i^T \right] \underline{r} \tag{11}$$

Equation (11) may be viewed as consisting of $(2n + 1)$ pertubations $\underline{u}_i$, $\underline{w}_i$ and $\underline{e}$. An appropriate Liapunov function should be positive definite in error as well as other perturbations. Therefore, one may choose a Liapunov function of the form

$$V = \underline{e}^T M \underline{e} + \sum_{i=1}^{n} \underline{u}_i^T N_i \underline{u}_i + \sum_{i=1}^{n} \underline{w}_i^T Q_i \underline{w}_i \tag{12}$$

where M, N_i and Q_i are positive definite symmetric matrices. For simplicity Q_i and N_i may be selected as diagonal matrices with positive elements, i.e.

$$N_i = \text{diagonal} \left[n_{ij} \right] \qquad 1 \le j \le n \tag{13}$$

and

$$Q_i = \text{diagonal} \left[q_{ij} \right] \qquad 1 \le j \le n \tag{14}$$

The time derivative of V yields

$$\dot{V} = \underline{e}^T (K^T M + MK) \underline{e} + 2 \sum_{i=1}^{n} \left[\dot{\underline{u}}_i^T N_i + \underline{z}^T (\underline{b}_i^T M \underline{e}) \right] \underline{u}_i +$$
$$+ 2 \sum_{i=1}^{n} \left[\dot{\underline{w}}_i^T Q_i + \underline{r}^T (\underline{d}_i^T M \underline{e}) \right] \underline{w}_i \tag{15}$$

Liapunov's criterion for stability calls for $V > 0$ and $\dot{V} \le 0$. One way to comply with Liapunov's criterion for stability and to generate the controller equations is to let

$$K^T M + MK = - D \tag{16}$$

$$\dot{\underline{u}}_i^T = - \underline{z}^T (\underline{b}_i^T M \underline{e}) N_i^{-1} \tag{17}$$

$$\dot{\underline{w}}_i^T = - \underline{r}^T (\underline{d}_i^T M \underline{e}) Q_i^{-1} \tag{18}$$

where $D = D^T (> 0) = \text{diagonal} \left[d_{ii} \right] \quad 1 \le i \le n$ \tag{19}

Differentiating Eqs. (6) and (7) and assuming that the system matrices A and H can be considered time invariant during the identification interval, one obtains

$$\dot{B} = \sum_{i=1}^{n} \underline{b}_i \dot{\underline{u}}_i^T \tag{20}$$

696

and
$$\dot{C} = \sum_{i=1}^{n} \underline{d}_i \underline{w}_i^T \tag{21}$$

Substitution of (17) and (18) into (20) and (21) respectively yields

$$\dot{B} = - \sum_{i=1}^{n} \underline{b}_i \underline{z}^T (\underline{b}_i^T \underline{P} \underline{e}) N_i^{-1} \tag{22}$$

$$\dot{C} = - \sum_{i=1}^{n} \underline{d}_i \underline{r}^T (\underline{b}_i^T \underline{P} \underline{e}) Q_i^{-1} \tag{23}$$

Integrating (22) and (23) yields

$$B = B_0 - \int_0^t \left[\sum_{i=1}^{n} \underline{b}_i \underline{z}^T (\underline{b}_i^T \underline{P} \underline{e}) N_i^{-1} \right] dt \tag{24}$$

and
$$C = C_0 - \int_0^t \left[\sum_{i=1}^{n} \underline{d}_i \underline{r}^T (\underline{d}_i^T \underline{P} \underline{e}) Q_i^{-1} \right] dt \tag{25}$$

where B_0 and C_0 are initially assumed model matrices. Substitution of (24) and (25) into Eq. (2) gives the final model representation

$$\dot{x} = K\underline{x} + \left\{ B_0 - \int_0^t \left[\sum_{i=1}^{n} \underline{b}_i \underline{z}^T (\underline{b}_i^T \underline{P} \underline{e}) N_i^{-1} \right] dt - K \right\} \underline{z} +$$

$$+ \left\{ C_0 - \int_0^t \left[\sum_{i=1}^{n} \underline{d}_i \underline{r}^T (\underline{d}_i^T \underline{P} \underline{e}) Q_i^{-1} \right] dt \right\} \underline{r} \tag{26}$$

The dotted block in Fig. 1. shows the part of the identification process to be realized by the microcomputer system and the next section describes the microcomputer hardware needed for implementing the identification process.

MICROCOMPUTER HARDWARE FOR IDENTIFICATION PROCESS

The identification process based upon the adaptive laws described in the previous section can be implemented on a microcomputer system shown in Fig. 3. The microcomputer system accepts the reference system input and states as

analog inputs and initial model and identification matrices as digital inputs. The analog signals are converted to digital equivalents by A/D converters such as Datel's DAS-16-L8B which takes in an analog signal and puts out an 8-bit digital signal. For entering the initial model and identification matrices, a teletype may be used along with proper interface to the microcomputer. One such interface is Intel's 8251 - programmable, synchronous/asynchronous communication interface, which accepts serial information from the teletype, constructs 8-bit words and presents to the computer. The same interface can be used to print out the identified model parameters. In transmitting mode, it accepts 8-bit words and converts to serial information to drive the teletype.

The initial and intermediate model parameters along with the identification matrices and signals from the reference system are stored in 256 byte RAM memory which can be constructed from a pair of 256x4 RAM chips. Input and output buffering for the RAM memory can be constructed using Intel's 8212 data buffers.

The identification algorithm is stored in 8 different ROM chips such as Intel's 8308 ROM which is 1024x8 bit and stores up to 1024 bytes. The total programming memory will be 8K, which is quite sufficient for the identification of a second order system. ROM memory chip selection unit can be constructed using Intel's 8205 - one out of eight decoder. For a higher order reference system it may be necessary to expand the ROM memory.

The program execution takes place in the CPU such as Intel's 8080 microprocessor. The CPU is run by a two phase clock generator and driver such as Intel's 8224. The total system consisting of ROMs, RAMs, A/D converters, teletype and CPU is coordinated by the system controller unit such as Intel's 8228. To service interrupts from various I/O devices, Intel's 8214 priority interrupt control unit may be used.

CONCLUDING REMARKS

We have described an identification technique based upon Liapunov's direct method in conjunction with a model-reference system configuration. The adaptive laws are partitioned so that they can be implemented on a microcomputer system. The later part of the paper shows directions for implementing the identification technique on a microcomputer system. Faster implementation can be achieved by using the microprocessor in conjunction with hardware multipliers and linear circuits (such as integrators).

REFERENCES

1. Graupe, D.: Identification of Systems. Van Nostrand Reinhold Co. 1972

2. Kalman, R. E.; and Bertram, J. E.: Control System Analysis and Design Via the Second Method of Lyapunov. Trans. of ASME, June 1960.

3. Mekel, R.: Nonlinear and Digital Man-Machine Control Systems Modeling. NASA Langley Research Center, Report No. 2-447-01, Nov. 1972.

4. Mekel, R.; Montgomery, R. C.; and Dunn, H. J.: An Adaptive Learning Control System for Aircraft. Eighth Asilomar Conference on Circuits, Systems and Computers, Dec. 3-5, 1974.

5. Datel Systems, Inc.: Engineering Products Handbook, A/D and D/A Converters, 1974.

6. Intel Corporation: 8080 Microcomputer Systems User's Manual, Sept. 1975.

7. Graupe, D.: Multifunctional Control of Artificial Upper Limbs Based on Parameter Identification of Myoelectric Signals. Decision and Control Conference, 1975.

8. Torrero, E. A.: Microprocessors, New Directions for Designers. Hayden Book Company Inc., July 1975.
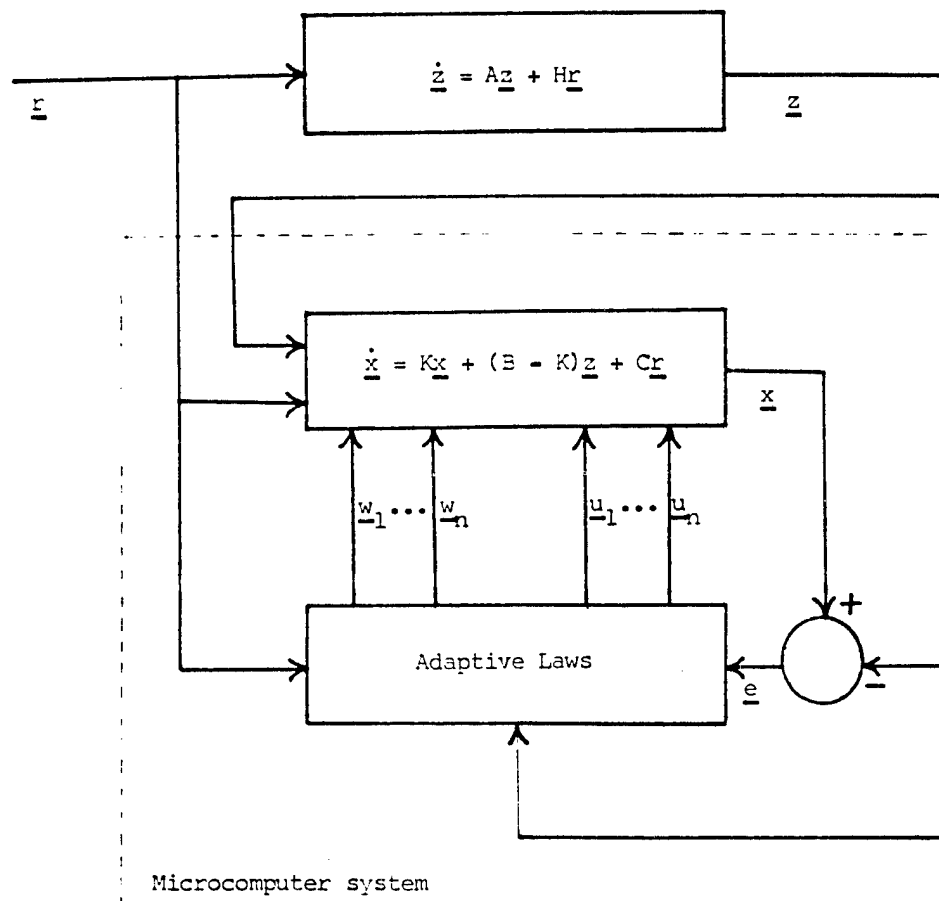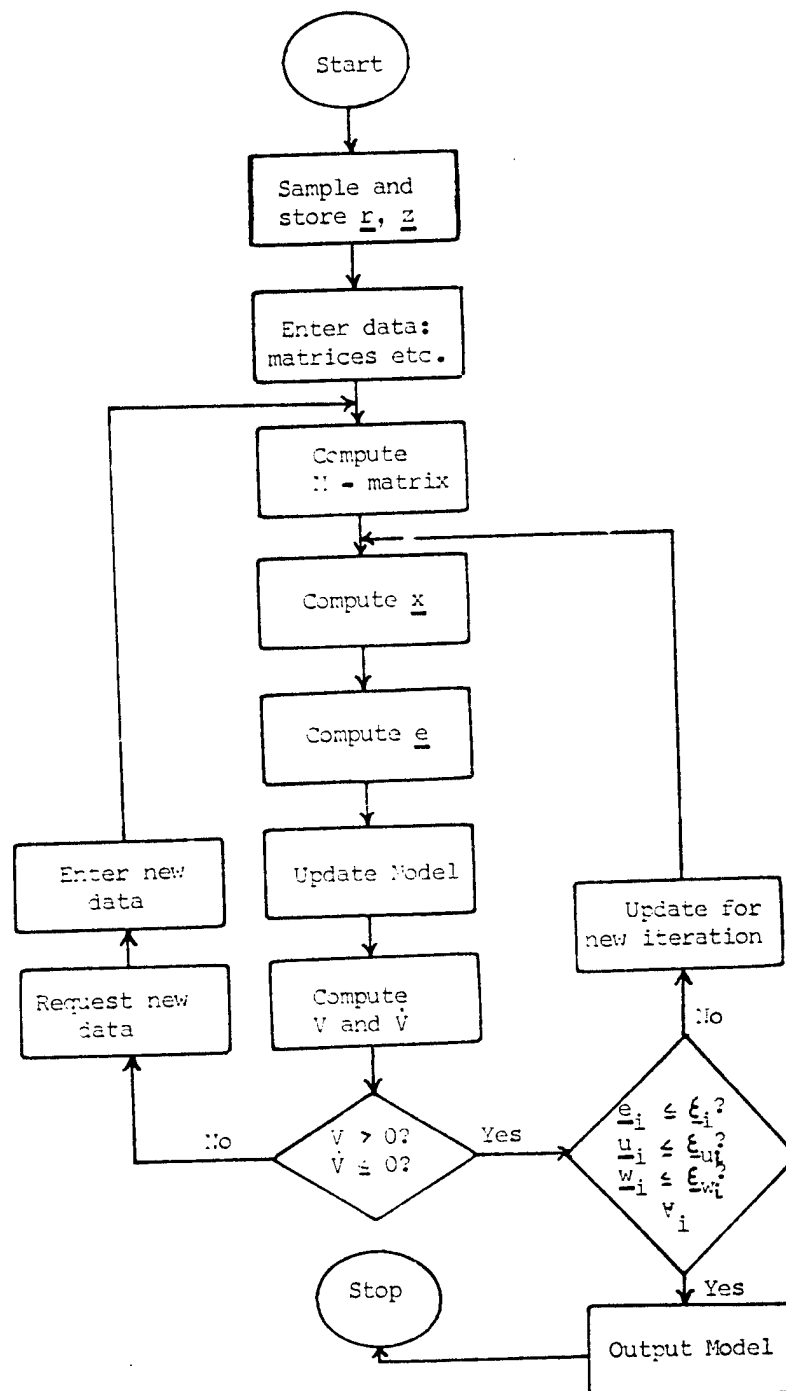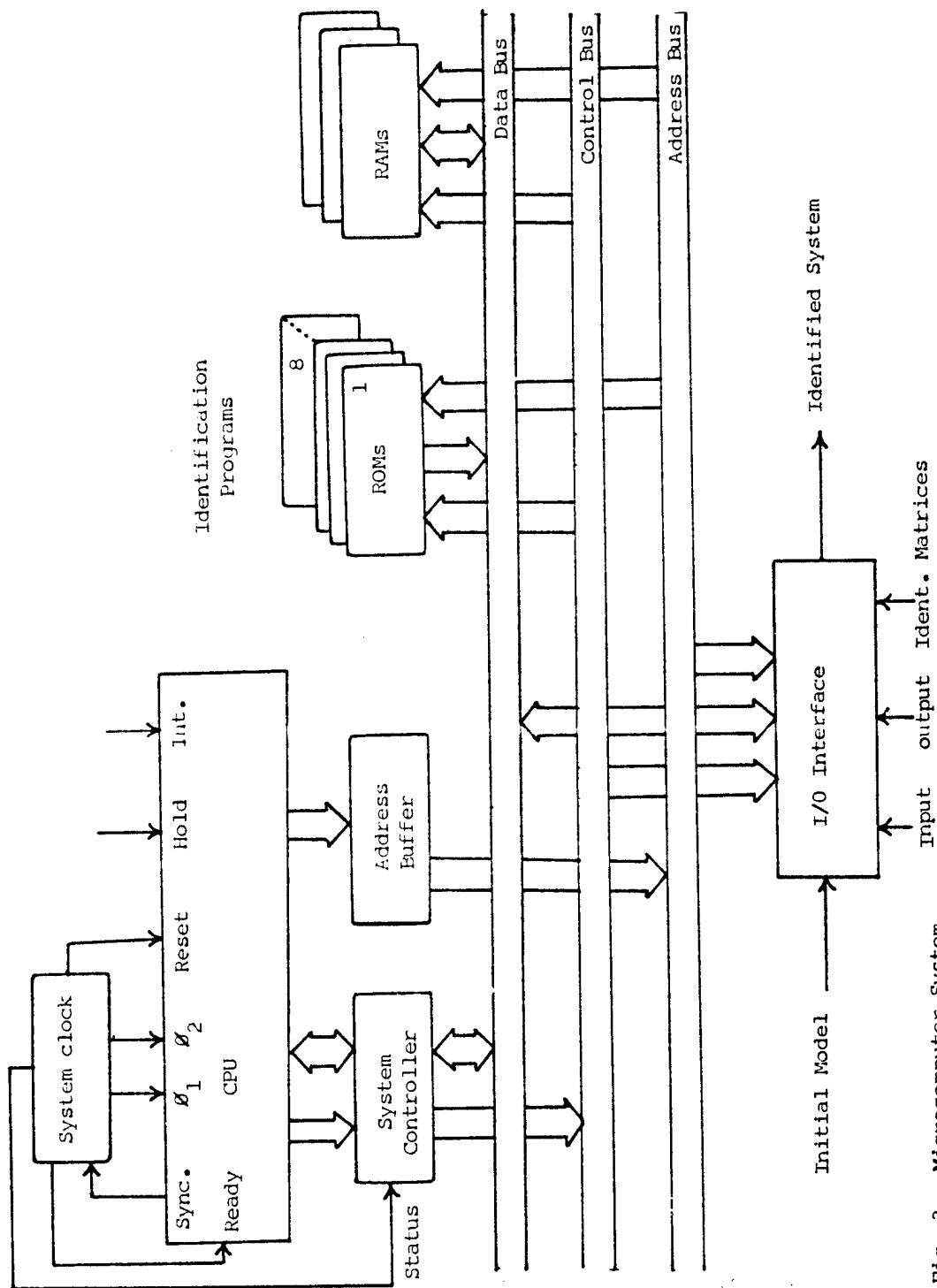
Fig. 1. Identification Process.

Fig. 2. Logic Flow Chart.

Fig. 3. Microcomputer System.